UNIVERSITÉ DU LUXEMBOURG

PhD-FSTC-2017-11

The Faculty of Life Sciences, Technology and Communication

DISSERTATION

Defence held on 13/02/2017 in Luxembourg

to obtain the degree of

DOCTEUR DE L´UNIVERSITÉ DU LUXEMBOURG

EN BIOLOGIE

by

Remon SOLIMAN

Born on 18th February, 1986 in El-Fayoum (Egypt)

NEW MODELS TO STUDY THE CROSS-TALK BETWEEN THE PROTEIN REPAIR L-ISOASPARTYL METHYLTRANSFERASE AND CELL SIGNALLING

Dissertation defence committee

Dr Carole Linster, — Scientific supervisor
Principle investigator, Université du Luxembourg

Dr Alexander Crawford
Principle investigator, Université du Luxembourg

Prof Rudi Balling — Dissertation supervisor
Professor, Université du Luxembourg

Prof. Serge Haan — Chairman
Professor, Université du Luxembourg

Prof. Hans-Ulrich Demuth
Professor, Fraunhofer Institute for Cell therapy and Immunology IZI

Prof. Diego Ingrosso
Associate Professor, Second University of Naples

UNIVERSITY OF LUXEMBOURG

New Models to Study the Cross-talk Between the Protein Repair L-Isoaspartyl Methyltransferase and Cell Signalling

by

Remon Soliman

Supervisor

Dr. Carole Linster

A thesis submitted in the fulfilment of the requirements
for the degree of Doctor of Philosophy

in the

Enzymology and Metabolism group

Luxembourg Centre for Systems Biomedicine

2017

Affidavit

I hereby confirm that the PhD thesis entitled “New models to study the cross-talk between the protein repair L-isoaspartyl methyltransferase and cell signalling” has been written independently and without any other sources than cited.

Luxembourg, _____ _____

Name

Acknowledgments

First of all, I would like to thank Dr. Carole Linster for giving me the opportunity to continue working on the amazing enzyme PCMT. Dr. Linster was the direct supervisor of my PhD thesis and the majority of the financial resources to support my PhD project were obtained with her help. Thanks to Carole, I really gained a lot of knowledge, not only related to PCMT, but also about the concept of damage and repair in biology, the way to approach scientific problems and the state-of-the-art technology in research. I would also like to thank her for the thorough revision and precious comments she provided for my thesis document.

I would like to thank Dr. Alexander Crawford for his generosity to let me work in his lab and learn a lot about the zebrafish model, also for his patience during the learning process and the time I consumed from his group for learning. Moreover, his zebrafish experience and scientific input from the zebrafish field was of great help. I also would like to thank Prof. Rudi Balling, first for creating this nice environment for research at the LCSB and second for accepting the official supervision of my PhD thesis, interesting scientific discussions and helpful inputs.

EM group, aka BCM group, it was really fun working with you guys. I had a lot of great moments with you, learned for the first time how to brew amazingly delicious beer, tried skiing for the first time (although I was skiing most of the time backwards). I want to thank you all for the nice working environment, Jeff, Danny, Julia, Ursula, Zaya, Charan. Especially Paul, with his weekends spent on reading my NICELY written thesis (I think he knows what I mean); without his feedback on my writings I think the thesis would have not reached this stage. Thanks also for humorous jokes ;-), motivation and the continuous scientific feedback during my PhD work. I also want to thank Ken for his great expertise in enzymology, his scientific feedback and not to forget his Canadian expertise in beer brewing. A big thank you goes to Nicole not only for the mass spectrometry experiments and the incredibly amazing results she produced for me, but also for the very big enthusiasm when discussing science.

CHE group, Max, Anastasia, Alice and Vincent, you are wonderful. Everybody in the group was really cheerful and always helpful. I would like to thank Lorena for teaching me how to work with zebrafish. The different techniques starting from feeding the fish (that was challenging for me ☺) to 1-cell injection of fish eggs (which was extremely easy). The scientific background, the different skills and tricks for handling zebrafish, etc., I learned all of this thanks to Lorena's help. Also Teresa, thanks to her I learned a lot about the zebrafish brain, how to perform EEG recordings, calcium imaging in the GCaMP6f line, and not to forget her help for last minute revision of the thesis. Also Simon, for his

suggestions on the zebrafish experiments as well as teaching me zebrafish organ dissection; and of course his patience when I killed some of his fishes.

I also cannot forget the great help from Mahsa, with calcium imaging in the mammalian cells, the time she spent with me to perform the calcium experiments in cells, and the great scientific discussions about calcium signalling in biology.

I would like to thank our dear former neighbours and now part of our team, Xiangyi and Christian, for all the support and fun we had together.

I would also like to thank my external reviewers Prof. Ingrosso and Prof. Demuth for taking the time to review my thesis and coming over to Luxembourg for my defense. It was in Prof. Demuth's lab where I first started working on PCMT and the work done in his lab qualified me to start my PhD in Dr. Linster's lab at LCSB.

I would like to thank the Fonds National de la Recherche Luxembourg for providing the main financial support of this thesis (AFR PhD grant number 4939112). This work was also partially supported by a Marie Curie International Reintegration Grant (number 276814) obtained under the European Union Seventh Framework Programme by Dr. Linster.

Finally, I would like to thank my family and friends. Especially my parents, Fayez and Hanaa, for their continuous love, support, and patience when staying away from them for long periods of time. And last but not least, thanks to my sisters Shery and Rania and their kids and babies Mathew, Thomas, Natalie and Evraam.

Abbreviations

ACSF	Artificial cerebrospinal fluid
AD	Alzheimer's disease
ADP	Adenosine diphosphate
AP	Alkaline phosphatase
ATP	Adenosine triphosphate
BCIP	5-Bromo 4-chloro 3-indolyl phosphate
bFGF	Basic fibroblast growth factor
bp	base pair
BSA	Bovine serum albumin
CaM	Calmodulin
CaMKII	Calmodulin-dependent kinase II
Cas9	CRISPR associated protein 9
CRISPR	Clustered regularly interspaced short palindromic repeats
DAG	Diacylglycerol
DCLK1	Doublecortin like kinase 1
DMEM	Dulbecco's Modified Eagle Medium
DMSO	Dimethyl sulfoxide
DNA	Deoxyribonucleic acid
dNTPs	Deoxy-nucleotide triphosphates
dpf	days post-fertilization
DSB	Double-strand break
ECL	Enhanced chemiluminescence
EDTA	Ethylenediaminetetraacetic acid
eef1a1l1	Eukaryotic translation elongation factor 1 alpha 1, like 1
EGF	Epidermal growth factor
EGTA	Ethylene glycol tetraacetic acid
ENU	Ethyl-*N*-nitrosourea
ERK	Extracellular signal-regulated kinase
FBS	Fetal bovine serum
g	Gravitational constant
GAPDH	Glyceraldehyde 3-phosphate dehydrogenase
gDNA	Genomic Deoxyribonucleic acid
GDP	Guanosine diphosphate

GFP	Green fluorescent protein
GPCR	G-protein coupled receptor
gRNA	Guide ribonucleic acid
GSK3β	Glycogen synthase kinase 3β
GTP	Guanosine triphosphate
HDR	Homology-directed repair
HEK293	Human embryonic kidney cells
hpf	hours post-fertilization
HRP	Horseradish peroxidase
HT22	Murine immortalized hippocampal cell line
IGF-1	Insulin growth factor 1
IP_3	Inositol (3,4,5)-trisphosphate
IPTG	Isopropyl β-D-1-thiogalactopyranoside
ISH	*In situ* hybridization
KASAisoDALKY	Nonapeptide of the sequence Lys-Ala-Ser-Ala-isoAsp-Ala-Leu-Lys-Tyr
kbp	kilo base pair
MAPK	Mitogen-activated protein kinase
MEK	Mitogen-activated protein kinase kinase
Mitfa	Microphthalmia-associated transcription factor a
MKP-3	MAP Kinase Phosphatase 3
MO	Morpholino oligomer
mTOR	Mechanistic target of rapamycin
NBT	Nitro blue tetrazolium
NHEJ	Nonhomologous end joining
OptiMEM®	Improved Minimal Essential Medium
PAM	Protospacer adjacent motif
PBS	Phosphate-buffered saline
PC-12	Pheochromocytoma cells derived from *Rattus norvegicus* adrenal gland
PCR	Polymerase chain reaction
PD	Parkinson's disease
PDK1	Phosphoinositide-dependent kinase-1
PEG	Polyethylene glycol
PFA	Paraformaldehyde
PIMT	Protein L-isoaspartyl methyltransferase

PIP_2	Phosphatidylinositol (4,5)-bisphosphate
PIP_3	Phosphatidylinositol (3,4,5)-trisphosphate
PMSF	Phenylmethylsulfonyl fluoride
PNK	Polynucleotide Kinase
PTU	Phenylthiourea
PTZ	Pentylenetetrazol
PVDF	Polyvinylidene fluoride
qPCR	Quantitative PCR
RISC	RNA-induced silencing complex
RKIP	Raf kinase interacting protein
RNAi	RNA interference
ROS	Reactive oxygen species
rpl13a	Ribosomal protein L13a
RT	Room temperature
SAH	*S*-adenosyl homocysteine
SAM	*S*-adenosyl methionine
SDS-PAGE	Sodium dodecyl sulfate – polyacrylamide gel electrophoresis
shRNA	Short hairpin RNA
SSC	Saline-sodium citrate buffer
U2OS	Human bone osteosarcoma cell line
U-87 MG	Uppsala 87 Malignant Glioma (Human glioblastoma cell line)
WB	Western blot

Table of Contents

Table of figures

Table of tables

Summary

Isomerization of L-aspartyl and L-asparaginyl residues to form L-isoaspartyl residues in proteins is one type of protein damage that can occur under physiological conditions and can potentially lead to conformational change, loss of function and enhanced protein degradation. Protein L-isoaspartyl methyltransferase (PCMT or PIMT)[1] is a repair enzyme, which allows the reconversion of L-isoaspartyl residues to L-aspartyl residues in protein. Although the catalytic function of PCMT is known, its physiological roles remain less well understood. *Pcmt1* gene knockout in mice leads for example, via molecular mechanisms that remain mostly obscure, to activation of insulin/IGF-1 and MAPK signalling pathways in the brain, and premature death due to massive epileptic seizure events.

In this doctoral research project, we have used both mammalian cells and zebrafish models to investigate the impact of PCMT deficiency on insulin/IGF-1, MAPK and calcium signalling as well as how PCMT may be involved in epilepsy. In mammalian cells we used shRNA and CRISPR/Cas9 technology to reduce or completely silence PCMT expression, with the main objective being to mimic, in cell culture, the activation of the IGF-1 and MAPK signalling pathways observed in *Pcmt1* knockout mice in the hope to thereby increase the chances to elucidate the underlying molecular mechanisms. In zebrafish we used an antisense morpholino-based strategy to knock down both PCMT homologs and thereby establish a new whole organism model to further study the physiological functions of PCMT, more particularly in the brain.

Our results indicate that insulin/IGF-1 signalling is not affected by *PCMT* knockdown or knockout in mammalian cells whereas a time-dependent MAPK pathway activation could be detected in a *Pcmt1* knockout mouse hippocampal cell line. In zebrafish, we showed that the two PCMT homologs Pcmt and Pcmtl (Pcmt/l) possess isoaspartyl methyltransferase activity. In *pcmt/l* knockdown (or morphant) zebrafish larvae we did not detect abnormal electrical activity in the brain, but we identified movement impairment and strongly perturbed brain calcium fluxes. Abnormal calcium responses were also observed in the *Pcmt1* knockout mouse hippocampal cell line. We concluded that the interplay between PCMT and growth signalling pathways is highly dependent on experimental model and may not be amenable to investigation in cell culture. Importantly, our results clearly show that PCMT plays a pivotal role in calcium signalling and suggest that PCMT-dependent repair mechanisms may be important to prevent calcium-related neurological disorders.

[1] Gene-protein acronym conventions: followed in this thesis: PCMT is used, in an organism-independent way, as the general acronym for the L-isoaspartyl protein carboxyl methyltransferase (also known as protein L-isoaspartyl methyltransferase). As organism-specific acronyms we used: *PCMT1*, human gene; PCMT1, human protein; *Pcmt1*, mouse gene; Pcmt1, mouse protein; *pcmt*, zebrafish gene; Pcmt, zebrafish protein.

1 Introduction

1.1 Damage and repair in biology

Every day human beings are exposed to different environmental stressors, e.g. radiation that leads to damage of various molecules in the cells. Nevertheless, cells are still functioning normally due to repair mechanisms in charge to maintain cell homeostasis. While DNA damage and repair have been intensively studied, only few repair mechanisms for proteins have been described. Even more recently, small molecules or metabolites were found to be prone to damage and cellular mechanisms for their repair are being uncovered. A considerable body of evidence suggests that cellular inability to repair damaged molecules like DNA and proteins plays an important role in neurological disorders as well as aging (CAMPISI and VIJG 2009). Therefore, extending our understanding of those cellular functions should contribute to gain insights into the physio-pathological processes involved and may be key for improving our quality of life.

1.1.1 DNA damage and repair

DNA is the keeper of all the genetic information essential for life. Yet, it is continuously subjected to damages either by endogenous (e.g. reactive oxygen species (ROS), endonucleases, or defective replication machinery) or exogenous sources (e.g. radiation or mutagenic compounds). Excessive, uncontrollable damage can lead to accumulation of mutations that can eventually result in cellular dysfunctions associated with human diseases such as cancer or neurodegenerative disorders (POIRIER 2004; COPPEDE and MIGLIORE 2015). In 2015, the Nobel Prize in chemistry was awarded to Tomas Lindahl, Paul Modrich and Aziz Sancar for their work on DNA repair. They showed that in order to keep DNA integrity, cells developed different repair mechanisms depending on the type of damage (LINDAHL *et al.* 2016). These repair mechanisms include, among others, mismatch repair (MMR), single-strand or double-strand break repair, base excision repair (BER) or nucleotide excision repair (NER). Deficiency in one of those repair mechanisms can lead to different disorders like Xeroderma Pigmentosum, Cockayne syndrome and Huntington disease (JEPPESEN *et al.* 2011). One example, is the MMR deficiency resulting in trinucleotide expansion in the gene encoding huntington protein leading to polyglutaminyl residues in Huntington disease (KOVTUN and MCMURRAY 2001). The discoveries in the DNA repair mechanisms opened the door for the development of many therapeutic agents such as olaparib which targets DNA repair for treatment of ovarian cancer (WIGGANS *et al.* 2015). Likewise, development of drugs modulating repair mechanisms of proteins and metabolites might offer new perspectives for therapeutic strategies targeting other diseases.

1.1.2 Metabolite damage and repair

Similarly to DNA, metabolites are also prone to damage, which may appear spontaneously or as a result of endogenous processes (mostly enzyme side reactions) (LINSTER *et al.* 2013). Enzymes, particularly in primary metabolism, are proteins that are generally thought to specifically catalyse one reaction, allowing the formation of one product. However, it is now known that the specificity of metabolic enzymes is weaker than expected and that side activities of various enzymes may lead to the production of abnormal or 'damaged' metabolites. Accumulation of these potentially harmful metabolites in the cell can interfere with normal cell function and lead to development of diseases. A growing number of metabolite repair enzymes is being identified and for some of them the physiological relevance is well illustrated by the fact that their dysfunction leads to debilitating disease (VAN SCHAFTINGEN *et al.* 2013; KREMER *et al.* 2016). One example is the production of the neurotoxic molecule L-2-hydroxyglutarate (L-2HG) as a side product of L-malate dehydrogenase. L-2HG is recognized by the repair enzyme L-2-hydroxyglutarate dehydrogenase (L2HGDH), which converts it to the non-toxic α-ketoglutarate. L2HGDH deficiency leads to L-2HG aciduria, a severe neurometabolic disorder (VAN SCHAFTINGEN *et al.* 2009). To illustrate the concept further, (*S*,*S*)-adenosyl methionine (SAM), the second most used cofactor in the cell, is prone to damage as (*R*,*S*)-SAM can form spontaneously from (*S*,*S*)-SAM (HOFFMAN 1986). A repair mechanism was identified in *Saccharomyces cerevisiae* involving the Mht1 and Sam4 enzymes which transfer the methyl group from (*R*,*S*)-SAM to homocysteine to form methionine and adenosyl homocysteine, which are both normal metabolites in the cell, and by this limiting the accumulation of the abnormal (*R*,*S*)-SAM form (VINCI and CLARKE 2007). The field of metabolite damage and repair is still young and growing, but the work accomplished already so far shows that, similar to DNA, proofreading enzymes are needed also in metabolism to correct for unavoidable enzymatic mistakes or reverse unwanted chemical modifications.

1.1.3 Protein damage and repair

Protein degradation is known to take place in the cell via two major mechanisms: proteolysis via the proteasome or via autophagy. In the former mechanism, misfolded, damaged or unneeded proteins are tagged with ubiquitin through enzymatic reactions prior to their degradation by the proteasome protein complex. In the latter mechanism, autophagy uses a transport mechanism into the lysosome where proteins, protein complexes or organelles can be degraded. In contrast to both proteasome and lysosome-based mechanisms, enzyme-based mechanisms exist where damaged proteins are not degraded but rather repaired. Indeed, similarly to DNA and metabolites, proteins can acquire damages by oxidation reactions or intramolecular rearrangements through which the amino acid sequence is altered and proteins can become non-functional. However, repair systems exist that are specific to amino acid damages and allow the restoration of functional proteins (CLARKE 2003). Imbalance

between protein damages, proteolytic pathways and protein repair systems can lead to accumulation of pathological forms of proteins and disease development especially in the nervous system (ROSS and POIRIER 2005). Various forms of protein damage and repair are explained in more detail in the following section.

1.2 Forms of protein damage and repair

1.2.1 Methionine oxidation

Methionine, either free or in proteins, can be oxidized to methionine sulfoxide by hydrogen peroxide, oxygen radicals, or other oxidizing agents. Methionine oxidation (Figure 1-1) was found to affect various cell functions. In calmodulin, methionine oxidation leads to structural alteration and declined affinity to calcium (GAO *et al.* 1998). Another example is inactivation of voltage gated K^+ channels affecting cellular excitability (CHEN *et al.* 2000). The repair system for this type of protein damage involves methionyl-sulfoxide reductases (MsrA and MsrB) that reduce methionyl-sulfoxide back to methionine (WEISSBACH *et al.* 2002). MsrA overexpression was found to extend the lifespan in *Drosophila melanogaster* and increased its ability to resist oxidative stress (RUAN *et al.* 2002). Similarly, MsrA and MsrB overexpression were found to protect mammalian cells against oxidative stress induced by H_2O_2 (MOSKOVITZ *et al.* 1998). In this regard, Msr enzymes are proposed to not only play a role in protein repair but also in ROS scavenging since the reduction reaction is NAD(P)H dependent. The cycles of the oxidation by ROS and reduction by Msr, scavenges molecules like H_2O_2 and drives an NAD(P)H oxidation reaction (LEVINE *et al.* 1996). Finally, MsrA overexpression in mice increased survival rate and improved insulin sensitivity in aged mice (SALMON *et al.* 2016). All the previous findings show that the protein damage caused due to methionine oxidation can be repaired directly by the Msr enzymes rather than protein degradation and *de novo* synthesis.

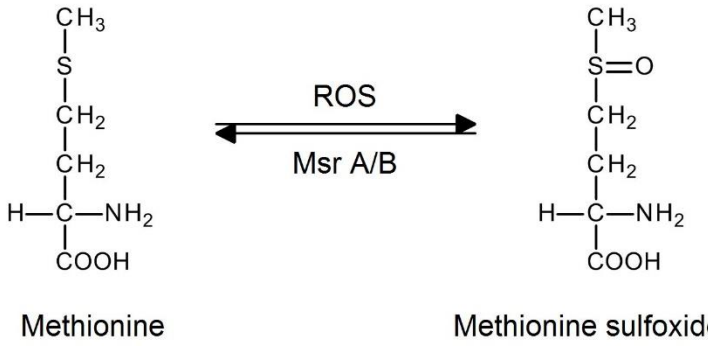

Figure 1-1: Oxidation of methionine and its reduction by methionyl-sulfoxide reductases (Msr A/B). Reactive oxygen species (ROS) oxidize methionine, either free or in proteins, to S- or R-methionyl-sulfoxides, which are recognized by MsrA or MsrB, respectively, and reduced back to methionine by these enzymes.

1.2.2 Tyrosine nitration

Another form of protein damage due to oxidative stress is tyrosine nitration. Nitric oxide reacts with superoxide forming peroxynitrite, which in turn interacts with macromolecules in the cell causing modulation of cellular functions. Tyrosine residues in proteins were found to be a potential target of peroxynitrite (Figure 1-2), which was confirmed when tyrosine-containing peptides were able to rescue PC12 cells from peroxynitrite-induced apoptosis (YE *et al.* 2007). Later, heat shock protein 90 (Hsp90) was identified as a major target for nitration and this kind of damage induces neuronal cell death (FRANCO *et al.* 2013). In addition, one noticeable consequence of tyrosine nitration is blocking of phosphorylation sites as it has been shown that tyrosine protein kinases were inhibited via peroxynitrite-mediated nitration of tyrosine (GOW *et al.* 1996). Signalling pathways involving phospholipase C_γ were found to be inhibited by tyrosine nitration (DREW and LEEUWENBURGH 2002). A proposed repair mechanism was assumed to exist when protein extracts from rat spleen and lung were able to modify nitrotyrosine-containing peptides but not free nitrotyrosine. However, the enzyme responsible for this activity has not been identified yet. (KAMISAKI *et al.* 1998). Furthermore, denitrase activity, from mouse spleen protein crude extract, was found to restore glutamine synthase activity inhibited by tyrosine nitration (KAMISAKI *et al.* 1998; GORG *et al.* 2007). In summary, tyrosine residues in proteins are prone to nitration altering protein function and there is a potential enzymatic repair mechanism whose molecular identity remains until now unknown.

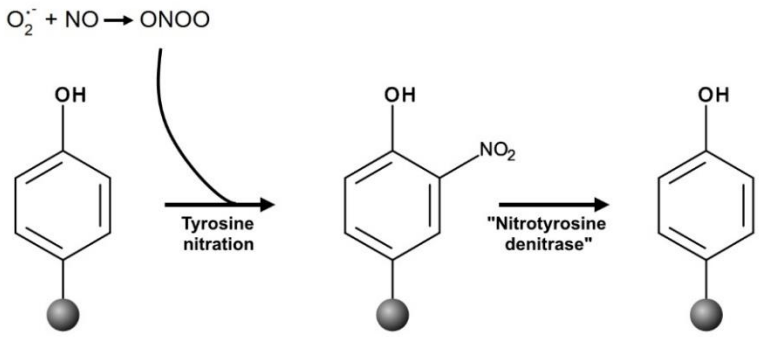

Figure 1-2: Tyrosine nitration. Oxygen radicals oxidize NO leading to the formation of peroxynitrite which in turn is able to react with tyrosine to form nitrotyrosine. A nitrotyrosine denitrase activity was detected in cellular crude extracts, but the enzyme responsible for this activity has not been identified yet.

1.2.3 Protein glycation

Unlike controlled, enzymatically catalysed, addition of sugar to protein (protein glycosylation), non-enzymatic addition of sugar to protein (protein glycation) is another type of protein damage. In general, aldehyde or ketone groups can react with free primary amines forming a Schiff base through an S_N2 nucleophilic attack (JOHNSON *et al.* 1983). In case of protein glycation, the Schiff base can be formed from the interaction between the aldehyde group of glucose and free amine groups in

proteins, in particular the ε-amine group of lysine side chains. Although the reaction is reversible, the Schiff base can undergo rearrangement giving rise to the more stable Amadori structure (fructosamine in case of glucose as the reacting sugar) (Figure 1-3). Glycation at lysine residues in proteins was reported as a sort of damage that can affect protein function. For example, RNase A as well as human erythrocyte bisphosphoglycerate mutase were found to have lower enzymatic activity when glycated (WATKINS *et al.* 1985; FUJITA *et al.* 1998). Moreover, glycated calmodulin failed to activate three of its downstream kinases (KOWLURU *et al.* 1989). Recently, protein glycation was found to enhance aggregation of β-amyloid (Aβ) and α-synuclein, increasing their pathogenicity (VICENTE MIRANDA and OUTEIRO 2010; VICENTE MIRANDA *et al.* 2016). Fructosamine-3-kinase (FN3K) is a protein repair enzyme that phosphorylates fructosamine residues in proteins and facilitates deglycation, restoring the original free amine group (DELPIERRE and VAN SCHAFTINGEN 2003). Although, the physiological relevance of the repair mechanism of FN3K is still not well understood, it is notably assumed that it might play a role in neurodegenerative diseases considering the impact of protein glycation on protein aggregation.

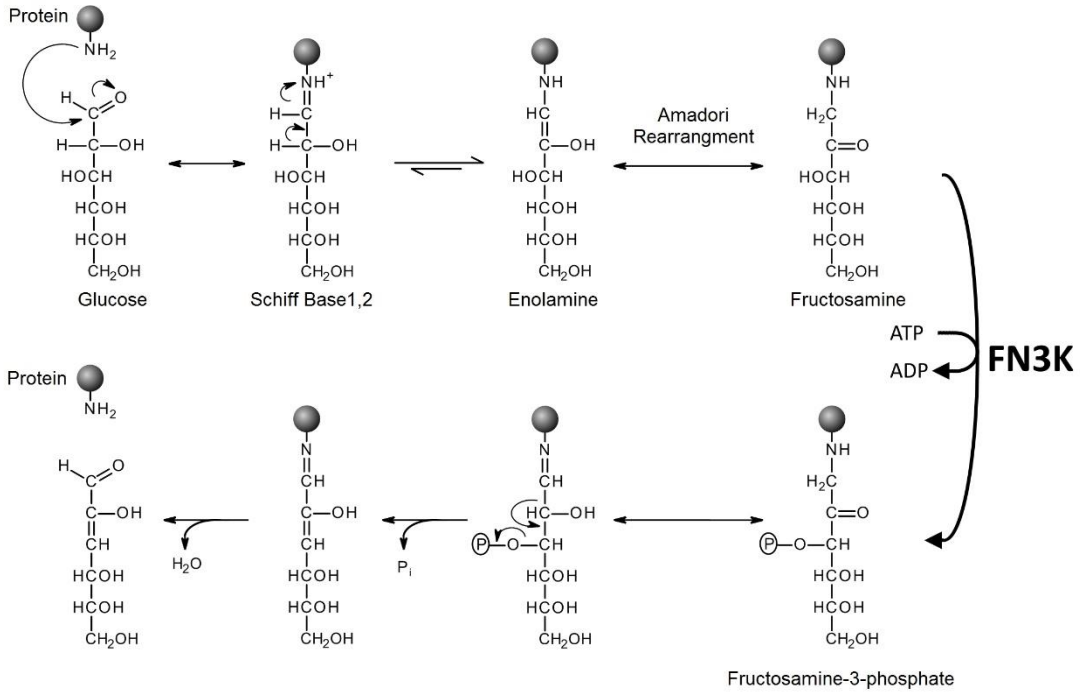

Figure 1-3: Protein glycation and repair by fructosamine 3-kinase (FN3K). Unlike enzymatically controlled glycosylation of proteins, glucose can react spontaneously with amine groups in proteins forming fructosamines. FN3K phosphorylates fructosamine residues in proteins, initiating the repair mechanism (deglycation). Adapted from (COLLARD 2004).

1.2.4 Proline isomerization

Although the majority of peptide bonds in proteins are in the *trans* conformation, those preceding prolyl residues are often in the *cis* conformation. Prolyl residues are however, prone to *cis*/*trans* interconversion, leading to conformational alterations, which in turn might lead to protein aggregation. An example of this process is observed in β-2-microglobulin (β2m) where *trans* conformation preceding prolyl residues together with Cu^{2+} ions trigger its amyloidogenesis (EAKIN *et al.* 2006). Since the isomerization process can happen spontaneously, an enzymatic system is required to maintain the correct conformation of prolyl residues in native proteins. Peptidylprolyl isomerase (Pin1) catalyses the *cis*/*trans* isomerization of prolyl residues in proteins (SCHIENE and FISCHER 2000). It appears that the repair mechanism by Pin1 is important for protein homoeostasis since the two hallmark proteins of Alzheimer's disease, Aβ and tau, were found to be affected by the cellular Pin1 activity. *Pin1* knockout in mammalian cells increased Aβ secretion while overexpression reduced the secretion, which was confirmed in a mouse *Pin1* knockout as it showed higher levels of insoluble Aβ42 in the brain (PASTORINO *et al.* 2006). Moreover, Pin1 was found to restore the ability of phosphorylated tau to bind to microtubules and remarkably, *Pin1* knockout mice experience motor and behavioural deficits (LU *et al.* 1999; LIOU *et al.* 2003). Thus, Pin1 is needed for conformational control of proline and protein homeostasis and shows interesting links to neurodegenerative disease.

1.2.5 Aspartyl and asparaginyl isomerization

Formation of isoaspartyl residues and the repair mechanism by protein L-isoaspartyl methyltransferase (PCMT) is the main focus of the work presented in this thesis and will be discussed in more detail below.

Interestingly, all protein repair enzymes discovered so far, i.e. PCMT, Msr, Pin1 and FN3K, are usually ubiquitously expressed in all tissues, but show highest expression in the brain (MIZOBUCHI *et al.* 1994; KUSCHEL *et al.* 1999; COLLARD *et al.* 2003; FANGHANEL *et al.* 2006). This suggests that targeted repair of proteins in post-mitotic cells such as neurons is essential, in addition to protein degradation and resynthesis, to prevent the accumulation of damaged proteins that may otherwise lead to disease development and notably neurodegenerative diseases. Protein repair enzymes are therefore also potentially promising targets for drug interventions.

1.3 Protein L-isoaspartyl methyltransferase

1.3.1 Isoaspartyl formation from aspartyl and asparaginyl residues

Under physiological conditions, the carbonyl carbons in the side chains of L-aspartyl and L-asparaginyl, after deamidation, residues in proteins are prone to a nucleophilic attack by the loan pair of electrons

on the nitrogen atom of the peptide bond formed with the next amino acyl residue (Figure 1-4). As a result, deamidation, in case of L-asparaginyl, or dehydration, in case of L-aspartyl, takes place leading to the formation of an L-succinimide intermediate. At this stage, racemization can take place to form D-succinimide. L-succinimide and D-succinimide are unstable and spontaneously form L-isoaspartyl as the major product (70%), L-aspartyl (30%), and minor amounts of D-aspartyl and D-isoaspartyl (GEIGER and CLARKE 1987). The conversion of aspartyl to isoaspartyl residues leads to an introduction of an extra $-CH_2-$ group in the peptide backbone with conformational changes in the 3D structure of the protein. Remarkably, the rate of isoaspartyl formation from asparaginyl residues was found to be 15 – 36 times faster in case of asparaginyl than from aspartyl residues (STEPHENSON and CLARKE 1989). Furthermore, asparaginyl deamidation was found to be faster when it is followed by an amino acid with a relatively small or hydrophilic side chain, such as alanine, glycine, histidine and serine, in contrast to bulky amino acids, such as phenylalanine, tyrosine or tryptophan (ROBINSON and ROBINSON 2001b). Secondary and tertiary protein structures were also found to influence isoaspartyl formation, small peptides being for example more prone to isomerization than bigger and highly structured proteins. Also, flexible regions in calmodulin were found to accumulate more isoaspartyl residues than non-flexible regions (CLARKE 1987; OTA and CLARKE 1989b; OTA and CLARKE 1989a). Additionally, asparaginyl residues in α-helices and β-turns were found to be more resistant against isomerization (XIE and SCHOWEN 1999).

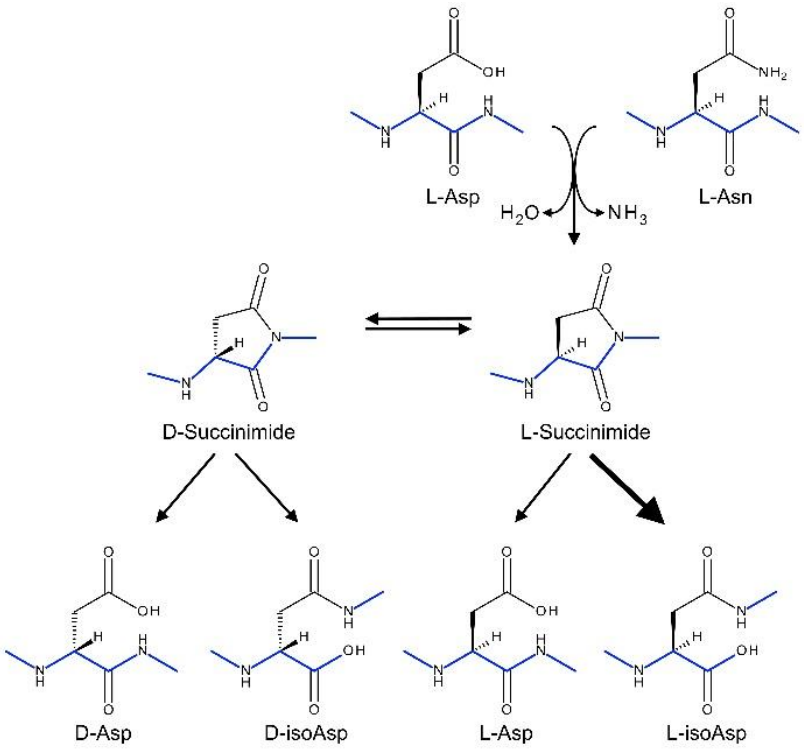

Figure 1-4: Formation of isoaspartyl residues in proteins. L-asparaginyl (L-Asn) and L-aspartyl (L-Asp) residues undergo spontaneous modification to form L-succinimide, which in turn can racemiz to D-succinimide. L- and D-succinimide are unstable and will eventually form either D-aspartyl (D-Asp), D-isoaspartyl (D-isoAsp), L-aspartyl (L-Asp) or L-isoaspartyl (L-isoAsp), with the major product being L-isoAsp. The L-Asn or L-Asp conversion to L-isoAsp shifts the peptide backbone (blue line) to the side chain, introducing an extra CH_2 group into the peptide backbone.

1.3.2 Influence of isoaspartyl formation on protein structure and function

Isoaspartyl formation can have different effects on proteins including conformational changes, loss-of-function, gain-of-function, protein aggregation and higher susceptibility to degradation. Isoaspartyl formation is a major concern in the field of therapeutic protein production, where recombinant IgG antibodies can lose for example up to 70% of potency due to isoaspartyl formation (HARRIS *et al.* 2001), also recombinant human stem cell factor loses half of the biological activity due to isoaspartyl formation (HSU *et al.* 1998). Another example of functional decline is in creatine kinase B, which loses the ability to phosphorylate creatine due to isomerization events (DIMITRIJEVIC *et al.* 2014). On the other hand, isoaspartyl formation was also shown to be a mechanism for gain-of-function. For example, conversion of asparaginyl to aspartyl, which involves the intermediate formation of the isoaspartyl residue, enables fibronectin to bind to integrin $\alpha_v\beta_3$ in the process of extracellular matrix activation (CURNIS *et al.* 2006; CORTI and CURNIS 2011). Aggregation is another consequence of isoaspartyl formation. Aβ isolated from Alzheimer's disease patients, was found to contain isoaspartyl residues at position 1, 7 and 23 (SARGAEVA *et al.* 2009); isomerization of Asp23, but not Asp7, enhanced Aβ aggregation (ROHER *et al.* 1993; SHIMIZU *et al.* 2002). Enhanced degradation due to isoaspartate

formation was observed in calmodulin, which during *in vitro* aging accumulated isoaspartyl residues over time and when injected into *Xenopus laevis* oocytes was degraded faster than a native calmodulin as a control (SZYMANSKA *et al.* 1998). Finally, an *in vivo* study showed that autoimmune mice strains like MRL mice have higher levels of isoaspartyl residues in protein compared to the control strains B10.BR nonautoimmune mice and the authors suggested that isoaspartyl formation in protein can trigger autoimmunity by T cell hyperproliferation (YANG *et al.* 2006). It appears that isoaspartyl formation can lead to different outcomes under normal physiological or pathological conditions, depending on the identity of the protein as well as on the position of the isomerized residue in the protein (REISSNER and ASWAD 2003).

In addition, as already indicated above, isoaspartyl formation has been associated with neurodegenerative conditions like Alzheimer's disease (AD), Parkinson's disease, and multiple sclerosis (MS). In AD patients, higher levels of isoaspartyl residues have been found in plasma proteins, tau, and as mentioned above, Aβ (WATANABE *et al.* 1999; SHIMIZU *et al.* 2000; YANG *et al.* 2011). Also in MS patients, myelin basic protein was found to accumulate higher isoaspartyl residues than control individuals (FRIEDRICH *et al.* 2016). Finally, α-synuclein, a hallmark in PD, was found to having the tendency for isoaspartyl formation, however, this observation is still under debate since another group could not confirm this observation (VIGNESWARA *et al.* 2006; MORRISON *et al.* 2012; VIGNESWARA *et al.* 2013). Therefore, isoaspartyl formation in proteins can be a risk factor for neurodegenerative diseases.

1.3.3 PCMT transfers a methyl group to isoaspartyl residues initiating their repair to aspartyl residues

Back in 1965, when Axelrod and Daly studied SAM-dependent methyltransferases in bovine pituitary gland extracts using radiolabelled *S*-adenosyl methionine (SAM), they reported the release of radiolabelled methanol. The production of radiolabelled methanol was inhibited upon boiling the extracts and they concluded that the SAM-dependent methanol production is catalysed enzymatically (AXELROD and DALY 1965). Almost ten years later, the methanol-forming enzyme was purified from bovine pituitary gland and it was found to methylate hormones secreted from the anterior lobe of the pituitary gland (DILIBERTO and AXELROD 1974). This enzyme is identified now as PCMT, which specifically recognizes L-isoaspartyl residues and to a lesser extend D-aspartyl residues in proteins and methylates them using SAM as the cofactor, thereby initiating their reconversion to L-aspartyl residues (JOHNSON *et al.* 1987b; MCFADDEN and CLARKE 1987; LOWENSON and CLARKE 1992) (Figure 1-5). It can be noted that PCMT activity can lead to complete repair if the original residue was an aspartyl residue; if the isoaspartyl residue was formed from an asparaginyl residue, the 'repaired' residue will also be an aspartyl residue, which thus represents a net asparaginyl to aspartyl conversion for the protein.

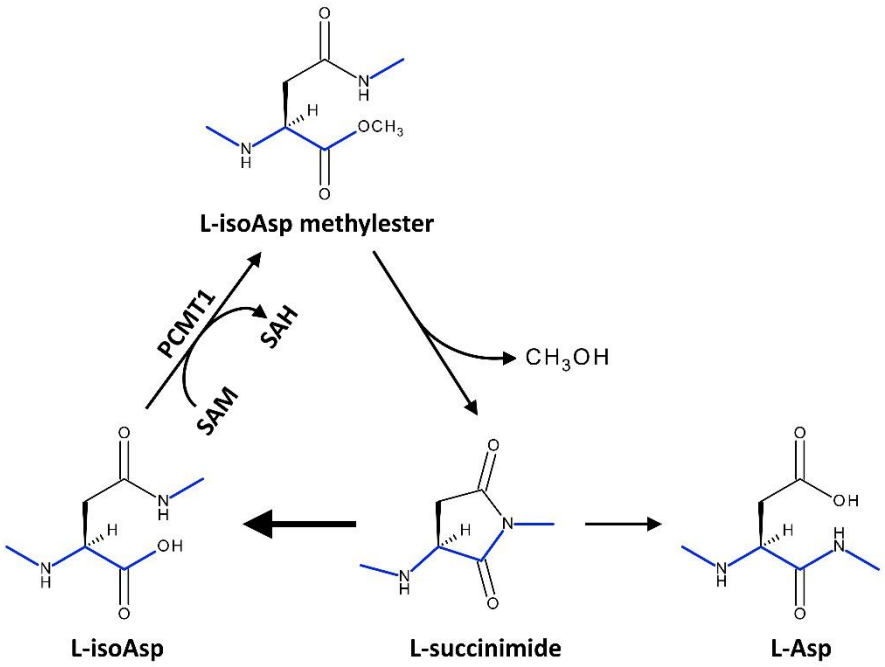

Figure 1-5: Isoaspartyl repair mechanism by PCMT. PCMT catalyses the transfer of a methyl group from the cofactor SAM to the carboxyl group in isoaspartyl residues, facilitating the formation of the L-succinimide intermediate. There is still a higher chance that L-succinimide will revert to the isoaspartyl form than to form an aspartyl residue, but since aspartyl residues are not methylated by PCMT, the reaction equilibrium is shifted towards aspartyl formation.

PCMT is widely conserved from bacteria to humans (JOHNSON *et al.* 1991a; LI and CLARKE 1992) with very few species, such as notably *Saccharomyces cerevisiae*, lacking a PCMT homolog (Figure 1-6). It appears that PCMT1 is the key enzyme to limit the accumulation of isoaspartyl residues in proteins, since protein extracted from tissues of *Pcmt1* knockout mice contain high levels of isoaspartyl (KIM *et al.* 1997b). Isoaspartyl containing peptides were found to be resistant to peptidase activity, limiting their removal through proteolysis and highlighting the importance of PCMT activity not only for protein repair but also for efficient protein degradation (JOHNSON and ASWAD 1990). Nevertheless, other mechanisms to limit isoaspartyl formation may exist, more particularly in the few species that do not encode PCMT, as recently proposed by Patananan et al., (PATANANAN *et al.* 2014). The authors showed indeed that in *S. cerevisiae*, isoaspartyl accumulation is very low despite the absence of PCMT activity in this species and proposed that there is an alternative mechanism for isoaspartyl degradation implying metalloproteases.

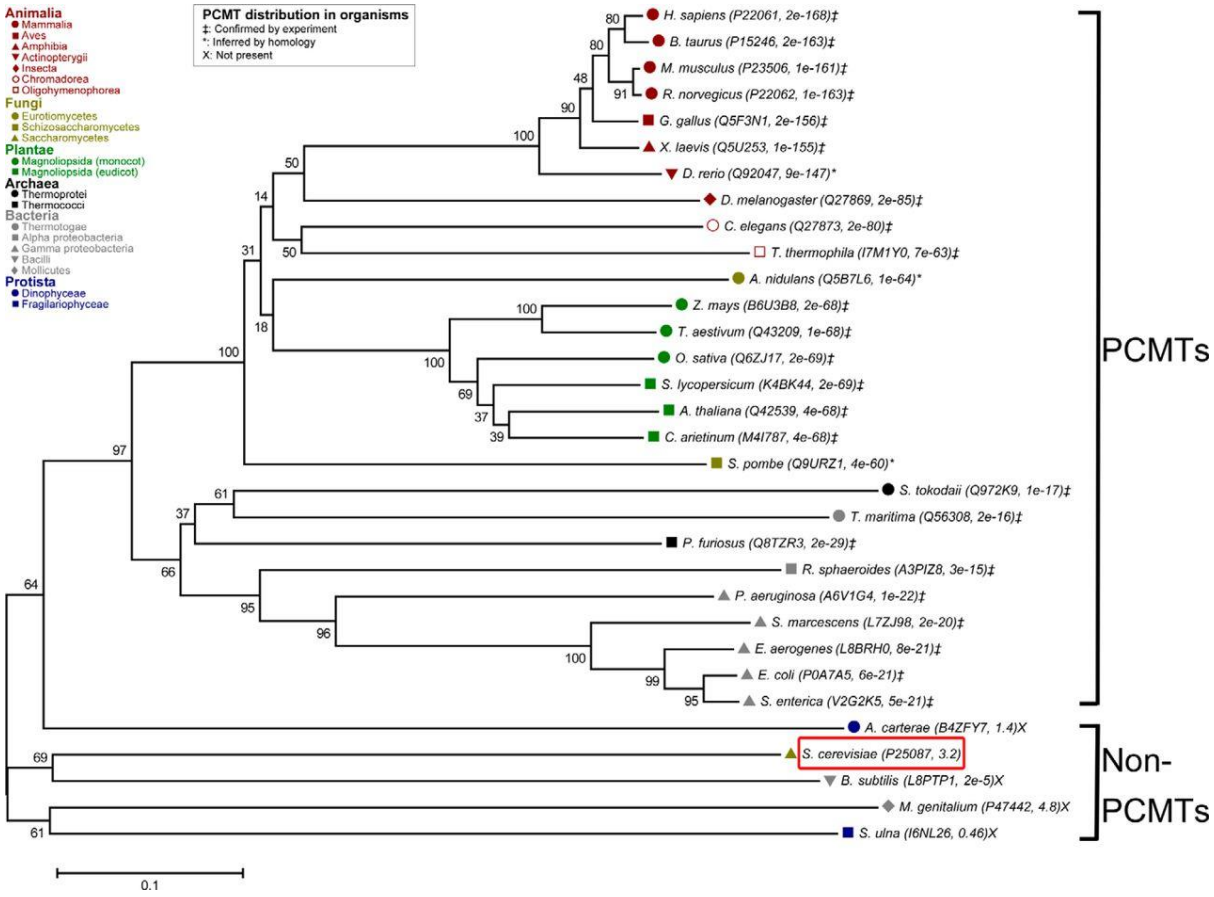

Figure 1-6: PCMT distribution in organisms. PCMT is highly conserved among many species except for a few Gram-positive bacteria and fungal species. Adapted from (PATANANAN et al. 2014).

PCMT being a SAM-dependent methyltransferase, the enzyme possesses a nucleotide-binding domain, which is highly conserved among different phyla (KAGAN *et al.* 1997; SMITH *et al.* 2002). The mechanism by which PCMT1 methylates isoaspartyl was thought earlier to be a random sequential mechanism (JOHNSON and ASWAD 1993), but later structural studies showed that it is an ordered sequential mechanism where SAM binds first, followed by the isoaspartyl peptide, then release of the methyl ester followed by SAH (SMITH *et al.* 2002; BENNETT *et al.* 2003). Two isoenzymes were described for human PCMT1 (PCMT I and PCMT II) sharing virtually identical primary structure with differing C-termini arising from alternative splicing resulting in the 226 amino acids PCMT I ending with Arg-Trp-Lys and the 227 amino acids PCMT II ending with Arg-Asp-Glu-Leu (MACLAREN *et al.* 1992; TAKEDA *et al.* 1995). The PCMT I is more basic than PCMT II and ratio of the second isoform to the first (II/I) varies between 0.52 to 1.2 as estimated in human blood samples (OTA *et al.* 1988). Nevertheless, difference in their function has not been reported until now. Human PCMT1 exhibits a polymorphism at residue 119, with 77% Ile and 23% Val in Caucasian populations (DEVRY and CLARKE 1999). The enzyme containing Val119 exhibits lower activity, but higher thermal stability and an increased affinity for endogenous substrates (DAVID *et al.* 1997; RUTHERFORD and DAGGETT 2009). This phenomenon was

explained by enforced van der Waals interactions between the residue Val119 and Leu130 (compared to Ile119 and Leu 130) (RUTHERFORD and DAGGETT 2010). Overall, PCMT is a SAM-dependent methyltransferase widely distributed enzyme with relatively small molecular weight (25 kDa) that initiates the conversion of isoaspartyl in proteins to aspartyl residues.

1.3.4 Tissue distribution and subcellular localization of PCMT

Different approaches have been used to study the tissue distribution and subcellular localization of PCMT including measuring transcript levels, enzyme activity levels or immunostaining techniques. It is accepted that PCMT is a soluble enzyme present in the cytosol (ASWAD and DEIGHT 1983) which is also supported by the fact that many of its substrates are cytosolic proteins, as will be described in the following section. Using Western blot analysis, Boivin *et al* showed that PCMT1 is ubiquitously expressed in rats in different organs like thymus, heart, pancreas, testes, kidney, spleen, liver, intestine, stomach, lung, muscles, and brain (BOIVIN *et al.* 1995). They also showed that, despite the solubility of the enzyme, it was abundant in membranous protein extracts when they tested different fractions from kidney including brush border membrane, basolateral membrane, intracellular membranes as well as mitochondrial fractions and nuclei (BOIVIN *et al.* 1995). Although PCMT has substrates in the nucleus, the enzyme is lacking a nuclear targeting sequence. However, the small size of the enzyme (25 kDa) suggests that it can easily diffuse through the nuclear pores since the cut off is about 60 kDa (WANG and BRATTAIN 2007). Finally, as mentioned above, there are two isoenzymes of PCMT1 resulting from alternative splicing. One of them ends with the amino acid sequence RDEL (POTTER *et al.* 1992), which is very similar to the endoplasmic reticulum (ER) retention signal KDEL (PELHAM 2000). Nevertheless, experimental evidence for ER localization has not been yet reported. The presence of this potential ER retention signal suggests the requirement of isoaspartyl repair during protein synthesis or a chaperon role for PCMT (KINDRACHUK *et al.* 2003; SAITO *et al.* 2016).

PCMT transcript levels in the brain and testes of rats were the highest in comparison to the other organs, which was also confirmed later with enzymatic activity levels. In the brain, the highest transcript levels were found more specifically in the cerebral cortex and the hippocampus (MIZOBUCHI *et al.* 1994; KIM *et al.* 1997b). Immunostaining results were consistent with the enzymatic assays, but expanded the expression levels to potential other brain regions by showing high staining in the substantia nigra, locus coeruleus and paraventricular nucleus as well (BILLINGSLEY and BALABAN 1985). Interestingly, neuronal cells expressed more PCMT1 compared to glial cells as indicated by the immunostaining intensity (BILLINGSLEY and BALABAN 1985; BILLINGSLEY *et al.* 1985a). PCMT activity was also detected in synaptosomes, but whether this activity is membrane-associated or soluble inside the synaptosomes remains unknown (DILIBERTO and AXELROD 1976). The second highest expression levels for PCMT was found in the reproductive organs, especially in germinal cells. Testes depleted from

sperm from rats, either by X-ray or genetically in infertile rats, have lower enzyme isoaspartyl methyltransferase activity than control, suggesting higher levels in germ cells than somatic cells (GAGNON *et al.* 1979; O'CONNOR *et al.* 1989). PCMT1 activity increases with the spermatogenesis process, most likely to limit protein damage during sperm storage and preserve damage free gametes for fecundation. In agreement with this assumption, low levels of PCMT1 were found in the sperm tail in asthenozoospermia, reduced sperm motility, compared to normozoospermia (HASHEMITABAR *et al.* 2015). Thus, PCMT has the potential to also be involved in a kind of rejuvenation mechanism where the molecules in the gametes have to be damage-free (BOUCHARD *et al.* 1980; CHAVOUS *et al.* 2000; UNAL *et al.* 2011).

1.3.5 PCMT substrates

In principle, any aspartyl or asparaginyl residue in a peptide chain can potentially undergo isomerization; in practice, it was observed, however, that certain residues in certain proteins are more prone to isoaspartyl formation than others (ROBINSON and ROBINSON 2001b; ROBINSON and ROBINSON 2001a). Since the discovery of the catalytic activity of PCMT1 in 1974, many proteins have been identified to be methyl accepting substrates for this enzyme and many of them, including hormones secreted from the pituitary gland, the hormonal carrier proteins neurophysins, calmodulin and epidermal growth factor (EGF), were identified independently in several studies (DILIBERTO and AXELROD 1974; EDGAR and HOPE 1974; GAGNON *et al.* 1981; DIAUGUSTINE *et al.* 1987). In 2006, two different groups independently used a proteomics approach to identify Pcmt1 substrates in mouse brains. They extracted total proteins from brains of *Pcmt1* knockout mice to enrich the potential substrates for Pcmt1. While the first group (VIGNESWARA *et al.* 2006) labelled the protein extract with radioactive SAM using exogenous recombinant PCMT and resolved them by 2-D gel electrophoresis, the second group (ZHU *et al.* 2006b) resolved the proteins and then used on-blot labelling with radioactive SAM and recombinant PCMT. Finally, both groups analysed the radiolabelled proteins by mass spectrometry. The difference in the sequence of their procedures is also important since isoaspartyl formation in the protein extracts can be induced *in vitro* enriching isoaspartyl residues in specific proteins (MORRISON *et al.* 2012) which might explain the differences in the identified substrates in both studies. Both groups identified thereby many Pcmt1 substrates for the first time, but also confirmed previously reported substrates. The methodology used did, however, not allow for detection of low abundant proteins and low molecular weight proteins and peptides (< 14 kDa). The broad functional diversity of the PCMT substrates identified so far suggests that PCMT deficiency has the potential to affect numerous different cellular pathways and that PCMT plays an overall housekeeping function in the cell.

Table 1-1: Pcmt1 substrates identified in the Zhu et al. (2006) and the Vigneswara et al. (2006) proteomic studies.

Substrate	Reference
α-Synuclein	(VIGNESWARA *et al.* 2006)
β-Synuclein	(VIGNESWARA *et al.* 2006)
Calreticulin	(VIGNESWARA *et al.* 2006)
Clathrin light chains a and b	(VIGNESWARA *et al.* 2006)
Collapsin response mediator protein 2 (CRMP2/ULIP2/DRP-2)	(ZHU *et al.* 2006b)
Dynamin 1	(ZHU *et al.* 2006b)
Microtubule-associated protein-2	(VIGNESWARA *et al.* 2006)
Phosphatidylethanolamine-binding protein (PEBP or RKIP)	(VIGNESWARA *et al.* 2006)
Stathmin	(VIGNESWARA *et al.* 2006)
Synapsin I	(PARANANDI and ASWAD 1995; REISSNER *et al.* 2006; ZHU *et al.* 2006b)
Synapsin II	(ZHU *et al.* 2006b)
Tubulin	(ZHU *et al.* 2006b)
Ubiquitin carboxyl-terminal hydrolase L1	(VIGNESWARA *et al.* 2006)

1.3.6 Physiological roles of PCMT

As mentioned above, given its broad tissue distribution and the wide range of substrates, PCMT may potentially interact with many biochemical pathways and cellular processes. Previous studies indicate that PCMT plays a role in aging, autoimmunity, various disease conditions, apoptosis and growth signalling pathways (JOHNSON *et al.* 1991b; DOYLE *et al.* 2003; FARRAR *et al.* 2005a; ZHU *et al.* 2006a). However, the molecular mechanisms underlying these interactions are generally not understood. So far, the well-documented biochemical function of PCMT is the catalytic transfer of a methyl group from SAM to isoaspartyl residues in proteins. To add to the complexity of its biological role, a PCMT protein engineered to lack this catalytic function was able to increase the survival of *E. coli* cells under stress induced by heat shock (KINDRACHUK *et al.* 2003). This observation suggested an additional, more chaperone-like role for PCMT. Given the focus of this thesis work on the cross-talk between PCMT and cell signalling, this section describes more specifically current knowledge on how this protein is involved in apoptosis as well as the MAPK, insulin/IGF-1, and calcium signalling pathways.

1.3.6.1 PCMT1 protects against apoptosis

Several studies have reported a role of PCMT in apoptosis. Overexpression of PCMT was first demonstrated to protect primary mouse cortical neurons against apoptosis when treated with Bax, a proapoptotic protein (HUEBSCHER *et al.* 1999). PCMT1 overexpression was also found to protect SH-SY5Y neuroblastoma cells from dopamine-mediated apoptosis (OUAZIA *et al.* 2015). Several mechanisms were suggested for the anti-apoptotic role of PCMT1. The first involves the Bcl-x_L protein, which had been reported to lose its anti-apoptotic function upon deamidation of two critical asparaginyl residues (with formation of isoaspartyl residues); this protein was found to be a substrate of PCMT1, methylation of the isoaspartyl residues by PCMT1 in the Bcl-x_L protein being proposed to allow for recovery of its anti-apoptotic function (CIMMINO *et al.* 2008). This was later confirmed by showing that microRNAs 15a and 16-1 downregulated PCMT1 expression, a down-regulation which was associated with increased susceptibility to apoptosis due to non-repaired (deamidated and isomerized) and therefore non-functional through Bcl-x_L (SAMBRI *et al.* 2011). A second proposed mechanism involves the inhibition of the proapoptotic mammalian sterile 20-like kinase 1 (Mst1). In a yeast-two hybrid system screen looking for binding partners of Mst1, PCMT1 was identified as an Mst1-interacting protein. Follow-up work showed that PCMT1 binds to the kinase domain of Mst1 based on co-immunoprecipitation experiments and that overexpression of PCMT1 attenuates Mst1 activity in response to apoptosis inducing conditions like hypoxia (YAN *et al.* 2013). A third proposed mechanism, implicates a potential regulation of the genome guardian (and pro-apoptotic) p53. It has been observed that p53 protein levels in the cell are inversely proportional to PCMT1 levels and that Asn29 and Asn30 in p53 are prone to deamidation. These and other observations led the authors to suggest that higher PCMT1 activity could lead to deactivation of p53 and cell death inhibition via isoaspartyl methylation (LEE *et al.* 2012). These conclusions should, however, be taken with caution since Asn29 and Asn30 are not among the hotspots for deamidation in p53, and could have been induced artificially (ROBINSON and ROBINSON 2001b; MORRISON *et al.* 2012). In conclusion, several lines of evidence show that PCMT1 plays a role in negative regulation of apoptosis and some mechanistic interactions have been proposed with Bcl-x_L, Mst1 and p53.

1.3.6.2 PCMT1 downregulation leads to activation of the Mitogen-activated protein kinase (MAPK) pathway

Protein phosphorylation is a major regulatory mechanism for many cellular functions, including signalling cascades mediating extracellular stimuli to the cell nucleus (COHEN 2000). Among the latter, the MAPK signalling pathway was found to be affected by PCMT1 activity. Kosugi *et al* knocked down *PCMT1* in HEK293 cells and analysed phosphorylation levels of three intermediates in the MAPK pathway (MEK, ERK, and Raf) (Figure 1-7) upon stimulation with EGF. They found that the MAPK

pathway was hyperactivated in response to EGF stimulation by showing higher phosphorylation levels of the three intermediates in the *PCMT1* knockdown cells as compared to control cells (KOSUGI *et al.* 2008). In apparent contradiction with the observations by Kosugi *et al* (2008), *PCMT1* knockdown in MDA-MB-231 epithelial cells under detachment conditions led to lower phosphorylation levels of Erk1/2 (RYU *et al.* 2011). One potential mechanism underlying the interaction between PCMT1 and MAPK signalling could be through the Raf inhibitor phosphatidylethanolamine-binding protein (PEBP) (also known as Raf kinase inhibitory protein RKIP), which is a PCMT substrate (VIGNESWARA *et al.* 2006). Whether the function of RKIP is affected by isoaspartyl formation has not been investigated yet, but one could assume a decrease in activity under PCMT1 deficiency (resulting in a lack of isoaspartyl repair in RKIP), leading to hyperactivation of the MAPK signalling pathway at least under certain conditions and in certain cell types. Another possibility is through increase of the total protein levels of Erk1/2 as reported by Yang *et al* (YANG *et al.* 2013) in a proteomics study in *Pcmt1* knockout mice. However, this wouldn't explain the increase in phosphorylation levels of intermediates upstream to Erk1/2 and would contradict other observations Kosugi *et al* (2008) showing the same levels of total Erk1/2 in *PCMT1* knockdown and control cells. Thus, while several lines of evidence suggest a regulation of the MAPK pathway by PCMT activity, this interaction appears to be strongly dependent on cell type and physiological state of the cell and the molecular mechanism(s) involved remain completely obscure.

1.3.6.3 PCMT1 downregulation leads to activation of the Insulin signalling (IGF-1) pathway

Components of insulin/insulin-like growth factor I (IGF-1) signalling pathway (hereafter designated as IGF-1 pathway) have emerged in the past two decades as being critically involved in the regulation of lifespan, and this in a conserved way from yeast to humans (BARBIERI *et al.* 2003). A key observation that was followed by an avalanche of research activity in this direction in the aging field was that *Caenorhabditis elegans* worms deficient in the DAF-2 (insulin-like receptor homolog) live twice as long as wild type worms (KENYON *et al.* 1993). IGF-1 pathway downregulation was subsequently found to extend lifespan in other model organisms including *Saccharomyces cerevisiase* (yeast), *Drosophila melanogaster* (fruit fly), and mice (HOLZENBERGER *et al.* 2003; KENYON 2010).

In this context, two interesting observations were made in the course of the characterization of the *Pcmt1* knockout mice: (1) the drastically shortened lifespan of these mice and (2) an increase in the size of their brains. More than 95% of *Pcmt1* knockout mice die before day 60 and the remaining animals do not make it beyond day 100 (KIM *et al.* 1997b). On the other hand, overexpression of *Pcmt* in *D. melanogaster* extended their lifespan by about 35% under stress conditions (CHAVOUS *et al.* 2001). Similar results were obtained in *C. elegans* where overexpression of *Pcmt* led to a lifespan extension under heat stress (BANFIELD *et al.* 2008; KHARE *et al.* 2011). Concerning the second key observation

mentioned above, despite the small body weight of the *Pcmt1* knockout mice, their brains were found to be 10% – 30% larger than the wild type brains (YAMAMOTO *et al.* 1998; FARRAR *et al.* 2005a). This enlargement was proposed to be due to increased cell proliferation, since $CD4^+$ cells deficient in *Pcmt1* showed higher proliferation rates in response to stimulators (DOYLE *et al.* 2003; FARRAR *et al.* 2005b) and subsequently evidence was presented in *Pcmt1* knockout mice for increased neurogenesis (FARRAR *et al.* 2005b).

The effects on lifespan and the brain enlargement, which phenocopy IGF-1 overexpression in mice (CARSON *et al.* 1993), suggested a possible interaction between PCMT1 and IGF-1 signalling. This hypothesis was supported by findings by Farrar *et al* (2005) as they found higher phosphorylation levels of intermediates in the IGF-1 signalling pathway, including Akt and GSK3β, in *Pcmt1* knockout mouse brains by Western blot analysis. Further investigation by immunohistochemistry showed the highest increases in phosphorylation levels of IGF-1 pathway intermediates in the *Pcmt1* knockout mice to be localized in the hippocampus (FARRAR *et al.* 2005a). Additional support for the PCMT/IGF-1 pathway/aging connection was provided by MacKay *et al* (2012) (MACKAY *et al.* 2012), who showed that Wortmannin (inhibitor of the phosphoinositide 3-kinase PI3K, an early intermediate in the IGF-1 pathway) administration to *Pcmt1* knockout mice increased their lifespan and decreased brain weight. Pcmt-dependent regulation of lifespan via insulin-like signalling may be a conserved feature as the lifespan extension observed in *C. elegans* animals overexpressing PCMT was shown to depend on DAF-16, the downstream transcription factor of the insulin-like signalling pathway in worms (KHARE *et al.* 2011).

Taken together, the evidence supporting a cross-talk between PCMT and the IGF-1 signalling pathway is thus strong, but the molecular mechanism behind this interaction remains completely unknown. It could be that, as proposed for the interaction with apoptosis, one of the IGF-1 pathway intermediates has an isoaspartyl molecular switch through which PCMT1 could modulate protein function via methylation. Another possibility, in the context of the damage theory, is that in the absence of PCMT1, the overall accumulation of isoaspartyl residues in proteins leads to inactivation of one or several protein phosphatases that are more susceptible to this kind of damage, resulting in increased protein phosphorylation levels across several signalling pathways, including the MAPK and IGF-1 pathways. Reproducing these effects of PCMT1 deficiency on signalling in cell culture models to investigate the molecular mechanisms in play was a major focus of the first part of this thesis.

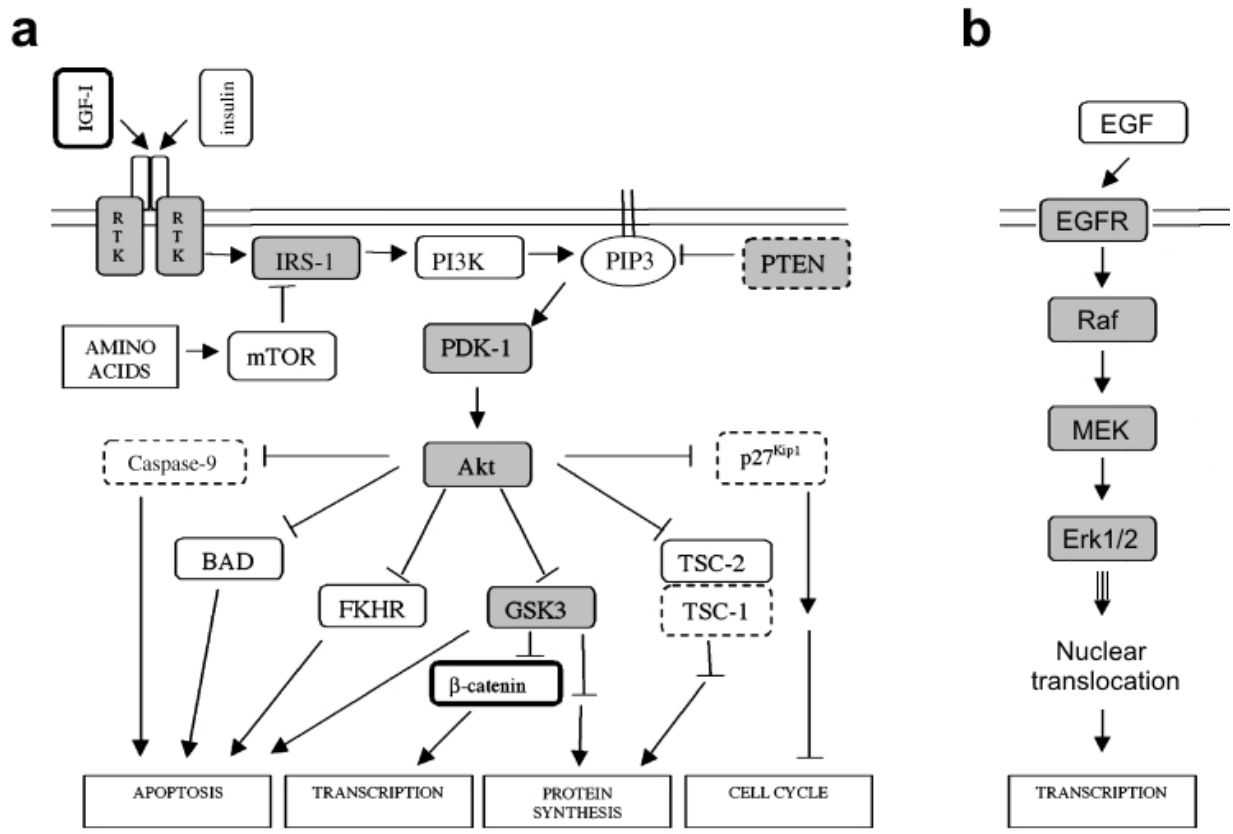

Figure 1-7: (a) Insulin/IGF-1 signalling pathway. (b) MAPK pathway adapted from (FARRAR et al. 2005a)

1.3.6.4 PCMT1 and calcium signalling

Similar to phosphorylation, calcium regulates many functions in the cell. Free cytosolic calcium concentrations are very low and tightly controlled to remain around a 100 nM basal levels. Different calcium regulator proteins were identified as substrates for PCMT1 including, among others, calmodulin (VIGNESWARA *et al.* 2006). Calmodulin was first reported as an exceptionally good substrate for enzymatic carboxyl methylation by Gagnon *et al* in 1981 (GAGNON *et al.* 1981), before even the molecular identification of PCMT, and they showed that this post-translational methylation inhibits the stimulatory effect of calmodulin on cyclic nucleotide phosphodiesterase. It has later been confirmed by different groups that calmodulin is among the major substrates for PCMT (BILLINGSLEY *et al.* 1985c; JOHNSON *et al.* 1985; JOHNSON *et al.* 1987a). Isoaspartyl residues were identified in the calcium binding motifs as well as in flexible regions of the calmodulin protein. (JOHNSON *et al.* 1985; OTA and CLARKE 1989a; POTTER *et al.* 1993). Furthermore, it has been shown that calcium binding affects methylation of calmodulin by PCMT1 (OTA and CLARKE 1989a) and this observation has been confirmed *in vivo* by simultaneous injection of aged calmodulin and [methyl-^{3}H]SAM into *Xenopus* oocytes, as the authors showed that calmodulin pre-incubated with EDTA was a better substrate than calmodulin pre-incubated with $CaCl_2$ for carboxyl methylation in these experiments (DESROSIERS *et al.* 1990).

Calmodulin was also identified as an interaction partner binding PCMT1 in a yeast two-hybrid screen and here, an effector function of calmodulin on PCMT1 was proposed in addition to the enzyme-substrate interaction, as calmodulin was found to stimulate the activity of PCMT1 (O'CONNOR and O'CONNOR 1998). During the phenotyping of the new PCMT-deficient cell and animal models created in this thesis, important perturbations in calcium signalling were observed, providing further *in vivo* evidence for a role of PCMT in this process.

1.4 Zebrafish as a model organism in biomedical research

1.4.1 General considerations

Danio rerio – zebrafish – is a freshwater teleost fish belonging to the Cyprinid family, which has emerged as a new vertebrate animal model organism (Figure 1-8a). Over the past 35 years, it has been used more and more frequently in diverse areas of developmental biology, biomedical research, toxicology, and as an excellent *in vivo* platform for drug discovery (ZON and PETERSON 2005), as indicated by the increasing number of zebrafish-related publications during that period (Figure 1-8b).

The prominent starting point of zebrafish as a model organism in research goes back to 1994, when two highly ambitious projects aimed to generate a large-scale ethyl-*N*-nitrosourea (ENU) genome-wide mutational screen in zebrafish. This ENU screen led to the identification of important genes for development and organogenesis and subsequent description and characterization of the mutations were published in an historic special issue – exclusive to zebrafish – of Development (MULLINS *et al.* 1994; DRIEVER *et al.* 1996; HAFFTER *et al.* 1996). This represented the first implementation of such a large genetic screen in a vertebrate organism, putting the zebrafish model intro the spotlight.

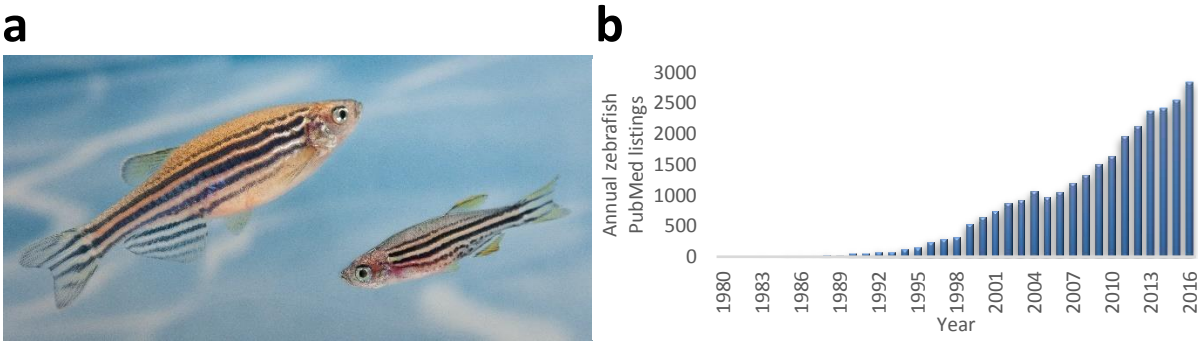

Figure 1-8: Zebrafish model (a) Adult zebrafish, female on the left and male on the right (Copyright Thierry Marysael) (b) Increasing number of publications retrieved from PubMed using 'zebrafish' as the search keyword for the period going from 1980 to 2016.

1.4.2 Advantages setting zebrafish apart as a model organism

Zebrafish has become an attractive model organism in biomedical research due to several reasons. First, its genome was fully sequenced revealing high similarity to the human genome (~70%) and suggesting high conservation in many biochemical pathways and cellular processes between humans and zebrafish (HOWE *et al.* 2013). Second, zebrafish develops very fast from a single cell zygote to an early larva in only 3 days (Figure 1-9), which allows to efficiently study the impact of genetic manipulation on early stages of development, and reaches adulthood to become sexually mature in three months, also speeding up experiments compared to many other vertebrate models (KIMMEL *et al.* 1995). Third, many diseases have been already modelled in zebrafish, offering platforms for disease mechanism identification (LIESCHKE and CURRIE 2007). Fourth, the small size of embryos and larvae (0.5 – 5 mm depending on the developmental stage) enables high-throughput, whole animal *in vivo* screenings (MURPHEY and ZON 2006). Fifth, there is an increasing number of genetic and molecular methods and tools (antisense morpholino oligonucleotides, Tol2 transgenesis, CRISPR-Cas9 genome editing, a well-established cDNA library (TON *et al.* 2002)) and of publically available online database resources (see for example http://zfin.org/) for zebrafish. Finally, the ex-uterus development, the high number of progeny (100 – 300 eggs per week), the ease of genetic manipulation, the transparency at early developmental stages, and its cost-effective husbandry are other important aspects that make zebrafish an excellent vertebrate model.

The advantages of working with zebrafish appear substantial; nevertheless, some overall limitations of this model should be mentioned as well. Phylogenetic studies have shown that early during teleost lineage (more than 150 million years ago), zebrafish underwent a teleost-specific genome duplication. From an anatomical and physiological point of view, although being a vertebrate, there are relevant differences between zebrafish and mammals, such as for example the lack of lungs, limbs, synovial joints, and heart separations.

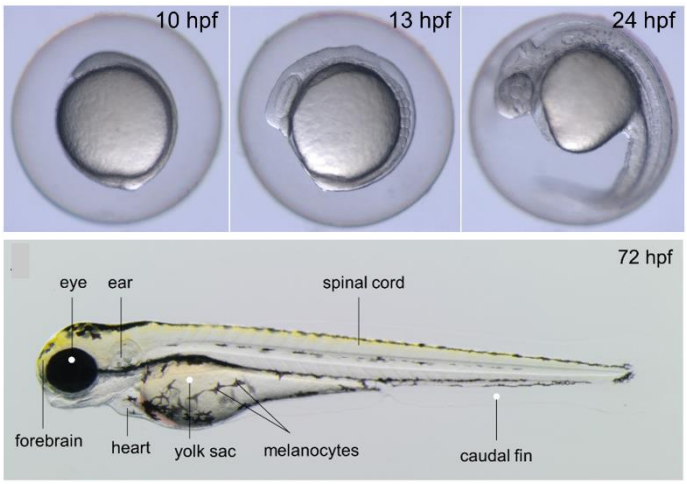

Figure 1-9: Zebrafish at different early developmental stages. ***hfp****: hours post fertilization*

1.4.3 Zebrafish as a model for neurological disorders

Epilepsy is one of the most common chronic neurological disorders affecting about 1% of the world population, with up to 30% - 40% of cases presenting resistance to available treatments (GO and SNEAD 2008; THURMAN *et al.* 2011). Although zebrafish was originally used primarily as a model to study embryogenesis and development, it is becoming a valuable *in vivo* tool to study many other physiological and patho-physiological processes like angiogenesis, cardiovascular diseases, cancer (WHITE *et al.* 2013) and neurological disorders (MARTIN-JIMENEZ *et al.* 2015). Particularly in the field of neurobiology, zebrafish has proven to be a good vertebrate model to study diseases affecting the central nervous system, and it has become a well-established model for epilepsy (CUNLIFFE 2016). Pentylenetetrazol (PTZ) for example, a gamma-aminobutyric acid receptor antagonist that is used widely to induce epilepsy in animals, was found to elicit an epileptic response in zebrafish characterized by behavioural, electrographic, and molecular changes reminiscent of the ones observed in rodent seizure models (BARABAN *et al.* 2005). The PTZ-induced electrical discharges were also attenuated by the commonly used anti-convulsant drugs valproate and diazepam in zebrafish.

Since *Pcmt1* knockout mice experience epileptic seizures (KIM *et al.* 1997b; YAMAMOTO *et al.* 1998) for reasons that remain poorly understood, it seemed tempting to try using a simpler vertebrate model to investigate the connection between PCMT1 and epilepsy. We identified two PCMT1 homologs in zebrafish and after establishing and validating a PCMT-deficient zebrafish model, we used it to investigate, amongst other things, its response to PTZ exposure.

1.5 Reverse genetic approaches

Different reverse genetic approaches were used in the present thesis to downregulate PCMT expression levels either in mammalian cells in culture or in zebrafish.

1.5.1 Lentiviral transduction of shRNA for gene knockdown in mammalian cells

RNA interference (RNAi) is an endogenous regulatory process through which cells control gene transcription (FIRE *et al.* 1998). Short hairpin RNAs (shRNAs) imitate RNAi and can be used to specifically knock down genes of interest. After transcription of shRNA constructs, the Dicer enzyme cleaves the generated RNA molecules to release 21 – 23 oligo small interfering RNAs (siRNAs) that will specifically bind a target mRNA through base pair complementarity. The siRNA/mRNA complexes are then incorporated into RNA-induced silencing complex (RISC) that will degrade them (Figure 1-10).

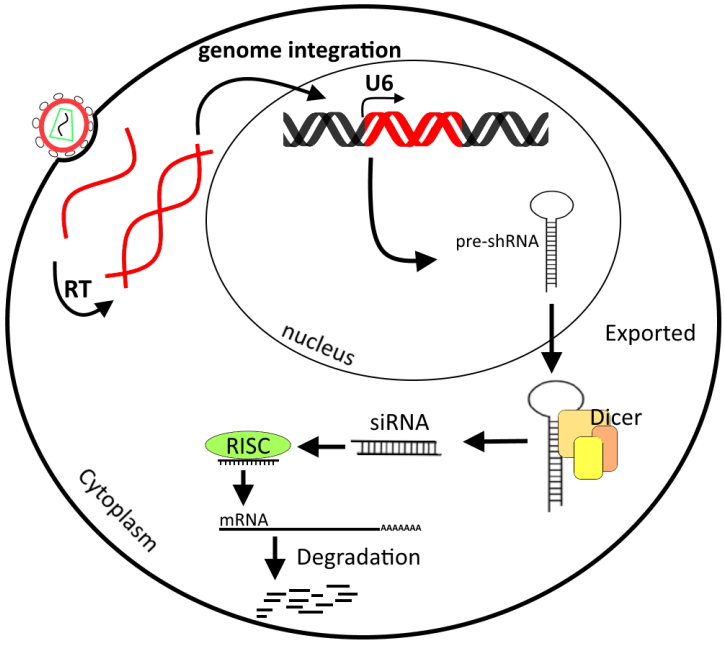

Figure 1-10: Schematic representation of lentiviral delivery of shRNA for gene knockdown in a mammalian cell. After insertion of the viral genetic material (RNA) into the cell, the viral reverse transcriptase (RT) converts it to DNA. which is transported into the nucleus and integrated into the genome by homologous recombination. The encoded shRNA is then transcribed, processed by Dicer to guide the RISC complex and finally degrade the target mRNA transcript.

Lentiviral technology provides a highly efficient method for delivery of nucleic acids into cells with genome integration of the desired DNA sequence. Unlike other transient gene knockdown techniques, integration of shRNA into the genome of a cell allows generating stable cell line with lower transcription levels of the target gene. ViraPower™ (ThermoFisher Scientific) is a mix of three plasmids (pLP1, pLP2 and pLP/VSVG) that, combined with the pLenti6/BLOCK-iT™-DEST plasmid, encode all the components (Section 6.1.1) necessary to form lentiviral particles having the ability to transduce

mammalian cells and integrate encapsulated cloned shRNA constructs into the cell genome for constitutive expression and efficient knockdown of the target gene.

1.5.2 CRISPR/Cas9 technology for gene knockout in mammalian cells

Clustered regularly interspaced short palindromic repeats (CRISPR) was discovered in prokaryotes as an acquired immune system against viruses (HORVATH and BARRANGOU 2010). Indeed, it has been shown that some bacteria and archaea become resistant to a virus after their first exposure. Those prokaryotes can keep a short viral DNA sequence and integrate them into their genome. This latter DNA sequence can then be transcribed to act as a guide RNA (gRNA). Upon the second exposure to the same virus, a CRISPR-associated (Cas) nuclease, guided by the gRNA, recognizes the invading DNA and causes a double strand break (DSB). Those acquired sequences from foreign DNA are always associated with a protospacer adjacent motif (PAM), which can vary depending on the specific CRISPR system (FENG *et al.* 2016).

The CRISPR/Cas9 system has been exploited to develop the current state-of-the-art methodology for precise genome editing. It relies on the co-expression of the Cas9 endonuclease, initially isolated from *Streptococcus pyogenes*, with a gRNA targeting a specific DNA sequence in the genome to edit. In this specific genome location, the Cas9 endonuclease generates a DSB that will be repaired through either Non-Homologous End Joining (NHEJ) or Homology-Directed Repair (HDR). The HDR mechanism requires a repair template and is used to insert a desired mutation into the target genomic locus (Figure 1-11). In contrast, NHEJ does not require any template and may lead to the insertion or deletion (InDel mutation) of several nucleotides at the DSB site. The acquisition of such indel mutations has the potential of leading to a frameshift that could generate a non-functional protein and thereby result in gene silencing or knockout.

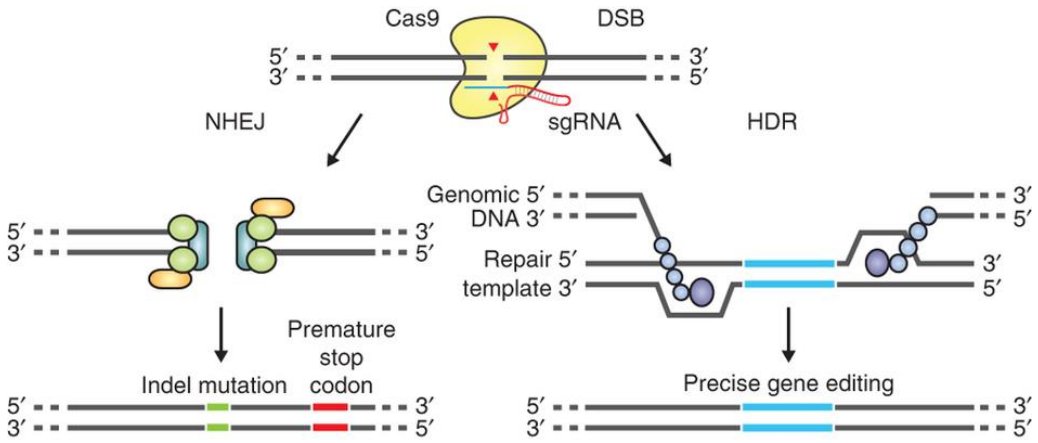

Figure 1-11: Schematic representation of the CRISPR/Cas9 strategy for gene knockout or editing. ***Cas9****: CRISPR associated protein;* ***DSB****: double strand break;* ***HDR****: Homology-directed repair;* ***NHEJ****: Nonhomologous end joining Adapted from (RAN et al. 2013)*

1.5.3 Morpholino oligomers for gene knockdown in zebrafish

Morpholinos (MOs) are of nucleic acid analogs where the ribose or deoxyribose sugar ring is replaced by a 6-membered morpholine ring and the polar phosphodiester linkage by a nonpolar phosphorodiamidate linkage. They contain the same four default bases that can bind to nucleic acids (SUMMERTON and WELLER 1997). They can be chemically synthesized to specifically target a gene of interest in order to decrease the amount of the encoded protein. They have been developed as a standard and efficient tool for gene knockdown in zebrafish (EKKER 2000; DRAPER *et al.* 2001).

The chemical structure of MOs confers a higher chemical stability compared to DNA or RNA and a higher resistance to nucleases. MOs can exert their knockdown effect through two mechanisms. The first one corresponds to the binding of the MO at the translational initiation site in the 5'UTR region of the target mRNA transcript to inhibit protein translation. The second corresponds to the binding of the MO either at the intron-exon or exon-intron junction interfering thereby with the correct splicing of the target transcript leading ultimately to the skipping of an exon or inclusion of an intron (Figure 1-12).

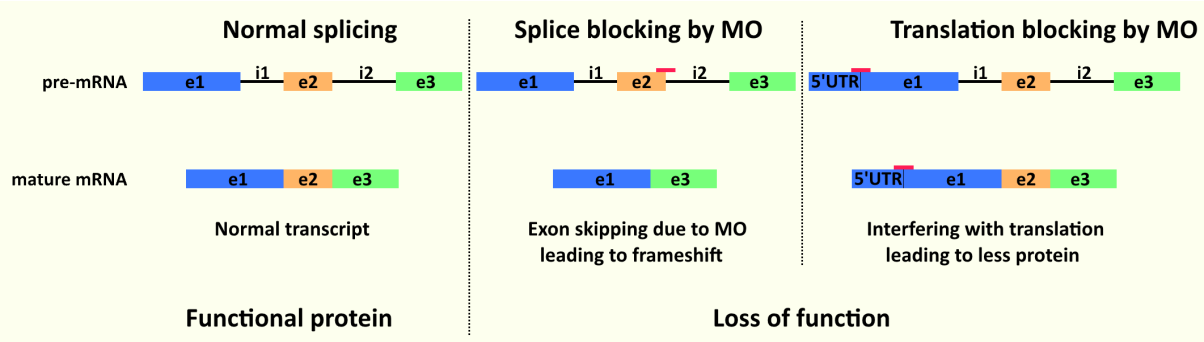

Figure 1-12: MO mechanism of action for gene downregulation. MOs can interfere with correct transcript splicing when binding at the exon/intron or intro/exon junction. They can also lead to translation blocking through binding to the translational initiation site in the target transcript.

Aims

The main aims of the presented thesis work were to 1) a) establish a mammalian cell culture model that mimics the effects of *PCMT* deficiency on the IGF-1 signalling pathway that was observed in *Pcmt1* knockout mice and b) use that model to elucidate the molecular mechanism underlying the crosstalk between PCMT and IGF-1 signalling 2) establish a more simple whole animal model of *PCMT* deficiency in zebrafish to better understand the role of PCMT in epilepsy that was also observed in the more difficult to handle mouse model and 3) use the cell culture and zebrafish models to investigate the influence of PCMT on calcium signalling *in vivo*.

In the frame of the first objective, we used lentiviral transduction of shRNAs to establish a stable *PCMT1* knockdown human HEK293 cell line and the CRISPR/Cas9 system to knock out *Pcmt1* in the mouse hippocampal cell line HT22. Following model establishment and validation, we compared the activation status of the MAPK and IGF-1 signalling pathways after various stimuli in the *PCMT* deficient and control cells.

For the second aim, as isoaspartyl methyltransferase activity had never been reported in zebrafish before, we started by identifying *PCMT* homolog gene candidates in the zebrafish genome and validate them by testing the enzymatic activity of their expression products *in vitro*. We then proceeded to knock down the identified *PCMT* orthologs using morpholino technology, validated *PCMT* deficiency in the generated morphant larvae and started phenotyping them by performing morphological analyses. Finally, we studied their suitability to develop seizures by tracking their locomotor behaviour and recording the electrical activity of their brains.

In the third aim, we wanted to take advantage of the newly established PCMT deficient cell culture and animal models to study the interaction between the isoaspartyl methyltransferase and calcium signalling *in vivo*. A strong body of evidence for such an interaction has been gathered through in vitro studies, but *in vivo* evidence remained more scarce. We notably took advantage of the transgenic zebrafish line that expresses the fluorescent calcium sensor GCaMP6F to monitor calcium fluxes and confirmed that PCMT activity also heavily interferes with intracellular calcium movements and therefore most likely signalling *in vivo*. Similar observations were done on the mouse hippocampal cells in culture, which now puts us in a position to take investigations of this physiological role of PCMT to the next level.

2 Materials and methods

2.1 Materials

2.1.1 Antibodies used in the present thesis

Table 2-1: Antibodies used for Western blot analysis

Antibody	Species	Clonality	Company	Catalog #	MW of target protein (kDa)
β-Actin (13E5)	Rabbit IgG	Monoclonal	Cell Signalling	4970	45
Akt (pan) (C67E7)	Rabbit IgG	Monoclonal	Cell Signalling	4691	60
p44/42 MAPK (Erk1/2)	Rabbit	Polyclonal	Cell Signalling	3264	42, 44
GAPDH (D16H11) XP® (HRP Conjugate)	Rabbit	Monoclonal	Cell Signalling	8884	37
MEK1/2 (47E6)	Rabbit	Monoclonal	Cell Signalling	9126	45
Phospho-p44/42 MAPK (Erk1/2) (Thr202/Tyr204) (D13.14.4E) XP®	Rabbit IgG	Monoclonal	Cell Signalling	4370	44, 42
Phospho-Akt (Ser473) (D9E) XP®	Rabbit IgG	Monoclonal	Cell Signalling	4060	60
Phospho-GSK3β (Ser9) (5B3)	Rabbit	Monoclonal	Cell Signalling	9323	46
Phospho-MEK1/2 (Ser217/221) (41G9)	Rabbit IgG	Monoclonal	Cell Signalling	9154	45
Anti-PCMT1	Rabbit	Polyclonal	Abcam	ab97446	25
Anti-rabbit IgG HRP-linked	Goat IgG	Polyclonal	Cell Signalling	7074	N/A

2.1.2 Mammalian cell lines used in the present thesis

Table 2-2: Mammalian cell lines

Cell line	Purpose	Source
Human embryonic kidney cells (HEK293)	Study of the interplay between PCMT1 and growth signalling pathways.	the American Type Culture Collection (ATCC)
Human embryonic kidney fast-growing cells (HEK293FT)	Production of lentiviral particles carrying shRNA for PCMT1 knockdown experiments.	ThermoFisher Scientific Catalog number: K4944
Human glioblastoma cells (U-87 MG)	Study of the interplay between PCMT1 and growth signalling pathways.	the American Type Culture Collection (ATCC)
Murine hippocampal cells (HT22)	Study of the interplay between PCMT1 and growth signalling pathways as well as calcium signalling.	a generous gift from Dr. David Schubert at the Salk institute, La Jolla, San Diego, California, USA

2.1.3 Chemicals used in the present thesis

2-Propanol	Sigma-Aldrich Belgium
5-Bromo 4-chloro 3-indolyl phosphate	Sigma-Aldrich Belgium
Agarose	Sigma-Aldrich Belgium
Bis-Tris	Sigma-Aldrich Belgium
Blasticidin S HCl	ThermoFisher
Bovine serum albumin	Sigma-Aldrich Belgium
Bromophenol blue	Sigma-Aldrich Belgium
Carbenicillin	Sigma-Aldrich Belgium
Chloroform	Sigma-Aldrich Belgium
Epidermal growth factor	Sigma-Aldrich Belgium
Ethanol	VWR/Merk
Ethyl 3-aminobenzoate methanesulfonate (Tricaine)	Sigma-Aldrich Belgium
Formamide	ThermoFisher Scientific
Glycerol	Sigma-Aldrich Belgium
Glycine	Sigma-Aldrich Belgium
Heparin	Sigma-Aldrich Belgium
Imidazole	VWR
Insulin	Sigma-Aldrich Belgium
Insulin growth factor-1	Sigma-Aldrich Belgium
Liquid scintillation cocktail	PerkinElmer
Methanol	VWR
Methyl cellulose	Sigma-Aldrich Belgium
Nitro blue tetrazolium	Sigma-Aldrich Belgium
Pentylenetetrazol	Sigma-Aldrich Belgium
Phenylthiourea	Sigma-Aldrich Belgium
Polyethylene glycol	Sigma-Aldrich Belgium
Polybrene	Sigma-Aldrich Belgium
Protease inhibitor cocktail	Roche
Proteinase K	Prophac/Roche
Phosphatase inhibitor cocktail	Sigma-Aldrich Belgium
Resazurin	Sigma-Aldrich Belgium
S-Adenosyl methionine	Sigma-Aldrich Belgium
S-[Methyl-^{3}H]Adenosyl methionine	PerkinElmer
Sodium chloride	Sigma-Aldrich Belgium

Sodium deoxycholate	Sigma-Aldrich Belgium
Sodium dodecyl sulfate	Sigma-Aldrich Belgium
Sodium fluoride	Sigma-Aldrich Belgium
Sodium orthovanadate	Sigma-Aldrich Belgium
Triton X-100	Sigma-Aldrich Belgium
Trizma	Sigma-Aldrich Belgium
Tween 20	Sigma-Aldrich Belgium

2.1.4 Plasmids used in the present thesis

Table 2-3: Description of the different plasmids, for which purpose they are used and their source

Plasmid	Purpose	Source
pCS2+	Used for cloning of *pcmt* and *pcmtl* coding sequence for further IVT production of transcripts of both genes.	A kind gift from Dr. Uwe Irion, Max Planck Institute for Developmental Biology, Tübingen, Germany
pENTR™/U6	Used for transient expression of shRNA sequence for *PCMT1* knockdown in HEK293 and U-87 MG cells.	ThermoFisher Scientific Catalog number: K4945
pET100D	Used for Pcmt and Pcmtl recombinant protein expression.	ThermoFisher Scientific Catalog number: K100-01
pGEM-T	Used for rescue experiments in zebrafish by exogenous expression of *pcmt* and *pcmtl* under the control of the ubiquitous promoter eef1α.	A kind gift from Dr. Simon Perathoner (PERATHONER *et al.* 2014)
pLenti6/BLOCK-iT™-DEST	Used in combination with ViraPower™ plasmid mixture for production of lentiviral particles carrying shRNA	ThermoFisher Scientific Catalog number: K4944
pZFF001	Used for rescue experiments in zebrafish by exogenous expression of *pcmt* and *pcmtl* under the control of the neuronal promoter Her4	A kind gift from prof Gilbert Weidinger, institute of biochemistry and molecular biology, university of Ulm, Germany
pX459	Used for cloning gRNA and expression of the Cas9 nuclease for CRISPR/Cas9 mediated knockout of *Pcmt1* in HT22 cells	Addgene, plasmid #48139 (RAN *et al.* 2013)

ViraPower™ plasmid mix	A mixture of three plasmids pLP1, pLP2 and pLP/VSV-G contain the necessary elements for production of lentiviral particles in HEK293FT cells	ThermoFisher Scientific Catalog number: K4944

2.1.5 Morpholino oligomers used in the present thesis

Table 2-4: Sequence of splice-blocking morpholinos used for knockdown experiments in zebrafish

Name	Sequence
PCMT i2e3	GCTTGATAACCTGCATGAAATGAAC
PCMTL e1i1	AGAGCGGAGCAAAAATCTTACTCGT
PCMT e5i5	AAGATGGATGAGCAGACCAACCGAT
PCMTL e4i4	CATGTGTTTTTCTGACCTACCATAT
Control MO	CCTCTTACCTCAGTTACAATTTATA

2.1.6 Primers used in the present thesis

2.1.6.1 Primers for qPCR

Table 2-5: Primers used in qPCR for transcript level quantification of target genes

Target gene	Sequence 5' → 3'	Amplicon Size
H. sapiens PCMT1	FWD: AGAAGCCCCTTATGATGCCA REV: TGCTGCCATCTTGTAGCTTG	161
H. sapiens ACTB	FWD: AGAAAATCTGGCACCACACC REV: AGCACAGCCTGGATAGCAA	173
H. sapiens GAPDH	FWD: GCTCTCTGCTCCTCCTGTT REV: GCGCCCAATACGACCAAAT	124
M. musculus Pcmt1	FWD: TCTTTCCTCCTCCACACAGTC REV: GTCCAAAACAAGCTGTGATGC	135
M. musculus Actb	FWD: GGCTGTATTCCCCTCCATCG REV: CCAGTTGGTAACAATGCCATGT	154
M. musculus Gapdh	FWD: TGCGACTTCAACAGCAACTC REV: CTTGCTCAGTGTCCTTGCTG	200
D. rerio Pcmt	FWD: CCACAGACCGTTCCCATTTC REV: GCTCCTTCATAGAGGTGGTCA	139
D. rerio Pcmtl	FWD: CATGGAGTCATTCACAACGACA REV: TATCCACTTCCAGACCCCACA	215
D. rerio Rpl13-alpha	FWD: TCTGGAGGACTGTAAGAGGTATGC REV: AGACGCACAATCTTGAGAGCAG	148
D. rerio eEf1-alpha	FWD: CTGGAGGCCAGCTCAAACAT REV: ATCAAGAAGAGTAGTACCGCTAGCATTAC	87

2.1.6.2 Primers for cloning

Table 2-6: Primers used for cloning

Name	Sequence 5' → 3'	Melting temperature °C	Purpose
hPCMT1-His	FWD: ATATAAGCTTATGCACCATCACCATCACCATGCCTGGAAATCCGGCGGC REV: ATATCTCGAGTTACAATTCATCCCTGGACCAC	58	Cloning of N-terminally His-tagged human *PCMT1* into pCMV6
drPcmt FWD	FWD: CACCATGGCCTGGAAATCCGGAG REV: TCAAAGTTCATCCCTTGACCACTG	55	Cloning of *pcmt* into pET100
drPcmtl FWD	FWD: CACCATGGCATGGATGTCTAGTGGC REV: TCAGAGCTCATCGCCCGGCCAC	55	Cloning of *pcmtl* into pET100
Pcmt as	FWD: GACATTAATACGACTCACTATAGGGTCATTGCTTAGCAGTGAGTTTATTG REV: GCTGGATTTTGTAGCAGGGAAACAAC	50	Preparation of *in situ* hybridization template for *pcmt* antisense probe
Pcmt s	GACATTAATACGACTCACTATAGGGGCTGGATTTTGTAGCAGGGAAAC TCATTGCTTAGCAGTGAGTTTATTGG	50	Preparation of *in situ* hybridization template for *pcmt* sense probe
Pcmtl as	GACATTAATACGACTCACTATAGGGCG GTCCCACTGACAGACAAGCAACACC	50	Preparation of *in situ* hybridization template for *pcmtl* antisense probe
Pcmtl s	GACATTAATACGACTCACTATAGGGATGTCCCACTGACAGACAAG CGAATTGGGTACCGGGCCCCCCC	50	Preparation of in situ hybridization template for *pcmtl* sense probe
drPcmt_pCS2	FWD: CTTGTTCTTTTTGCAGGATCCGCCGCCACCATGGCCTGGAAATCCGGAGG REV: CTATAGTTCTAGAGGCTCGAGTCAAAGTTCATCCCTTG	58	Cloning of *pcmt* into pCS2+ plasmid
drPcmtl_pCS2	FWD: CTTGTTCTTTTTGCAGGATCCGCCGCCACCATGGCATGGATGTCTAGTGG REV: CTATAGTTCTAGAGGCTCGAGTCAGAGCTCATCGCCCG	58	Cloning of *pcmtl* into pCS2+ plasmid
drPcmt_pZFF	FWD: CAAGACACACAGCAATCATGGCCTGGAAATCCGGAGG REV: CAGGCTGAAGTTTGTAGCAAGTTCATCCCTTGACCAC	58	Cloning of *pcmt* into pZFF001 plasmid
drPcmtl_pZFF	FWD: CAAGACACACAGCAATCATGGCATGGATGTCTAGTGG REV: CAGGCTGAAGTTTGTAGCGAGCTCATCGCCCGGCCA	58	Cloning of *pcmtl* into pZFF001 plasmid
SDM_Pcmt_D-V	FWD: GGAGCAAAGGCTCTGGTGGTGGGATCGGGCTCC REV: GGAGCCCGATCCCACCACCAGAGCCTTTGCTCC	60	Site directed mutagenesis of *pcmt* to replace Asp83 with Val
SDM_Pcmtl_D-V	FWD: GGAGCCTCAGCGCTGGTGGTGGGGTCTGGAAGT REV: ACTTCCAGACCCCACCACCAGCGCTGAGGCTCC	60	Site directed mutagenesis of *pcmtl* to replace Asp83 with Val
mPcmtCRISPRcheck	FWD: AAGGATGACCCAATGCTCCT REV: GGGCTGCTGTTTCTACTTGG	58	Validation of *Pcmt1* gene deletion after CRISPR-mutated HT22 cells

2.1.7 Restriction enzymes used in the present thesis

- BamHI New England Biolabs
- BbSI New England Biolabs
- BsmBI New England Biolabs
- DpnI Agilent Technologies
- HindIII New England Biolabs
- NheI New England Biolabs
- NotI New England Biolabs
- SacII New England Biolabs
- XhoI New England Biolabs

2.1.8 Kits used in the present thesis

Kit	Purpose	Company
AccuPrime™ *Pfx*	PCR amplification of DNA	ThermoFischer Scientific
BLOCK-iT™ U6 RNAi Entry Vector kit	Transient expression of shRNA for PCMT1 knockdown in mammalian cells	ThermoFischer Scientific
BLOCK-iT™ Lentiviral RNAi expression system kit	Stable integration of shRNA in mammalian cell genome for PCMT1 knockdown in mammalian cells	ThermoFischer Scientific
Champion™ pET Directional TOPO® Expression kit	Cloning of Pcmt and Pcmtl for recombinant protein expression.	ThermoFischer Scientific
Fluo-4 AM	Intracellular calcium detection in mammalian cells.	ThermoFischer Scientific
Gel extraction kit	DNA extraction and purification from agarose gel	Qiagen
In-Fusion	Cloning of *pcmt* and *pcmtl* into pZFF001 plasmid	Clontech
MEGAclear™ kit	Purification of RNA after *in vitro* transcription reaction	Ambion
mMESSAGE mMACHINE® SP6 Transcription kit	*In vitro* transcription for production of *pcmt* and *pcmtl* for rescue experiments	Ambion
NucleoBond Xtra Maxi kit	Purification of plasmid DNA from 50 – 100 ml bacterial culture.	MACHEREY-NAGEL
PCR purification kit	DNA purification	Qiagen
Plasmid Miniprep kit	Purification of plasmid DNA from 1 – 5 ml bacterial culture.	Qiagen
Rapid DNA Dephos & Ligation kit	Dephosphorylation of DNA during cloning	Roche
RED Taq premix kit	Colony check for PCR	Sigma-Aldrich Belgium
RevertAid H Minus First Strand cDNA synthesis kit	Synthesis of first strand cDNA from total RNA template.	ThermoFischer Scientific

2.2 Methods

2.2.1 Handling of cellular and whole organism models

2.2.1.1 Mammalian cell culture

All cells were maintained in culture medium composed of Dulbecco's Modified Eagle Medium (DMEM) (Table 2-7), 10% (v/v) fetal bovine serum (FBS) and 1% (v/v) Penicillin-Streptomycin (100 units/ml of penicillin and 100 µg/ml of streptomycin final concentration). Cells were stored as aliquots of 1×10^6 cells in 1 ml culture medium supplemented with 5% DMSO at -150°C. When fresh cells were needed they were thawed, washed with culture medium to remove DMSO and passaged at least 2 times before using them in experiments. Cells were cultivated at 37°C and 5% CO_2 at 70 – 90 % confluency and passaged two times a week (except for HT22 cell passages 3 times a week). Experiments in this thesis were performed with cells that had been passaged 10 – 28 times.

Table 2-7: Dulbecco's Modified Eagle Medium (DMEM) composition

Components	Concentration [mg/l]	Concentration [mM]
AMINO ACIDS		
Glycine	30	0.400
L-Arginine hydrochloride	84	0.398
L-Cystine 2HCl	63	0.201
L-Glutamine	584	4.000
L-Histidine hydrochloride-H_2O	42	0.200
L-Isoleucine	105	0.802
L-Leucine	105	0.802
L-Lysine hydrochloride	146	0.798
L-Methionine	30	0.201
L-Phenylalanine	66	0.400
L-Serine	42	0.400
L-Threonine	95	0.798
L-Tryptophan	16	0.078
L-Tyrosine disodium salt dihydrate	104	0.398
L-Valine	94	0.803
VITAMINS		
Choline chloride	4	0.029
D-Calcium pantothenate	4	0.008
Folic Acid	4	0.009
Niacinamide	4	0.033
Pyridoxine hydrochloride	4	0.019
Riboflavin	0.4	0.001
Thiamine hydrochloride	4	0.012
i-Inositol	7.2	0.040

INORGANIC SALTS		
Calcium Chloride ($CaCl_2$) (anhyd.)	200	1.802
Ferric Nitrate ($Fe(NO_3)_3*9H_2O$)	0.1	0.000
Magnesium Sulfate ($MgSO_4$) (anhyd.)	97.67	0.814
Potassium Chloride (KCl)	400	5.333
Sodium Bicarbonate ($NaHCO_3$)	3700	44.048
Sodium Chloride (NaCl)	6400	110.345
Sodium Phosphate monobasic (NaH_2PO_4-H_2O)	125	0.906
OTHER COMPONENTS		
D-Glucose (Dextrose)	4500	25.000
Phenol Red	15	0.040

2.2.1.2 Zebrafish (Danio rerio) maintenance

The zebrafish strains used in this thesis were the AB strain (wild type) and the *nacre* and beta-actin:GCaMP6f transgenic lines. The AB strain (Figure 2-1) was originally offspring of two lines named A and B, which were initially bought by Prof. George Streisinger from a pet shop in Albany, Oregon, USA. The *nacre* transgenic line (Figure 2-1) is lacking the microphthalmia-associated transcription factor a (*mitfa*) gene in the AB background, leading to deficiency in melanocytes and transparency of the animals (LISTER *et al.* 1999).

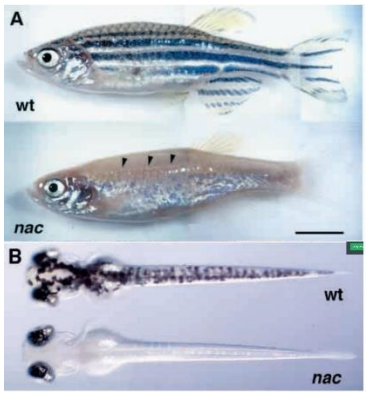

Figure 2-1: Wild type strain (top) and nacre strain (mitfa$^{-/-}$ mutant) lacking melanocytes (bottom) of adult zebrafish (A) and 3 dpf larvae (B). Adapted from (LISTER et al. 1999)

The beta-actin:GCaMP6f transgenic zebrafish line was a generous gift from Dr. Francesca Peri, head of the Developmental Biology Unit at EMBL, Heidelberg, Germany. This transgenic line expresses calmodulin (CaM) fused to a circularly permuted green fluorescent protein (GFP) through an M13 peptide in the cytoplasm of the cells (CHEN *et al.* 2013) under the control of the beta-actin promoter, expected to lead to ubiquitous expression in all cell types of the body. Upon binding of calcium to CaM, the CaM/M13 domain undergoes conformational changes leading to increase in the fluorescence intensity of the GFP. Transparency is essential to obtain a good visualization of

fluorescent signal. To achieve transparency, the beta-actin:GCaMP6f strain was crossed with the *nacre* strain and their non-pigmented, green fluorescent heart progeny were selected for the experiments. The beta-actin:GCaMP6f positive larvae shows green fluorescence in the heart due to continues calcium release for contractility.

Adult zebrafish and embryos were raised and maintained in the LCSB Zebrafish Core Facility at 28 (±0.5) °C with light/dark cycles of 14/10 hours, respectively, according to standard protocols (WESTERFIELD 2000). Embryos were obtained by natural spawning and after collection and sorting out unfertilized eggs, they were reared in 0.3 × Danieau's solution (17 mM NaCl, 2 mM KCl, 0.12 mM $MgSO_4$, 1.8 mM $Ca(NO_3)_2$, 1.5 mM HEPES pH 7.5 and 0.03 M methylene blue) until needed for experiments.

2.2.1.2.1 Ethics statement for animal experimentation

In this project, all procedures with zebrafish were performed in accordance with European laws, guidelines and policies for animal experimentation, housing and care (European Directive 2010/63/EU on the protection of animals used for scientific purposes of 20 October 2010), and following the principles of the Three Rs – to replace, reduce and refine the use of animals used for scientific purposes. By using non-mammalian vertebrates (zebrafish embryos and larvae) for *in vivo* experiments, the use of mammalian models (e.g. adult rodents such as mice and rats) is minimized.

The operation of the Luxembourg Centre for Systems Biomedicine (LCSB) Zebrafish Core Facility and the performance of the aforementioned experiments with zebrafish embryos and larvae in the LCSB has been allowed, with regard to European Directive 2010/63/EU, by the relevant agencies of the Government of Luxembourg, both the Ministère de la Santé and the Ministère de l'Agriculture, de la Viticulture et du Développement Rural (Arrêté ministériel du 20 décembre 2012).

2.2.2 Molecular biology

2.2.2.1 Genomic DNA (gDNA) extraction

Extraction of gDNA from mammalian cells was adapted from Meeker *et al*. (MEEKER *et al.* 2007). Briefly, 1×10^6 cells were disrupted by vortexing in 100 µl of 50 mM NaOH and boiling for 10 minutes at 95°C. Subsequently, samples were put on ice and 10 µl of 1 M Tris/HCl pH 8.0 were added to neutralize the pH. Finally, samples were centrifuged for 5 minutes at 16 100 × *g* at 4°C and the supernatants were used for PCR analysis.

2.2.2.2 Total RNA extraction

RNA extraction, either from mammalian cells or zebrafish, was carried out using TriPure reagent according to the supplier's protocol. One ml of TriPure reagent was added to either 1×10^6 cells, 15 –

20 larvae or dissected adult zebrafish organ. In case of the larvae and dissected organs, tissues were homogenized using the Precellys-24 homogenizer (3 cycles each of 10 seconds at 6000 rpm and 15 seconds off between each cycle) while mammalian cells were homogenized by pipetting. Regardless of the sample origin, all samples were treated the same for subsequent steps. Homogenates were left 5 minutes at room temperature, transferred to 2-ml tubes containing 200 µl chloroform, shaken vigorously for 15 seconds and then centrifuged at 12 000 × *g* for 15 minutes at 4°C for phase separation. The upper aqueous phase, containing RNA, was transferred to a new tube containing 500 µl isopropanol for RNA precipitation. Tubes were left at room temperature for 5 minutes for the precipitate to form, followed by centrifugation at 12 000 × *g* for 10 minutes at 4°C. The pellet was then washed with 1 ml of 70% ethanol and left to air-dry. Finally, the pellet was solubilized in 50 µl nuclease-free H_2O and incubation for 10 minutes at 55°C. RNA samples were stored at -80°C until used.

2.2.2.3 In vitro transcription

In vitro transcription (IVT) was performed using the mMESSAGE mMACHINE® SP6 Transcription kit to produce full sequence capped mRNA for injection into zebrafish eggs. Prior to IVT, the coding sequences of target genes were cloned into the pCS2+ plasmid, which was then linearized using NotI restriction enzyme and purified using the Qiagen PCR purification kit. IVT reactions (20 µl total volume) contained 10 µl 2× NTP/CAP (mixture of NTPs and capped GTP), 2 µl 10× reaction buffer, 2 µg of linearized and purified plasmid and 2 µl of SP6 enzyme mix. The reaction mixture was incubated for 2 hours at 37°C. Residual plasmid DNA was removed by the addition of 1 µl of TURBO DNase and incubation at 37°C for 15 minutes. Finally, transcribed RNA was purified using the MEGAclear™ kit.

2.2.2.4 Complementary DNA (cDNA) synthesis

The RevertAid H Minus First Strand cDNA synthesis kit from ThermoFisher was used following the manufacturer's protocol for cDNA synthesis. Briefly, 1 µg total RNA was used as a template in 20 µl reactions containing 1 µl of dT10 primer (stock 100 µM), 4 µl 5× reaction buffer, 1 µl RiboLock (RNase inhibitor 20 U/µl), 2 µl of dNTPs (stock 10 mM) and 1 µl of RevertAid enzyme (stock 200 U/µl). The reaction mixtures were incubated at 42°C for 1 hour followed by 15 minutes at 70°C for enzyme deactivation. cDNA samples were stored at -20°C until further analysis.

2.2.2.5 Transformation of chemically competent E. coli cells

Transformation of Stbl3, TOP10 or BL21(DE3) chemically competent *E. coli* cells (Table 2-8) was performed by incubating the cells with either 50 – 100 ng purified plasmid or 2 µl of a ligation product following cloning (Section 2.2.2.9) for 5 minutes on ice, followed by 30 seconds at 42°C and 2 minutes back on ice. Cells were regenerated in 250 µl of SOC medium (20 g/l Tryptone, 5 g/l yeast extract, 4.8 g/l $MgSO_4$, 3.603 g/l dextrose, 0.5 g/l NaCl, 0.186 g/l KCl) at 37°C for 1 hour with constant agitation

(225 rpm). Finally, cells were spread on LB-agar plates supplemented with the appropriate antibiotic for selection.

Table 2-8: Bacterial strains used for cloning and recombinant protein expression

Strain	Purpose	Company
***E. coli* BL21(DE3)**	Recombinant protein expression	TermoFischer Scientific
***E. coli* Stbl3**	Propagation of plasmids containing direct repeats found in lentiviral expression vectors	TermoFischer Scientific
***E. coli* TOP10**	Propagation of plasmids	TermoFischer Scientific

2.2.2.6 Plasmid purification

Depending on the desired quantity of the purified plasmid, either the Qiagen MiniPrep kit (to produce 5 – 10 µg of DNA) or the NucleoBond MaxiPrep kit (to produce 500 – 1000 µg of DNA) were used. 5 ml or 100 ml bacterial culture hosting the plasmid to be purified were prepared for the MiniPrep or MaxiPrep kits, respectively. Cells were cultivated overnight with constant shaking (200 rpm) at 37°C in LB medium supplemented with the appropriate antibiotic for selection (ampicillin was used at 100 µg/ml and kanamycin at 50 µg/ml). Cells were harvested by centrifugation at 4000 × *g* and pellets were used for plasmid purification following the manufacturers' protocols, with final elution of plasmid in nuclease-free H_2O.

2.2.2.7 Polymerase chain reaction (PCR), colony PCR and qPCR

A standard PCR protocol was used for amplification of genes of interest prior to cloning. Briefly, the AccuPrime™ *Pfx* DNA polymerase was used in a 50 µl reaction mixture containing 5 µl of 10 × reaction buffer () supplied with the enzyme kit, 25 pmol of each forward and reverse primers, 10 – 100 ng DNA template and 1 unit of the enzyme. The template was denatured at 98°C for 2 minutes followed by 30 cycles of 98°C for 15 seconds; X°C for 15 seconds; and 72°C for 1 min/kb for extension (where X is the annealing temperature specific to each primer pair (Table 2-6)). An additional final extension step at 72°C for 10 minutes was used after these 30 cycles.

For colony PCR, Taq DNA polymerase was used, where 20 µl reaction mixtures were set up containing 10 µl of 2× REDTaq premix and 5 pmol of each forward and reverse primers. By opposition to the standard PCR where purified DNA served as a template, a freshly picked bacterial colony, resuspended in the reaction mixture, was here used as the DNA source. Thermocycler parameters were similar to the ones described for standard PCR but an initial step (98°C for 5 minutes) was added to allow for cell lysis.

A qPCR approach was used to quantify transcript levels of genes of interest. Briefly, 2 µl of 1:5 diluted cDNA, prepared from 1 µg RNA as described before (Section 2.2.2.4), were used as a template. In each qPCR reaction (total volume of 20 µl), the cDNA was mixed with 5 pmol of each forward and reverse primers specific for the target gene and 10 µl 2× iQ SYBR green mix from BioRad. A denaturation step at 95°C for 5 minutes was followed by 40 cycles of 95°C for 30 seconds, 60°C for 30 seconds, and 72°C for 30 seconds for extension, with acquisition of fluorescence information followed by a melting curve. Calculation of relative fold changes in expression of a target gene normalized to expression of a reference gene was done using the $2^{-\Delta\Delta Ct}$ method (PFAFFL 2001).

2.2.2.8 Quality and quantification of nucleic acid

The concentration of DNA and RNA samples were evaluated by UV absorbance measured on a NanoDrop2000 from ThermoFisher Scientific. Concentration was estimated based on UV absorbance at 260 nm where 1 absorbance unite corresponded to 50 ng/µl for DNA and 40 ng/µl for RNA.

2.2.2.9 Cloning

During this thesis work, various DNA fragments had to be cloned into plasmids. Based on the desired application and the plasmid, different cloning strategies and different bacterial strains were used.

2.2.2.9.1 Restriction-ligation cloning

Standard restriction-ligation cloning was done by amplification of the target DNA with primers containing restriction site sequences compatible with the restriction sites available in the plasmid. PCR products were purified using the Qiagen PCR purification kit and incubated with the restriction enzymes and the respective buffer at the recommended temperature. In parallel, destination plasmids were also incubated with compatible restriction enzymes and buffer. Restricted plasmids were dephosphorylated using the Rapid Dephos kit. Restricted PCR fragments and plasmids were mixed together at 1:3 molar ratio in ligation buffer with T4 DNA ligase and incubated at room temperature for 15 minutes. The ligation reactions were stopped by placing the reaction tubes on ice and 2 µl of ligation reaction were used for chemical transformation of *E. coli* TOP10 cells (Section 2.2.2.5).

2.2.2.9.2 TOPO cloning

The Champion™ pET100 Directional TOPO® Expression Kit was used to insert an ORF of interest into a pET100 plasmid downstream to a His-tag for recombinant protein expression in *E. coli* and for later affinity purification on His-Trap Ni-column (GE Healthcare).

Cloning was carried out according to the manufacturer's protocol. Briefly, primers were designed including the 4 bp sequence CACC in 5' of the forward primer necessary for directional cloning. The ORF of interest was amplified using the respective primers by the standard PCR protocol (Section

2.2.2.7) from clones obtained from SourceBioscience clone IRBOp991B0677D for *pcmt* and clone IRBOp991C012D for *pcmtl*. The PCR product was loaded into a 1% agarose gel for separation by electrophoresis and the DNA band migrating at the correct size was excised out of the gel for subsequent purification using the Qiagen gel extraction kit. The purified PCR product was mixed with the pET100 vector at a 2:1 molar ratio, 1 µl salt solution (provided with the kit) and H_2O to reach a total volume of 10 µl. The reaction mixture was incubated for 15 minutes at room temperature and then kept on ice until used (2 µl) for transformation of *E. coli* TOP10 cells.

2.2.2.9.3 In-Fusion cloning

In-Fusion Enzyme fuses DNA fragments (e.g. PCR-amplified DNA sequences) with linearized vectors by recognizing a 15 bp overlap at their ends. PCR was done using the standard protocol followed by loading into a 1% agarose gel and amplicon purification using the Qiagen gel extraction kit. An In-Fusion cloning reaction was set up by mixing 2 µl of 5× In-Fusion HD Enzyme Premix with 100 ng linearized plasmid, 30 ng insert and nuclease-free H_2O up to 10 µl. The reaction was incubated for 15 min at 50°C, then placed on ice. 2.5 µl of this reaction mixture were used to transform chemically competent *E. coli* TOP10 cells (Section 2.2.2.5).

2.2.2.9.4 shRNA cloning into pENTR™/U6 vector

shRNAs against human PCMT1 were designed using the BLOCK-iT™ RNAi Designer web tool from ThermoFisher Scientific and default parameters. The shRNA was aimed to be inserted into the pENTR™/U6 vector with a sense-loop-antisense orientation and the default loop sequence CGAA. The designer tool returned 8 different regions to target in the transcript and the three with the highest score were selected for further use. Top and bottom strand oligonucleotides were ordered from Eurofins with HPLC grade of purification.

Table 2-9: shRNA design for the human PCMT1 gene: sequence of the three targeted regions in the PCMT1 transcript and the corresponding top and bottom strands for shRNA synthesis

	Target sequence in PCMT1 transcript	**Top Strand 5' → 3'**	**Bottom Strand 5' → 3'**
shRNA1	GCTAGTAGATGACT CAGTAAA	CACCGCTAGTAGATGACTCAGTAAACGA ATTTACTGAGTCATCTACTAGC	AAAAGCTAGTAGATGACTCAGTAAATTC GTTTACTGAGTCATCTACTAGC
shRNA2	GCGCTAATAGATCA GTTAAAG	CACCGCGCTAATAGATCAGTTAAAGCGA ACTTTAACTGATCTATTAGCGC	AAAAGCGCTAATAGATCAGTTAAAGTTC GCTTTAACTGATCTATTAGCGC
shRNA3	GCAGTATGACAAGC TACAAGA	CACCGCAGTATGACAAGCTACAAGACGA ATCTTGTAGCTTGTCATACTGC	AAAAGCAGTATGACAAGCTACAAGATTC GTCTTGTAGCTTGTCATACTGC
Ctrl shRNA	N/A	CACCGAGAAGACATCGTACTGTAATCGA AATTACAGTACGATGTCTTCTC	AAAAGAGAAGACATCGTACTGTAATTTC GATTACAGTACGATGTCTTCTC

For transient expression of shRNA and to test the efficiency of the three different shRNAs, each was cloned into the pENTR™/U6 vector. The top and bottom strand oligonucleotides were mixed together at a concentration of 200 µM, heated to 95°C for 4 minutes and then left to anneal at RT for 10 minutes. 0.0025 pmol of the annealed oligonucleotides were mixed with 0.5 ng pENTR™/U6 vector together with 0.5 U of T4 DNA ligase and ligation buffer provided with the kit in a total volume of 10 µl and incubated for 5 minutes at room temperature. 2 µl of the ligation product were used for transformation of chemically competent *E. coli* TOP10 cells (Section 2.2.2.5).

2.2.2.9.5 Gateway cloning to generate lentiviral shRNA expression plasmid

The Gateway® Technology is a universal cloning method that takes advantage of the site-specific recombination properties of bacteriophage lambda to provide a rapid and highly efficient way to move a DNA sequence of interest into multiple vector systems. Gateway cloning was used to move the shRNA sequences cloned into the pENTR™/U6 vector to the pLenti6/BLOCK-iT™-DEST vector by LR recombination to create lentiviral shRNA expression vectors. The LR recombination reaction was set up by mixing 150 ng of empty pLenti6/BLOCK-iT™-DEST vector with 150 ng of recombinant (shRNA containing) the pENTR™/U6 entry construct together with 2 µl of Gateway® LR clonase® II enzyme mix in a total volume of 10 µl and the reaction mixture was incubated at 25°C for 1 hour. 2 µg proteinase K were then added followed by a 10 minutes incubation at 37°C. 2 µl of this final mixture were used for transformation of chemically competent *E. coli* Stbl3 cells (Section 2.2.2.5).

2.2.2.9.6 gRNA cloning into the pX459 plasmid

Guide RNAs (gRNA) were designed using an online tool from the Sanger institute (http://www.sanger.ac.uk/htgt/wge/find_crisprs). Since CRISPR/Cas9 was going to be used to knock out *Pcmt1* in HT22 cells, which are of murine origin, Mouse (GRCm38) was selected as the 'Species' and the search was focused on exons 1 – 5 of the *Pcmt1* gene. As the search returned hundreds of results, it was refined by selecting both the 'paired Crispr' and 'best 25%' at the off-target filters. The two gRNAs with the lowest number of putative off-targets were selected. Scrambled gRNA was generated by shuffling gRNA1 sequence to be used as a control. Oligonucleotides were ordered from Eurogentec.

Table 2-10: gRNA sequences used in this study to guide the Cas9 nuclease to the Pcmt1 gene in HT22 cells

Name	gRNA sequence	Oligos ordered for gRNA cloning into pX459	
		Top 5'→ 3'	Bottom 5'→ 3'
gRNA 1	GCCGCACTCGCCCCGAGGAC	CACCGCCGCACTCGCCCCGAGGAC	AAACGTCCTCGGGGCGAGTGCGGC
gRNA 2	GTGAGTGGCAGAACGCTTAC	CACCGTGAGTGGCAGAACGCTTAC	AAACGTAAGCGTTCTGCCACTCAC
Scramble gRNA	GCGCGCACGTCGCACGCACC	CACCGCGCGCACGTCGCACGCACC	AAACGGTGCGTGCGACGTGCGCGC

To clone the gRNAs into the pX459 plasmid, 10 pmol of each the top and bottom oligonucleotides were mixed together with 1 µl of T4 Polynucleotide Kinase (PNK) and 1 µl of 10× T4 ligation buffer in a final volume of 10 µl reaction. The reaction mixture was incubated at 37°C for 30 minutes for phosphorylation of the oligonucleotides. The temperature was increased to 95°C for 5 minutes and then decreased to 25°C at a rate of -5°C/minute, allowing annealing of the top and bottom oligonucleotides. The phosphorylated annealed oligonucleotides were diluted 1:250. In parallel, the pX459 vector was digested with BbSI restriction enzyme followed by purification using the Qiagen gel extraction kit. The purified plasmid was dephosphorylated in a reaction mixture containing 22.5 µl of gel purified product (i.e. 800 ng), 3 µl H_2O, 3 µl 10× rAPid Alkaline Phosphatase buffer and 1.5 µl rAPid alkaline phosphatase and incubated for 30 min at 37°C following by deactivation for 2 min at 75 °C. Ligation of the phosphorylated annealed oligos with the digested dephosphorylated pX459 plasmid was performed using the T4 DNA ligase protocol: a 20 µl reaction mixture containing 2 µl of linearized pX459, 1 µl of diluted annealed and phosphorylated oligos, 2 µl of DNA dilution buffer, 5 µl of H_2O, 10 of µl 2× ligation buffer and 1 µl of T4 DNA ligase was incubated for 15 min at room temperature. 2 µl of this ligation reaction were used to transform chemically competent *E. coli* TOP10 cells.

2.2.2.10 Site-directed mutagenesis

The D83V non-synonymous mutation was introduced into the coding sequence of both the *pcmt* and *pcmtl* zebrafish genes by substitution of a GAT codon by a GTT codon through site-directed mutagenesis. Plasmids containing either the *pcmt* or *pcmtl* coding sequences were used as templates and PCR-amplified, using two different pairs of primers designed specifically to introduce the desired mutation using PCR standard protocol (Section 2.2.2.7). In contrast to the newly PCR-produced plasmids (with the mutation of interest), the template plasmids were methylated at various positions. The Dpn I restriction enzyme specifically recognizes and cuts methylated DNA sequences. The addition of this enzyme to a mixture containing template plasmid and the newly produced plasmids allowed the digestion of only the template plasmid without the mutation. Chemically competent *E. coli* cells were transformed with 2 µl of the resulting point mutated plasmid preparation.

2.2.3 Biochemical assays

2.2.3.1 Protein quantification through Bradford assay

Protein concentration was determined using the Bradford assay. Briefly, Bradford reagent was prepared by diluting commercially available Bradford solution from Biorad 5-fold in H_2O, followed by filtration through a 0.2 µm filter. Bovine serum albumin (BSA) standards were prepared in the range of 0.1 – 0.9 mg/ml. For each sample or standard, 20 µl were mixed with 1 ml of Bradford reagent and incubated 5 minutes in the dark at room temperature. Absorbance was measured at 595 nm. Protein

concentration in the samples was calculated using the standard curve generated based on the BSA standard measurements.

2.2.3.2 SDS-PAGE and Western blot analysis

Protein extracts or purified protein samples were mixed with SDS sample buffer (63 mM Tris/HCl pH 6.8, 2% w/v SDS, 10% v/v glycerol, 0.002% w/v bromophenol blue, and 5% β-mercaptoethanol) and heated at 95°C for 5 minutes. Unless otherwise mentioned, the equivalent of 20 µg protein of each sample was loaded into pre-cast SDS-PAGE gels from BioRad. Separation was achieved at a constant voltage (160 V) for 1 hour using migration buffer (25 mM Tris pH 8.3, 192 mM glycine and 1% SDS). Following the electrophoretic separation, the gel was either used for protein detection by Coomassie blue staining or for Western blot analysis. For Coomassie blue detection, the gel was stained with Coomassie blue (ThermoFisher Scientific, catalog no. 24620) in a microwave for 10 seconds followed by 15 min at room temperature on a shaker. Several washing steps with water were used to reduce background staining.

For Western blot analysis, the gel, alongside filter papers and methanol-activated PVDF membrane, were first equilibrated for 5 minutes in transfer buffer (25 mM Tris pH 8.3, 192 mM glycine, 10% (v/v) methanol). Proteins were blotted on the PVDF membrane using a semi-dry method. This membrane was washed briefly with TBS-T buffer (20 mM Tris/HCl pH 6.7; 137 mM NaCl 0.1% Tween20) and blocked in 5% BSA solution for 1 hour at room temperature on an orbital shaker. Unless otherwise indicated, primary antibody was diluted 1:1000 in TBS-T buffer containing 1% BSA and incubated with the membrane overnight at 4°C with shaking followed by three washing steps with TBS-T buffer for 5 minutes. The secondary antibody, diluted 1:5000 in TBS-T containing 1% BSA, was then added to the membrane followed by a 1-hour incubation at room temperature. Finally, the membrane was again washed 3 times with TBS-T buffer for 5 minutes. Antibody binding was revealed through addition of enhanced chemiluminescent (ECL) substrate from Amersham (Catalog no. RPN2232). Band detection was carried out on a Li-COR Odyssey FC Imaging System. Band intensity was quantified using Image Studio™ software from Li-COR with exposure times ranging from 30 seconds to 2 minutes.

2.2.3.3 Recombinant protein expression and purification

E. coli BL21(DE3) cells carrying the pET100 plasmid (containing either *pcmt* or *pcmtl* coding sequences) were grown on LB agar plates supplemented with 100 µg/ml ampicillin at 37°C. One clone served to inoculate a 5 ml starter culture (LB with ampicillin) that was grown for about 10 hours at 37°C. The complete starter culture was used to inoculate a 50 ml pre-culture that was grown overnight to obtain sufficient biomass for the main culture. This latter consisted in 1 L of LB medium supplemented with 50 µg/ml carbenicillin to which 20 ml of the pre-culture was added. Cells were grown at 37°C with

shaking until OD_{600} reached 0.7. Protein expression was then induced by addition of IPTG at a final concentration of 0.1 mM and cells were incubated with continuous shaking for 10 hours at 18°C. Finally, they were harvested by centrifugation at 4816 × *g* for 20 minutes and pellets were stored at -80°C until used for protein extraction and purification.

Cells were resuspended in 50 ml lysis buffer (25 mM Tris/HCl pH 8.0, 300 mM NaCl, 0.5 mM PMSF, 1 mM DTT, 0.1 mg/ml lysozyme, 1× protease inhibitor cocktail) and sonicated using a BRANSON Digital Sonifier 200W S-250D for 3 cycles with 1 minute breaks in between (each cycle was 0.5 second 'on', 1 second 'off' during 20 seconds total, with 50% amplitude). Lysates were centrifuged for 40 minutes at 15,000 × *g* at 4°C and the supernatant, containing soluble proteins, was filtered through a 5 µm cellulose acetate membrane.

An Äkta purifier system (GE Healthcare) was used for protein purification. The filtered protein extract (about 50 ml) was passed on a 1 ml HisTrap column at a constant flow rate of 1 ml/min. This column had been previously equilibrated with 10 column volumes (CVs) of buffer A (25 mM Tris/HCl pH8, 300 mM NaCl, 10 mM imidazole). After loading the cell free extract, buffer A was constantly run through the column until absorbance at 280 nm went back to baseline levels, indicating that all non-bound proteins had been removed. The column was then washed with another 10 CVs of buffer A followed by a second washing step with a buffer with equal composition as buffer A except for imidazole concentration (increased to 25 mM). Finally, His-tagged proteins were eluted with a linear gradient of imidazole (25 – 300 mM) applied over 20 ml with collection of 1 ml fractions. The fractions showing high protein concentration and high purity of the protein of interest by SDS-PAGE analysis were pooled. Pooled fractions were dialyzed overnight against a buffer containing 20 mM Tris/HCl pH 7.6, 25 mM NaCl and 20% glycerol with a 2-step dialysis each of 2 l and stored at -20°C until used.

2.2.3.4 Methanol vapour diffusion assay

To assess total isoaspartyl content and isoaspartyl methyltransferase activity in various sample types, a methanol vapour diffusion assay was applied as adapted from Patananan *et al* (PATANANAN *et al.* 2014) and illustrated in Figure 2-2. A 100 µl reaction mixture was prepared containing 0.2 M Bis-Tris pH 6.0, 73 µM *S*-adenosyl methionine (SAM), isoaspartyl containing substrate and the methyltransferase. The SAM cofactor solution was prepared by diluting 1 part of 7 µM [methyl-^{3}H]SAM (PerkinElmer, 78 Ci/mmol, 0.55 µCi/µl) in 9 parts 80 µM non-labelled SAM (Sigma-Aldrich). For the methyltransferase activity assays in cell extracts, the reaction contained 100 µM of KASAisoDLAKY peptide (Lys-Ala-Ser-Ala-isoAsp-Leu-Ala-Lys-Tyr) as the isoaspartyl substrate and 10 – 30 µg cytosolic protein extract as the isoaspartyl methyltransferase source. For measuring total isoaspartyl levels, the assay mixture contained 10 – 30 µg cytosolic protein extract as the isoaspartyl

substrate and 5 µg recombinant human protein L-isoaspartyl methyltransferase (rhPCMT1). For both types of assay, the reaction mixture was incubated at 30°C for two hours and stopped by addition of 10 µl of 0.2 M NaOH solution. 100 µl of the stopped reaction mixture were spotted on a filter paper (1×2 cm) and placed above 2 ml liquid scintillation cocktail (Ultima Gold XR, Perkin Elmer catalog no. 6013111) in a 4-ml tube. The closed tube was incubated for 4 hours at room temperature to allow the diffusion of radiolabeled methanol into the liquid scintillation cocktail. Finally, the filter paper was removed and tubes were placed into a MicroBeta2 plate counter from PerkinElmer. Counts per minute (cpm) were converted to moles of isoaspartyl using a standard curve prepared the same way using 5 µg rhPCMT1 and different concentrations (0.024 – 6.25 µM) of KASAisoDLAKY peptide.

For kinetic characterization of the purified *D. rerio* Pcmt and Pcmtl enzymes, the reaction mixture contained 2 µg of recombinant Pcmt or Pcmtl and different concentrations (2 – 500 µM) of the of KASAisoDLAKY substrate. Reactions were stopped at different time points to determine initial velocities. Dependency of enzyme initial velocity on substrate concentration indicated Michaelis-Menten kinetics.

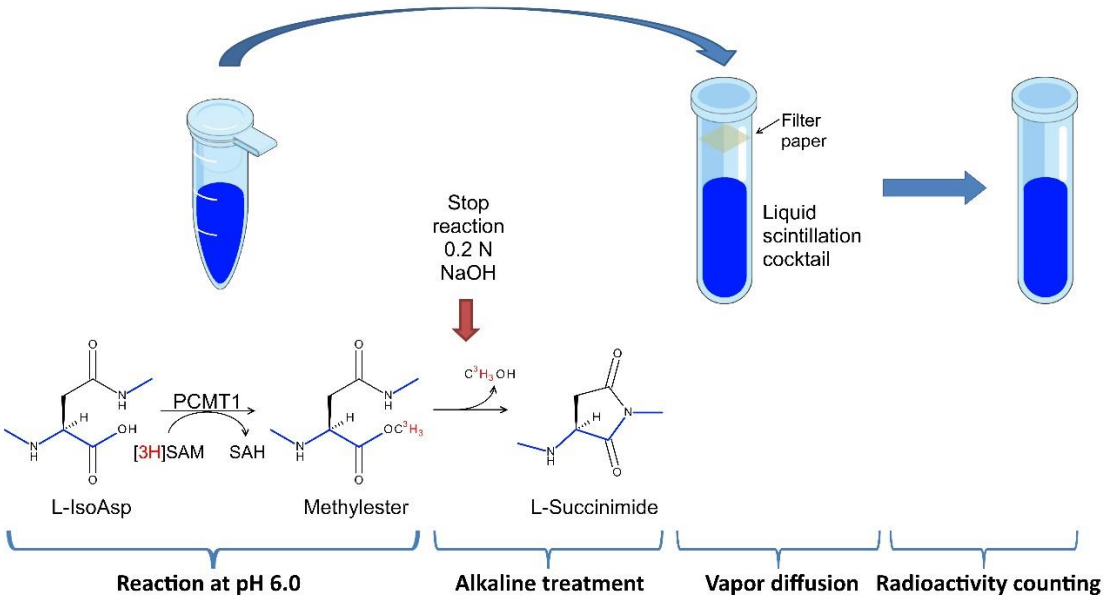

Figure 2-2: Methanol vapour diffusion assay used to assay L-isoaspartyl methyltransferase activity or L-isoaspartyl content in various types of samples.

2.2.4 Cell culture methods

2.2.4.1 Mammalian cell transfection

The mammalian cell transfection protocol described here was carried out to introduce plasmid DNA into cells. Cells were seeded 1 day before transfection in a 6-well plate and left to adhere, reaching 50 – 70% confluency at the time of transfection. Lipofectamine 2000 reagent and plasmid DNA were

mixed together at a ratio of 1 µg DNA per 3 µl lipofectamine in a total volume of 250 µl OptiMEM medium. The mixture was incubated for 5 minutes at room temperature for the lipid-DNA complex to form and then added drop-wise to the cells in the 6-well plate. Experiments were performed 24 to 72 hours later. For production of recombinant lentiviral particles containing shRNA constructs, the same transfection protocol was used (with HEK293FT cells) except that the lipid-DNA complexes were added on the same day as the cells were seeded, and lentiviral production was continued as described in the following section.

2.2.4.2 PCMT1 knockdown in human cell lines using lentiviral shRNA transduction

Lentiviral transduction of shRNAs was used to establish stable human-derived cell lines (HEK293 and U-87 MG) with lower transcription levels of PCMT1.

2.2.4.2.1 Production of lentivirus

HEK293FT cells were transfected as described before (Section 2.2.4.1) with a plasmid mix composed of ViraPower™ (containing pLP1, pLP2 and pLP/VSVG plasmids, see above) and pLenti6/BLOCK-iT™-shRNA expression vector for the production of recombinant lentiviral particles. After on overnight incubation in full growth DMEM medium, this latter was replaced by fresh medium. Virus-containing medium was harvested 48 hours post transfection and centrifuged at 3000 rpm for 5 minutes at 4°C. Viral particles were concentrated by mixing 40 ml of the resulting supernatant with 8 ml of 40% polyethylenglycol 1000 (PEG1000), overnight incubation at 4°C, and 30 minutes centrifugation at 1 500 × *g* at 4°C. The supernatant was discarded and the viral pellet was resuspended in 400 µl PBS. Aliquots of this concentrated viral preparation were stored at -80°C.

2.2.4.2.2 Transduction of U-87 MG and HEK293 cells

Since the lentivirus used introduces a blasticidin resistance to the transduced cells, a kill curve was set up for both the HEK293 and U-87 MG cell lines to find the minimum toxic concentration of blasticidin. Cells were incubated with 1 to 10 µM blasticidin and media were changed every 3 days for a total duration of 10 days.

HEK293 or U-87 MG cells were seeded in 6-well plates and grown overnight. The medium (2 ml/well) was replaced by a fresh one containing 20 µl of the virus preparation described in the previous section. Polybrene was added at a final concentration of 6 µg/ml to enhance cell transduction. After one day of incubation, the medium containing the virus was changed with fresh complete medium devoid of virus. On the third day, selection with blasticidin (at the minimal toxic concentrations determined as described above i.e. 2 µg/ml and 4µg/ml for U87 and HEK293 cells, respectively) was started by adding the antibiotic followed by renewal of the medium every 3 days during a total duration of 10 days. Six blasticidin-resistant colonies were selected and plated in fresh dishes. Total RNA was extracted and

the transcription level of *PCMT1* was determined by qPCR to identify clones with the highest knockdown efficiency.

2.2.4.3 Pcmt1 knockout in mouse HT22 cells using CRISPR/Cas9

The CRISPR/Cas9 strategy was used to knock out the *Pcmt1* gene in the mouse hippocampal HT22 cell line using the method described in Ran *et al* (RAN *et al.* 2013). gRNAs were designed and cloned into the pX459 plasmid as described before (Section 2.2.2.9.6). HT22 cells were transfected with the recombinant plasmid using the standard transfection protocol described earlier (Section 2.2.4.1). Puromycin was added one day after transfection at a final concentration of 1 µg/ml for selection of plasmid containing cells. Medium was refreshed after 3 days and 3 days later puromycin-resistant cells were trypsinized, counted and diluted to a density of 1 cell per 200 µl medium so that when seeding 100 µl per well in 96-well plates the chances to have only one cell per well is high. Single resistant cells were seeded in each well of a 96-well plate followed by clone expansion for one week. Ten wells with single clones were selected for genotyping. Clones showing the expected 40 bp deletion in the *Pcmt1* gene were propagated and stored thereafter in DMSO solution at -150°C.

2.2.4.4 Stimulation of mammalian cells with growth factors

To study the phosphorylation of different intermediates in growth signalling pathways in the established cell models, different growth factors were used to stimulate the different signalling pathways. Insulin and insulin growth factor-1 (IGF-1) were used for stimulation of the insulin/IGF-1 signalling pathway and epidermal growth factor (EGF) was used for stimulation of the MAPK signalling pathway. Cells were seeded in 6-well plates in 2 ml culture media and incubated under standard conditions for 24 hours. Stimulation was done when the cells were 70 – 80 % confluent and to achieve this confluency in 24 hours, HEK293 cells were seeded at 1×10^6 cells/well; U-87 MG cells were seeded at 0.4×10^6 cells/well; HT22 cells were seeded at 0.5×10^6 cells/well. Following the 24 hours incubation time cells were washed with pre-warmed PBS and then fresh medium without serum supplemented with the respective stimulator was added and cells incubated for the desired duration of stimulation. Following the desired stimulation time, medium was aspirated and the plates were placed on ice. Cells were scraped in 150 µl RIPA buffer and lysed using Bioruptor UCD-300 TO. Lysates were centrifuged at 16 100 × *g* for 20 minutes at 4°C. Protein concentration was determined using Bradford assay and phosphorylation analysed by Western blot.

2.2.4.5 Calcium imaging in HT22 cells

Pcmt1 knockout or control cells were seeded in 12-well plates at a density of 25,000 cells per well and incubated at 37°C and 5% CO_2 for 2 days. Cells were then washed with PBS and 1 ml of fresh medium was added (the medium used in this case was DMEM without phenol red and supplemented with 25

mM glucose, 4 mM glutamine, 10% FB and 1% (v/v)). Cells were stained by adding 250 µl of Fluo-4 AM reagent into each well followed by 30 minutes incubation at 37°C and 5% CO_2. Cells were then stimulated by addition of ATP at final concentrations of 10 – 80 µM and calcium signals were acquired using a Nikon widefield microscope in a controlled environment (37°C and 5% CO_2). Signals were extracted from acquired images using ImageJ and analyzed using CASA software.

2.2.4.6 Metabolite extraction from mammalian cells

Cells were seeded in 6-well plates at a density of 50,000 cells per well and grown to 80 % confluency. Cells were washed with 1 ml PBS, placed on ice and scraped into 300 µl quenching buffer (50% methanol, 10 mM Tris pH 7.5) at -20°C. Quenched cells were transferred to a tube containing 150 µl chloroform at -20°C. Tubes were vortexed for 2 hours at -20°C and then centrifuged at 10 000 × *g* for 10 minutes at -10°C. The upper aqueous phase was filtered through a 0.2 µm filter and kept at -80°C until metabolite analysis by LCMS.

2.2.4.7 Targeted metabolite analysis with LCMS

To quantify the nucleotides AMP, ADP, ATP, GMP, GDP, and GTP, a targeted HRES-LC-MS method was used. Measurements were performed on a Dionex UltiMate 3000 (Thermo Fisher Scientific) coupled to a Qexactive Orbitrap mass spectrometer (Thermo Fisher Scientific) equipped with a HESI electrospray ion source. Nitrogen was supplied by a NMG33 generator (CMC). Absolute concentrations were calculated based on external calibration curves prepared in 50 % LC-MS-grade MeOH. Analyte separation was achieved by hydrophilic interaction chromatography using a Sequant zicHilic column (3.5 µm, 100 Å, 150 X 2.1 mm, Merck) equipped with a SecurityGuard ULTRA precolumn (UHPLC HILIC for 2.1 ID Columns, Phenomenex) at a constant flow rate of 0.4 ml/min and a temperature of 40 °C. Target metabolites were eluted isocratic, using 70 % solvent B where solvent A is 100 mM Ammonium acetate pH 4.5 (adjusted by acetic acid addition) and solvent B is acetonitrile. 5 µl of sample were injected, while the autosampler was cooled down to 10 °C. Mass spectral data were obtained in a scheduled single ion monitoring in negative mode. Source settings and accurate masses are given in appendix 6.2.

For the analysis of inositol 1,4,5-trisphosphate a second targeted HRES-LC-MS method was applied using the same instrumental setup. Chromatographic separation was achieved in reversed phase mode on a C18EVO column (150 × 2.1 mm, 3.5 µm particle size, 100 °A pore size) (Phenomenex) connected to a guard column (SecurityGuard ULTRA cartridge, UHPLC C18EVO for 2.1 mm ID columns, Phenomenex) that was used at 20 °C and a flow rate of 0.25 ml/min in gradient mode where solvent A is 0 mM ammonium acetate pH 7 (adjusted by ammonium hydroxide) and solvent B is acetonitrile, according to the following profile: from 0 to 2 minutes, isocratic at 0 % B; 2 to 12 minutes, linear gradient to 100 % B; 12 to 15 minutes, isocratic at 100 % B, 15 to 16 minutes, linear gradient to 0 % B

followed by an equilibration of 4 minutes at starting condition. 5 µl of sample were injected, while the autosampler was cooled down to 10 °C. Mass spectral data were obtained in negative single ion monitoring mode. Source settings and mass transitions are given in the appendix 6.2.

2.2.5 Zebrafish methods

2.2.5.1 Collecting eggs

Female and male adult animals were transferred to mating cages with a physical barrier, which was removed on the morning of the next day when lights were switched on. At this time, the mating process started to take place and females started to lay eggs. Eggs were collected at regular intervals of 30 minutes after the beginning of the mating process.

2.2.5.2 Morpholino injection

Splice blocking morpholino oligomers (MOs) were designed and synthesized by Gene Tools, LLC (Philomath, Oregon, USA). MOs (1 mM stock solutions) were diluted in water with 0.1% phenol red and loaded into a glass capillary pulled in house. Pressure and time of injection were adjusted to obtain a droplet with 0.15 mm diameter to inject a volume of about 2 nl into eggs at 1 – 2-cell stage. The injected eggs were maintained at 28.5°C with standard light/dark cycles and medium exchange was done every day until the day of the esperiments.

2.2.5.3 Larvae deyolking and protein extraction

Deyolking was done according to a method described by Link *et al*. (LINK *et al.* 2006). About 100 larvae at 2 days post fertilization (dpf) or 4 dpf were collected in a tube containing 200 µl of deyolking buffer (55 mM NaCl, 1.8 mM KCl, 1.25 mM $NaHCO_3$). Larvae were pipetted up and down with a tip cut off at the extremity so as to match approximately the diameter of the yolk and favour yolk disruption through shear stress. Samples were then washed 3 times with 200 µl wash buffer (110 mM NaCl, 3.5 mM KCl, 2.7 mM $CaCl_2$, 10 mM Tris/HCl pH8.5) centrifuged briefly to collect the larvae at the bottom and pellets stored at -80°C until used.

For protein extraction, 200 µl of lysis buffer (50 mM Tris/HCl pH 7.5, 150 mM NaCl, 1% Triton X-100, 0.1% SDS, 1 mM EDTA, 1 × protease inhibitor cocktail) were added to about 100 larvae. Tissue homogenization was carried out using a Precellys-24 homogenizer for 3 cycles, each cycle consisting of vigorous shaking at 3000 rpm for 10 seconds and a 15 seconds break. Samples were then incubated on ice for 30 minutes and centrifuged at 16 100 × *g* for 20 minutes at 4°C. Protein concentration of the supernatants was determined using the Bradford assay (Section 2.2.3.1).

2.2.5.4 Embryo or larvae fixation

Embryos or larvae were collected at the desired stage, manually dechorionated with fine forceps if applicable, and incubated in 4% paraformaldehyde overnight at 4°C. After this incubation period, samples were washed with PBS and stored in methanol at -20°C until used.

2.2.5.5 In situ hybridization

In situ hybridization (ISH) was performed to determine the tissue distribution of the *pcmt* and *pcmtl* transcripts. Procedures were performed according to the protocol developed by Thisse and Thisse (THISSE and THISSE 2008) as illustrated in Figure 2-3 and described thereafter.

2.2.5.5.1 Probe preparation

Templates for IVT were prepared by PCR amplification of 500 bp for *pcmt* and 700 bp for *pcmtl* genes. Forward primers used were designed with T7 promoter sequence. IVT reaction contained 2 µg of PCR product, 2 µl of 10× reaction buffer DIG-labelling mix, 2 µl of T7 polymerase and 1 µl of RNase inhibitor in a final volume of 20 µl. This reaction was incubated 3 hours at 37°C. After this incubation, 1 µl DNaseI was added and reaction was incubated again for 15 minutes at 37°C. IVT products were purified using ammonium acetate precipitation. To the 20 µl IVT reaction, 10 µl of 7.5 M ammonium acetate were added and incubated 30 minutes at room temperature. Probes were centrifuged at 16,100 × *g* for 1 hour at 20°C and washed with 1 ml of 80% ethanol. Pellets were air-dried and finally re-suspended in 100 µl of RNase-free H_2O and stored at -80°C until used.

2.2.5.5.2 Probe hybridization

Fixed embryos or larvae stored in 100% methanol were rehydrated gradually with PBS by 5 minutes incubation in 25% methanol, 75% PBS and each step reducing the methanol by 25% until the last incubation with 100% PBS which was repeated 4 times. Following, rehydration, samples were permeablized by incubation in PBS supplemented with 10 µg/ml proteinase K and 0.1% tween 20. Incubation time was dependent on the developmental stage. It ranges from 10 second (or minutes) for samples harvested after 10 – 36 hpf to 30 minutes for samples harvested after the 36 hpf stage. Proteinase K digestion was stopped by transferring samples to 4% paraformaldehyde (PFA) and incubation for 20 minutes at RT. Samples were then washed 4 times in PBS, each for 5 minutes. Following this, PBS was replaced by 70°C-preheated hybridization buffer (50% deionized formamide, 5× SSC, 0.1% Tween 20, 50 µg/ml heparin, 500 µg/ml RNase-free tRNA adjusted to pH 6.0 by adding citric acid (460 µl of 1 M citric acid solution for 50 ml of HM)) and samples were incubated for 4 hours at 70°C. After this incubation, probes were added to a final concentration of 1 ng/µl and hybridization was carried out overnight, still at 70°C. After hybridization, probes were recovered and samples were gradually washed with increasing concentration of SSC buffer until achieving 100% of 2× SSC. Samples

were then washed with 0.2× SSC for 30 minutes and gradually brought to 100% PBS. After that, they were incubated during 4 hours at RT in blocking buffer (PBS with 0.1% tween 20, 2% (v/v) sheep serum and 2 mg/ml BSA). Further incubation with primary antibody anti-DIG, conjugated to the alkaline phosphatase (AP) diluted 1:5000, was done overnight at 4°C. Embryos were washed 6 times with PBST at RT each for 15 minutes, then washed 3 times 5 minutes with AP buffer (100 mM Tris HCl, pH 9.5, 50 mM MgCl2, 100 mM NaCl and 0.1% (v/v) Tween 20). After washing, samples were incubated in dark with colouring buffer (AP buffer containing 225 µg/ml of NBT and 175 µg/ml of BCIP). Colour development was checked every 10 minutes and stopped as soon as the desired intensity was reached. The reaction was stopped by replacement of the colouring buffer with PBS-T and samples were washed 4 times for 5 minutes with PBS-T. Samples were fixed for 10 minutes at RT in 4% PFA and then washed again 3 times in PBS-T. To decrease background, samples were incubated for 10 minutes in 100% ethanol and then gradually brought back to PBS-T. Finally, samples were mounted into 3% methylcellulose and images were taken using a Zeiss Stereomicroscope Discovery V8.

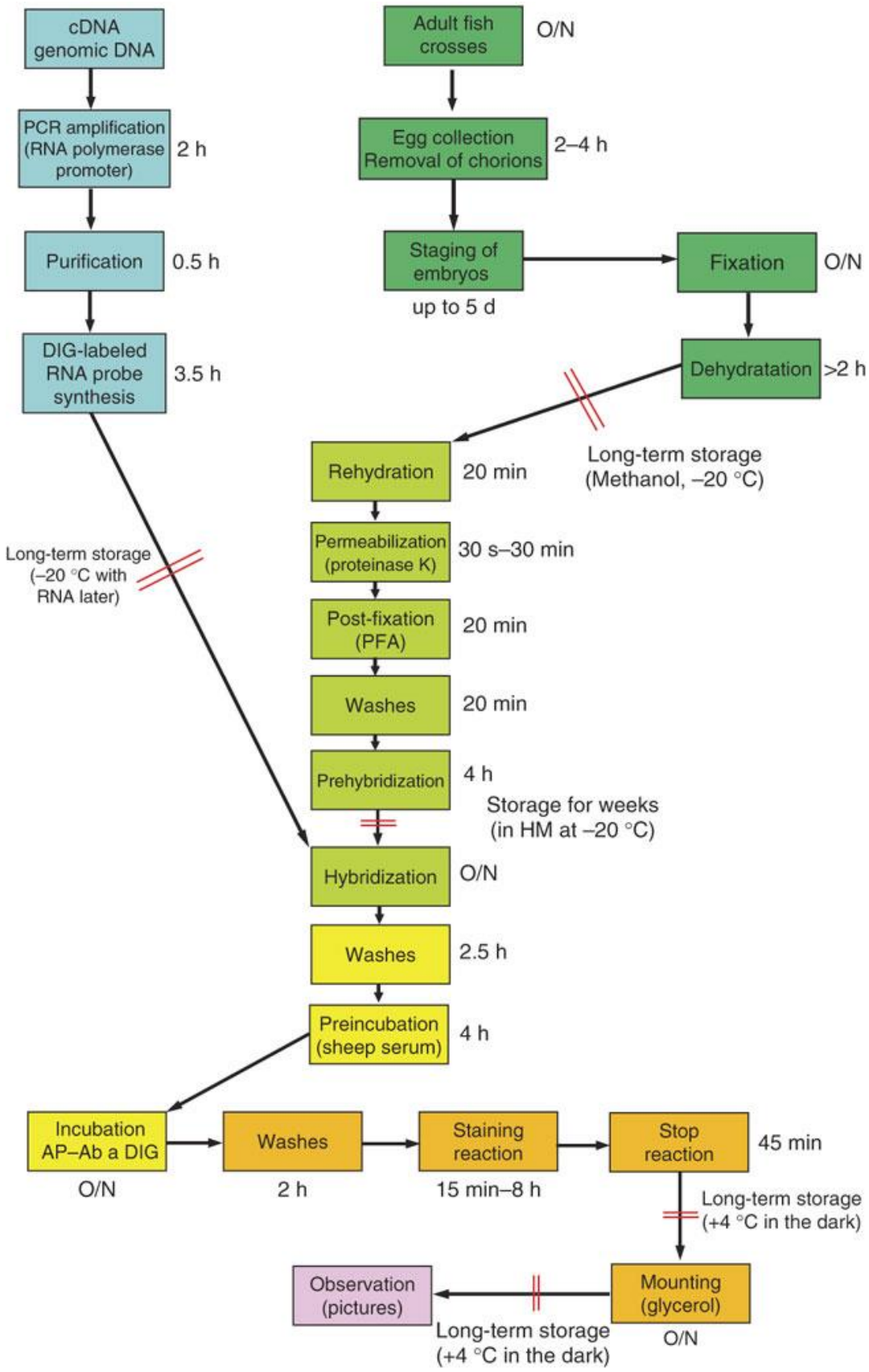

Figure 2-3: Flow chart summarizing steps for in situ hybridization. Adapted from (THISSE and THISSE 2008)

2.2.5.6 Locomotor tracking

Locomotor tracking system is usually used to evaluate changes in locomotor behaviour in zebrafish larvae. The system is equipped with a camera that records the movement of larvae and can measure the distance they move and their velocity. Larvae at 4 dpf injected with either Ctrl or *pcmt/l* MO were placed in a 96-well plate (1 larva per well) in 100 µl 0.3 × Danieau's. The plate was incubated in the dark for 1 hour and then placed into the DanioVision tracking system, where the exposure to light was minimized. Larvae movements were continuously tracked. After 2 cycles of tracking (10 minutes lights on followed by 10 minutes lights off), 100 µl 0.3 × Danieau's supplemented with 40 mM PTZ was added to each well (to reach a final concentration of 20 mM PTZ) and tracking was repeated.

2.2.5.7 Calcium signalling in beta-actin:GCaMP6f transgenic zebrafish

Larvae at 4 dpf injected with either Ctrl MO, Pcmt/l MO or Pcmt/l MO together with rescue plasmids, were incubated in 20 mM PTZ for 5 or 30 minutes at 28.5°C. They were then immobilized in 1.3% low melting agarose in 0.3 × Danieau's without methylene blue on a glass bottom dish (MatTek, MA, USA) and covered with Danieau's supplemented with 20 mM PTZ to avoid dryness of the gel. The immobilized larvae were positioned on the Nikon stereomicroscope SMZ25 and imaged for 15 or 30 minutes using a Nikon SHR Plan Apo 2× WD:60 lens and illuminated by an epi-fluorescence light source with a GFP-B filter cube. Images were acquired at 2 Hz (500 msec exposure time), 640×512 resolution, 8 Bit depth, and 5× zoom. The mean fluorescence intensity (F) of the brain over time was analysed using the Fiji software (SCHINDELIN *et al.* 2012) and expressed as F/F_0, where F_0 corresponds to the 35^{th} percentile of the acquired signal.

2.2.5.8 Tectal field potential recording

Larvae at 4dpf were immersed in 2% low melting agarose in artificial cerebrospinal fluid (ACSF - 124 mM NaCl, 2 mM KCl, 2 mM $MgSO_4$, 2 mM $CaCl_2$, 1.25 mM KH_2PO_4, 26 mM $NaHCO_3$ and 10 mM glucose). A glass electrode, filled with ACSF and connected to a high-impedance amplifier, was inserted into the optic tectum of the larval brain. Electrode resistance was set between 2–9 MΩ. Recordings were performed in current clamp mode with the following parameters: low-pass filtered at 1 kHz, high-pass filtered at 1 Hz, digital gain 10 and sampling interval 10 µs (MultiClamp 700B amplifier, Digidata 1550A digitizer, both Axon instruments, USA). Each recording was done for 10 minutes. Spontaneous epileptiform events were taken into account when the amplitude exceeded three times the background noise. The analysis of spikes was carried out using the Clampfit 10.2 software (Molecular Devices Corporation, USA).

2.2.5.9 Statistical analysis

All statistical analyses were done using the GraphPad Prism 5 software version 5.04 applying two-tailed, unpaired Student's t-test in case of comparing two data sets or ANOVA for comparison of more than two data sets.

3 Results

3.1 Establishment of *PCMT*-deficient models to study

3.1.1 *PCMT1* knockdown in HEK293 and U-87 MG cells

The insulin/IGF-1 signalling pathway (hereafter simply designated IGF-1 pathway) is highly conserved among species and one of the major regulators of aging (KENYON *et al.* 1993). Interestingly, phosphorylation levels of intermediates in the IGF-1 pathway (including Akt and GSK3β) were found to be higher in the brains of *Pcmt1* knockout mice (FARRAR *et al.* 2005a). One of our aims was to elucidate the mechanism by which *Pcmt1* deficiency affects the phosphorylation levels in IGF-1 pathway intermediates. Since the highest expression of *Pcmt1* is found in the brain, we started using U-87 MG and HEK293, which are brain and kidney derived human cell lines, respectively. Although HEK293 cells are not derived from brain, they have been reported to express neuronal markers for example neurofilament (NF) subunits NF-L, NF-M and NF-H (SHAW *et al.* 2002). Moreover, phosphorylation levels of c-Raf, Erk1/2 and MEK, intermediates of the mitogen-activated protein kinase (MAPK) pathway, were found to be higher in *PCMT1* knockdown HEK293 cells (KOSUGI *et al.* 2008) suggesting that this cell line might be appropriate for studying effects of *PCMT1* deficiency on other signalling pathways as well. We decided to use lentivirus mediated integration of shRNA to knock down *PCMT1* in the chosen cell lines since it could potentially result in more efficient gene silencing and allow for creation of more easy to handle stable knockdown cell lines as compared to transient transfection with siRNAs.

3.1.1.1 shRNA design and knockdown efficiency test

As described in the methods (Section 2.2.4.2), lentiviral delivery of shRNA was used to knock down the expression of *PCMT1* in both the HEK293 and U-87 MG cell lines. shRNA target regions in the *PCMT1* coding sequence were identified using the freely available BLOCK-iT™ RNAi Designer web tool from ThermoFisher. The designer tool returned eight target regions and ranked them according to their knockdown probability (Table 3-1). We chose three target sequences (#2, #4 and #8 in Table 3-1) and designated them shRNA1, shRNA2 and shRNA3. The decision was based on the fact that #4 and #8 had the highest score, and #2 was chosen randomly. Simultaneously, a scrambled shRNA sequence was designed by shuffling the sequence of shRNA1. This control shRNA (designated below shCtrl) doesn't target any transcript encoded by the human genome.

These four shRNAs were independently inserted into the pENTR™/U6 vector to be expressed under the control of the U6 promoter. A transient transfection approach was then used to test the

knockdown efficiency of the different shRNAs in both the HEK293 and U-87 MG cell lines. Cells were maintained under standard conditions and harvested for RNA extraction 48 hours after transfection. *PCMT1* transcript levels were measured by qPCR, the β-actin gene (*ACTB*) being used as the reference gene for normalisation. Cells expressing the control shRNA showed the same levels of *PCMT1* transcript as non-transfected cells (data not show). Cells expressing either of the three *PCMT1* targeting shRNAs showed a reduction in *PCMT1* transcript levels (Figure 3-1) with knockdown efficiencies of 52%, 59% and 35% (HEK293 cells) and 63%, 56% and 47% (U-87 MG cells) for shRNA1, shRNA2, and shRNA3, respectively. Based on these results, we decided to use shRNA2 (hereafter designated shPCMT) for subsequent experiments.

Table 3-1: Different shRNA target regions in the PCMT1 transcript and their rank according to knockdown probabilities. The yellow highlighted sequences were tested for PCMT1 knockdown efficiency.

No.	Start (bp)	Target sequence (DNA)	GC%	Rank	Name
1	33	GGAGCTAATCCACAATCTCCG	52.39	★★★☆☆	
2	342	GCTAGTAGATGACTCAGTAAA	38.1	★★★★☆	shRNA1
3	501	GGCGCTAATAGATCAGTTAAA	38.1	★★★★☆	
4	502	GCGCTAATAGATCAGTTAAAG	38.1	★★★★★	shRNA2
5	573	GTTGGAGCAGTATGACAAGCT	47.62	★★★☆☆	
6	576	GGAGCAGTATGACAAGCTACA	47.62	★★★★☆	
7	577	GAGCAGTATGACAAGCTACAA	42.86	★★★☆☆	
8	579	GCAGTATGACAAGCTACAAGA	42.86	★★★★★	shRNA3
		GAGAAGACATCGTACTGTAAT	38.1		shCtrl

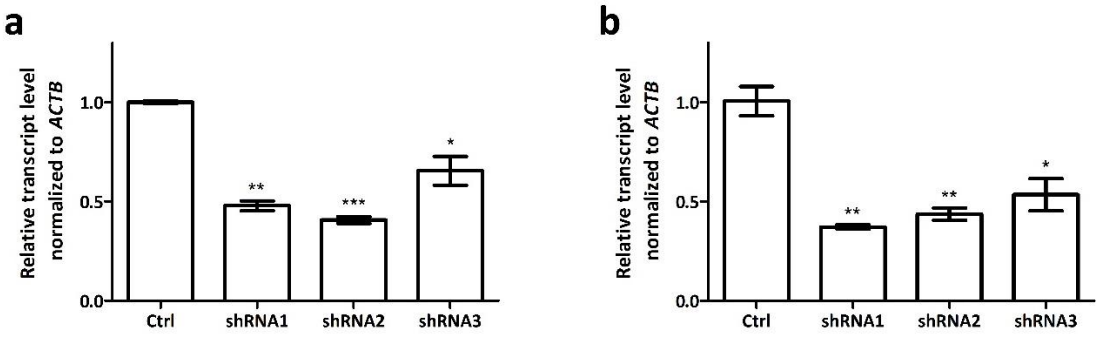

Figure 3-1: Relative PCMT1 transcript levels determined by qPCR following transient knockdown in HEK293 (a) and U-87 MG (b) cells by transfection with plasmids for transient expression of different shRNAs against PCMT1 (Ctrl, non-targeting scrambled shRNA). The values shown are mean ± SEM of 3 biological replicates. The statistical significance of the differences between Ctrl and PCMT1 targeting shRNAs was estimated using a Student t-test (p-value < 0.05, ** p-value < 0.01, *** p-value < 0.001).*

3.1.1.2 Generation of a stable PCMT1 knockdown cell lines

For stable integration of the shRNA into the genome of the target cells, we first had to produce lentiviral particles carrying the shRNA sequence. Recombinant lentivirus production was performed as described in details in the methods (Section 2.2.4.2) in HEK293FT cells, after transfection of the cells with ViraPower plasmids provided with the kit along with the pLenti6/BLOCK-iT™ expression plasmid carrying the sequence of either shCtrl or shPCMT1. Viral particles were purified, concentrated, and used for stable integration of shCtrl or shPCMT into the genome of HEK293 and U-87 MG cells. Stable cell lines were selected based on blasticidin resistance and tested further. As for the transient shRNA expression trials, we estimated the *PCMT1* expression levels in blasticidin resistant cell lines stably expressing shCtrl or shPCMT through qPCR. Results showed that *PCMT1* expression was reduced to 30% and 20% in the stable knockdown HEK293 and U-87 MG cell lines, respectively, by the PCMT1 targeting shRNA as compared to cell lines stably expressing shCtrl (Figure 3-2). The knockdown efficiency is clearly stronger in the stable cell lines as after transient expression of the shRNA. This difference in knockdown efficiency between transient and stable expression of shRNA could be due to two reasons. The first is the plasmid dilution taking place in transient expression during cell division, where shRNA copy number gets diluted with every cell division, whereas in the stable cell lines the genome integrated shRNA is duplicated with each cell division. The second reason may be that in transient expression we estimated the knockdown efficiency in a heterogeneous population of cells, where some might have had low levels of the shRNA, while for the stable cell lines, generated from single clones each, homogenous cell populations are analysed in which each cell in principle expresses similar levels of the shRNA.

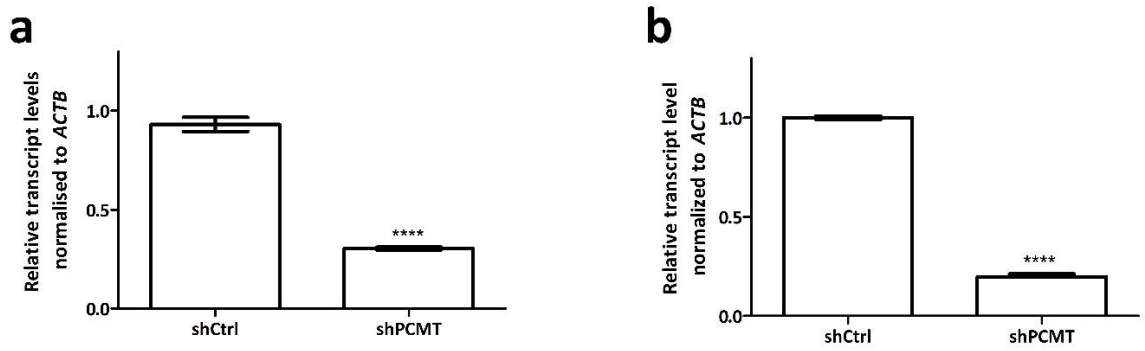

*Figure 3-2: Relative PCMT1 transcript levels in HEK293 (a) or U-87 MG (b) cell lines stably expressing non-targeting control shRNA (shCtrl) or PCMT1-targeting shRNA (shPCMT) after lentiviral transduction and selection by blasticidin. The values shown are mean ± SEM of 3 biological replicates The values shown are means ± SEM of 3 biological replicates (**** p-value < 0.0001).*

We further determined the PCMT1 knockdown efficiency in the two stable cell lines at the protein level. We seeded cells expressing shCtrl or shPCMT in a 6-well plate and kept it for 24 hours under

standard conditions followed by protein extraction in SDS sample buffer. Protein samples were resolved with 12% SDS-PAGE denaturation gel and blotted onto a PVDF membrane. We used two primary antibodies (Table 2-1) for protein quantification: an anti-PCMT1 antibody (from Abcam; polyclonal antibody raised against a recombinant fragment, corresponding to amino acids 1-197 of human PCMT1 (NP_005380)) and an anti-β-Actin antibody (13E5; from Cell Signalling) for loading control.

The Western blot analysis clearly showed a decrease of PCMT1 protein in both knockdown cell lines (Figure 3-3 a). Comparison of relative band intensities (PCMT1/ACTB) using the Imagej software revealed a decrease in PCMT1 protein levels of 80% and 62% in knockdown HEK293 and U-87 MG cells, respectively, compared to control cells (Figure 3-3 b & c). Intriguingly, the transcript and protein levels variations in HEK293 and U-87 MG cells were inconsistent. On the one hand, *PCMT1* transcript levels were higher in HEK293 cells than in U-87 MG cells (Figure 3-2). On the other hand, PCMT1 protein levels were lower in HEK293 cells than in U-87 MG cells (Figure 3-3 b & c). These results suggested either a more efficient translational machinery or higher protein stability in the U-87 MG cells.

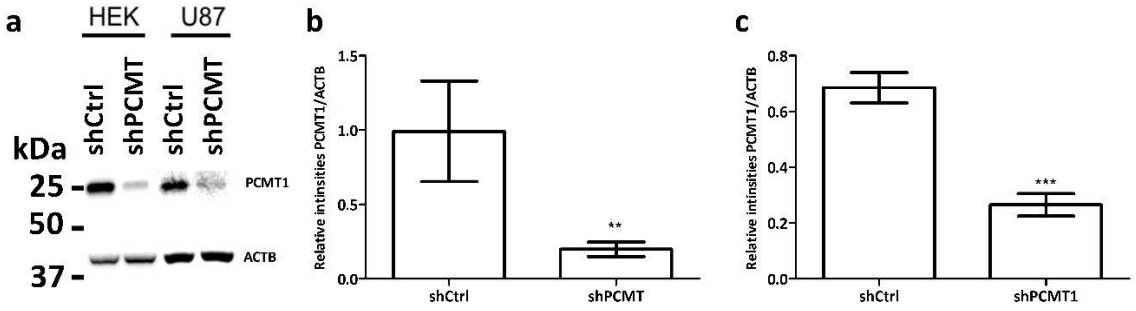

*Figure 3-3: PCMT1 protein levels in HEK293 and U-87 MG cells stably expressing shPCMT. Western blot analysis of protein extracts from HEK293 and U-87 MG cells (a). Quantitative analysis of PCMT1 protein levels in HEK293 (b) and U-87 MG (c) cells. The values shown are means ± SEM of 6 biological replicates (** p-value < 0.01, *** p-value < 0.001).*

3.1.1.3 Isoaspartyl methyltransferase activity and isoaspartyl levels in stable PCMT1 knockdown cell lines

We assumed that lower PCMT1 protein levels in the cells expressing shPCMT would lead to a decrease of the activity of the enzyme and subsequent accumulation of the enzyme substrates, isoaspartyl-containing proteins. To validate this hypothesis, we assayed the isoaspartyl methyltransferase activity and isoaspartyl levels in protein extracts derived from the above described HEK293 and U-87 MG cell lines using a methanol vapour diffusion assay (PATANANAN *et al.* 2014). To determine the endogenous PCMT1 enzyme activity, we incubated protein extracts with the KASAisoDLAKY peptide as a substrate

and *S*-[^{3}H-methyl]adenosyl methionine ([^{3}H]SAM). KASAisoDLAKY is a nonapeptide of the following sequence (Lys-Ala-Ser-Ala-isoAsp-Leu-Ala-Lys-Tyr) where the middle amino acid is an L-isoaspartyl residue that serves as a methyl acceptor for the PCMT1 activity. In addition, for isoaspartyl level quantification, we incubated the protein extracts with recombinant human PCMT1 and [^{3}H]SAM. In both cases, the reactions were run for 2 hours at 37°C and stopped by adding NaOH. The base-labile [^{3}H]methanol released from the carboxymethyl ester bond on isoaspartyl residues was measured by the vapour diffusion assay described in the methods (Section 2.2.3.4) and illustrated in Figure 2-2.

In comparison to the control cells, the isoaspartyl methyltransferase activity levels were significantly reduced to 17% and 38% in the *PCMT1* knockdown HEK293 and U-87 MG cell lines, respectively (Figure 3-4a, c). This activity analysis is in perfect agreement with the knockdown efficiency at protein level (Figure 3-3). Furthermore, the impact of the lower PCMT1 protein and activity levels on isoaspartyl accumulation was determined in total protein extracts. Our results show only a slight increase of about 10% in isoaspartyl levels in both the HEK293 and U-87 MG cell lines (Figure 3-4b, d). These data suggest that the low residual PCMT1 activity levels in the PCMT1 knockdown cell lines are sufficient to repair the bulk of isoaspartyl residues forming under our cultivations conditions and therefore prevent an important isoaspartyl accumulation. Similarly, heterozygous *Pcmt1*$^{+/-}$ mice did not show a significant difference in isoaspartyl levels compared to wild type mice despite the fact that they have only 50% of the enzyme activity (KIM *et al.* 1997b; YAMAMOTO *et al.* 1998). Given this very moderate effect on isoaspartyl levels by the partial *PCMT1* deficiency in our stable HEK293 and U-87 MG knockdown cell lines, we decided to apply the more recently established CRISPR/Cas9 technology to try to achieve a full knockout of PCMT activity in another cell line.

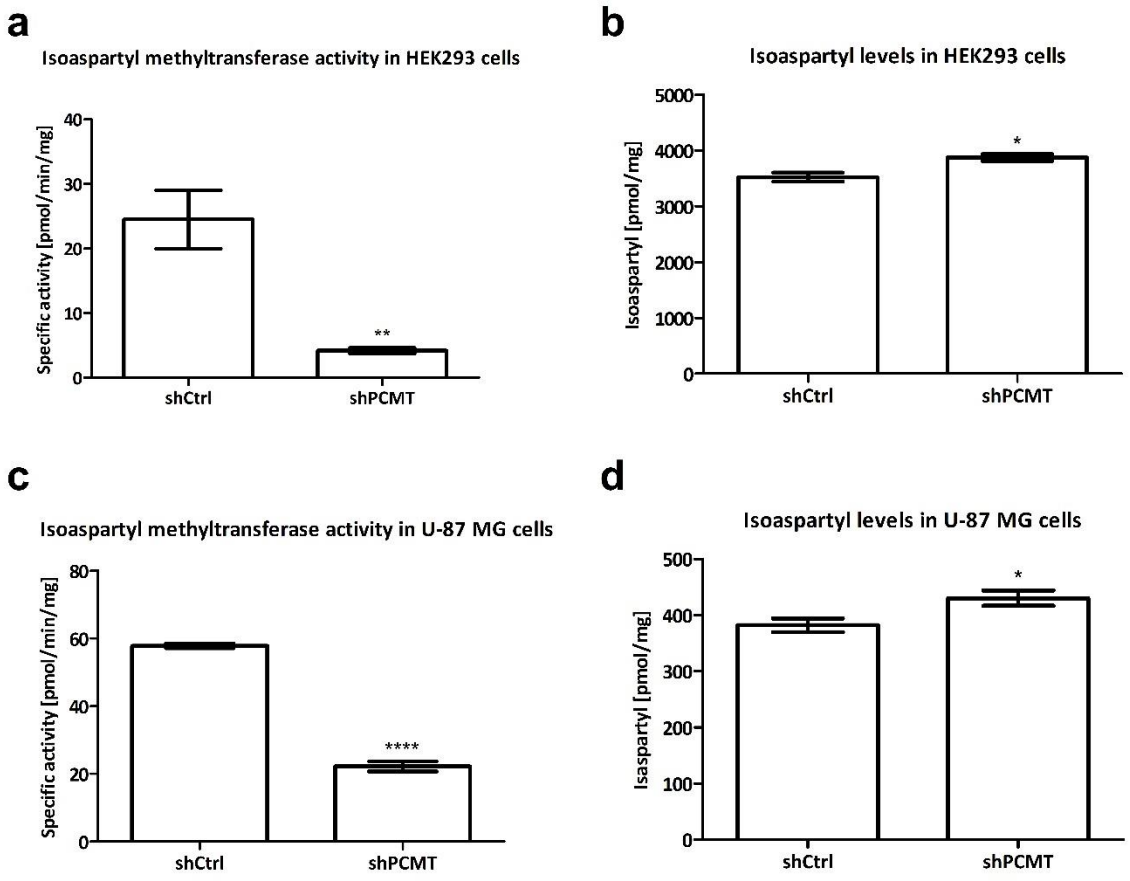

*Figure 3-4: Isoaspartyl methyltransferase activity and isoaspartyl levels in HEK293 (a, b) and U-87 MG (c, d) PCMT1 knockdown cells. The methanol vapour diffusion assay was used for quantification of the isoaspartyl methyltransferase activity as well as isoaspartyl levels in protein extracts derived from the cells. The values shown are means ± SEM of 4 biological replicates (*p-value < 0.05, **p-value < 0.01, **** p-value < 0.0001).*

3.1.2 *Pcmt1* knockout in mouse hippocampal HT22 cells

In *Pcmt1* knockout mice, immunostaining of phosphorylated Akt showed most pronounced elevations in phosphorylation levels specifically in the hippocampus region of the brain (FARRAR *et al.* 2005a). We decided therefore not only to use CRISPR/Cas9 technology to knock out *Pcmt1* (instead of only knocking down by shRNA), but to also switch from HEK293 and U-97 MG cells to HT22 cells, which have been derived from immortalized murine hippocampal cells (LIU *et al.* 2009).

3.1.2.1 CRISPR/Cas9 mediated knockout of Pcmt1

We designed two guide RNAs (gRNAs) to specifically target the Cas9 nuclease towards two sites in the *Pcmt1* gene, distant of 40 bp, to induce double strand breaks (DSB). The expected deletion would be expected to either interfere with mRNA splicing and maturation or lead to frameshift mutation and in both cases this would lead to early stop codon and truncated protein. We cloned these two gRNAs into the pX459 plasmid carrying a puromycin resistance gene, as described in the methods section

(2.2.4.3), and transfected the recombinant plasmid into the HT22 cells. In parallel, we also transfected cells with the same plasmid expressing a scrambled gRNA as control (scrambled gRNA was generated by shuffling gRNA1 sequence; see section 2.2.2.9.6). Puromycin-resistant cells were seeded in 96-well plates at a density of 1 cell/well for clonal selection. After one week of incubation, we selected 10 clones from cells transfected with *Pcmt1* gRNAs and 3 clones from cells transfected with scrambled gRNA for validation of *Pcmt1* gene mutation.

A PCR-based approach was performed using primers pairs surrounding the expected deletion region (Table 2-6). The expected amplicon size corresponded to 155 bp for the control HT22 cells and 115 bp for cells carrying the correct deletion. While clones 1 – 9 showed only the smaller amplicon, clone number 10 showed two amplicons (expected 115 bp amplicon and a second one that is smaller than the wild type amplicon, but bigger than the mutated one (Figure 3-5a)). The clone number 10 thus did not seem to be a heterozygous cell line (one wild-type and one mutated *Pcmt1* allele), but the indel mutation might have led, in one of the alleles, to the introduction of extra nucleotides between the two DSBs by the repair machinery that performs the nonhomologous end joining (NHEJ) and which is prone to mistakes. We randomly selected three of the positive clones (C3, C6 and C7) for further experiments and the data shown hereafter are from clone number C6 (designated *Pcmt1* knockout from here on).

Similarly, as for the knockdown in HEK293 and U-87 MG cell lines, we next determine the knockout efficiency at both mRNA and protein levels in the selected *Pcmt1* knockout HT22 line. Using qPCR, we found an 82% decrease in the transcript in the *Pcmt1* knockout line compared to the control line (Figure 3-5b). This difference could be explained by a decrease of the transcription of edited *Pcmt1* gene or a lower stability of the corresponding mRNA. As mentioned previously, the 40-bp deletion is predicted to lead to a premature stop codon in the transcript. Thus we may assume that the nonsense-mediated decay mechanism (BAKER and PARKER 2004), which could take place when translational termination is in close proximity to the initiation site, is more pronounced for *Pcmt1* carrying the 40-bp deletion. The difference in expression was even more striking at the protein level. After protein separation by SDS-PAGE, Western blot analysis showed that the PCMT1 protein was not detectable in the knockout cells even though, the anti-PCMT1 antibody used was raised against the first 197 amino acids which are not before the DSB induced by CRISPR/Cas9 (Figure 3-5c). We thus concluded that our CRISPR/Cas9 strategy had allowed for the creation of an HT22 cell line with a complete knockout of *Pcmt1* expression, in which the low but detectable residual *Pcmt1* transcripts were not translated into Pcmt1 protein levels detectable by Western blot.

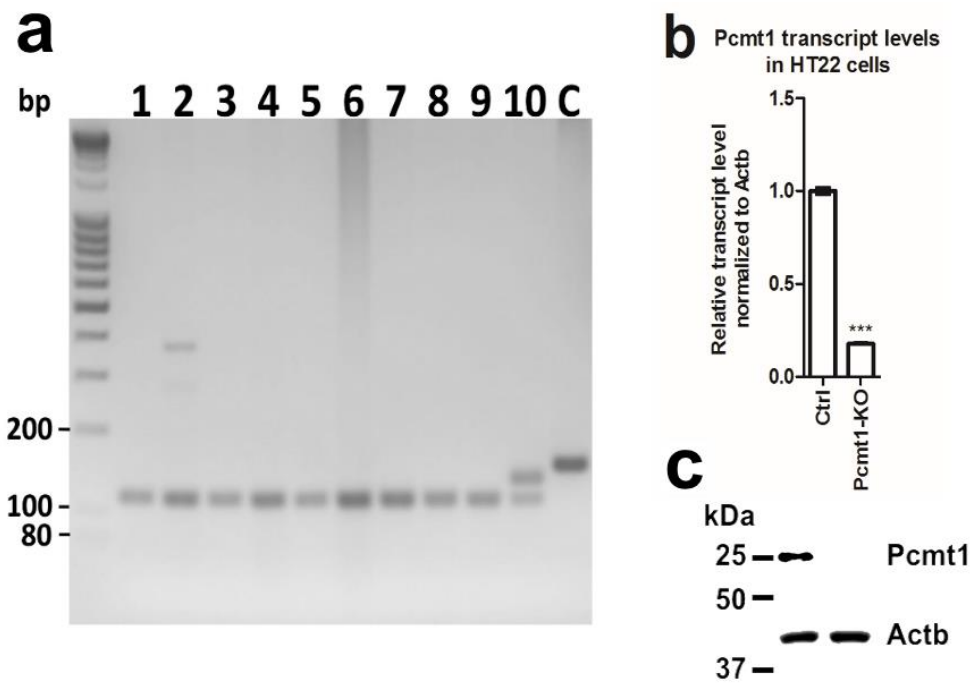

*Figure 3-5: Pcmt1 knockout in HT22 cells. (a) PCR amplicons of genomic Pcmt1 from different CRISPR/Cas9 edited HT22 cell lines analysed on a 3% agarose gel. Ten clones were tested (1 – 10) in addition to control cells (C) transfected with a scrambled gRNA. Wild type amplicon is 155 bp while CRISPR/Cas9 mutant amplicon is 115 bp (b) Pcmt1 transcript level in Pcmt1 knockout HT22 cells relative to control cells as determined by qPCR. The values shown are means ± SEM of 3 biological replicates (*** p = 0.0005) (c) Pcmt1 protein levels in control and Pcmt1 knockout HT22 cells analysed by Western blot.*

3.1.2.2 Isoaspartyl methyltransferase activity and isoaspartyl levels in Pcmt1 knockout HT22 cells

We then also investigated the impact of the *Pcmt1* deletion on both the isoaspartyl methyltransferase activity and isoaspartyl levels in protein extracts derived from the *Pcmt1* knockout HT22 cells, using the methanol vapour diffusion assay described above. Cells were seeded in 6-well plates and incubated for two days under standard cultivation conditions. Consistent with the total lack of Pcmt1 protein in the *Pcmt1* knockout cells, no residual isoaspartyl methyltransferase activity was detected (Figure 3-6). Moreover, we found that the proteins in the *Pcmt1* knockout cells contained significantly more isoaspartyl residues than the control cells. By comparison to the *PCMT1* knockdown HEK293 or U87 cell lines, there was a higher accumulation of damaged proteins containing isoaspartyl residues in the *Pcmt1* knockout HT22 cell line (1.1-fold increase in both the HEK293 or U87 knockdown cells compared to control cells *versus* 1.6-fold increase in the HT22 knockout cells compared to control cells). For further comparison, it has been reported previously that *Pcmt1* knockout mice accumulate 4- to 8-fold higher isoaspartyl levels in various tissues than control mice. But it was also shown that this accumulation is age-dependent, with a 2.7-fold increase of isoaspartyl levels in proteins extracted

from red blood cells taken from *Pcmt1* knockout mice at the age of 24 or 59 days (KIM *et al.* 1997b). In addition, isoaspartyl levels were found also to increase in response to oxidative stress. Isoaspartyl levels increased in membrane proteins of human erythrocytes under oxidative stress due to exposure to *t*-butyl hydroperoxide and H_2O_2 (INGROSSO *et al.* 2000). It is therefore possible that higher isoaspartyl accumulations can be reached in our HT22 *Pcmt1* knockout cell line after more prolonged cultivation times (aging) or following exposure to certain stress conditions. In any case, given the complete absence of isoaspartyl methyltransferase activity in a cell line of a relevant type (hippocampal origin), we concluded that we had now created a promising tool to mimic the effects of *Pcmt1* knockout on growth signalling pathways previously observed in the hippocampus of *Pcmt1* knockout mice.

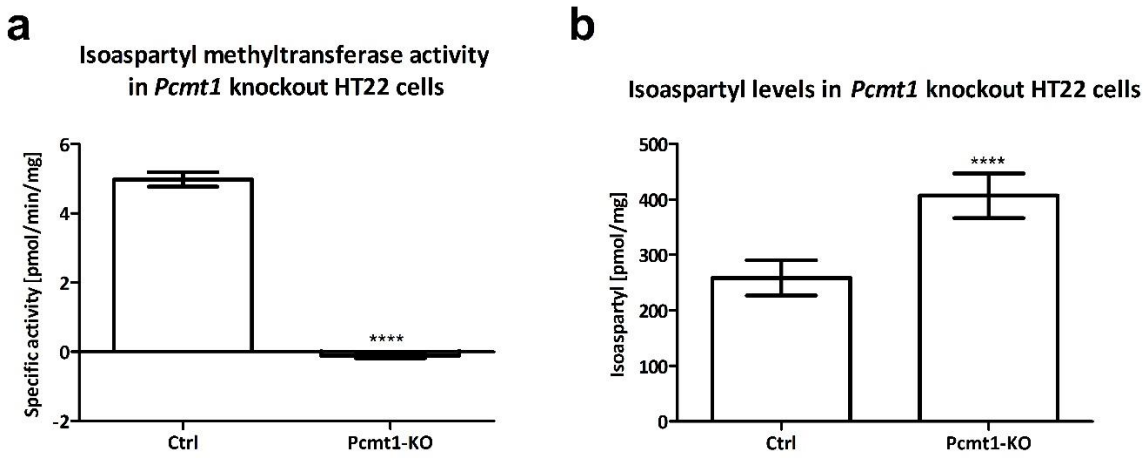

*Figure 3-6: Isoaspartyl methyltransferase activity and isoaspartyl levels in protein extracts of Pcmt1 knockout cells. The values shown are means ± SEM of 6 biological replicates (**** $p < 0.0001$).*

3.1.3 *PCMT* knockdown in zebrafish

Pcmt1 knockout mice die prematurely due to fatal epileptic seizures (KIM *et al.* 1997b), however, the mechanism underlying the connection between seizure development and *Pcmt1* function is not known. Zebrafish is used as a model organism to investigate neurological disorders, including epilepsy (BARABAN 2007; MARTIN-JIMENEZ *et al.* 2015). As the zebrafish model enables *in vivo* imaging of the brain, is amenable to high-throughput approaches (ZON and PETERSON 2005) and is for a number of aspects more convenient and easy to handle than the mouse model (Section 1.4.2), we aimed at developing a zebrafish model with PCMT deficiency to further study the physiological relevance of the isoaspartyl repair mechanism and more particularly its apparent role in seizure development.

A BLASTp search using the human PCMT1 protein sequence (Accession: AAH07501.1) as query against *D. rerio* (taxid: 7955) and using default parameters (ALTSCHUL *et al.* 1997; ALTSCHUL *et al.* 2005) revealed 5 hits (Table 3-2). Three out of the five protein hits had less than 50% query cover and were excluded.

They only shared similarity with the human protein in the methyltransferase domains, which suggested that they are methyltransferase enzymes but not specifically related to the isoaspartyl methyltransferase family. The other two matches correspond to the expression products of the zebrafish *pcmt* and *pcmtl* genes, annotated as L-isoaspartyl methyltransferases based on the high sequence similarity with established isoaspartyl methyltransferases. Pcmt and Pcmtl are paralogs, resulting from an ancient genome duplication event in teleost fishes (TAYLOR *et al.* 2001), and the share 85% and 69% amino acid sequence identity, respectively, with the human PCMT1 protein. To see the sequence similarity between the three homologues as well as the mouse one, since we are also using a mouse derived cells line, a multiple sequence alignment performed with the CLUSTAL Omega software version 1.2.4 (SIEVERS *et al.* 2011) using default settings. The alignment (Figure 3-7) showed that the SAM-dependent methyltransferase domains, AdoMet I – III, as well as isoaspartyl methyltransferase domains, pre-I and post-III, highlighted in yellow in Figure 3-7 are well conserved between the four sequences as well as amino acid residues found to directly interact with *S*-adenosylhomocysteine from crystal structure data (PDB: 1I1N) (KAGAN and CLARKE 1994; KAGAN *et al.* 1997; SMITH *et al.* 2002).

Table 3-2: Blastp results from searching for homologs of human PCMT1 in zebrafish.

Description	Query cover	E value	Ident	Accession
protein-L-isoaspartate(D-aspartate) O-methyltransferase [*Danio rerio*]	100%	5.19E-151	85%	NP_571540.1
l-isoaspartyl protein carboxyl methyltransferase, like [*Danio rerio*]	100%	4.22E-117	69%	NP_957062.1
Select seq ref|XP_017206506.1| PREDICTED: uncharacterized protein LOC767695 isoform X1 [*Danio rerio*]	45%	0.003	32%	XP_017206506.1
Select seq ref|NP_001070101.1| uncharacterized protein LOC767695 [*Danio rerio*]	45%	0.004	32%	NP_001070101.1
Zgc:153372 [*Danio rerio*]	20%	0.004	43%	AAI52084.1

*Figure 3-7: Sequence alignment of the human PCMT1, mouse Pcmt1 and their two homologs from zebrafish Pcmt and Pcmtl. Residues highlighted in yellow are conserved methyltransferase domains; AdoMet I – III are SAM specific domains and pre-I and post-III are isoaspartyl methyltransferase-specific domains (KAGAN et al. 1997). Residues in red were found from crystallography data to be directly interacting with S-adenosylhomocysteine (SMITH et al. 2002). An * (asterisk) indicates positions which have a single, fully conserved residue. A : (colon) indicates conservation between groups of strongly similar properties. A . (period) indicates conservation between groups of weakly similar properties.*

3.1.3.1 Biochemical properties of the zebrafish Pcmt and Pcmtl proteins

Gene duplication is a powerful tool to the acquisition of new function. In 1970, Susumu Ohno has presented a new classical view of the evolution of duplicated genes: whereas one gene must conserve the function, the second one may acquire mutations, either in the coding or non-coding regions, that have the potential to lead to dosage compensation, sub- or neo-functionalization (CONANT and WOLFE 2008). Pcmt and Pcmtl, arising from the genome duplication of the ancestor of teleost fishes, both share high sequence identity with human and mouse PCMT, with virtually total conservation in the SAM methyltransferase domains as well as the more isoaspartyl methyltransferase specific domains pre-I and post-III (Figure 3-7). Based on this sequence analysis, both Pcmt and Pcmtl thus qualified has highly likely ortholog candidates of the mammalian PCMT1 protein. As even single amino acid changes in protein sequences can critically affect protein function, however, predictions based on sequence similarity should never be taken as granted and need to be verified experimentally. In our case, to determine if we had to focus on the *pcmt* or the *pcmtl* gene or both for the establishment of our PCMT deficient zebrafish model, we first aimed at answering the following two questions: (i) do Pcmt and/or Pcmtl catalyse the same enzymatic reaction as their human homologue and (ii) if yes, do the kinetic

properties vary significantly between human PCMT1 and zebrafish Pcmt and Pcmtl? A second aspect, that we analysed in a second stage, was a comparison of the expression properties of the *pcmt* and *pcmtl* genes, both in time (when during development?) and in space (in which tissues?).

3.1.3.1.1 Pcmt and Pcmtl recombinant protein expression and purification

To answer the first two questions regarding the catalytic function of Pcmt and Pcmtl, we expressed both enzymes in *E. coli* for subsequent purification and *in vitro* enzymatic characterization. After cloning of the coding sequences of both proteins independently into pET100 plasmids downstream of a 6×His-tag sequence (Section 2.2.2.9.2), *E. coli* BL21(DE) cells were transformed with each plasmid and transformants were cultivated in LB medium supplemented with 50 µg/ml carbenicillin for selection. Protein expression was induced with 0.1 mM IPTG at 18°C for 10 hours. To purify the recombinantly expressed proteins, we lysed the cells by sonication and separated soluble proteins from cell debris and other insoluble material by centrifugation followed by a filtration step. The filtered supernatant was loaded onto a His-trap Ni^{2+} column for affinity purification of His-tagged proteins.

We started with the purification of Pcmtl. Following protein binding to the His-trap column, the latter was washed with 25 mM imidazole, to remove non-specifically bound proteins, followed by gradient elution with 25 – 300 mM imidazole over 20 minutes (Figure 3-8 b). Based on SDS-PAGE analysis we prepared two pools of fractions, the first corresponding to volumes 179 – 182 ml (contained higher Pcmtl amount) and the second corresponding to volumes 182 – 186 ml collected during the elution step (Figure 3-8 b&d). As the SDS-PAGE showed some remaining protein impurities in the peak elution fractions, we modified our strategy for the Pcmt purification by adding a second washing step in the aim of increasing the purity. After the protein binding step, we washed the column with 25 mM and 50 mM imidazole, followed by protein elution using a linear imidazole gradient (50 – 300 mM imidazole) over 20 ml (Figure 3-8 a). Based on SDS-PAGE analysis (Figure 3-8 c) we prepared two pools of fractions containing purified Pcmt, the first corresponding to the protein peak that eluted during the 50 mM imidazole wash and the second corresponding to the fractions eluted between volumes 129 – 136 ml during the imidazole gradient.

Following affinity purification, to desalt our purified enzyme pools we dialyzed them twice against a buffer containing 20 mM Tris pH 7.4, 25 mM NaCl and 20% glycerol and stored them in dialysis buffer at -20°C.

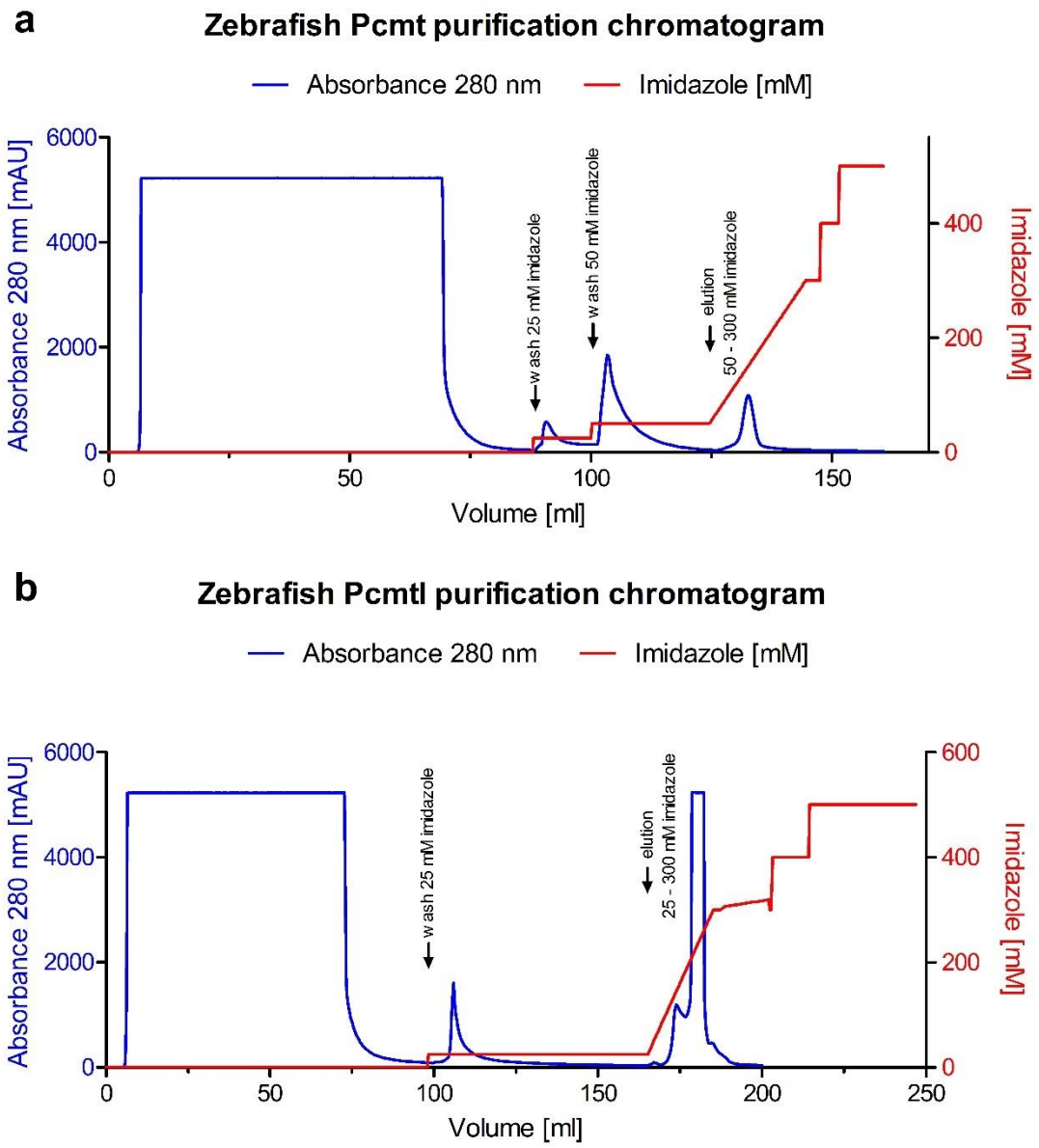
a
Zebrafish Pcmt purification chromatogram
Absorbance 280 nm
Imidazole [mM]
Absorbance 280 nm [mAU]
Imidazole [mM]
wash 25 mM imidazole
wash 50 mM imidazole
elution
50 - 300 mM imidazole
Volume [ml]
b
Zebrafish Pcmtl purification chromatogram
Absorbance 280 nm
Imidazole [mM]
Absorbance 280 nm [mAU]
Imidazole [mM]
wash 25 mM imidazole
elution
25 - 300 mM imidazole
Volume [ml]

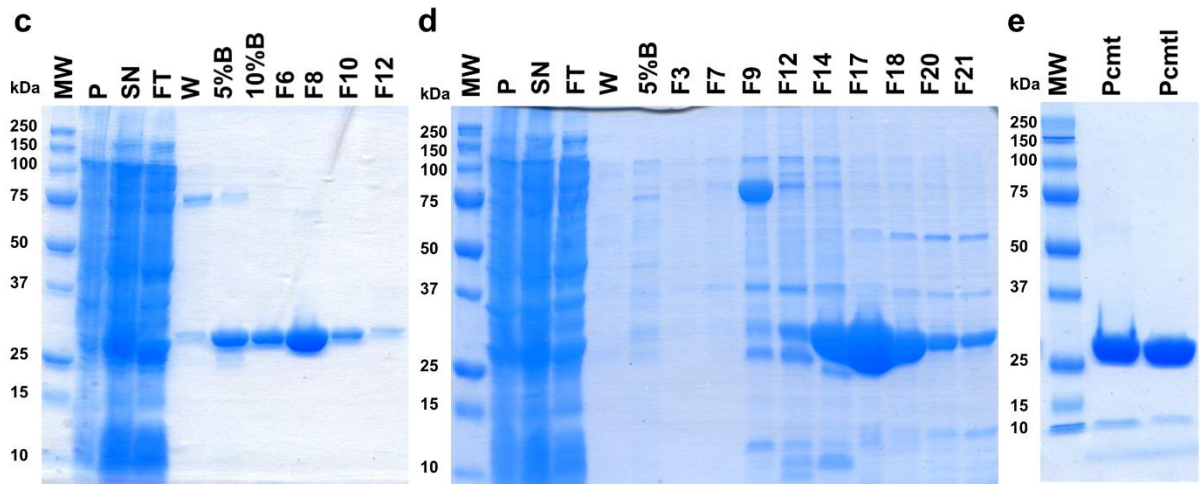
c
kDa
MW
P
SN
FT
W
5%B
10%B
F6
F8
F10
F12
d
kDa
MW
P
SN
FT
W
5%B
F3
F7
F9
F12
F14
F17
F18
F20
F21
e
kDa
MW
Pcmt
Pcmtl

Figure 3-8: Recombinant protein purification of N-terminally His-tagged Pcmt and Pcmtl. Chromatography profile for purification of zebrafish Pcmt (a) and Pcmtl (b) protein on nickel affinity column. Protein concentration was monitored spectrophotometrically by measuring the absorbance at 280 nm (blue line). Imidazole concentration was adjusted into the running buffer for washing and elution of His-tagged protein (red line). (c and d) SDS-PAGE analysis of samples collected during the purification MW: molecular weight markers; P: pellet; SN: supernatant FT: flow through; W: wash; %B: buffer B percentage used for extra washing steps; F6, F8, F10, F12 in (c) fractions collected during gradient elution corresponding to volumes 130, 132, 134 ml in chromatogram (a), respectively; F3, F7, F9, F12, F14, F18, F20, F21 in (d) corresponds to volumes 167, 171, 173, 176, 178, 181, 182, 184, 185 ml in chromatogram (b), respectively.

As can be deduced from the chromatograms and SDS-PAGE analyses shown in Figure 3-8, the second purification strategy (for Pcmt) was not necessarily more successful than the first one (for Pcmtl), His-tagged Pcmt protein eluting already during the washing steps at the increased imidazole concentrations. Nevertheless, after affinity purification and desalting, SDS-PAGE analysis of the desalted protein pools showed that we had obtained highly homogenous protein preparations of both enzymes (Figure 3-8e), with a total protein yield of 24 mg and 55 mg of purified Pcmt and Pcmtl, respectively.

3.1.3.1.2 Catalytic activity of Pcmt and Pcmtl

We used the purified recombinant Pcmt and Pcmtl proteins for *in vitro* enzymatic characterization using the methanol vapour diffusion assay (Section 2.2.3.4). Briefly, we incubated 0.5 µg of either enzyme with different concentrations (0.2 – 60 µM) of an isoaspartyl-containing peptide (KASAisoDLAKY) and radiolabelled [^{3}H]-*S*-adenosyl methionine [^{3}H]-SAM in a total volume of 50 µl. The assay was in an 'end-point' format with the reaction being stopped after 7, 14 and 21 minutes after incubation at 30°C. The [^{3}H]-methanol released from the methylated isoaspartyl-containing peptide during incubation at basic pH was measured via the vapour diffusion assay and initial velocities were determined by the rate of [^{3}H]-methanol formation over time. The determined initial velocities were plotted against the substrate concentration and the data were fitted to the Michaelis-Menten kinetics model was used to determine the Michaelis-Menten constant (K_M) and maximum velocity (V_{max}) and thereby evaluate the substrate affinity, turnover number (k_{cat}) and catalytic efficiency (k_{cat}/K_M) of Pcmt and Pcmtl.

Our results showed that both Pcmt and Pcmtl catalyse the transfer of methyl group from the cofactor SAM to the isoaspartyl residue in the tested peptide substrate (Figure 3-9). Based on the K_M values (4.2 µM and 3.6 µM for Pcmt and Pcmtl, respectively) both enzymes show a high substrate affinity. This substrate affinity was intermediate compared to isoaspartyl methyltransferase enzymes from other species tested with the same substrate. It was higher compared to Pcmt from *A. thaliana* (K_M = 21 µM) and lower compared to PCMT1 from *H. sapiens* (K_M = 0.4 µM) (LOWENSON and CLARKE 1991;

THAPAR and CLARKE 2000). We found that the maximum velocity is about 1.5-fold higher for Pcmtl compared to Pcmt.

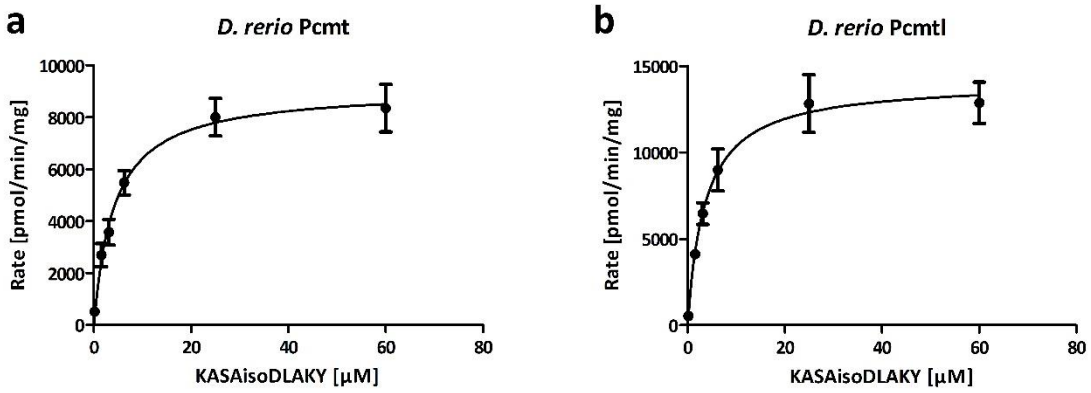

Figure 3-9: Substrate saturation curves for zebrafish Pcmt and Pcmtl. Each of the recombinant purified enzymes was incubated with different concentrations of the methyl acceptor substrate KASAisoDLAKY and initial reaction velocities were determined using methanol vapour diffusion assay. The values shown are mean ± SD of 3 biological replicates.

Table 3-3: Kinetic properties of Pcmt and Pcmtl using KASAisoDLAKY as a methyl acceptor. K_M and V_{max} values were determined from the data shown in Figure 3-9 using nonlinear regression curve fitting in GraphPad Prism 5.

	K_M [µM]	V_{max} [pmol/min/mg]	k_{cat} [s^{-1}]	k_{cat}/K_M [$M^{-1}s^{-1}$]
Pcmt	4.2 ± 0.51	9096 ± 313	4.30 ± 0.12 × 10^{-3}	1031
Pcmtl	3.6 ± 0.48	14112 ± 515	6.72 ± 0.25 × 10^{-3}	1845

3.1.3.2 pcmt and pcmtl expression and tissue distribution

We first compared the *pcmt* and *pcmtl* mRNA expression over time during early larval development using qPCR. We next used two approaches to determine the tissue localization of the *pcmt* and *pcmtl* transcripts: *in situ* hybridization in embryos and mRNA quantification by qPCR in different organs dissected from adult zebrafish.

3.1.3.2.1 *pcmt* and *pcmtl* expression during early development

To determine if both *pcmt* and *pcmtl* genes are expressed during early zebrafish development, total RNA was extracted from embryos/larvae collected at different stages: from 7 hours post fertilization (hpf) up to 6 days post fertilization (dpf). Using qPCR, we found that both *pcmt* and *pcmtl* transcripts were detectable as early as 7 hpf, the first time point tested (Figure 3-10). *Pcmtl* transcript levels were stable for the first 3 days and then doubled from the fourth day, while the *pcmt* transcript levels

showed (reproducibly) more variations during the first 3 days and then also started to stabilize at an overall higher level. This discrepancy between *pcmt* and *pcmtl* transcript levels could be due to differential transcription regulation or transcript stability.

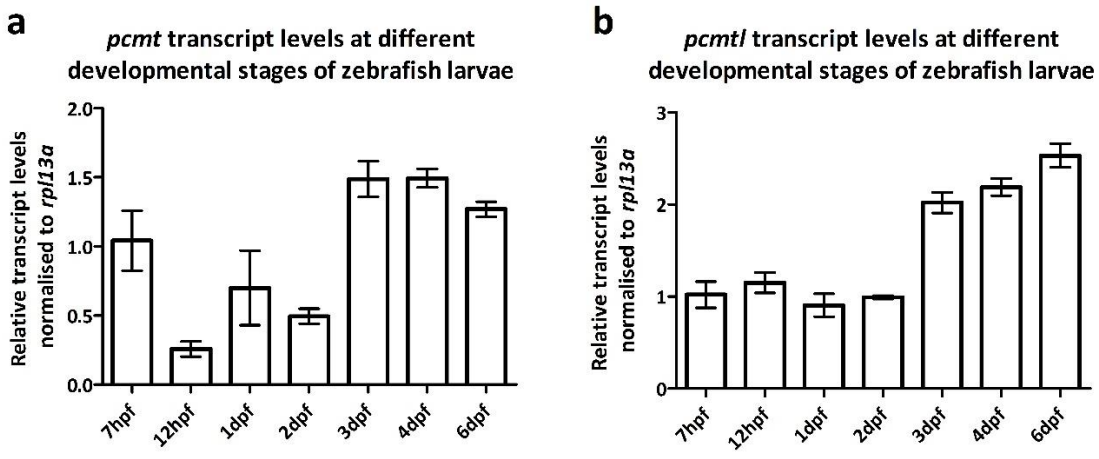

Figure 3-10: Pcmt and pcmtl transcript levels during early development of zebrafish as determined by qPCR (Relative fold changes compared to 7 hpf. The values shown are mean ± SEM of 3 biological replicates.

The dynamics observed for *pcmt* expression, where the transcript levels decreased at 12 hpf and start to increase again at 24 hpf were unusual. One possible explanation for the early drop in transcript level is that at the first time point there is still a high proportion of maternally transmitted mRNA, which then starts to decrease while the endogenous machinery is taking over for the transcript production. To test this hypothesis, we collected eggs directly after they were laid for yolk RNA extraction. RNA extraction was done as before and in parallel we also extracted RNA from fertilized eggs at 12 and 24 hpf followed by first strand cDNA synthesis. Agarose gel electrophoresis analysis showed the presence of both transcripts in the eggs confirming the transmission of maternal mRNA (Figure 3-11). Our results show that both pcmt and pcmtl are maternally transmitted and both genes are expressed during early stages of development. In addition, the results suggest an important role of *pcmt/l* during development since, at least in mice, isoaspartyl levels are low at young age and increase with age (KIM *et al.* 1997b). Therefore, the repair mechanism to limit isoaspartyl accumulation is unusable suggesting an alternative function during development.

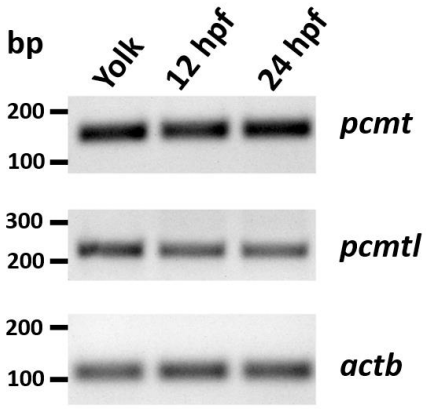

Figure 3-11: Agarose gel showing DNA fragments amplified from pcmt and pcmtl cDNA from zebrafish egg yolk, 12 hpf and 24 hpf embryos.

3.1.3.2.2 Tissue distribution of *pcmt* and *pcmtl* transcripts at embryonic stage

For tissue localization of both the *pcmt* and *pcmtl* transcripts at embryonic stage, we performed *in situ* hybridization as previously described (Section 2.2.5.5). We prepared sense and anti-sense RNA probes for both transcripts by *in vitro* transcription during which uridine bases were labelled with digoxigenin (DIG). The antisense probe should hybridize to endogenous transcript for visualization of the transcript localization, while the sense probe should not bind specifically and is used as a negative control. Embryos were collected at 1 dpf, fixed in 4% paraformaldehyde and incubated with either sense or antisense probes followed by immunodetection using anti-DIG antibody.

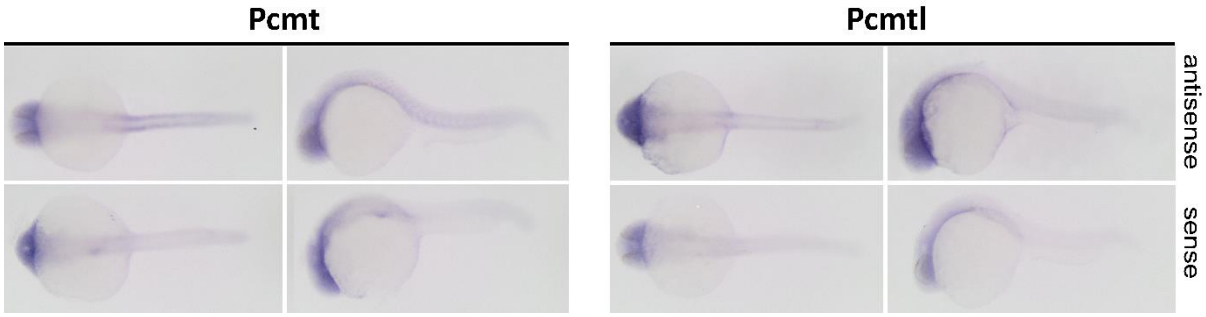

Figure 3-12: Tissue distribution analysis by in situ hybridization for pcmt and pcmtl transcripts in 1 dpf embryos.

Our results showed colour development over the whole embryos using the antisense probes with no preferential localization to specific tissues for either *pcmt* or *pcmtl* transcripts (Figure 3-12). Noticeably, a very slight difference between *pcmt* and *pcmtl* can be seen where the *pcmt* transcript showed higher levels in the trunk and tail while *pcmtl* transcript was more intense in the head region. The results suggest a ubiquitous expression of both genes in all tissue of the embryo, but the high background detected in the control samples (sense probe) renders the experiment somewhat inconclusive. Similar experiments done previously for *pcmtl* in a high-throughput analysis by Thisse,

B. and Thisse, C. also indicated that the transcript is not spatially restricted to a specific tissue in zebrafish at stages between 1-cell to 3 dpf (THISSE and THISSE 2004). Experiments in mice also showed that *Pcmt1* is ubiquitously expressed in all the tissue tested (DILIBERTO and AXELROD 1976; BOIVIN *et al.* 1995).

3.1.3.2.3 Tissue distribution of *pcmt* and *pcmtl* transcripts in adult zebrafish

Tissue-specific localization can also be estimated through gene expression analysis by qPCR in various cell types or organs. We dissected different organs (brain, heart, testes/ovaries, spleen, kidney and liver) from 2 year-old adult fish (n=3) for RNA extraction and subsequent *pcmt* and *pcmtl* transcript quantification through qPCR. All gene expression data were normalized to the eukaryotic elongation factor 1a (*eef1a*) housekeeping gene (TANG *et al.* 2007). Independently of the gender, we found the same trend for both the *pcmt* and *pcmtl* genes, with the highest expression levels being found in brain and testes/ovaries (Figure 3-13). The results are in good agreement with the tissue distribution found for *Pcmt1* in mice, which also showed ubiquitous expression, but higher expression levels in the brain and testes (KIM *et al.* 1997b; LOWENSON *et al.* 2001).

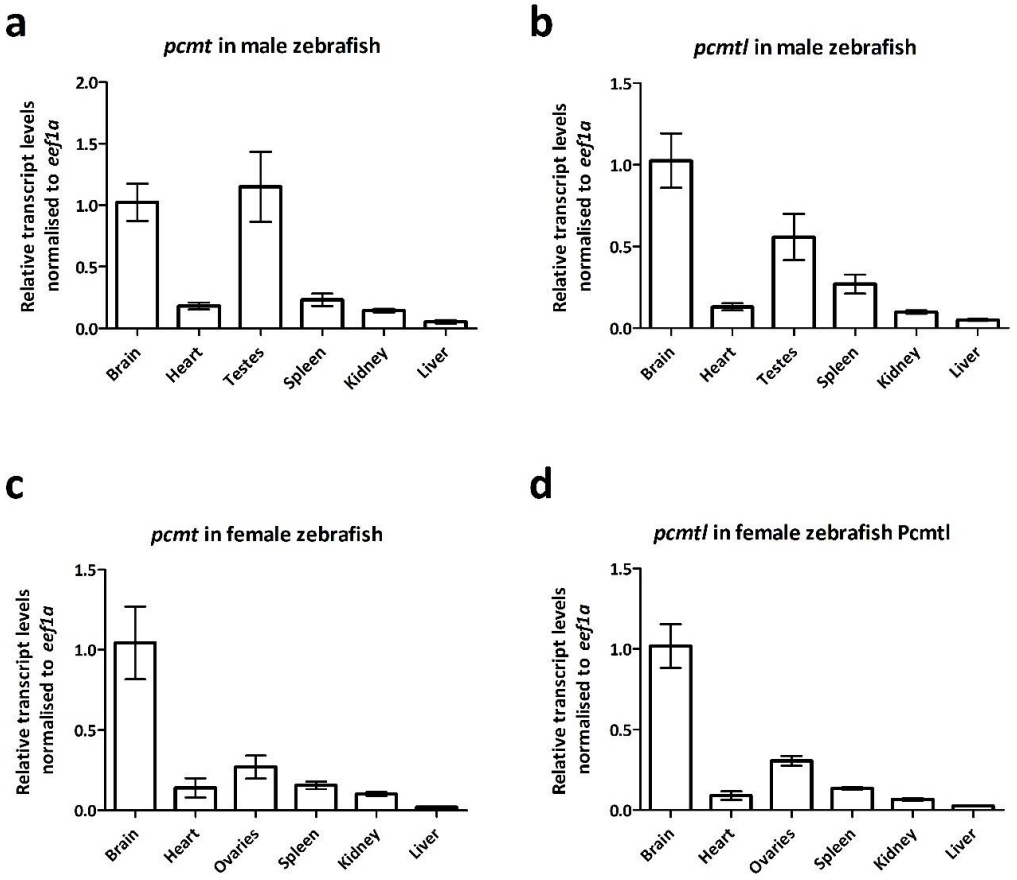

Figure 3-13: Pcmt and Pcmtl transcript levels determined by qPCR in different organs of 2-year old adult zebrafish. Relative fold changes compared to the expression levels in brain were determined. The values shown are mean ± SEM of 3 biological replicates.

All together, these results suggest that both Pcmt and Pcmtl conserved the same catalytic activity and similar expression patterns, suggesting that the two paralogue genes have not functionally diverged since the gene duplication event. In practical terms, this meant that both genes had to be targeted in zebrafish to achieve efficient knockdown of isoaspartyl methyltransferase function and investigate the *in vivo* impact of a deficiency in this function. The evolution of duplicated genes is still a hot topic in biology, especially in zebrafish (ZHONG *et al.* 2016), and could be investigated further for *pcmt* and *pcmtl* genes. However, this evolutionary aspect goes beyond the scope of this thesis.

3.1.3.3 Morpholino mediated knockdown of pcmt and pcmtl in zebrafish

3.1.3.3.1 Morpholino efficiency and toxicity testing

Morpholinos (MOs) are oligomers that are often used for gene expression knockdown in zebrafish (EKKER 2000; DRAPER *et al.* 2001). Five different MOs were designed by GeneTools LLC (Philomath, Oregon, USA) (Table 2-4): two specific to *pcmt* (*pcmt* i2e3 and *pcmt* e5i5), two specific to *pcmtl* (*pcmtl* e1i1 and *pcmtl* e4i4) and one scrambled sequence serving as control MO. The MOs designed for *pcmt* specifically target the intron2-exon3 (*pcmt* i2e3) and the exon5-intron5 junctions (*pcmt* e5i5). Similarly, MOs designed for *pcmtl* specifically target the exon1-intron1 (*pcmtl* e1i1) and the exon4-intron4 (*pcmtl* e4i4) junctions. As described previously, MOs binding at the intron-exon or at the exon-intron junctions should impair mRNA splicing leading to the loss of one exon and eventually to non-functional protein. Thus the efficiency of MOs can be estimated by PCR analysis at the cDNA level with primers located up- and downstream of the predicted skipped exon leading to a smaller amplicon due to the missing exon (Figure 3-14).

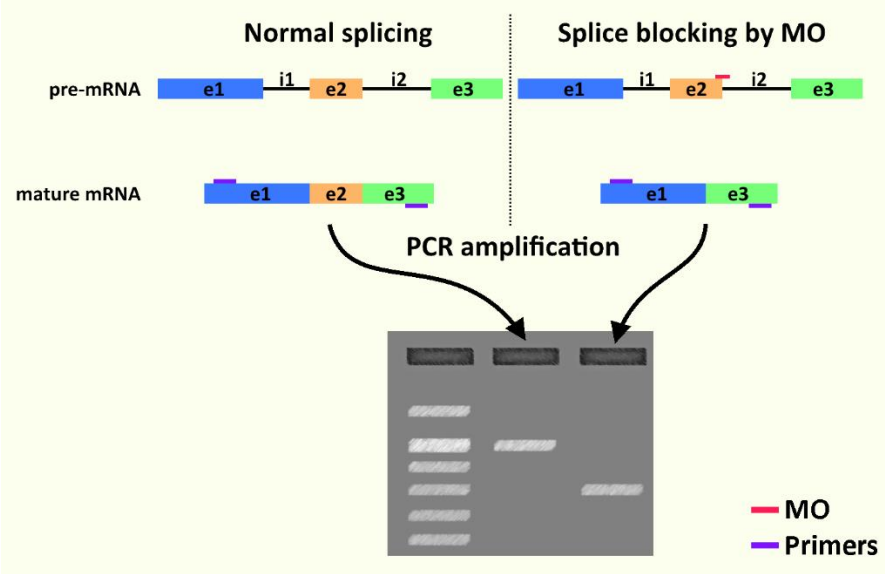

Figure 3-14: Schematic representation of MO effect on mRNA splicing and of the PCR analysis strategy that can be used to check for MO efficiency.

To test the efficiency of the MOs, we injected 9 ng of each of the above mentioned five MOs independently into wild type AB eggs at 1 – 2 cell stage, followed by total RNA extraction at 2 dpf. After cDNA synthesis and PCR with primers chosen as described above, amplicons were resolved by on a 3% agarose gel. Depending on the MO, the size of the PCR amplicon was expected to vary from 100 to 225 bp or to be totally absent in case of *pcmtl* e1i1 since the forward primer had been designed to bind to MO-target exon 1 (Table 3-4). Figure 3-15 shows the DNA agarose gel analysis of the obtained PCR amplicons. In *pcmt* i2e3 MO-injected larvae, the wild type (wt) amplicon was still predominant with a faint band of smaller size representing the morphant amplicon lacking the 32 bp exon 3. In contrast, in case of the *pcmt* e5i5 MO, the wt amplicon was totally absent while two morphant smaller bands were observed. Sequencing of the latter two amplicons showed both total skipping of the 115 bp exon 5 or partial skipping of 52 bp from the same exon. *pcmtl* e1i1 did not seem to interfere with *pcmtl* transcript splicing, but *pcmtl* e4i4 led to skipping of the 32 bp exon 4, with low levels of residual wt amplicon. In summary, *pcmt* e5i5 and *pcmtl* e4i4 were more efficient than *pcmt* i2e3 and *pcmtl* e1i1 in interfering with correct splicing of the *pcmt* and *pcmtl* pre-mRNAs, respectively. We thus decided to use *pcmt* e5i5 and *pcmtl* e4i4 for further experiments.

Table 3-4: Expected amplicon size from wt or morphant transcripts.

	***pcmt* i2e3**	***pcmt* e5i5**	***pcmtl* e1i1**	***pcmtl* e4i4**
Target exon (size)	Exon 3 in *pcmt* (32bp)	Exon 5 in *pcmt* (115 bp)	Exon 1 in *pcmtl* (161 bp)	Exon 4 in *pcmtl* (32bp)
Wt amplicon size (bp)	139	225	101	215
Morphant amplicon size (bp)	107	110	0	183

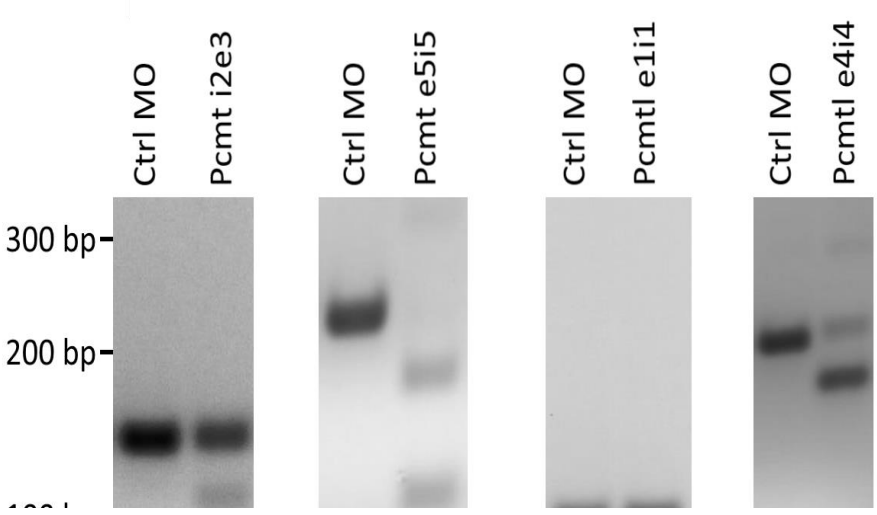

Figure 3-15: Agarose gel electrophoresis analysis for MO efficiency validation. Eggs were injected with either control MO or MO targeting pcmt or pcmtl (9 ng of each MO). RNA was extracted at 2dpf, converted into cDNA and used for PCR with primers spanning the exon targeted by the MO.

To find the efficient MO concentration with the lowest toxicity, we injected different amounts of each MO (7, 11, or 14 ng) at 1 – 2-cell stage and followed the development of the injected larvae over time. Both MOs resulted in amount-dependent dysmorphology (Figure 3-16). MOs higher than 7 ng in the case of *pcmt* e5i5 and 11 ng in the case of *pcmtl* e4i4 led to larvae with strong curvature of the trunk at 4 dpf, which is reported as a common side-effect of many MOs (KOK *et al.* 2015).

Interestingly, the swim bladder was found to be affected by MOs injection. In *pcmt* e5i5 the swim bladder is totally absent even with the lowest concentration, while in the case of *pcmtl* e4i4, the effect is dose-dependent (red arrows in Figure 3-16). It has previously been reported in MO-mediated knockdown of genes related to neurological disorders, such as Dravet syndrome and Batten disease (ZHANG *et al.* 2015; WAGER *et al.* 2016) that the swim bladder development was affected and failed to inflate.

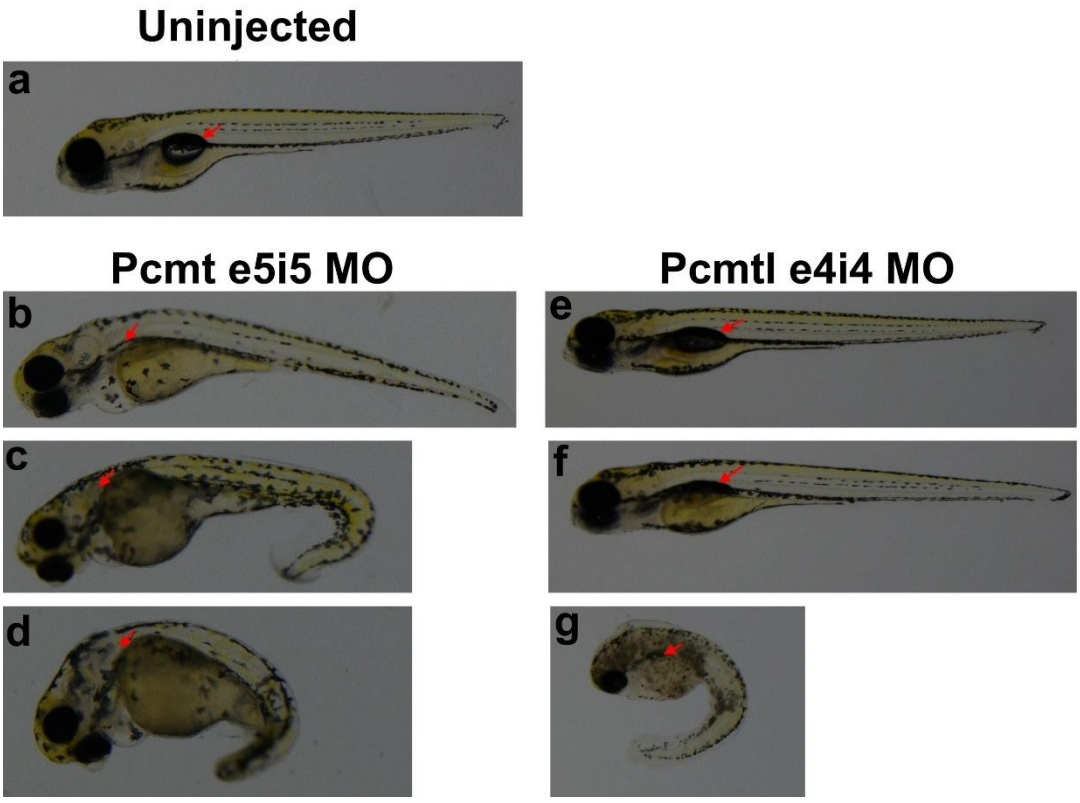

Figure 3-16: MO titration: AB eggs were injected with different amounts of either Pcmt e5i5 MO or Pcmtl e4i4 MO to find the maximum tolerated concentration. b and e: 7 ng; c and f: 11 ng; d and g: 14 ng. Increasing MO amounts led to developmental delay and morphological abnormalities. Swim bladder development was also affected by the MOs (red arrows).

Since we have found both Pcmt and Pcmtl to catalyse the same biochemical reaction, we decided to knock down both genes simultaneously (*pcmt/l*) in order to study the phenotypic effects of isoaspartyl methyltransferase downregulation. We continued with the titration of the MOs by co-injection of 7 ng

of each MO (14 ng in total), but this led to death of all the larvae. Amounts were reduced to 5 ng of each MO, which also led to severe dysmorphology in a large proportion of larvae and finally we used co-injection of 3.5 ng of each MO as an efficient and minimally toxic working amount for simultaneous knockdown of both genes.

3.1.3.3.2 Morpholino-mediated knockdown of *pcmt/l* leads to loss of methyltransferase activity and limited accumulation of isoaspartyl residues in the *pcmt/l* morphants

In order to determine the impact of simultaneous *pcmt* and *pcmtl* knockdown on isoaspartyl methyltransferase activity and accumulation of isoaspartyl levels, we used the vapour diffusion assay as described for mammalian cells. We injected AB eggs with *pcmt/l* MO (3.5 ng of each *pcmt* e5i5 and *pcmtl* e4i4) followed by protein extraction at 2 and 4 dpf (Section 2.2.5.3). Independently of the day of sampling, the methyltransferase activity was drastically decreased in *pcmt/l* morphant larvae compared to age-matched uninjected or MO control-injected larvae (Figure 3-17 a). Concerning the isoaspartyl levels, at 2 dpf we observed a slight but not significant increase in *pcmt/l* morphant extracts, which could be due to the residual methyltransferase activity detected at this stage. At 4 dpf, where the methyltransferase activity was not detectable, we observed a statistically significant, 1.5-fold increase in isoaspartyl residues in the *pcmt/l* morphant extracts (Figure 3-17b).

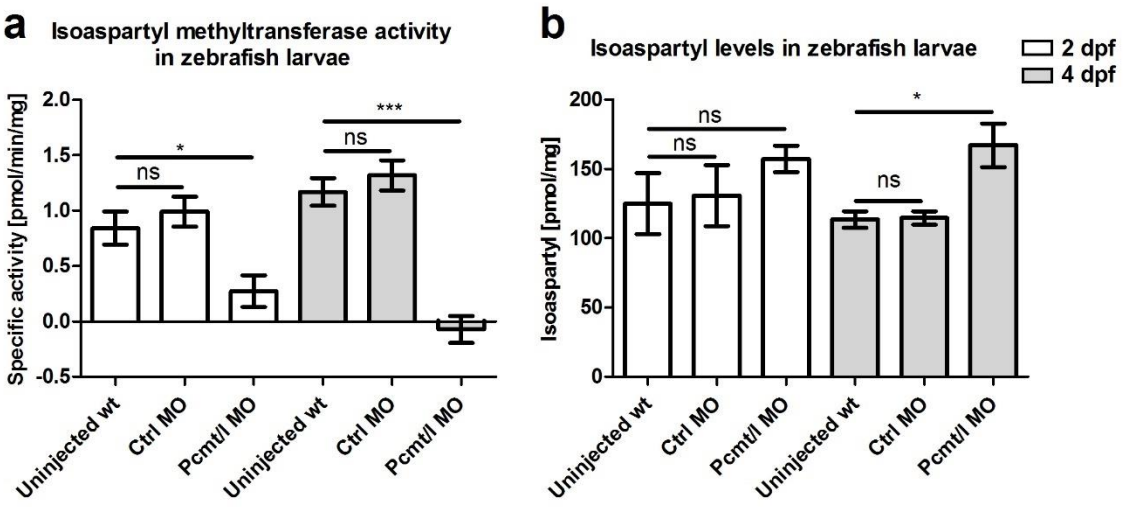

*Figure 3-17: Isoaspartyl methyltransferase activity and isoaspartyl levels in protein extracts of zebrafish larvae at 2 and 4 dpf. (a) Isoaspartyl methyltransferase activity in zebrafish estimated by incubation of protein extracts with methyl acceptor KASAisoDLAKY and [^{3}H]SAM. (b) Isoaspartyl levels in protein estimated by incubation of protein extracts with recombinant human PCMT1 and [3H]SAM (done at Clarke's lab). The values shown are means ± SEM of 4 biological replicates (ns, not significant; * p-value < 0.05; *** p-value < 0.001).*

We were also interested to see if the isoaspartyl residues detected in the zebrafish protein extracts were uniformly distributed among proteins of all sizes or were found more specifically in certain

proteins only, with a special interest in the proteins accumulating more isoaspartyl residues in the *pcmt/l* morphants. We therefore implemented fluorography experiments in collaboration with Prof. Steven Clarke's laboratory at UCLA (Los Angeles, CA). At LCSB, we prepared the protein extracts from zebrafish larvae at 2 and 4 dpf (uninjected, control MO-injected or *pcmt/l* MO-injected). In the Clarke lab, isoaspartyl residues were labelled with radioactive methyl groups from [^{3}H]SAM using recombinant human PCMT1 enzyme and the labelled proteins were resolved by SDS-PAGE. The protein gels were then incubated in EN^{3}HANCE, dried and exposed to a film for 1 day for detection of the labelled protein bands as described by Patananan *et al* (PATANANAN *et al.* 2014).

Interestingly, Coomassie blue staining of the SDS-PAGE gels showed decreased staining intensity for all proteins above 31 kDa in the protein extracts from 2 dpf *pcmt/l* morphant embryos (Figure 3-18b), despite loading the same amount of protein (as normalized based on Bradford assay). This could be due to increased protease activity levels specifically in the *pcmt/l* morphants at this developmental stage. Indeed, isoaspartyl accumulation and PCMT downregulation was reported to activate protease activity (SZYMANSKA *et al.* 1998; DAI *et al.* 2013; DHO *et al.* 2013). Accordingly, the fluorography also showed lower radioactive labelling after incubation with human recombinant PCMT1 for the 2 dpf *pcmt/l* morphant embryos (Figure 3-18a). Given that, when measuring total isoaspartyl levels in protein extracts derived from embryos at that stage, we detect equal or even slightly higher levels of isomerized residues in the *pcmt/l* morphants compared to the control embryos (Figure 3-17b), this suggests again that the lower labelling in the fluorograph for the *pcmt/l* morphants does not reflect overall lower accumulation of isoaspartyl residues in their proteins, but higher rates of proteolysis with formation of small labelled peptides that are not detected by fluorography, but are well measurable in the isoaspartyl assay in total protein extracts. In strong contrast, nothing points at this increased proteolysis in extracts derived from *pcmt/l* morphant larvae 2 days later (equal Coomassie blue staining intensities in all the lanes for 4 dpf samples, as expected given equal loading amounts for all the samples to be compared (Figure 3-18b). In addition, fluorography confirmed the increase in the isoaspartyl levels in the *pcmt/l* morphant larvae at 4 dpf observed also during isoaspartyl assays in total protein extracts (Figure 3-17b), but was, at first sight, not associated to specific proteins (Figure 3-18a).

Our results confirm the efficiency of the combined *pcmt/l* MO knockdown strategy, with a profound downregulation of the isoaspartyl methyltransferase activity and higher accumulation of isoaspartyl residues in pcmt/l morphant larvae. Both effects were more pronounced at 4 dpf than at 2 dpf. It is noteworthy that in the *Pcmt1* knockout mice, isoaspartyl levels are positively correlated with age (KIM *et al.* 1997b). To our knowledge, isoaspartyl level measurements have not been reported for mice at

developmental stages that would correspond to the early stages of life investigated here in zebrafish due to practical constraints (MO efficiency decreases after 5 dpf due to dilution by cell division; experiments have thus to be performed before that time point). One concern was therefore that the zebrafish model could from that point of view limit us to see phenotypic impacts of isoaspartyl methyltransferase deficiency. The results obtained with the 4 dpf larvae indicate, however, that the zebrafish model should allow to also investigate consequences of increased isoaspartyl damage accumulation, at least to a certain extent.

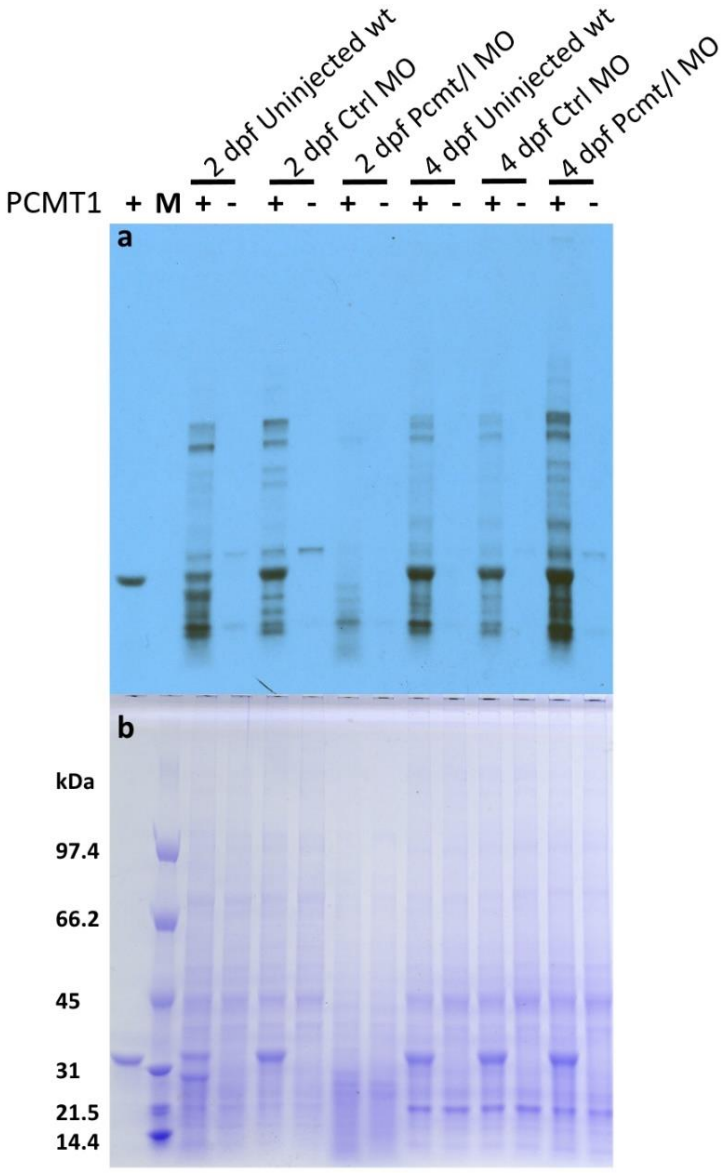

Figure 3-18: Fluorography and SDS-PAGE analysis of isoaspartyl in protein extracts from zebrafish Protein extracts from uninjected, Ctrl MO-injected and pcmt/l MO-injected of 2 dpf and 4 dpf were labelled with [^{3}H]-SAM and recombinant human PCMT1 then resolved in SDS-PAGE. Fluorography (a) showed lower incorporation levels of [^{3}H]-methyl in protein extract from pcmt/l morphants at 2 dpf compared to control but higher levels at 4 dpf. Coomassie blue staining (b) showed same protein levels loaded in all sample except for 2 dpf pcmt/l morphant where lower staining intensity was observed.

3.2 IGF-1 and MAPK Signalling pathways in *PCMT1* deficient cells

A number of previous findings support a connection between PCMT1 and growth signalling pathways such as the insulin/IGF-1 signalling pathway (FARRAR *et al.* 2005a; KHARE *et al.* 2011; MACKAY *et al.* 2012) or the mitogen-activated protein kinase pathway (MAPK) (DOYLE *et al.* 2003; KOSUGI *et al.* 2008). The IGF-1 pathway is conserved across almost all eukaryotes and plays a central role in the regulation of several downstream signalling cascades such as the well-documented TOR pathway. The latter is notably associated with macromolecule biosynthesis, autophagy or specific phenotypes such as aging. Investigations in a number of model organisms, including mice and *C. elegans*, showed that silencing of genes associated with the IGF-1 pathway can induce a lifespan extension (HOLZENBERGER *et al.* 2003; KENYON 2010). As already mentioned several times in this thesis before, homozygous *Pcmt1* knockout mice exhibit a shortened lifespan. Combined with the observed hyperphosphorylation of intermediates of the IGF1 pathway in these mice, it is tempting to link *Pcmt1* deficiency to accelerated aging via activation of the IGF1 signalling pathway. In this part, we aimed at reproducing these effects of PCMT1 on growth signalling pathways in the different *PCMT1* deficient cell models established and validated in section (3.1.1) and (3.1.2) in order to investigate the mechanism(s) by which PCMT1 interacts with these pathways.

3.2.1 Growth signalling pathways in PCMT1-knockdown cells

We first tested the previously described HEK293 cells stably expressing an anti-PCMT1 shRNA. To investigate differences in phosphorylation status of intermediates in the IGF-1 and MAPK pathways between the PCMT1 knockdown and control cell lines, we used the known corresponding activators IGF-1 (insulin-like growth factor-1) and EGF (epidermal growth factor). EGF was reported before to activate the MAPK pathway in HEK293 cells at 1 µg/ml cell medium (KOSUGI *et al.* 2008); the EC50 for IGF-1 was reported to be around 10 ng/ml in mouse bone marrow cells (FDC-P1) (MCCUBREY *et al.* 1991). Based on this, we decided to use 1 µg/ml EGF and 100 ng/ml (10× EC50) IGF-1 in the medium of our HEK293 cell lines. We seeded 1×10^6 cells, expressing either of the above defined shCtrl or shPCMT, per well in 6-well plates. The next day, we washed the cells with PBS and stimulated them with either IGF-1 or EGF. We incubated the cells with the stimulating media for different durations (5 – 30 minutes) followed by washing with PBS and scraping of the cells into ice-cold RIPA buffer. We analysed the protein extracts by Western blotting as described in the methods (Section 2.2.3.2). We found that in the control cells, the phosphorylation levels of protein kinase B (Akt) did not change after exposures to IGF-1 up to 30 minutes. Also, PCMT1 knockdown did not seem to affect Akt phosphorylation under the conditions tested: Akt phosphorylation levels were the same in cells expressing shCtrl and shPCMT and exposed to 100 ng/µl IGF-1, at all the time points tested (Figure 3-19).

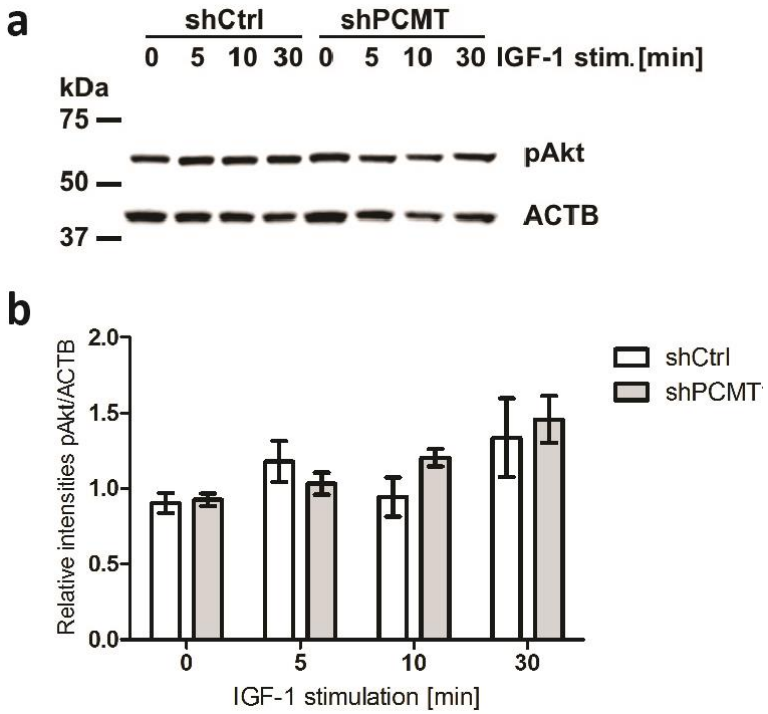

Figure 3-19: pAkt levels in PCMT1 knockdown HEK293 cells. Western blot analysis (a) and relative band intensity quantification (b) showing the Akt phosphorylation levels in PCMT1 knockdown HEK293 cells and corresponding control cells after stimulation with IGF-1 for different durations. The values shown are means ± SEM of 3 biological replicates.

We then tested if we can reproduce the activation of MAPK pathway intermediates (cRaf, Erk1/2, MEK) that had previously been reported in different *PCMT1* deficient cell models (DOYLE *et al.* 2003; KOSUGI *et al.* 2008). Using a similar experimental setup as Kosugi *et al* (KOSUGI *et al.* 2008), shCtrl and shPCMT cells were exposed to EGF for different durations followed by protein extraction for Western blot analysis. We found that both cell lines show a transient response to EGF, where phosphorylation of Erk1/2 increases within 5 minutes from EGF addition, drops after 10 minutes and then remains stable up to 30 minutes (Figure 3-20). There was no difference in our experiments in Erk1/2 phosphorylation levels between shCtrl and shPCMT cells, in contrast to what had been reported before (KOSUGI *et al.* 2008). This discrepancy may be explained by the fact that in the HEK293 cell model used by Kosugi *et al*., no residual PCMT1 protein levels could be detected by Western blot anymore, while in our cell line a residual PCMT1 level corresponding to 20% of control levels was still present (Figure 3-3). Also, in the cell line used by Kosugi *et al*., an about 2-fold increase in isoaspartyl levels was measured in cellular proteins, while we only detected a 1.1-fold increase in our cell lines (Figure 3-4 b).

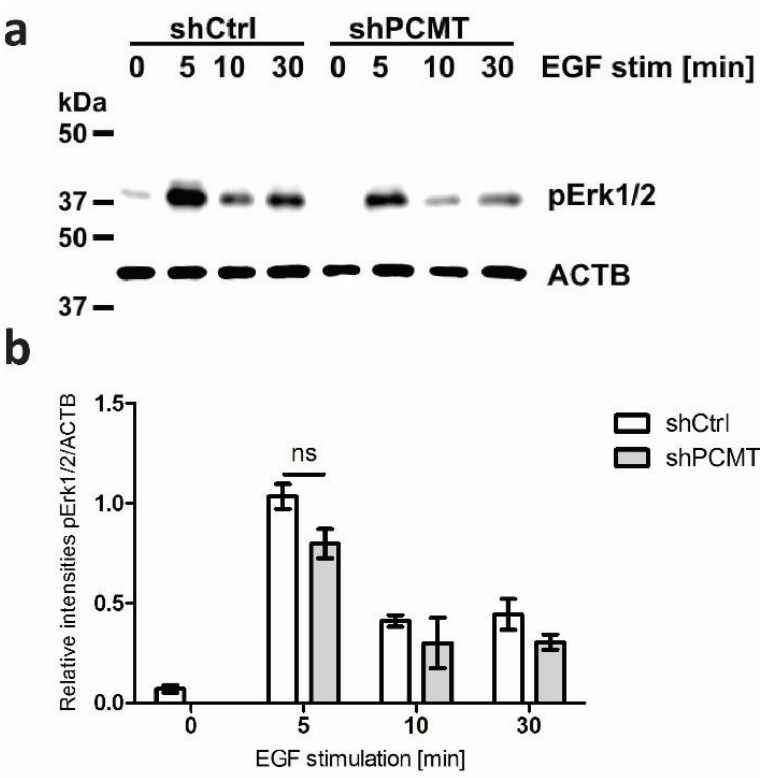

Figure 3-20: pErk1/2 levels in PCMT1 knockdown HEK293 cells Western blot analysis (a) and relative band intensity quantification (b) showing the Erk1/2 phosphorylation levels in PCMT1 knockdown HEK293 cells and corresponding control cells after stimulation with EGF for different durations. The values shown are means ± SEM of 3 biological replicates.

We concluded that, under our conditions, *PCMT1* knockdown in HEK293 cells did not affect the phosphorylation levels of either Akt or Erk1/2. Farrar and colleagues had shown that Akt hyperphosphorylation in *Pcmt1* knockout mice was particularly pronounced in the hippocampus (FARRAR *et al.* 2005a). As potential reasons for our negative results in these first trials in a HEK293 *PCMT1* knockdown cell line were (1) only partial silencing of the protein of interest, (2) lack of significant accumulation of isoaspartyl residues in the knockdown cells and (3) use of a cell line from a different species (human versus mouse) and a different tissular origin (embryonic kidney versus hippocampus), we decided to repeat these experiments in a mouse hippocampal cell line (HT22) in which the *Pcmt1* gene had been knocked out using the CRISPR/Cas9 technology (Section 2.2.4.3).

3.2.2 Growth signalling in *Pcmt1* knockout HT22 cells

As described in the first part of the results (Section 3.1.2) we successfully created a *Pcmt1* knockout HT22 cell model and validated it in terms of total loss of isoaspartyl methyltransferase activity and detectable accumulation of isoaspartyl substrates (Figure 3-6 b). In this section, we used the cell model to test whether we can reproduce the hyperphosphorylation pattern of intermediates of the IGF-1 pathway previously observed in *Pcmt1* knockout mice (FARRAR *et al.* 2005a). We started by optimizing

the conditions for activation of the IGF-1 signalling pathway by IGF-1 and insulin (RINDERKNECHT and HUMBEL 1978), testing exposure of the cells to different concentrations of the activators for different durations. Different concentrations of both IGF-1 and insulin were added to the cell media as described before and stimulation was stopped 10 minutes later by washing the cells with PBS and addition of ice-cold RIPA buffer for subsequent Western blot analysis.

IGF-1 stimulation induced a dose response effect where phosphorylation of Akt increased in response to increasing IGF-1 concentrations (Figure 3-21). However, there was no significant difference in the phosphorylation levels of Akt between control and *Pcmt1* knockout cells.

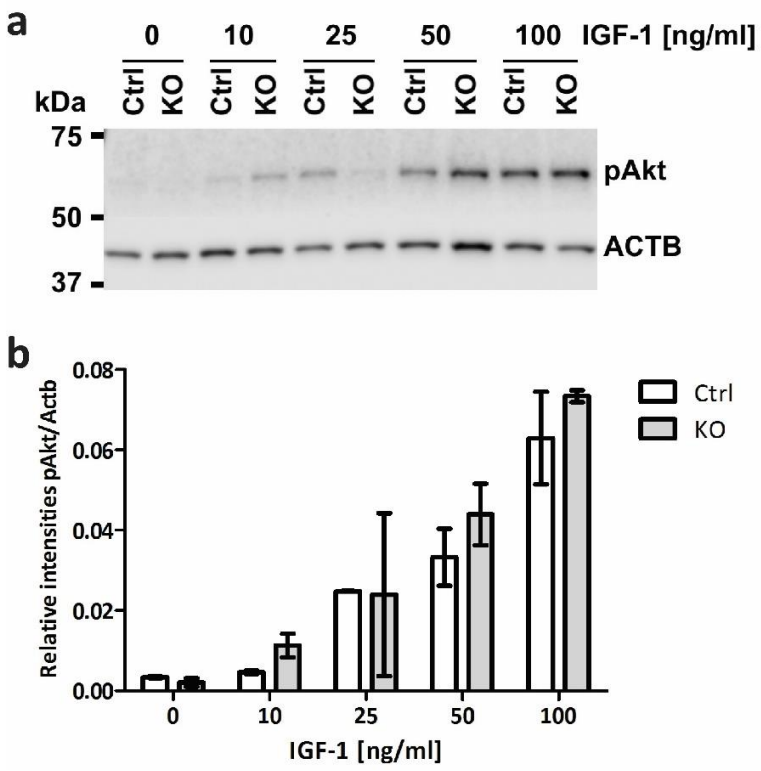

Figure 3-21: Phosphorylation levels of Akt in HT22 control and Pcmt1 KO cells in response to exposure to different concentrations of IGF-1 for 10 minutes. (a) Representative Western blot analysis for one of the tested replicates and (b) relative quantification based on band intensities. The values shown are means ± SEM of 2 biological replicates

We repeated a similar experiment, but stimulating the cells for different durations with 100 ng/ml IGF-1. The resulting time course showed a dynamic response of Akt phosphorylation to IGF-1 with the highest phosphorylation levels being reached at 5 and 10 minutes after addition of the growth factor, followed by a progressive decrease in phosphorylation over the next 24 hours. Again, we did not find significant differences in Akt phosphorylation levels between control and *Pcmt1* knockout cells (Figure 3-22).

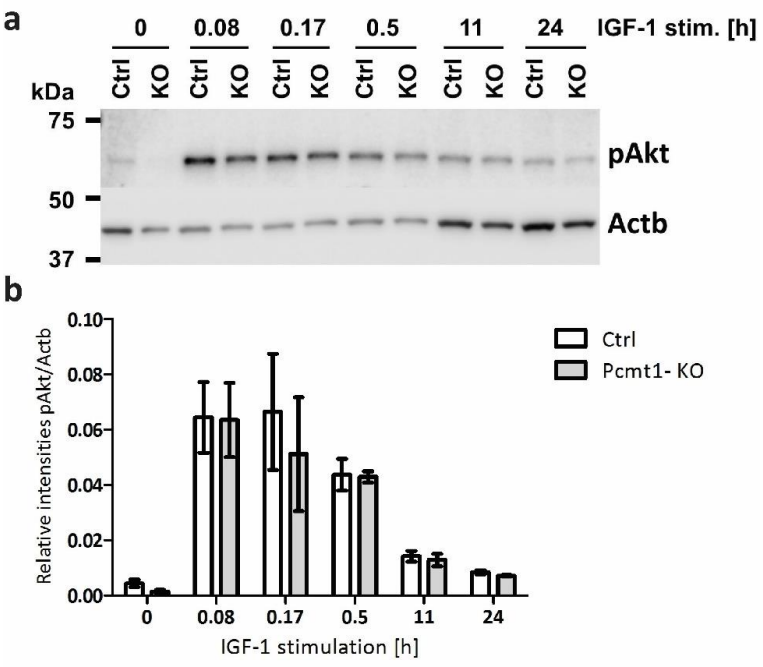

Figure 3-22: Phosphorylation levels of Akt in HT22 control and Pcmt1 KO cells in response to exposure to 100 ng/ml IGF-1 for the indicated durations. (a) Representative Western blot analysis for one of the tested replicates and (b) relative quantification based on band intensities. The values shown are means ± SEM of 3 biological replicates

We then tested the effect of insulin, a hormone which should also stimulate phosphorylation of Akt. Exposure of the HT22 cells to one dose of insulin (10 µg/ml) for different durations also led to a dynamic response of Akt phosphorylation levels, but to a lesser extent and with a different time course as with IGF-1 (Figure 3-23) but not as strong as the IGF-1 effect. Similar to IGF-1 we did not see differences in the phosphorylation levels of Akt in *Pcmt1* knockout cells compared to control cells in response to insulin either. The dynamics of the responses in Akt activation following insulin and IGF-1 addition hint at the complexity of studying these signalling pathway in cell culture models. This may have prevented us from observing a potential effect of *Pcmt1* deficiency on IGF-1 pathway activation. Other reasons may of course be linked to the fact that we tried to reproduce effects that had been observed in the complexity of the brain tissue environment in a living animal, in a much more simple monoculture cell model.

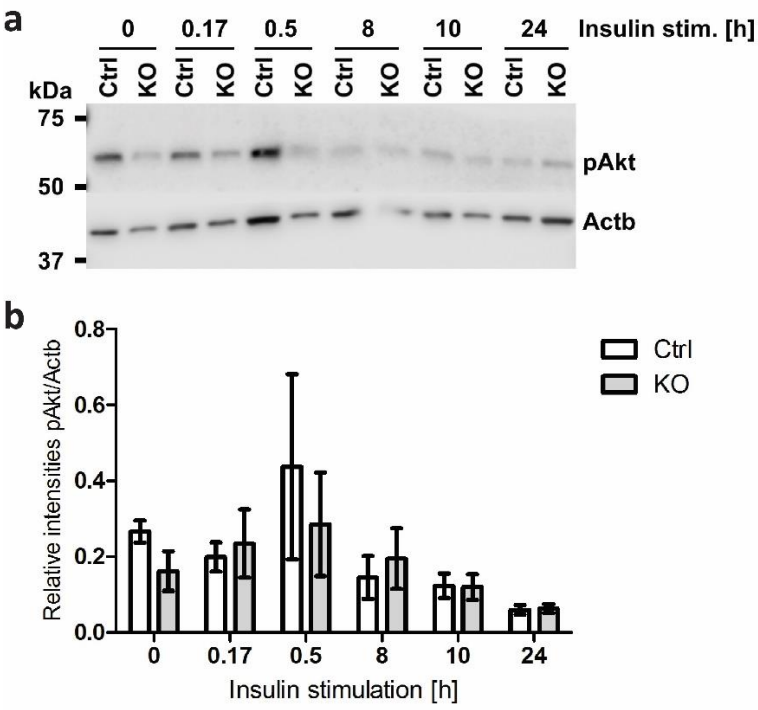

Figure 3-23: Phosphorylation levels of Akt in HT22 control and Pcmt1 KO cells in response to exposure to 10 µg/ml insulin for the indicated durations. (a) Representative Western blot analysis for one of the tested replicates and (b) relative quantification based on band intensities. The values shown are means ± SEM of 3 biological replicates

In our previous experiments where we investigated the phosphorylation levels of Erk1/2 in HEK293 cells, we stimulated the cells with 1 µg/ml EGF as in Kosugi *et al*. (Kosugi *et al.* 2008). In the HT22 cell model we decided to test different concentrations of EGF in the range of 25 – 1000 ng/ml (10-minute exposures). Interestingly, highest phosphorylation levels of Erk1/2 were found after exposure to the lower EGF doses at 25 to 100 ng/ml (Figure 3-24). As opposed to all the previous trials, in this cell model with EGF stimulation we were now also able to detect, at all the EGF concentrations tested, higher ERK1/2 phosphorylation levels in the *Pcmt1* knockout cells compared to the control cells (Figure 3-24).

We were also interested in the dynamics of the phosphorylation response, so we stimulated the cells with 100 ng/ml EGF for different durations from 10 minutes to 23 hours. We found that highest phosphorylation levels were reached at 10 minutes of stimulation and went down at 30 minutes (Figure 3-25). Stimulations over several hours did not lead to higher phosphorylation levels or reveal a second wave of phosphorylation response. These results suggested that EGF stimulation induces a fast phosphorylation response at the level of Erk1/2 within a few minutes. Hyperphosphorylation of Erk1/2 in the *Pcmt1* KO versus control cells was also the most pronounced for the short 10-minute exposure (Figure 3-25).

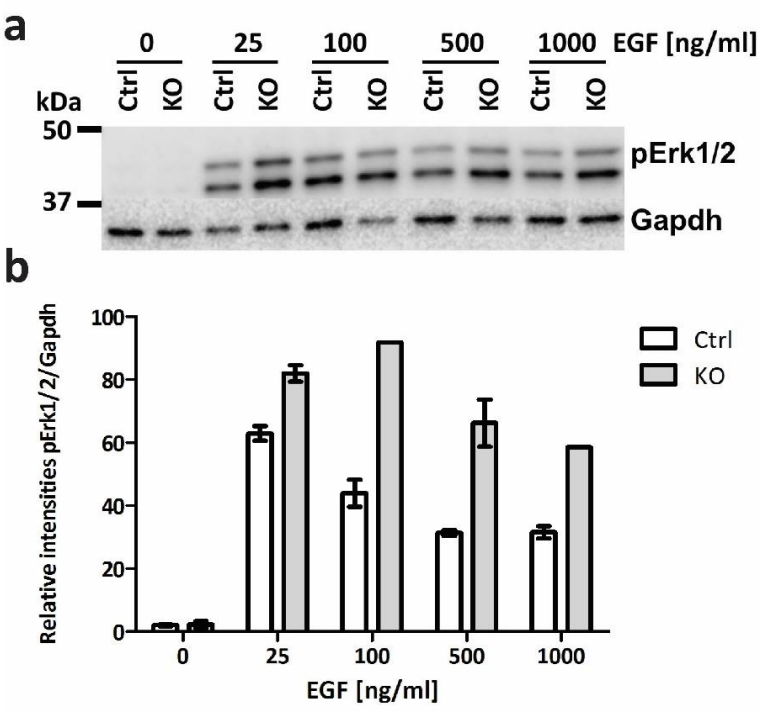

Figure 3-24: Phosphorylation levels of Erk1/2 in HT22 control and Pcmt1 KO cells in response to a 10-minute exposure to the indicated concentrations of EGF. (a) Representative Western blot analysis for one of the tested replicates and (b) relative quantification based on band intensities. The values shown are means ± SEM of 2 biological replicates

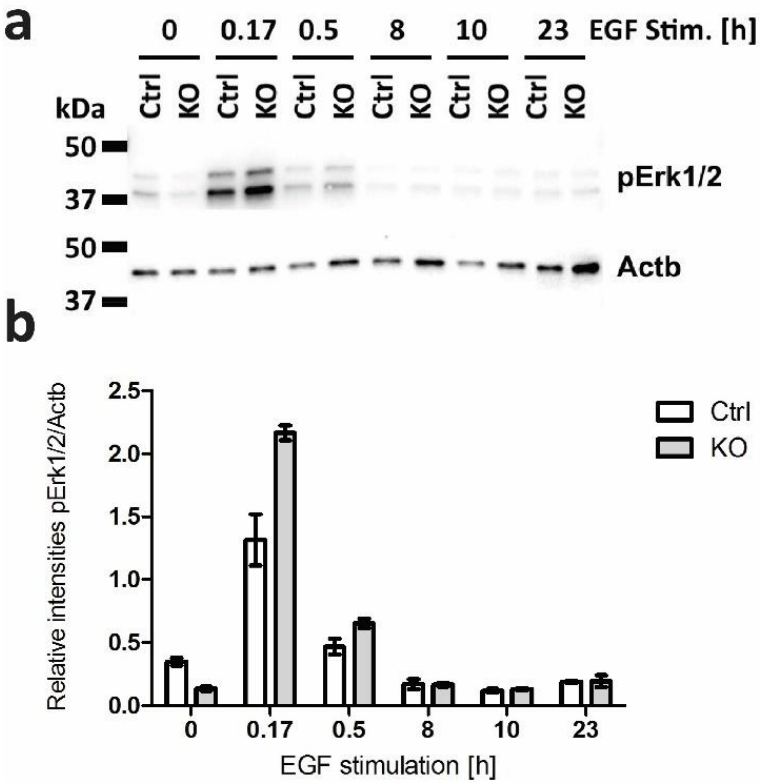

Figure 3-25: Phosphorylation levels of Erk1/2 in HT22 control and Pcmt1 KO cells in response to exposure to 100 ng/ml EGF for the indicated durations. (a) Representative Western blot analysis for one of the tested replicates and (b) relative quantification based on band intensities. The values shown are means ± SEM of 3 biological replicates

We therefore repeated a time course experiment with 100 ng/ml EGF, but testing shorter exposure times to investigate the dynamics of the Erk1/2 phosphorylation response. We confirmed that the effect of EGF is quite transient, with highest phosphorylation levels of Erk1/2 reached at 5 and 10 minutes and then going down at 30 minutes (Figure 3-26). Again, the most pronounced difference in Erk1/2 phosphorylation levels between the *Pcmt1* knockout and control cells was observed for the 10-minute exposure.

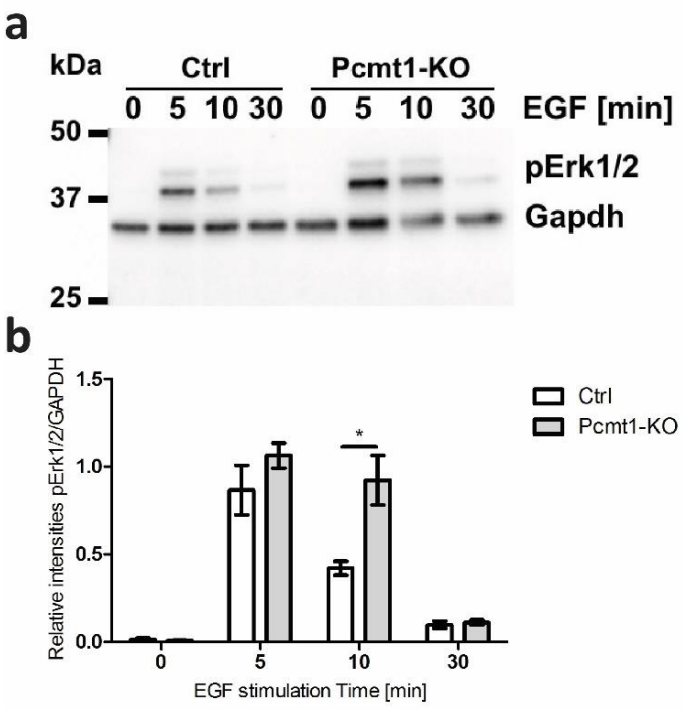

Figure 3-26: Phosphorylation levels of Erk1/2 in HT22 control and Pcmt1 KO cells in response to exposure to 100 ng/ml EGF for the indicated durations. (a) Representative Western blot analysis for one of the tested replicates and (b) relative quantification based on band intensities. The values shown are means ± SEM of 3 biological replicates

We extended this investigation by also measuring the phosphorylation levels of another intermediate in the MAPK pathway, namely Mitogen-activated protein kinase (MEK), which is just upstream of Erk1/2 (phosphorylating the latter). We tested the phosphorylation levels of MEK after stimulation with 100 ng/ml EGF for 0 and 10 minutes and we found that MEK is less phosphorylated in the *Pcmt1* KO cells directly after addition of EGF ('0 min'), but shows the same phosphorylation level as the control cells after 10 minutes of stimulation (Figure 3-27). In the study by Kosugi *et al* in the *PMCT1* knockdown HEK293 cells, both Erk1/2 and MEK were more phosphorylated in the knockdown cells compared to the control cells, but the fold change for phospho-Erk1/2 was higher than for phospho-MEK (KOSUGI *et al.* 2008). Together with our data, this suggests that the higher phosphorylation levels of Erk1/2 in *Pcmt1* deficient cells is not due to higher activity of upstream kinases, but may be due to lower activity of downstream protein phosphatases.

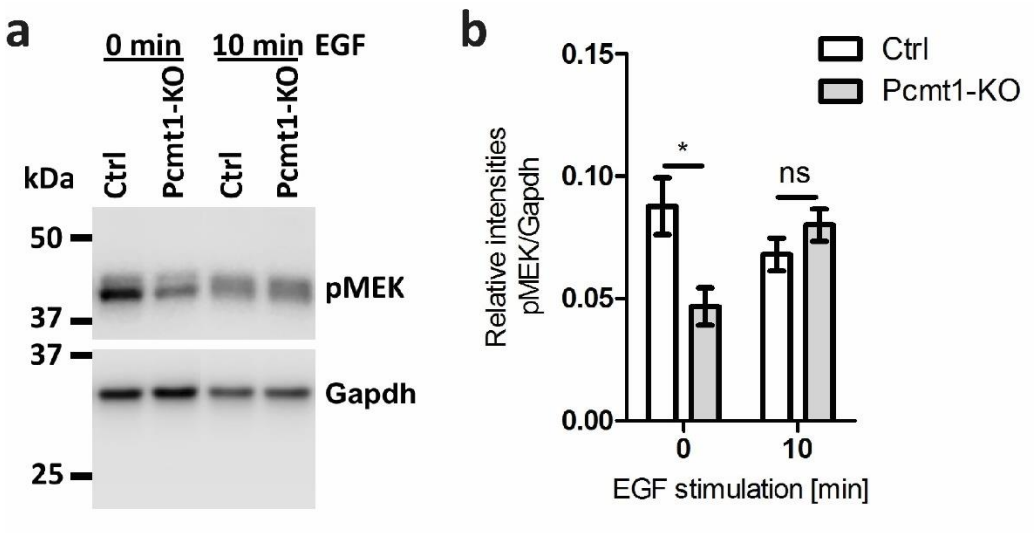

Figure 3-27: Phosphorylation levels of MEK in HT22 control and Pcmt1 KO cells in response to exposure to 100 ng/ml EGF for the indicated durations. (a) Representative Western blot analysis for one of the tested replicates and (b) relative quantification based on band intensities. The values shown are means ± SEM of 3 biological replicates.

In summary, phosphorylation levels of Akt (an intermediate in the insulin/IGF-1 signalling pathway) are not affected by *PCMT1* knockdown in HEK293 and U-87 cells upon IGF-1 stimulation. Similarly, in HT22 *Pcmt1* knockout cells Akt phosphorylation levels are the same upon stimulation with IGF-1 or insulin. Regarding the Erk1/2 (an intermediate in the MAPK signalling pathway), *PCMT1* knockdown in HEK293 and U-87 MG cells did its affect phosphorylation levels. However, Pcmt1 knockout seems to have higher phosphorylation levels of Erk1/2 than control cells upon stimulation with EGF.

3.3 Phenotyping of *pcmt/l* knockdown zebrafish

3.3.1 MO-mediated knockdown of *pcmt* and *pcmtl* leads to developmental delay and dysmorphology in zebrafish larvae

We have shown previously (Section 3.1.3.2) that that the expression products of the *pcmt* and *pcmtl* genes, arising from the genome duplication in teleost fish evolution (TAYLOR *et al.* 2001), do not differ markedly in terms of catalytic properties and expression/tissue distribution patterns (Figure 3-9 and Figure 3-13). One of the implications thereof is that both genes need to be targeted for morpholino-mediated knockdown to achieve a maximal silencing effect of the associated function. In practice, this was achieved by co-injection of both *pcmt* e5i5 MO and *pcmtl* e4i4 MOs (3.5 ng of each).

Survey of morphological changes following this co-injection revealed that embryos at 2 or 4 days post fertilization (dpf) showed various phenotypes. We ranked the severity of dysmorphology from mild to severe. At 2 dpf, a slight body curvature was ranked as a mild phenotype, a curved trunk and small body size as a moderate phenotype, and a reduction of melanin formation and a strong malformation

as a severe phenotype. At 4 dpf, a lack of swimming bladder, a curved trunk, and strong malformation were ranked as mild, moderate, and severe phenotypes, respectively (Figure 3-28). Relative quantification of these phenotypes in *pcmt/l* MO-treated embryos highlighted an increase of dysmorphic trait in comparison to uninjected and control MO-treated embryos (Figure 3-29). At 2 dpf, 15% of *pmct/l* morphant larvae did not survive and 22%, 26%, and 17% showed severe, moderate, and mild dysmorphologies, respectively; 19% of the 2 dpf morphant embryos were normal. The deleterious effect was even higher at 4 dpf where about 50% of the *pmct/l* morphant larvae were dead. In contrast, more than 95% and 85% of embryos injected with control MO (as well as uninjected embryos) showed a normal phenotype at 2 dpf and 4 dpf, respectively (Figure 3-29).

These results suggest a crucial role for *pcmt* and *pcmtl* in embryonic zebrafish development and are consistent with the drastically reduced life span of *Pcmt1* knockout mice (Kim *et al.* 1997b). However, they should be considered with some caution since MO treatment can lead, independently from the targeted gene, to similar dysmorphic phenotypes, due to off-target effects of MOs, that cannot be reproduced by gene deletion strategies (Kok *et al.* 2015).

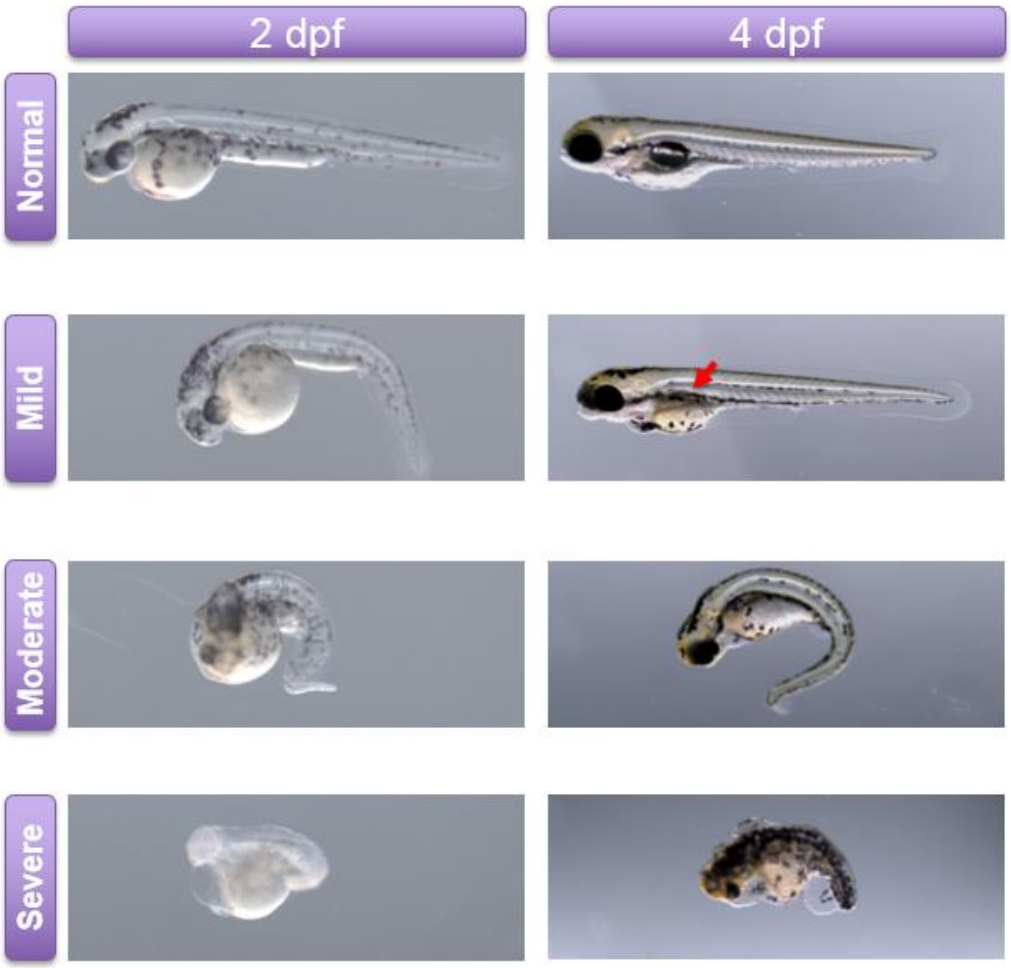

Figure 3-28: Morphological phenotype ranking in morphant zebrafish larvae deficient in pcmt and pcmtl

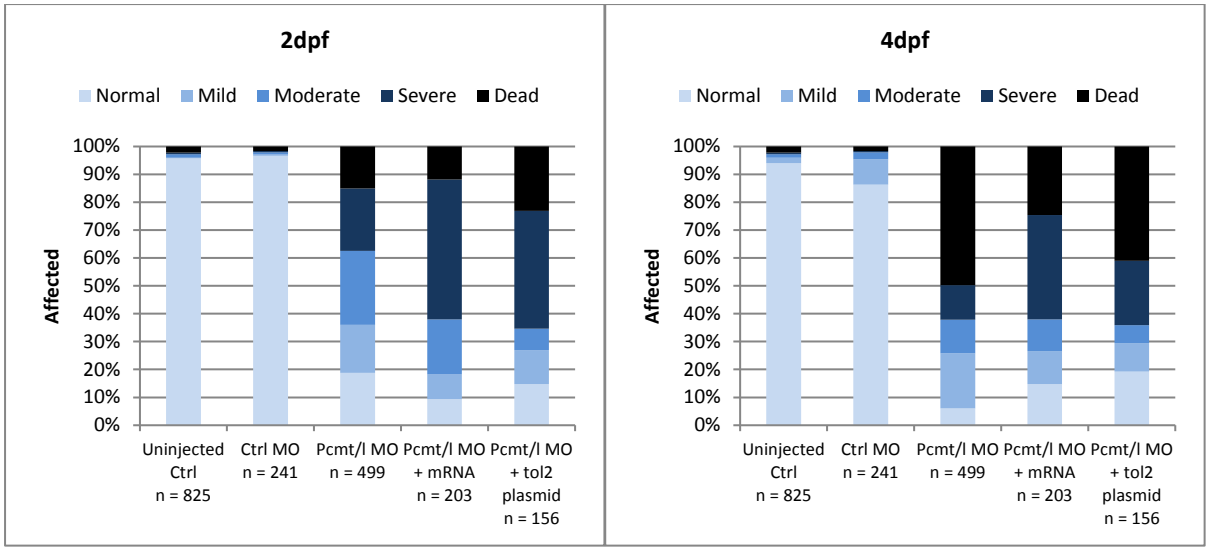

Figure 3-29: Morphological phenotype in morphant zebrafish deficient in pcmt and pcmtl as well as rescuing attempt by exogenous expression of both genes either by direct injection of mRNAs or of plasmids carrying the coding sequence of pcmt and pcmtl genes.

In order to confirm these morphological phenotypes to be specifically caused by *pcmt/l* deficiency, rescue experiments were carried out using two different approaches: by direct injection of *pcmt* and *pcmtl* mRNAs or of rescue plasmids carrying the coding regions of either *pcmt* or *pcmtl*. To generate the mRNAs, the coding sequences of both *pcmt* and *pcmtl* were cloned into the pCS2+ plasmid and the recombinant plasmids were used for IVT production of both transcripts. For creation of the rescue plasmids, the coding sequences of *pcmt* and *pcmtl* were cloned into the pGEMT vector under the control of eukaryotic elongation factor 1 α (eEF1α) ubiquitous promoter to be injected directly. Both the prepared transcripts and plasmids were first titrated to find the maximum tolerated amounts to be injected without causing toxicity and we ended up with 100 pg for mRNA transcripts and 20 pg plasmid DNA as the maximum safe amount to be injected. To perform the rescue experiments we injected either 100 pg of the *pcmt* and *pcmtl* transcripts or 20 pg of the *pcmt* and *pcmtl* rescue plasmids simultaneously with the *pcmt/l* MOs into AB eggs.

For the 2 dpf larvae, neither the mRNA transcripts nor the plasmids expressing *pcmt* and *pcmtl* showed a rescue effect; at the contrary, they even amplified the severity of the dysmorphology (Figure 3-29). By contrast, for the 4 dpf larvae, both rescue strategies reversed, although only very partially, the deleterious effects of the *pcmt/l* MOs, with a higher proportion of normal larvae and a lower proportion of dead larvae (Figure 3-29). The most straightforward explanation for these observations would be that most (4 dpf), if not all (2 dpf) of the dysmorphology phenotype is due to non gene specific, off-target effects of the *pcmt/l* MOs. It could, however, also be hypothesized that the MO knockdown effect takes place faster than the rescue effect through the exogenous expression of both

genes and that reversion of the phenotypes can therefore only be observed at later time points after injection (starting at 4 dpf and maybe even more pronounced at later stages, but not detectable yet at 2 dpf).

3.3.2 Seizure quantification by locomotor tracking system

As a reminder, it had previously been shown that *Pcmt1* knockout mice develop epileptic seizures starting at a young age and that their premature death coincided with a final massive epileptic episode (YAMAMOTO *et al.* 1998; KIM *et al.* 1999). In preliminary tests conducted on *pcmt/l* morphant embryos, we observed twitching events at 2 dpf, reminiscent of epileptic seizures (a personal communication by Alexander Crawford). The twitching events were characterized by abnormal fast moving of the tail which occurs irregularly over different durations of time making it difficult to quantify. Our observations indicated that they were substantially more frequent in the *pcmt/l* morphants than control MO injected larvae and suggested that isoaspartyl methyltransferase deficiency may induce seizure-like events in young zebrafish larvae (or embryos).

Tracking of the locomotor behaviour has been shown to be a good read-out for the epilepsy phenotype in zebrafish PTZ epilepsy model (AFRIKANOVA *et al.* 2013). DanioVision is a high-throughput locomotor tracking system that is based on a camera placed on top of a 96-well plate and recording the movement of zebrafish larvae in each well. Based on the movements, the system can measure the total distance each larva traveled during the time of the experiment and its velocity which correlates positively with increased seizure activity. By combination of the DanioVision system and stimulation with pentylenetetrazol (PTZ), a gamma-aminobutyric acid (GABA) receptor antagonist that induces seizures (HUANG *et al.* 2001; BARABAN *et al.* 2005), we aimed at investigating the impact of *pcmt/l* knockdown on seizure development in zebrafish. As a proof-of-concept experiment, uninjected embryos were placed in a 96-well plate (one larva per well containing each 100 µl of Danieau). The plate was incubated for one hour in the dark prior to recording. Results showed that both the total distance travelled and the velocity were increased in embryos treated with 20 mM PTZ as compared to non-treated control larvae (Figure 3-30). This pilot experiment confirmed that the experimental setup allowed for detection of PTZ-induced seizures and that it was suitable for further characterization of the pcmt/l morphants.

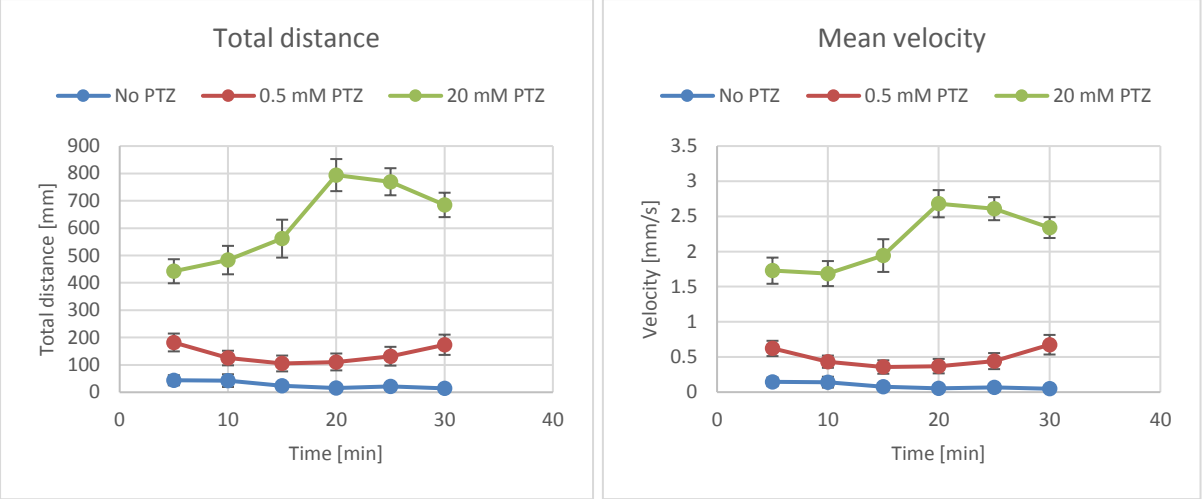

Figure 3-30: Locomotor behaviour of wild type zebrafish larvae without or with exposure to PTZ. Larvae were incubated in 96-well plate and their movements tracked using the DanioVision system. PTZ dose dependency of the total distance travelled (left panel) and the mean velocity (right panel) of zebrafish larvae is shown. Values are the mean ± SEM of 20 biological replicates.

Using the same protocol, control and *pcmt/l* morphant larvae were surveyed at 4 dpf in three conditions, without PTZ, with 0.5 mM PTZ or with 20 mM PTZ. Only mild and normally looking larvae (Figure 3-28) were selected for the experiment. Larvae injected with control MO showed a similar profile as the ones observed for the proof-of-concept experiment where both total distance and velocity were increased in a dose-dependent manner in response to PTZ. In the absence of PTZ, the *pcmt/l* morphant larvae showed a similar locomotor behaviour as the control larvae. In the presence of 0.5 mM or 20 mM PTZ, the total distance travelled by *pcmt/l* morphants was drastically reduced compared to the control larvae although the mean velocity was only slightly decreased (Figure 3-31). The results indicate that *pcmt/l* deficiency reduces the overall locomotor activity of the zebrafish larvae, but that the residual movements are performed at the same speed as for control larvae. These observations do therefore not support that those young zebrafish larvae deficient in isoaspartyl methyltransferase activity, as opposed to *Pcmt1* knockout mice (Kim *et al.* 1997b) , experience epileptic seizure events (lack of increased velocity of movements in response to PTZ), but the decreased total distance travelled shows that they experience an impairment of locomotor behaviour. The decreased locomotor activity of the *pcmt/l* morphants could be due to neurological deficits due to the impaired brain development that we observed in these morphants (Figure 3-36). A more trivial explanation would be locomotor constraints imposed by the more general developmental delay caused by the *pcmt/l* MOs, with for instance an underdeveloped swimming bladder and trunk curvatures, which may of course affect the swimming behaviour of the larvae.

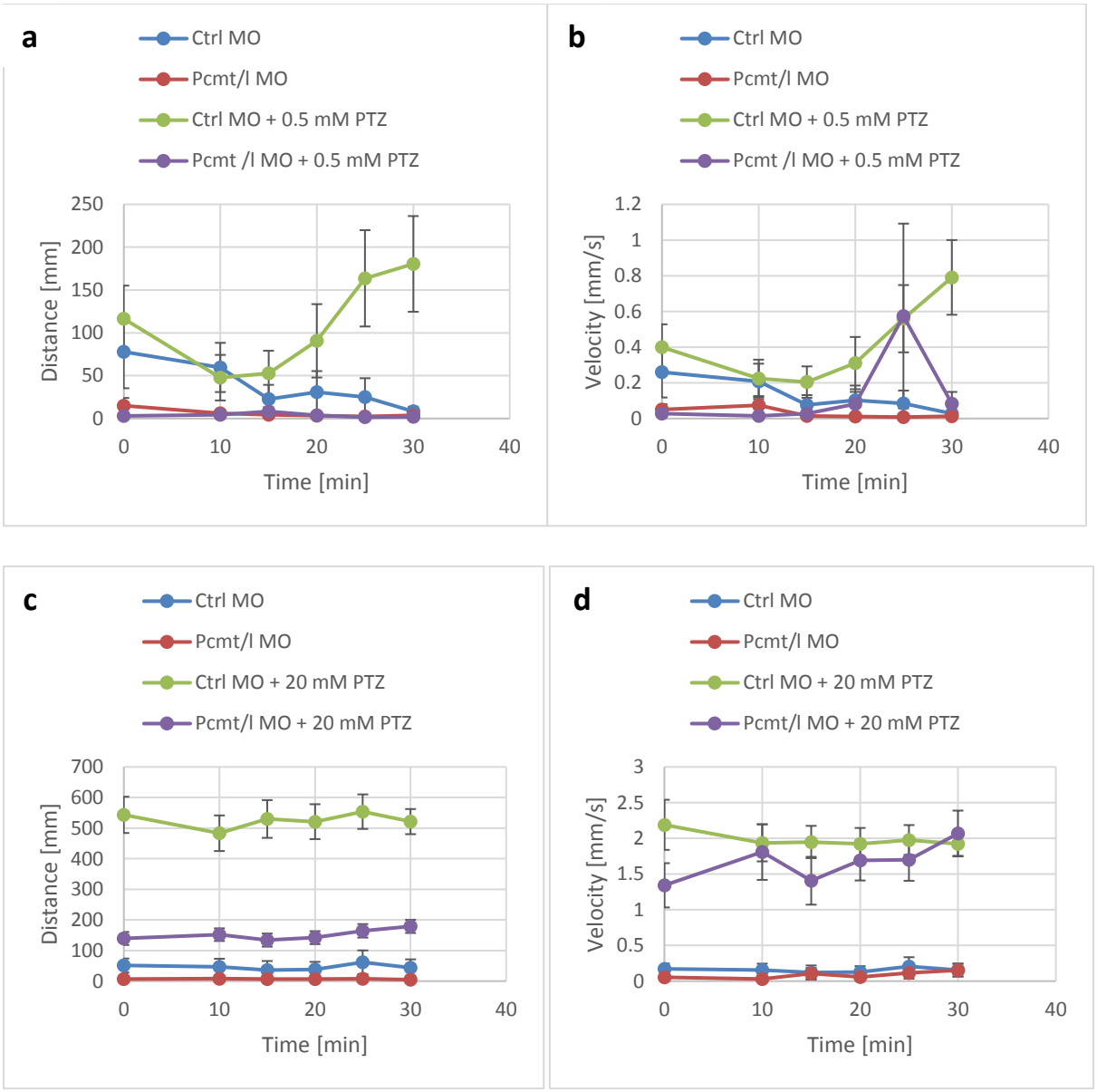

Figure 3-31: Locomotor behaviour of control MO and pcmt/l MO injected zebrafish larvae without or with exposure to PTZ. (a) Total distance travelled with exposure to 0.5 mM PTZ (b) Mean velocity with exposure to 0.5 mM PTZ (c) Total distance travelled with exposure to 20 mM PTZ (d) Mean velocity with exposure to 20 mM PTZ. Values are the mean ± SEM of 20 biological replicates.

3.3.3 Brain electrical activity by tectal field potential recordings

It has been shown previously that *Pcmt1* knockout mice experience abnormal electrical brain activity (Kim *et al.* 1999) and our *pcmt/l* morphant zebrafish model opened the perspective to provide more insights into this phenotype. Given the difficulty to interpret the locomotor tracking results obtained in the previous section due to the potential bias introduced by dysmorphologies of the morphant larvae potentially limiting swimming movements, it was also important to use a second approach, free of this bias, to try to detect and quantify seizure activity in the morphants. We therefore decided to proceed to measurements of the electrical brain activity in the brain using the technique of tectal field

potential recordings. At 5 dpf, larvae were immobilized into 2% low melting agarose and an electrode was placed into the optic tectum (Figure 3-32a) for local field potential recording as previously described (Section 2.2.5.8). As a proof of concept, tectal field potential recording of 5 dpf wild type AB larvae exposed to 20 mM PTZ showed massive electrical discharges indicating seizure development in response to PTZ that was detectable with our experimental setup (Figure 3-32b).

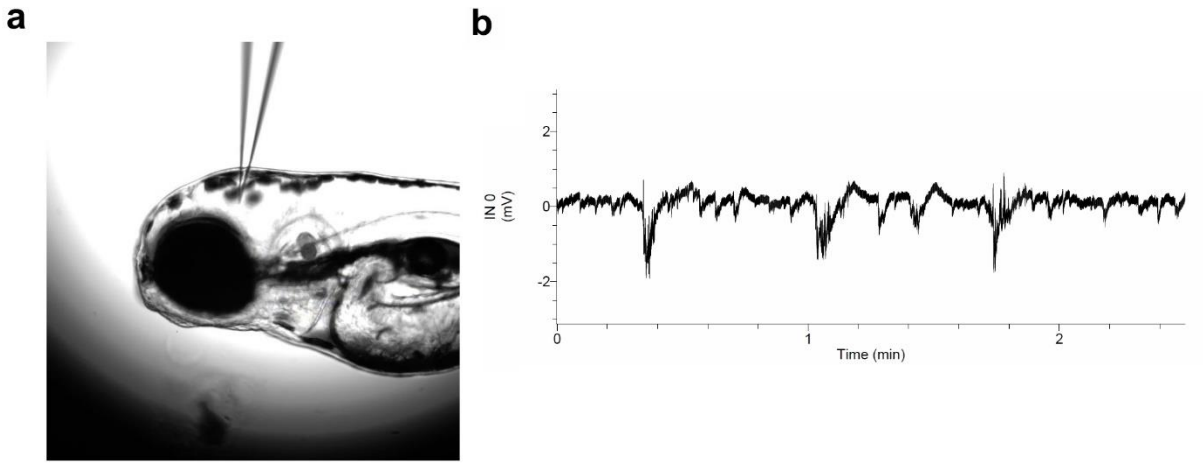

Figure 3-32: Tectal field potential recording. (a) Representative image of an agar-immobilized 5dpf wild type AB larva with the electrode placed in the optic tectum. (b) representative trace of the electric field potential (in mV) in the optic tectum over a 10-minute recording of a 5-dpf zebrafish larvae incubated with PTZ 20mM for 30 minutes.

We then proceeded to tectal field potential recordings, electroencephalography in the optic tectum, in control MO and *pcmt/l* MO injected larvae. As expected for control MO-injected larvae, we detected no epileptiform events in those animals (Figure 3-33 a). These recordings did not provide any evidence for increased epileptic activity in the brains of *pcmt/l* morphant larvae either (Figure 3-33 b). Despite our preliminary observations indicating increased twitching events reminiscent of epileptic seizures in the *pcmt/l* morphant larvae, the above described more quantitative methodologies for detecting epileptic activity in our model (locomotor tracking and tectal field potential recordings) did not lend further support to the assumption that isoaspartyl methyltransferase deficiency may trigger abnormal epileptic seizures in zebrafish, at least at the early developmental stages that were testable in our morpholino knockdown model.

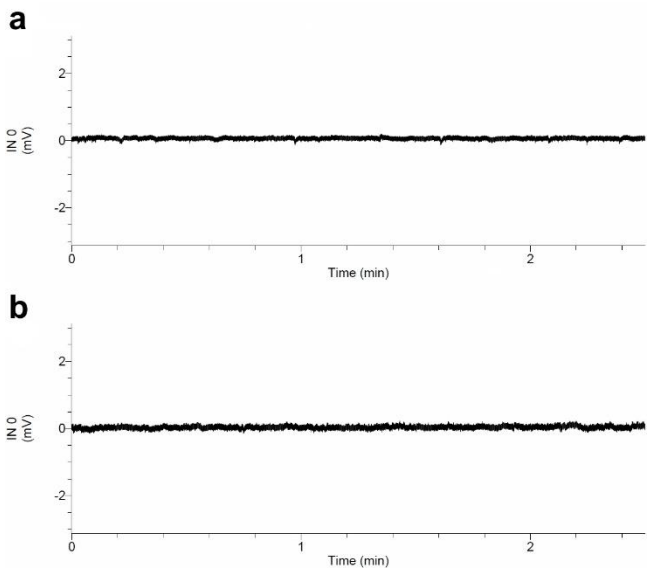

Figure 3-33: Tectal field potential recordings in control MO and pcmt/l MO larvae at 5 dpf. Traces of the electric field potential (in mV) in the optic tectum over a 10-minute recording in a control larva (a) and a pcmt/l morphant larva (b). A representative experiment out of 5 independent similar experiments with similar observations is shown.

3.4 Interplay between PCMT and calcium signalling

Calmodulin, a major regulator of calcium levels in the cell, was reported to be a major substrate for Pcmt1 (REISSNER *et al.* 2006; VIGNESWARA *et al.* 2006). It was also shown that calmodulin loses its activity upon deamidation of Asn residues, but recovers its activity when repaired by PCMT1 (JOHNSON *et al.* 1987a). Moreover, a yeast 2-hybrid system revealed that calmodulin doesn't only serve as a substrate for PCMT1, but that they seem to share other types of complex interactions (O'CONNOR and O'CONNOR 1998). Calcium homeostasis is essential for many physiological functions in the cells. The cytosolic concentration of calcium is generally very low and tightly regulated and a disturbance in that regulation can lead to many neurological disorders (WOJDA *et al.* 2008). Finally, there is also a link between calcium signalling and epilepsy and actually another approach to detect epileptic seizures is to monitor calcium fluxes in the brain as a result of the activation of voltage-gated calcium channels during neuronal firing (GRIENBERGER and KONNERTH 2012; LILLIS *et al.* 2015). Also, it appears that PTZ-induced seizures are calcium dependent, since calcium channel blockers attenuated the PTZ effect on seizure development (GATCH *et al.* 2001). One may assume that isoaspartyl accumulation in calmodulin in PCMT1-deficient models (or a missing regulatory interaction between calmodulin and PCMT1) affects calcium homoeostasis in the cell, contributing thereby to the neurological disturbances observed for example in the *Pcmt1* knockout mice. These observations motivated us to investigate the effects of *PCMT* deficiency on calcium fluxes in our zebrafish and mammalian cell models.

3.4.1 Calcium signalling in *pcmt/l* knockdown zebrafish

GCaMP6f is a genetically encoded calcium indicator consisting in a fusion protein between calmodulin and a circularly permuted GFP connected through an M13 peptide (CHEN *et al.* 2013). When calmodulin binds to calcium it undergoes conformational changes leading to increasing fluorescence intensity of the fused GFP. We took advantage of the beta-actin:GCaMP6f transgenic zebrafish line to monitor cytoplasmic calcium levels in the brain in the context of *PCMT* deficiency. We injected eggs from the beta-actin:GCaMP6f line at the 1 – 2 cell stage with either control or *pcmt/l* MOs. Larvae at 4 dpf were immobilized in 1.5% low melting agarose on a glass slide and covered with 0.3× Danieau's containing 20 mM PTZ. Time-lapse image acquisition was started 5 minutes after addition of the PTZ-containing solution for 15 minutes and the mean fluorescence intensity measured using the ImageJ software.

A shown by the oscillations of the fluorescence signal in the brain of larvae injected with control MO, PTZ induced large calcium transients over the whole duration of the experiment (Figure 3-34). Interestingly, *pcmt/l* deficient larvae showed no major calcium peaks during the whole time-lapse imaging, indicating much less transient calcium fluxes into the cytoplasm of the brain cells of these larvae

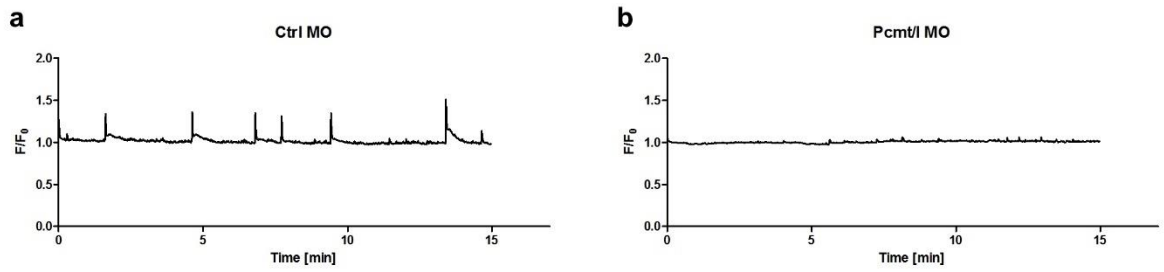

Figure 3-34: Calcium transients in 4 dpf beta-actin:GCaMP6f pcmt/l morphants. Calcium signalling in 4 dpf larvae either control (a) or pcmt/l (b) morphants n=5. Larvae exposed to 20 mM PTZ 5 minutes prior to fluorescence signal acquisition for 15 minutes. Signal (F) was extracted using ImageJ and normalized to the 35th percentile signal (F_0). Normalized signal (F/F_0) were plotted against time.

In order to confirm these results, we performed rescue experiments in which we injected beta-actin:GCaMP6f eggs with mixtures of *pcmt/l* MOs and pGEMT expression plasmids containing the coding sequences for wild type *pcmt* and *pcmtl* or mutated coding sequences leading to the expression of D83V mutant proteins that correspond to catalytic null mutants lacking isoaspartyl methyltransferase activity (CIMMINO *et al.* 2008). In the rescue experiment, we pre-incubated the larvae for 30 minutes in 20 mM PTZ prior to acquiring the fluorescence signal over another 30-min period. Clearly, restoring expression of wild type Pcmt and Pcmtl, but not expression of the catalytically inactive proteins, rescued the calcium transients induced by PTZ (Figure 3-35), similarly

to what was previously observed in control MO injected larvae. These observations suggest that the strong calcium signalling defect observed in the *pcmt/l* morphant larvae is specifically caused by the down-regulation of the *pcmt* and *pcmtl* gene expression (and not due to off-target effects) and moreover, that this effect is dependent on the methyltransferase activity of the enzymes.

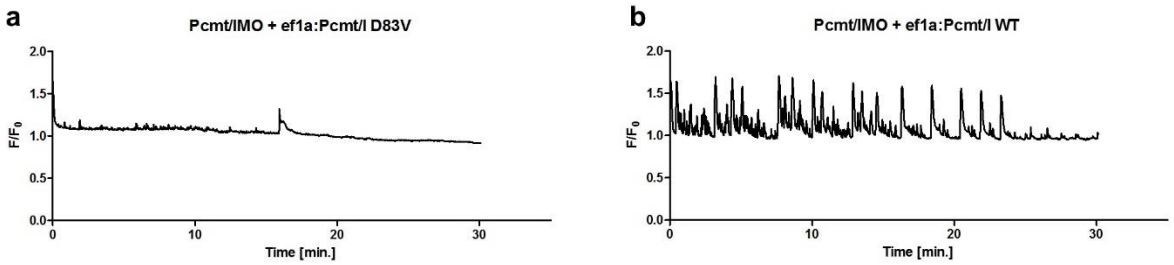

Figure 3-35: Calcium signalling in beta-actin:GCaMP6f zebrafish larvae – rescue experiment. Calcium signalling in 4 dpf pcmt/l morphant larvae either control (a) D83V mutant pcmt/l (b) wt pcmt/l n=5. Larvae exposed to 20 mM PTZ 30 minutes prior to fluorescence signal acquisition for 30 minutes. Signal (F) was extracted using ImageJ and normalized to the 35th percentile (F_0). Normalized signal (F/F_0) were plotted against time.

Another interesting observation in the *pcmt/l* MO injected larvae was the small size of the head. We noticed during the first experiments that the *pcmt/l* MO injections resulted in a general developmental delay and smaller body size, which seemed consistent with the smaller body size observed for the *Pcmt1* knockout mice (YAMAMOTO *et al.* 1998). However, the latter mice displayed increased brain size, which contrasts with the smaller brains observed in *pcmt/l* morphant larvae (Figure 3-36). It should be noted though that a direct comparison between the zebrafish model and the mouse model is again not possible, since our observations in zebrafish were made in the first days of life while body and brain size measurements were reported for mice that were 4 – 7 weeks old (YAMAMOTO *et al.* 1998; FARRAR *et al.* 2005a). Our observation in the zebrafish larvae suggested that *pcmt/l* deficiency interferes with normal brain development, which may contribute to the strongly decreased calcium fluxes observed in these same larvae.

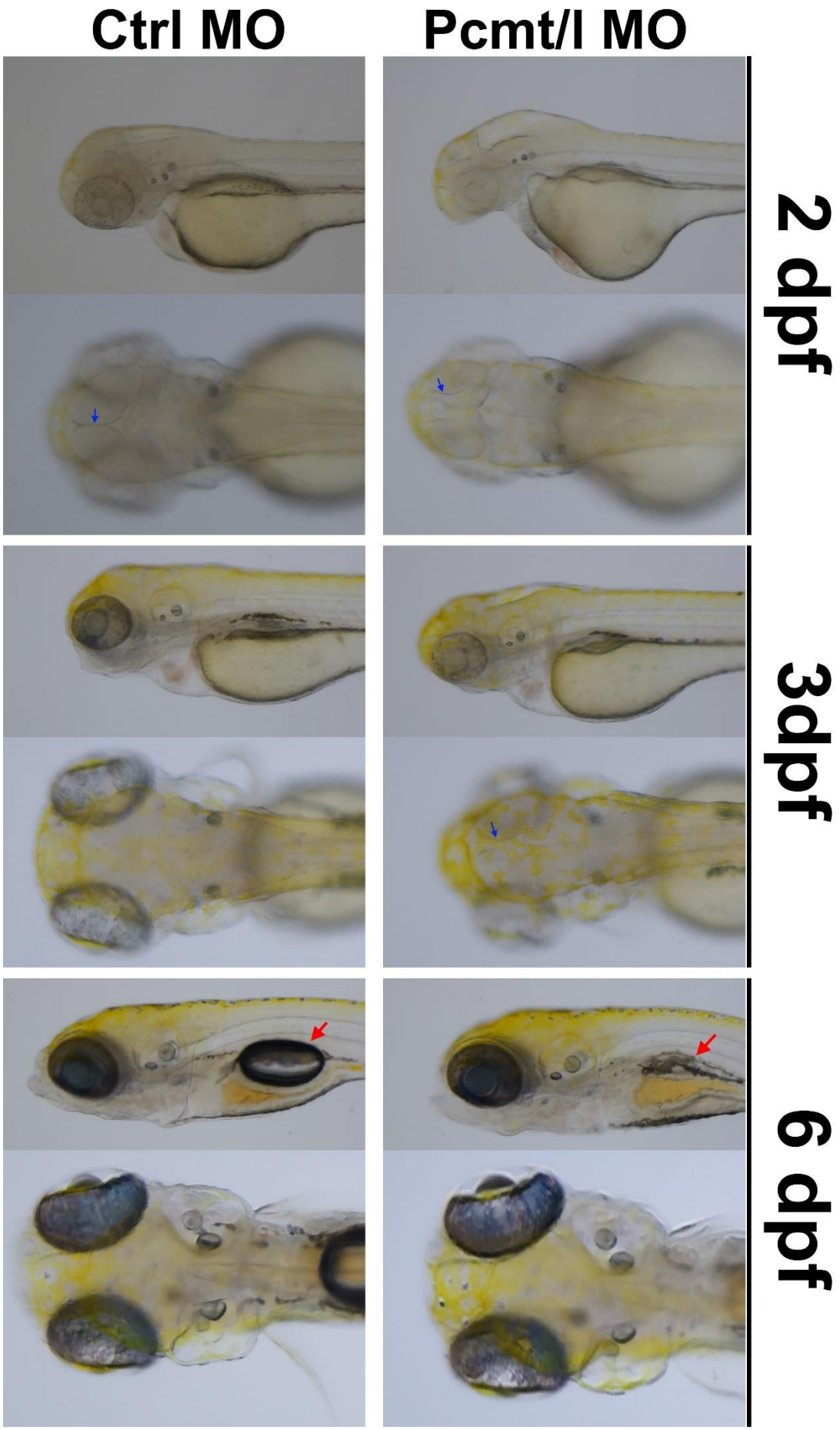
Ctrl MO
Pcmt/l MO
2 dpf
3dpf
6 dpf

Figure 3-36: Brain developmental delay in pcmt/l morphant larvae shown for different ages. The profile pictures taken at 2 and 3 dpf show a smaller head size as compared to the age-matched control MO injected larvae. The top-down view pictures allow to see the smaller size of the developing optic tectum (blue arrows) in the pcmt/l morphant larvae as compared to the control larvae. In the 6 dpf larvae, the most obvious difference between pcmt/l morphants and controls was the underdeveloped swimming bladder (red arrows), while the differences in head and brain size had become less pronounced at that developmental stage.

As a main conclusion, the results from this subsection indicate that the isoaspartyl methyltransferase activity of Pcmt/l plays an important role in the regulation of calcium fluxes towards the cytoplasm in brain cells during early zebrafish development. Via this hypothetical function, the isoaspartyl methyltransferases may therefore affect a panoply of downstream calcium-dependent pathways.

3.4.2 Calcium signalling in HT22 *Pcmt1* knockout cells

To test whether this effect of Pcmt on calcium fluxes is conserved and to understand more about the underlying mechanism, we went back to our HT22 *Pcmt1* knockout cell model (see section 3.1.2). To monitor calcium movements in our mouse cell line, we used the chemical fluorescent calcium indicator Fluo-4 from ThermoFisher scientific. We seeded 25,000 control or *Pcmt1* knockout HT22 cells per well in 12-well plates and incubated them under standard conditions for 48 hours. Cells were then washed with PBS and fresh media without phenol red added in addition to 250 µl of Fluo-4 staining solution. Cells were stained for 30 minutes before we place the plate under the microscope and acquire signal. We acquired signal for 20 minutes followed by stimulation with 20 µM ATP and continuation of signal acquisition for another 40 minutes and finally stimulated them a second time with 40 µM ATP.

We found that both control and *Pcmt1* knockout cells responded to the first ATP stimulation by a spike in cytosolic calcium concentration while upon the second ATP stimulation only the control cells responded with a similar calcium transient (Figure 3-37a). Comparison of the first spike between control and *Pcmt1* knockout cells showed a smaller peak area with a lower amplitude but with a larger width in the knockout cells (Figure 3-37 b – d). The lower peak area and amplitude indicate lower calcium concentration; in addition, the larger width of the peak indicates a slower decrease in the intracellular calcium concentration back to basal levels. This delay suggests a lower buffering capacity in the knockout cells, which could be due to a lower calcium binding capacity or affinity of calmodulin or to a defect in the ion channels releasing the calcium extracellularly. These results are reminiscent of the observations in the *pcmt/l* morphant zebrafish larvae in that they point towards Pcmt being important to sustain cellular calcium fluxes.

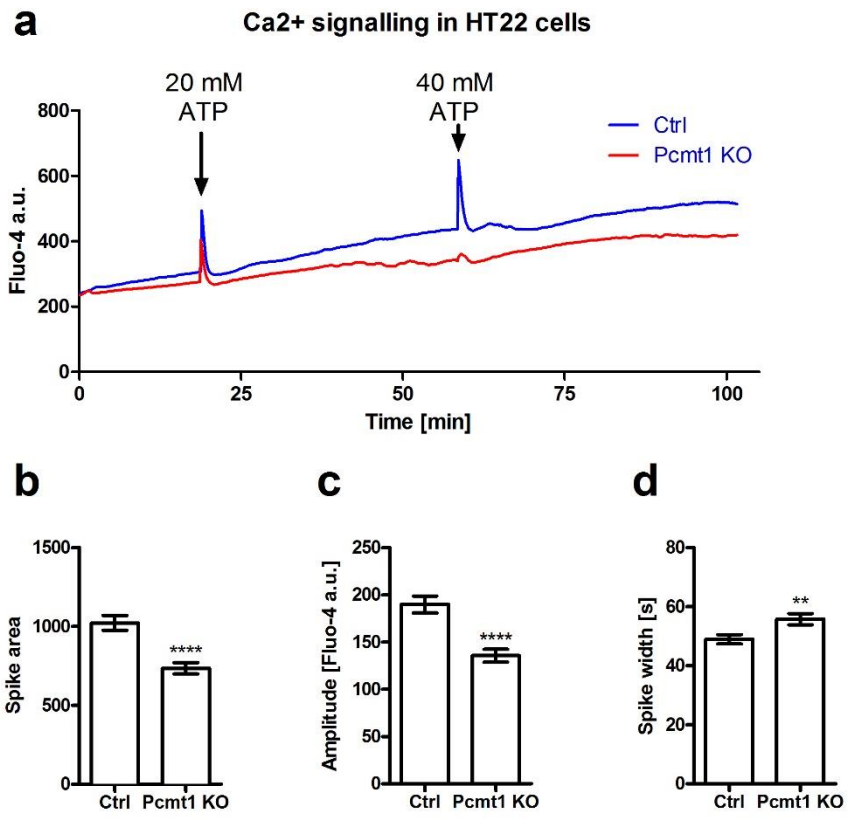

*Figure 3-37: Calcium transients in HT22 cells in response to ATP stimulation. (a) Fluo-4 fluorescence signal acquired by microscopy in control (blue trace) and Pcmt1 KO (red trace) cells to monitor intracellular calcium concentrations in response to ATP stimuli. (b – d) Analysis of the first spike in response to the 20 µM ATP stimulation showing a decrease in spike area (b) and amplitude (c), but an increase in spike width in the KO cells compared to control cells. (**** p-value <0.0001; **p-value <0.001)*

Intracellular calcium release from the endoplasmic reticulum to the cytosol in response to ATP is mediated through the G-protein coupled receptor and phospholipase C (PLC) activation that in turn catalyses the cleavage of phosphatidylinositol (3,4,5)-trisphosphate (PIP_3) into inositol (3,4,5)-trisphosphate (IP_3) and diacylglycerol (DAG) (SALTER and HICKS 1995). To try to understand why the *Pcmt1* knockout cells are less responsive to ATP stimulation in terms of calcium transients, we aimed to quantify GTP, GDP and IP_3 levels in *Pcmt1* knockout and control cells. Polar metabolites were extracted from the cells using a cold methanol extraction protocol followed by phase separation as described in the methods (Section 2.2.4.6) and metabolite extracts were analysed using a targeted LC-MS-based approach (Section 2.2.4.7). These analyses did not reveal any significant difference in the GTP/GDP ratio, but a 4-fold decrease in intracellular IP_3 concentration in the *Pcmt1* knockout cells compared to the control cells (Figure 3-38). In addition, we found that the ATP/ADP ratio was lower in the *Pcmt1* knockout cells compared to the control cells (Figure 3-38 b), which is consistent with previous results showing lower ATP levels in A549 cells deficient in *PCMT1* (OGASAWARA *et al.* 2016). In

the latter study, a 70% decrease in cellular ATP levels was reported upon *PCMT1* knockdown. Our results suggest that *Pcmt1* deficiency may lead to a metabolic state that is less responsive to stimuli normally inducing spikes in cytosolic calcium concentrations. Due to reasons that remain currently unclear, lower isoaspartyl methyltransferase activity in cells seems to lead to lower intracellular concentrations of IP_3, which is an important second messenger for intracellular calcium release.

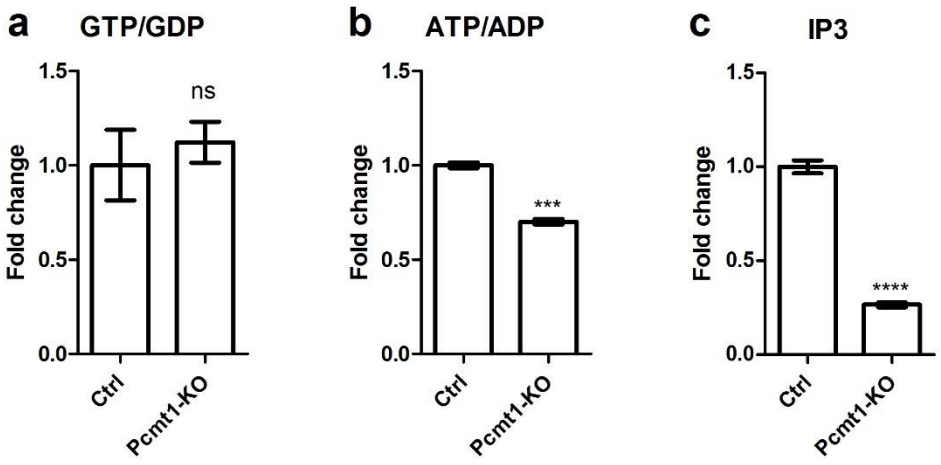

*Figure 3-38: Comparison of nucleotide and inositol-3,4,5-trisphosphate (IP_3) levels in control and Pcmt1 KO HT22 cells. Targeted LC-MS analyses showed no change in the GTP/GDP ratio, a 1.5-fold decrease in the ATP/ADP ratio and a 4-fold decrease in IP_3 levels in the Pcmt1 knockout cells compared to the control cells. The values shown correspond to peak areas of m/z ions of interest normalised to the corresponding peak areas in control cells and are means ± SEM of 3 biological replicates (ns, non-significant; ***p-value < 0.001; ****p-value < 0.0001).*

4 Discussion

The Protein L-isoaspartyl methyltransferase (PCMT) recognizes isoaspartyl residues arising from aspartyl as well as asparaginyl residues in proteins and initiates their reconversion to aspartyl residues. The work described in the present thesis aimed to understand more about molecular mechanisms involving PCMT and which are vital for cellular homeostasis, more specifically in the brain. Although the only known catalytic function of PCMT is the transfer of a methyl group from the cofactor SAM to isoaspartyl residues in proteins initiating their 'repair' back to aspartyl residues, this methylation can lead to different outcomes as follows: (1) inhibition of protein aggregation through limiting isoaspartyl content in specific proteins (β-amyloid (Aβ) aggregability has for example been shown to be suppressed by PCMT *in vitro* (JUNG *et al.* 2011)); (2) modulation of catalytic activity of enzymes (e.g. creatine kinase B activity is decreased in the absence of *Pcmt1* in mice due to formation of isoaspartyl residues (DIMITRIJEVIC *et al.* 2014)); (3) modulation of susceptibility to proteolysis of certain proteins (e.g. deamidation of asparaginyl residues in Bcl-xL and in calmodulin enhances their proteolysis (SZYMANSKA *et al.* 1998; DHO *et al.* 2013)); (4) modulation of protein function as conversion of asparaginyl to aspartyl residues can activate certain functions (e.g. deamidation of an asparaginyl residue in the N-terminal region of fibronectin is required to generate a binding site for $\alpha_v\beta3$-integrin for activation of extracellular matrix (CURNIS *et al.* 2006)); (5) D/L racemization of aspartyl residues (e.g. PCMT was found to be necessary for racemization of Asp25 in histone H2B (YOUNG *et al.* 2005). The diversity of these outcomes and of the protein substrates on which PCMT can act, the high conservation of PCMT among many species, and its wide distribution in various tissues indicate that this enzyme plays a fundamental role in living organisms and has the potential to interfere with numerous cellular pathways and processes.

4.1 PCMT differentially regulates growth signalling pathways

Among the different pathways found to be affected by PCMT are the IGF-1 and the MAPK signalling pathways. The insulin/IGF-1 signalling pathway has become a hallmark pathway of the aging process since the discovery that it's downregulation extends lifespan of *C. elegans*, but also in other organisms such as mice (KENYON *et al.* 1993; HOLZENBERGER *et al.* 2003; KENYON 2010). PCMT also has been shown to affect lifespan in mice, *C. elegans*, and *D. melanogaster* (KIM *et al.* 1997b; CHAVOUS *et al.* 2001; BANFIELD *et al.* 2008); in addition, *Pcmt1* knockout mice show hyperactivation of the IGF-1 pathway (FARRAR *et al.* 2005a). Therefore, a potential mechanism of lifespan regulation by PCMT could be through modulation of the IGF-1 signalling pathway. Interestingly, PCMT was also found to interact with the MAPK pathway, as *PCMT1* knockdown in HEK293 cells resulted in the transient activation of

different kinases in the MAPK pathway (KOSUGI *et al.* 2008). Nevertheless, the mechanism by which PCMT affects the IGF-1 and MAPK signalling pathways remains completely unknown.

One possible mechanism through which PCMT could interact with several signalling cascades is by modulation of the activity of one or several protein phosphatases; these phosphatases could be inactivated (or more rapidly degraded) due to the presence of one or several isoaspartyl residues in their sequence and lack of repair of those residues in PCMT-deficient organisms or cells could then lead to the hyperphosphorylation pattern of several signalling intermediates that has been observed (DOYLE *et al.* 2003; FARRAR *et al.* 2005a; KOSUGI *et al.* 2008) (Figure 4-1). Another more indirect mechanism could involve modulation of feedback regulations in affected signalling pathways (Figure 4-1). For example, a downstream target of Akt is the translational initiation repressor factor 4E-BP1/2 through the mTOR pathway. 4E-BP1/2 isolated from *Pcmt1* knockout mouse brain was found to accumulate isoaspartyl residues and be less active than the native form (BIDINOSTI *et al.* 2010) Lower activity of other downstream targets of Akt, e.g. the FOXO transcription factor, can lead to pathway activation via a positive feedback mechanism (PUIG *et al.* 2003). Similarly, *Pcmt* deficiency could thus lead to activation of intermediates of the IGF-1 pathway by lack of repair and inactivation of 4E-BP1/2. Also, proteomic analyses of *Pcmt1* knockout mice showed differential up- and downregulation of many proteins which are not direct substrates for Pcmt1. An example of this is the nonspecific serine/threonine-protein kinase DCLK1, which was found to be significantly upregulated in the *Pcmt1* knockout mouse brains (YANG *et al.* 2013) and could also contribute to activation of signalling pathways.

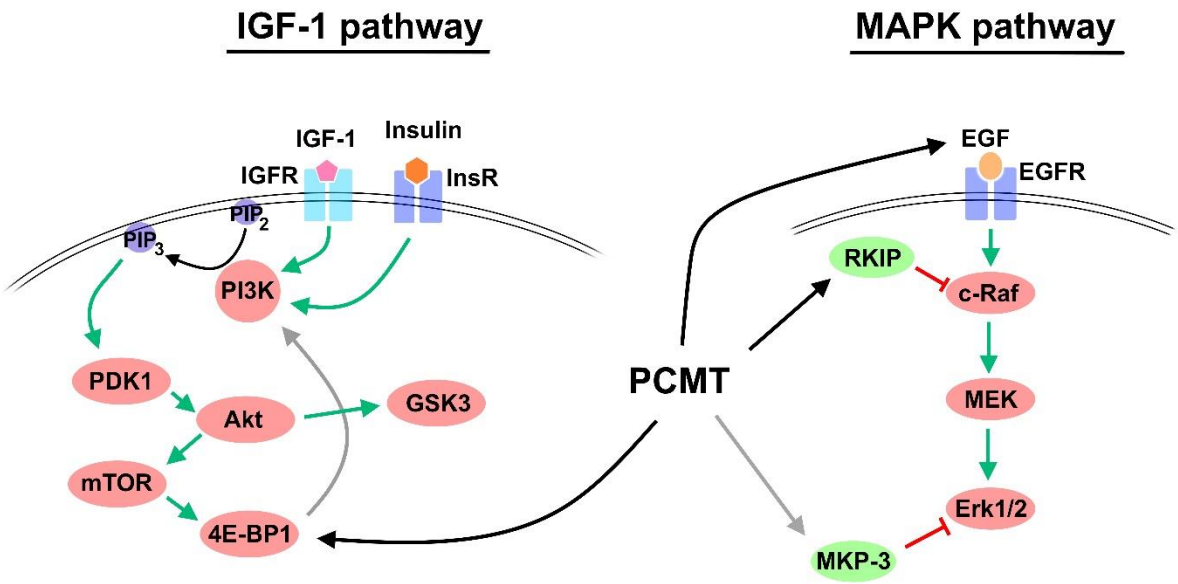

Figure 4-1: Possible interactions of PCMT with signalling pathways. Green arrows represent activation; red lines represent inhibition; black arrows point towards direct PCMT substrates; gray arrows represent potential regulatory

interactions. ***IGF-1****: Insulin growth factor-1;* ***IGFR****: IGF-1 receptor;* ***InsR****: Insulin receptor;* ***PIP_2****: Phosphatidylinositol 4,5-bisphosphate;* ***PIP_3****: Phosphatidylinositol (3,4,5)-trisphosphate;* ***PI3K****: Phosphatidylinositol 4,5-bisphosphate 3-kinase;* ***PDK1****: Phosphoinositide-dependent kinase-1;* ***Akt****: protein kinase B;* ***GSK3****: Glycogen synthase kinase 3;* ***mTOR****: mechanistic target of rapamycin;* ***4E-BP1****: Translation repressor protein* ***EGF****: Epidermal growth factor;* ***EGFR****: EGF receptor;* ***RKIP****: Raf kinase inhibitor protein;* ***MEK****: Mitogen-activated protein kinase kinase* ***Erk1/2****: extracellular signal–regulated kinase;* ***MKP-3****: MAP Kinase Phosphatase 3.*

To interrogate the mechanism underlying IGF-1 pathway activation in *PCMT* deficiency, we have established stable HEK293 and U-87 MG cell lines expressing low levels of *PCMT1* using lentiviral transduction of shRNAs. Unlike to what has been reported before by Farrar *et al* (2005a), i.e. hyperphosphorylation of IGF-1 pathway intermediates, including Akt and GSK3β, in *Pcmt1* knockout mouse brain compared to wild-type (FARRAR *et al.* 2005a), we did not detect a difference in the phosphorylation levels of Akt in our *PCMT1* knockdown cell models compared to control cells. We reasoned that two major differences might be at the basis of this discrepancy. First, the complete absence of Pcmt1 protein in the knockout mouse model as opposed to our knockdown models, where cells still retained 20 – 40% of isoaspartyl methyltransferase activity. Second, immunohistochemistry experiments in the Farrar *et al*. study showed that Akt hyperphosphorylation is by far the most pronounced in the hippocampus, indicating that our negative results might be related to the choice of cell type. We therefore switched to the HT22 cell line, an immortalized mouse hippocampal cell line, and, instead of using shRNA methodology to knock down *PCMT1* transcription levels, we used the CRISPR/Cas9 technology to completely suppress enzyme expression. The latter strategy led to the creation of a cell line in which no residual isoaspartyl methyltransferase activity was detectable, confirming total knockout of Pcmt1. Nevertheless, similar to what we had observed in the HEK293 and U-87 MG knockdown cells, *Pcmt1* knockout did not affect the phosphorylation levels of Akt in the HT22 cell line.

It appears therefore that the connection between PCMT and phosphorylation of Akt or IGF-1 signalling more generally is affected not only by cell type but by other factors like external stimulation factors, cell-cell interactions or cell state, differentiated or not. *PCMT1* knockdown in bone osteosarcoma cells (U2OS), similarly to our results, did not affect the phosphorylation levels of Akt (LEE *et al.* 2012). On the other hand, *Pcmt1* knockdown in adrenal gland pheochromocytoma cells (PC12) led not to up-, but downregulation of Akt phosphorylation in response to basic fibroblast growth factor (bFGF) during the differentiation process and the *Pcmt1* deficient cells showed poor differentiation (DUNG *et al.* 2016). The latter observations also suggest that PCMT might be involved in neuronal cell differentiation and that the PCMT effect on Akt phosphorylation levels also depends on the differentiation state of the cell. Unfortunately, our trials to differentiate HT22 cells to mature neurons failed and we therefore could not check whether this would have revealed effects of *Pcmt1* deficiency

on IGF-1 signalling. When Dung *et al* (DUNG *et al.* 2016) looked at the phosphorylation levels of Akt, they stimulated the cells with bFGF while Lee *et al* (LEE *et al.* 2012) did not use any stimulators and we tested both IGF-1 and insulin in our experiments; this could again lead to different outcomes, to not mention the complexity of the extracellular environment that cells are exposed to in the brain of a living animal and that we may just have missed critical factors in our cell culture models to reproduce what had been found in the brains of a whole organism mouse model.

Simultaneously, we wanted to validate our cell models by testing another signalling pathway, namely the MAPK pathway, reported previously to be activated in *PCMT1* knockdown HEK293 cells (KOSUGI *et al.* 2008). In our HEK293 *PCMT1* knockdown cell model, we did not find upregulation in the phosphorylation levels of Erk1/2 upon stimulation of the cells with 1 µg/ml EGF similar to their experimental set up. It seems that in the study by Kosugi *et al* (KOSUGI *et al.* 2008), they had a more efficient shRNA-mediated knockdown of *PCMT1* in HEK293 cells, since based on Western blot analysis they did not find detectable residual PCMT1 protein, while in our HEK293 knockdown cell line, an 'only' 80% reduction in PCMT1 protein levels was estimated using the same technique. In addition, in their model, *PCMT1* knockdown resulted in a 2-fold increase in the isoaspartyl levels in the knockdown cells compared to the control cells, while we only measured a 1.1-fold increase (Figure 3-4b). When we switched to *Pcmt1* knockout HT22 cells, we found higher phosphorylation levels of Erk1/2, but not MEK (also hyperphosphorylated in the Kosugi study), in the knockout cells compared to the control cells. The difference in results obtained in our two models, the *PCMT1* knockdown HEK293 and the *Pcmt1* knockout HT22 cells, suggests that the MAPK pathway is sensitive to enzyme and/or isoaspartyl levels in the cells in the sense that the lower the isoaspartyl methyltransferase activity levels and/or the higher the isoaspartyl levels, the more pronounced the effects on activation status of the MAPK signalling pathway will be (at least at the level of Erk1/2). Taken together, the observations also suggest that the effect of *Pcmt1* deficiency on the MAPK signalling pathway is not so strongly dependent on cell type, cell state and/or cell environment than the effect on IGF-1 signalling and that the former effect may therefore be mechanistically investigated further in a cell culture model.

A possible regulatory mechanism of the MAPK pathway by Pcmt is through the Raf kinase inhibitory protein (RKIP), which directly interacts with the Raf kinase, leading to less activation of the MAPK pathway (Figure 4-1). As already mentioned before (Table 1-1), RKIP was found to be a substrate for Pcmt1 through the proteomics analysis of *Pcmt1* mouse knockout brains (VIGNESWARA *et al.* 2006). Assuming that isoaspartyl accumulation would decrease its activity in *Pcmt1* deficient cells, this could lead to the activation of the MAPK pathway observed in these cells. In that scenario, one would expect, however, to find higher phosphorylation levels of MEK, which was not the case in our experiments,

and in the study by Kosugi *et al*. (KOSUGI *et al.* 2008), the effect on phosphorylation levels was also more pronounced on Erk1/2 than on MEK. The observation that a more downstream intermediate of the signalling cascade is the most hyperphosphorylated in *PCMT* deficient cells indicates that a decrease in protein phosphatase activity rather than an increase of protein kinase activity is a more likely mechanism involved in the effect of PCMT on the MAPK pathway.

In summary, PCMT interaction with growth signalling pathways, and more particularly with the IGF-1 signalling pathway, is affected by many factors and simple cell culture seems in this case not to allow to model an effect that has been observed in the much more complex brain environment. In addition to the potential influence of cell type, cell-cell interaction and differentiation state already mentioned above, absence of crucial extracellular signals may be a critical limitation in the cell culture model. For example, EGF was found to accumulate isoaspartyl residues (DIAUGUSTINE *et al.* 1987) and could contribute to abnormal signalling via the MAPK pathway in the absence of PCMT. Moreover, PCMT1 was originally discovered in the pituitary gland where many hormones were found to be substrates for the enzyme, including growth hormone and the hormonal carrier neurophysins (DILIBERTO and AXELROD 1974; EDGAR and HOPE 1974). The effect of PCMT deficiency on growth signalling might therefore depend on the presence of both the cells producing the growth factors as well as the target cells, which is more challenging to reproduce in simple cell culture.

4.2 Protein L-isoaspartyl methyltransferase in zebrafish

Pcmt1 knockout mice experience fatal epileptic seizures (KIM *et al.* 1997b; KIM *et al.* 1999). However, the interplay between *Pcmt1* and seizure development is still unclear. Zebrafish is emerging as a new model to study epilepsy for several reasons: both zebrafish larvae and adults recapitulate some features of the epileptic phenotype as described for humans and rodent models, namely convulsive behaviours associated with epileptiform brain discharges resulting from genetic mutations or after exposure to proconvulsant drugs; zebrafish larvae are highly amenable for genetic and/or pharmacological manipulations/treatments with implications for *in vivo* gene function and drug discovery; zebrafish larvae are optically transparent enabling the *in vivo* live imaging of neuronal activity and/or other cellular/molecular processes in the brain as reviewed by Cunliffe (CUNLIFFE 2016). For these reasons, zebrafish seemed like a valuable vertebrate model to investigate the role of isoaspartyl methyltransferase during brain development and susceptibility to epileptic seizures. However, the isoaspartyl methyltransferase function had not yet been reported in zebrafish.

In our search for homologs of human PCMT1 in zebrafish, we found two proteins annotated as Pcmt and Pcmtl and predicted to catalyse the same reaction as PCMT1, based on their amino acid sequence similarity to the human protein. Amino acid sequence analysis showed that human PCMT1 shares 85%

and 69% sequence identity with Pcmt and Pcmtl, respectively. In addition, the SAM-dependent methyltransferase domains as well as amino acids predicted to bind to the co-factor based on crystal structure data were highly conserved in both zebrafish proteins (KAGAN and CLARKE 1994; SMITH *et al.* 2002). Pcmt and Pcmtl proteins in zebrafish arise from two genes located on two different chromosomes (20 and 17, respectively). This duplication is common for many genes in zebrafish as a result of a genome duplication that occurred in the teleost fish lineage (TAYLOR *et al.* 2001). Our results showed that both *pcmt* and *pcmtl* are expressed during zebrafish development and at adult stage. Expression of two genes for the same function can, however, represent an energy burden for the cell and we wanted to first test whether both proteins catalyse the same reaction as human PCMT1 or if they had diverged in terms of molecular function and/or localization of expression.

4.2.1 Pcmt and Pcmtl catalyse the transfer of methyl group to isoaspartyl residues

For functional assay of both Pcmt and Pcmtl we expressed both enzymes in *E. coli* and successfully purified them to high homogeneity. To assay the catalytic activity of the two purified enzymes, we used a nonapeptide Lys-Ala-Ser-Ala-isoAsp-Leu-Ala-Lys-Tyr (KASAisoDLAKY) to serve as a substrate. Although many substrates have been identified for PCMT1, KASAisoDLAKY has proven to be a high affinity substrate for PCMT1 and was used to assay the activity of PCMT homologs from many different species (ICHIKAWA and CLARKE 1998). An advantage of also working with this substrate was thus to allow for direct comparison with previous studies. We assayed the enzymatic activity of Pcmt and Pcmtl *in vitro* using a radioactivity-based methyltransferase assay described before (PATANANAN *et al.* 2014). We found that both proteins catalyse the transfer of a methyl group from the co-factor SAM to isoaspartyl as revealed by the methanol release from the reaction product under alkaline conditions, thus suggesting that both Pcmt and Pcmtl are isoaspartyl methyltransferases. The slight difference in substrate affinity between Pcmt and Pcmtl may be explained by a difference in the amino acid residue in position number 120, i.e. in one of the highly conserved isoaspartyl methyltransferase domains, which corresponds to Ile in case of Pcmt and Val in case of Pcmtl. Human polymorphism at this amino acid residue showed higher substrate affinity in case of Val (RUTHERFORD and DAGGETT 2009).

Compared to PCMT homologs from other species, the substrate affinity of both zebrafish enzymes can be classified as intermediate among homologs with higher affinity, like human PCMT1, and lower affinity, like the *C. elegans* PCM-1, based on the reported K_M values (Table 4-1). The almost 10-fold lower substrate affinity of the zebrafish proteins compared to human PCMT1 cannot be attributed to differences in the isoaspartyl methyltransferase domains, since those are highly conserved between the proteins (see Figure 3-7 'multiple sequence alignment' in the Results section 3.1.3). Even more strikingly, the affinity of human PCMT1 for KASAisoDLAKY is 160-fold higher than the one of *A. thaliana* PCMT although the isoaspartyl methyltransferase domains are highly conserved between the two

proteins. Thus it appears that the affinity for the peptide substrate is highly influenced by amino acid residues outside of the isoaspartyl methyltransferase domains.

Table 4-1: K_M values of PCMT from different species for KASAisoDLAKY

Species	K_M [µM]	Reference
A. thaliana	80 ± 18	(THAPAR and CLARKE 2000)
***C. elegans* PCM-1**	9.12	(KAGAN and CLARKE 1995)
***D. Rerio* Pcmt**	4.2 ± 0.51	This work
***D. Rerio* Pcmtl**	3.6 ± 0.48	This work
***E. coli* pcm**	50.6	(FU *et al.* 1991)
***H. sapiens* PCMT1**	0.52 ± 0.08	(LOWENSON and CLARKE 1991)
Wheat germ	12.7	(MUDGETT and CLARKE 1993)
***T. maritima* pcm**	2.8 ± 0.24	(ICHIKAWA and CLARKE 1998)

4.2.2 *Pcmt* and *pcmtl* are expressed during early development

When we tested the presence of *pcmt* and *pcmtl* transcripts in fish eggs (i.e. eggs at 1-cell stage) we found that both of them are expressed as a result of maternal mRNA transmission through the oocyte. Following the transcript levels of both *pcmt* and *pcmtl* during development, we found that the *pcmt* transcript decreased up to 12 hpf followed by a gradual increase up to 3 dpf, and then stable levels up to 6 dpf. The variation in pcmt transcript level during the first day of development can be explained by the fact that the maternal contribution of the transcript is decreasing during the first hours of development and the embryos start expressing endogenous *pcmt* at later stages. On the other hand, *pcmtl* presents more stable transcription levels from 7 hpf to 2 dpf, and from 3 dpf the levels are doubled and become more stable up to 6 dpf.

Since PCMT plays a protein repair role, the presence of *pcmt/l* transcript in the eggs can represent a molecular function of PCMT in rejuvenation, a process taking place during gametogenesis where all damaged molecules are removed, yet the underlying mechanisms are still unclear (UNAL *et al.* 2011). Independently of this possible contribution to the rejuvenation process, the subsequent expression of *pcmt/l* during early developmental stages is interesting since isoaspartyl levels have been shown to positively correlate with age (KIM *et al.* 1997b; LOWENSON *et al.* 2001); such an early expression of the repair enzyme might thus indicate an alternative function, for instance a regulatory function via methylation of specific proteins as opposed to the more global housekeeping protein repair role that might become more important again during the aging process. In rats, the *Pcmt* transcript levels also increased in the brain from embryonic day 15 (E15) up to 28-week-old (28W) (SHIRASAWA *et al.* 1995).

This early expression of Pcmt in several species thus suggests a conserved role of this protein during embryonic development and this may be further supported by its importance for neuronal differentiation (*Pcmt1*-deficient fibroblasts fail to differentiate *in vitro*; (DUNG *et al.* 2016) and the developmental delay and lack of neuronal maturation in *Pcmt1* knockout mice (FARRAR *et al.* 2005b).

4.2.3 *pcmt* and *pcmtl* tissue distribution

Since we found that the catalytic function of zebrafish Pcmt and Pcmtl is very similar, one possible explanation that both of them are nevertheless actively expressed is a differential tissue distribution. We aimed at investigating the tissue distribution of both transcripts at different embryonic stages as well as in adult animals. Tissue distribution of PCMT homologs in other species were, to the best of our knowledge, not reported before at embryonic stage and the ex-uterus development of zebrafish offers in principle a unique opportunity to visualize gene expression during early development. The results obtained from the whole mount *in situ* hybridization of 1 dpf embryos for the *pcmtl* transcript agrees with previous results from a highthroughput expression analysis, which reported that the *pcmtl* transcript is not spatially restricted to a specific tissue (THISSE and THISSE 2004). Similar results were also obtained for *pcmt* showing ubiquitous expression in all tissues of the embryo. Yet, the high background in our negative controls during those experiments made it difficult to derive solid conclusions about the tissue localization of the *pcmt* and *pcmtl* transcripts during embryogenesis, since it might indicate a poor specificity of the hybridization probes used.

Our qRT-PCR results from adult zebrafish showed also ubiquitous expression of both transcripts, but with differential tissue expression levels. We found that both transcripts are present in all tested tissues, with the highest expression levels in the brain and testes or ovaries. A similar expression pattern, detected by transcript levels and isoaspartyl methyltransferase activity levels, was also found in rats (KIM *et al.* 1997b; LOWENSON *et al.* 2001). In addition, in *Pcmt1* knockout mice, the brain is the most affected organ with the mice dying due to fatal epileptic seizures. Interestingly, these seizures as well as the short lifespan phenotypes in *Pcmt1* knockout mice were rescued by adenoviral mediated expression of exogenous *Pcmt1* under the control of a neuron-specific promoter (KIM *et al.* 1997b; LOWENSON *et al.* 2001). These findings suggest that *Pcmt1* knockout in the organs other than the brain has much less critical pathological effects in mice. Moreover, many of the identified major substrates for PCMT are brain specific proteins (e.g. synapsin and dynamin 1; (VIGNESWARA *et al.* 2006; ZHU *et al.* 2006b)). Taken together these observations indicate a general support function of PCMT for all the tissues in the analysed species, including now zebrafish, but more critical roles in the brain.

The high levels of expression of PCMT in testes might be important to preserve fertilization competent sperm for several weeks of storage (CHAVOUS *et al.* 2000). Similarly, in plants protein homoeostasis in

seeds is essential since seeds experience long periods of quiescence before they start to germinate. In *Arabidopsis thaliana*, Pcmt affects seed longevity and germination vigor and protects the seeds from heat stress (OGE *et al.* 2008). And as mentioned before, like in the female eggs, the high expression levels of PCMT in the gametes of many species suggests a role in the rejuvenation process through removal of damaged molecules (UNAL *et al.* 2011).

While all the above helps justifying high expression of Pcmt and Pcmtl in brain, testes and ovaries, the reason for the conserved expression of two enzymes that catalyse the same reaction, with very similar kinetic parameters and spatial distribution in zebrafish is not clear yet. However, it is not the first organism in which the expression of two *PCMT* transcripts has been maintained. *Arabidopsis thaliana* expresses two genes encoding two active isoaspartyl methyltransferase enzymes and the one difference found so far is the subcellular localization, as one of the forms is targeted to the nucleus (XU *et al.* 2004; VILLA *et al.* 2006). Another difference for the two *A. thaliana* genes has been identified at the level of the regulation of expression: while one of them is constitutively expressed, the other one is expressed under stress or abscisic acid treatment (MUDGETT and CLARKE 1994; XU *et al.* 2004). We also saw differences in the transcription dynamics of the *pcmt* and *pcmtl* genes in zebrafish during early development. Further investigations on transcriptional regulation and subcellular localization of Pcmt and Pcmtl in zebrafish might provide rational explanations for the two corresponding genes being still actively expressed in this organism.

4.2.4 Physiological implication of *pcmt/l* knockdown in zebrafish

To assess the function of Pcmt and Pcmtl *in vivo*, we used MO technology to knock down the expression levels of both genes. We selected two splice blocking MOs targeting the *pcmt* and *pcmtl* transcripts and validated their knockdown efficiency. We can see clearly that both MOs interfere with the normal splicing as PCR amplification using primers flanking the region targeted by the MOs and gel analysis showed smaller PCR amplicons from the transcripts of both genes following MO injection (Figure 3-15). Sequencing of those transcripts confirmed the skipping of the MO-targeted exons. Moreover, the morphant larvae co-injected with both the *pcmt*- and *pcmtl*-targeting MOs showed a more than 73% decrease in the isoaspartyl methyltransferase activity at 2 dpf and no detectable activity at 4 dpf (Figure 3-17). All of these results confirmed the efficiency of the MO strategy used to simultaneously reduce the expression levels of *pcmt* and *pcmtl*.

Despite the drastic decrease in isoaspartyl methyltransferase activity in the *pcmt/l* morphant larvae, there was no increase in isoaspartyl levels at 2 dpf and only a 1.5-fold increase at 4 dpf. The absence of isoaspartyl accumulation at 2 dpf and the low accumulation at 4 dpf as compared to an up to 8-fold increase of isoaspartyl levels measured in the *Pcmt1* knockout mice (KIM *et al.* 1997b) can be due to

many reasons. First, the age difference of the analysed fishes and mice: the accumulation of isoaspartyl residues is age-dependent and the higher accumulation observed in the *Pcmt1* knockout mice might simply be due to the fact the samples were obtained from older animals (30 – 40 days old mice (KIM *et al.* 1997b)). Two or four days of development might not have been enough time for reaching isoaspartyl levels that would lead to clearly identifiable phenotypes, but this time constraint is imposed by MO technology as knockdown efficiency is going down starting at 5 dpf. Second, knockdown of the isoaspartyl methyltransferase activity might lead to activation of proteolytic pathways limiting the accumulation of isoaspartyl residues in proteins by an independent mechanism (PATANANAN *et al.* 2014). Indeed, SDS-PAGE analysis of protein extracts from 2 dpf *pcmt/l* morphants indicated increased proteolysis in those samples and comparison of results obtained by isoaspartyl assay in total protein extracts versus fluorography supported the idea of increased proteolysis of isoaspartyl-containing proteins specifically induced in the *pcmt/l* knockdown animals (Section 3.1.3.3.2). The latter might therefore be an interesting model for further investigations on proteases more specifically acting on isoaspartyl-containing proteins.

MO-mediated double knockdown of both *pcmt* and *pcmtl* led to morphological abnormalities in zebrafish larvae. The most obvious phenotypes in the *pcmt/l* morphants were the small size, curved trunk and a delayed swim bladder development. A recent publication showed disagreements between some phenotypes observed with MO-mediated knockdown and TALEN- or CRISPR/Cas9-mediated knockout of the same genes, suggesting that a number of phenotypes induced by MOs are due to off-target effects (KOK *et al.* 2015). The most common MOs off-target phenotypes reported by the latter study included curved and shortened trunk, and stalled intersegmental vessels. However, the poor correlation between gene knockout and knockdown in this study could have been due to several reasons. For example, gene knockout, but not to the same extent knockdown, can activate compensatory mechanisms masking phenotypic effects of the gene silencing; from this point of view it seems actually advantageous to use MO knockdown methodology over knockout technologies (ROSSI *et al.* 2015). Another reason for different results obtained with knockout versus knockdown strategy can be gene redundancy in knockout models due to gene duplication, alternative start codon, or partial overlapping function, especially in zebrafish where the genome duplication event has resulted in numerous paralogous gene pairs; this could again lead to rescue of effects caused by the knockout gene (BARBARIC *et al.* 2007). Therefore, despite the recent controversies around MOs as a good tool for gene knockdown in zebrafish, we believe that it remains a valuable strategy, especially if the injected MO concentrations are well titrated and used at a concentration where the targeted genes are efficiently downregulated, but where toxic, likely off-target effects are not seen yet. We did these titration efforts where we tried different amount of each MO individually and selected the maximum

amounts that does not lead to sever dysmorphology by itself. Even when combining the two MO against pcmt and pcmtl together we went more down with the MO amounts combined together. In addition, the gene specificity of phenotypic effects induced by MOs can be tested using rescue strategies, by exogenous expression of the target gene either by transcript injection or DNA vector carrying the coding sequence of the target gene. Although our trails to rescue the dysmorphological phenotype in the larvae did not lead to a significant recovery of those phenotypes, still *pcmt/l* knockdown could be the reason behind the observed morphological abnormalities since mice deficient in *Pcmt1* also experience growth retardation (KIM *et al.* 1997b).

The delay of development of the swim bladder was another interesting phenotype in the *pcmt/l* morphant larvae, specially it not a common off-target effect induced by many other MOs (KOK *et al.* 2015). The swim bladder development was found to be regulated by various signalling pathways like Notch and Hey2 (HOLTZINGER and EVANS 2005), but so far none of these pathways were investigated in the context of *PCMT* deficiency. Interestingly, swim bladder development hindrance has been recently reported in the context of other neurological disorders modelled in zebrafish (ZHANG *et al.* 2015; WAGER *et al.* 2016). Since PCMT is important for normal brain functioning (as also supported by work in zebrafish in this thesis), there could be a specific link to the swimming bladder development. This indicates that the zebrafish may be a valuable new model to explore interactions of PCMT with signalling pathways involved in development in addition to the growth signalling pathways to which connections have already been established in other models. The work performed in this thesis lays solid grounds to start these investigations.

MO-mediated knockdown studies of genes associated with epilepsy in humans were found to induce seizures in zebrafish larvae, which could be detected using electroencephalography in the optic tectum (EEG) (ZHANG *et al.* 2015; WAGER *et al.* 2016). Likewise, we pursued to use the same technique to analyse brain electrical activity and to test whether our *pcmt/l* morphant zebrafish larvae present a similar seizure phenotype as observed in *Pcmt1* knockout mice (KIM *et al.* 1999). Our EEG results did not reveal brain electrical activity reminiscent of epileptic discharges in the *pcmt/l* morphant larvae. We also performed locomotor tracking experiments in the same larvae; locomotor tracking is another method for the detection of abnormal brain activity as it can result in atypical movement behaviours (AFRIKANOVA *et al.* 2013). Locomotor tracking of 4 dpf larvae deficient in *pcmt/l* showed neither differences in their total distance travelled nor in the velocity of their movements under control conditions; even when using a sub-convulsant concentration of PTZ (0.5 mM), no difference was detected. Interestingly, with 20 mM PTZ stimulation, *pcmt/l* morphant larvae showed much less locomotor activity in terms of total distance travelled during the assay, although the velocity of the

remaining movements was similar to that of control larvae. On the one hand, these observations indicate that *PCMT* deficiency does not lead to seizure development in young zebrafish larvae. On the other hand, the locomotor tracking experiments revealed that PCMT deficiency in those larvae leads to abnormally low locomotor activity, which may be explained by delays in swimming bladder and/or brain development.

Despite both showing developmental abnormalities(YAMAMOTO *et al.* 1998), it is interesting to think about the possible reasons for the discrepancy between *Pcmt1* knockout mice and *pcmt/l* morphant larvae in terms of seizure development. One possible reason is that the downregulation of PCMT activity in the morphant zebrafish larvae is probably only effective at later stages than in the mouse knockout model. The MOs we used for *pcmt/l* knockdown interfere with mRNA splicing. This means that the maternal mRNA, which is already spliced, is not affected by those MOs and our results indeed indicated that wild type *pcmt/l* transcripts are present in the *pcmt/l* morphant embryos up to 12 hpf (data not shown). By contrast, in *Pcmt1* knockout mice, the enzyme is absent from the very start (1-cell zygote stage). It can be speculated that some critical events in terms of brain development are differentially affected depending on the presence or absence of PCMT in these first hours of life, which will later on lead (or not) to the development of seizures. Also, the *Pcmt1* knockout mice were reported to have a 15% increase in brain size compared to wild type littermates (YAMAMOTO *et al.* 1998), whereas *pcmt/l* morphant larvae actually showed smaller brain size compared to control larvae. Finally, a straightforward comparison between the zebrafish and mouse model may be hampered again by the difference in age of the analysed animals. Given the decrease in MO knockdown efficiency beyond 5 dpf, we tried to detect seizures via EEG recordings at 4 dpf in the zebrafish model, whereas the seizure events detected in the mice occurred at the age of 4 – 12 weeks (YAMAMOTO *et al.* 1998).

Despite all these observations pointing at the absence of seizure development in *PCMT* deficient zebrafish, some further deeper investigations may be required to fully formulate conclusions. Due to some developmental delays, interpretation of the locomotor tracking experiments is difficult in terms of epileptic seizure development and EEG recordings seem to be better adapted to pursue the epilepsy analyses in the *pcmt/l* morphant larvae. EEG recordings were so far only performed in control conditions. It might be worth repeating such recordings after exposure of the larvae to proconvulsant agents. However, given the apparent irresponsiveness of the *pcmt/l* morphants to the commonly used proconvulsant PTZ (see calcium signalling experiment and also the absence of increased locomotor activity after exposure to high doses of PTZ), different agents like pilocarpine and kainate should be tested here. Finally, it is worth considering that the epileptic seizures in the *Pcmt1* knockout mice may

be a secondary effect of Pcmt1 deficiency whereas the primary effect is impaired brain development. Similarly, mutations in the phenylalanine hydroxylase (*PAH*) gene lead to seizures in a mouse model and humans, but the primary effect of phenylalanine accumulation is a delay in brain development which then renders these animals prone to seizures (KAYAALP *et al.* 1997; MARTYNYUK *et al.* 2007).

4.3 Calcium signalling

4.3.1 Calcium homeostasis in the cell

Regulation of intracellular Ca^{2+} concentration is important for many cellular processes like differentiation, apoptosis and transcription (BERRIDGE *et al.* 2003). These processes depend on the dynamics of cytosolic Ca^{2+} concentrations as well as downstream targets. Most of the Ca^{2+} binding proteins are characterized with helix-loop-helix motives (also called EF-hands), which contain the conserved sequence Asp-X-Asp-X-X-Gly. Ca^{2+} binds to this motif causing conformational changes in the Ca^{2+} binding proteins that will allow the binding to their downstream (FRIEDBERG 1988). Well known examples of Ca^{2+} binding proteins are calmodulin, which regulates for example phosphorylation cascades via interactions with Ca^{2+}-calmodulin dependent kinases (CaMK), protein kinase C and protein kinase A and the Ca^{2+}-dependent phosphatase calcineurin B (BERRIDGE *et al.* 2003). Since intracellular Ca^{2+} concentration critically impacts many cellular processes, it is tightly controlled by a range of regulatory mechanisms.

Upregulation of cytosolic Ca^{2+} concentrations is achieved through either influx from extracellular space or release from intracellular Ca^{2+} pools, mainly the ER, but also other organelles like sarcoplasmic reticulum (SR), Golgi apparatus and mitochondria. Ca^{2+} influx from the extracellular space occurs through voltage-operated as well as ligand-gated Ca^{2+} channels upon stimulation. N-methyl-D-aspartate receptors (NMDARs) are one class of ligand-gated Ca^{2+} channels activated upon ligand binding like the excitatory neurotransmitter glutamate (RAO and FINKBEINER 2007). Voltage-operated Ca^{2+} channels, e.g. N and P/Q channels, are present on excitable neurons and are activated upon membrane depolarization and will lead to Ca^{2+} influx and neurotransmitter release (BURNASHEV and ROZOV 2005). Intracellular Ca^{2+} release in response to GPCR stimulation is achieved through the production of inositol 1,4,5 trisphosphate (IP_3), which binds to IP_3 receptors (IP3R) on the ER membrane, leading to calcium release from the ER to the cytosol (SALTER and HICKS 1995).

Downregulation of cytosolic Ca^{2+} concentrations was found to be kinetically controlled. Cells evolved mechanisms for rapid decrease in cytosolic Ca^{2+} concentration and others for slower decrease, in order to bring the Ca^{2+} concentration back to its basal levels following stimulation. Rapid decrease mechanisms depend on protein buffers like calbindin D-28k, calretinin, and calmodulin, present in the

cytosol and binding instantly to Ca^{2+} reducing its cytosolic free concentration (SCHWALLER 2007). Slower mechanisms are based on Ca^{2+} pumps and exchangers. Mitochondria also were found to be sensitive to cytosolic Ca^{2+} concentration and play an important role in its downregulation where they tend to take up Ca^{2+} to protect the cells from apoptosis (COLLINS *et al.* 2001; GIACOMELLO *et al.* 2007).

This brief summary illustrates that intracellular Ca^{2+} concentration is regulated through different mechanisms and should make it clear that interfering with one or more of those checkpoints would lead to perturbed Ca^{2+} homeostasis affecting many Ca^{2+}-dependent cellular functions.

4.3.2 Interplay between PCMT and calcium

Calmodulin is one of the early discovered substrates for PCMT. It accumulates high levels of isoaspartyl levels during *in vitro* as well as *in vivo* aging (GAGNON *et al.* 1981; JOHNSON *et al.* 1985; POTTER *et al.* 1993). In addition, one of the isoforms of PCMT1 contains the RDEL ER retention signal, suggesting a possible localization of the enzyme also in this Ca^{2+} hub organelle. Supporting this hypothesis is the isoaspartyl formation in calreticulin, an endoplasmic reticulum resident protein and Ca^{2+} regulator, which is one of the major substrates for Pcmt1 found through the proteomic analysis of *Pcmt1* knockout mouse brains (VIGNESWARA *et al.* 2006). Moreover, it has recently been reported that PCMT1 may play an important role in the preservation of mitochondrial function and that its knockdown leads to a significant decrease in ATP levels (OGASAWARA *et al.* 2016), which we confirmed in our *Pcmt1* knockout cell model. Finally, the EF-hand (Asp-X-Asp-X-X-Gly) in Ca^{2+} binding proteins contains two aspartate residues which are prone to isoaspartyl formation affecting Ca^{2+} binding (FRIEDBERG 1988). Due to all these established or potential connections between PCMT and Ca^{2+} homeostasis as well as known connections between the latter and epilepsy development, we were tempted to test the effect of PCMT on Ca^{2+} signalling in the PCMT deficient models created in this thesis.

We used a transgenic zebrafish line that encodes the GCaMP6f protein, a cytosolic Ca^{2+} indicator whose fluorescence intensity increases upon intracellular Ca^{2+} release. PTZ was reported to induce seizures through release of Ca^{2+} from intracellular pools like the endoplasmic reticulum (ER) (SUGAYA and ONOZUKA 1978; ONOZUKA *et al.* 1989). The knockdown of *pcmt/l* in zebrafish drastically hindered Ca^{2+} fluxes in the brain in response to PTZ stimulation, an effect that was rescued with exogenous expression of *pcmt/l* but not catalytically inactive forms of the enzymes. This observation strongly suggested that the isoaspartyl methyltransferase activity plays an important role to support Ca^{2+} movements in the cell. We sought further support for this role in our HT22 cell model where we used the Fluo-4 dye (GEE *et al.* 2000), a fluorescent Ca^{2+} indicator. Upon stimulation of the cells with ATP, both control and *Pcmt1* knockout cells showed a transient increase in intracellular Ca^{2+} concentrations.

Interestingly, upon a second stimulation with ATP, the control cells again responded with a spike in intracellular Ca^{2+} concentration, which was not observed in the *Pcmt1* knockout cells.

Even though the HT22 knockout cells responded to the first ATP stimulation, the Ca^{2+} spike area and width showed that a lower intracellular Ca^{2+} concentration was reached and that the subsequent Ca^{2+} buffering (to recover original Ca^{2+} concentrations) was less efficient as compared to control cells. As mentioned before, cytosolic Ca^{2+} binding proteins like calmodulin and organelles like the mitochondria are important players in Ca^{2+} buffering or downregulation. Non-repaired calmodulin in *Pcmt1* knockout cells could be one of the reasons behind the poor buffering of Ca^{2+} since the Ca^{2+} binding affinity of calmodulin might be affected with the accumulation of isoaspartyl residues (BILLINGSLEY *et al.* 1985b; OTA and CLARKE 1990). Another possibility of poor Ca^{2+} buffering could be mitochondrial dysfunction. Our results showed lower ATP/ADP ratios in *Pcmt1* knockout HT22 cells and a recent study also provided evidence for mitochondrial dysfunction in PCMT1 knockdown A549 cells(OGASAWARA *et al.* 2016).

To further investigate the mechanism involved in the crosstalk between PCMT and Ca^{2+} signalling, we used LC-MS analysis to measure the levels of Ca^{2+} related metabolites in HT22 *Pcmt1* knockout cells. The release of Ca^{2+} from the ER in response to ATP was found to be phospholipase C (PLC) dependent following activation of GTP-dependent GPCR. PLC catalyses the hydrolysis of phosphatidylinositol 4,5-bisphosphate (PIP_2) to diacylglycerol (DAG) and IP_3, which in turn binds to the IP_3 receptor (IP3R) in the ER membrane leading to the release of Ca^{2+} (SALTER and HICKS 1995). The GTP/GDP ratio was not affected by *Pcmt1* knockout, suggesting that GPCR activity may not be affected but rather a downstream target to it. By contrast, IP_3 levels in the *Pcmt1* knockout HT22 cells were found to be 4-fold lower as compared to control cells, which could contribute to the lower cytosolic calcium levels reached after ATP stimulation in the knockout cells. A possible reason for decreased IP_3 concentrations in the knockout cells could be a deficiency in PLC activity due to isoaspartyl residue accumulation in the enzyme, but this has not been investigated so far. Noticeably, similar to *Pcmt1* knockout mice, PLC knockout mice experience epilepsy, (KIM *et al.* 1997a) suggesting that the epileptic seizures in the *Pcmt1* knockout mice may be mechanistically connected to PLC function, although this remains highly speculative for the time being.

In summary, our work in PCMT deficient cell and zebrafish models suggests that the isoaspartyl methyltransferase activity of PCMT plays an important role in the calcium response of the cell to extracellular stimuli, that is conserved in fish and mammals. Possible mechanisms underlying this role of PCMT are as follows: 1) supporting PLC activity for the adequate production of IP_3 and Ca^{2+} release from the ER; 2) maintaining calmodulin levels or calcium affinity to guarantee adequate calcium

buffering capacity in the cytosol; and 3) preserving mitochondrial function and thereby its role in calcium re-uptake through an as yet unknown mechanism (Figure 4-2). Some evidence has been found to support the first mechanistic line proposed. However, this list is not exhaustive and further work is needed to better understand how PCMT contributes to regulating calcium uptake and/or downregulation after exposure of the cell to extracellular stimuli.

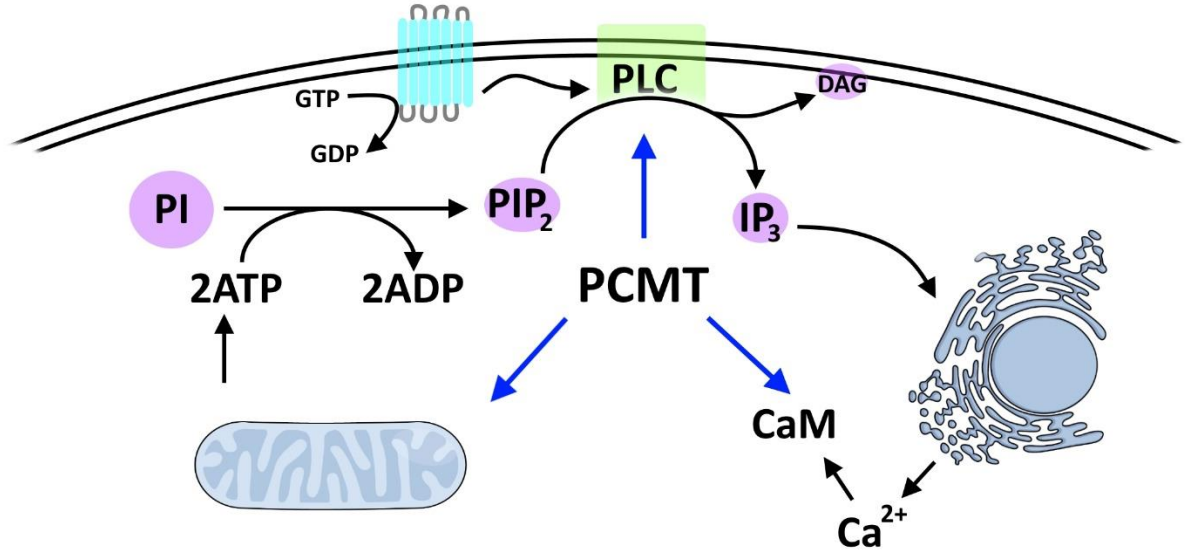

Figure 4-2: Possible mechanisms underlying the role of PCMT in supporting the cellular calcium response to extracellular stimuli.PCMT deficiency may lead to lower PLC activity and IP_3 production and/or mitochondrial dysfunction and lower ATP production. In addition, PCMT deficiency could affect the Ca^{2+} buffering capacity of the cytosol via effects on calmodulin levels or Ca^{2+}affinity. ***CaM****: Calmodulin;* ***DAG****: diacylglycerol;* ***IP_3****: inositol (3,4,5)-trisphosphate;* ***PIP_2****: Phosphatidylinositol 4,5-bisphosphate;* ***PLC****: phospholipase C.*

5 Conclusions and perspectives

Our work aimed at elucidating the mechanism by which the protein repair enzyme PCMT interacts with growth signalling pathways such as the insulin/IGF-1 and MAPK pathways. To address this aim, new models to investigate this and other physiological roles of PCMT have been established and validated and for the first time *in vivo* evidence could be produced to support and important role for PCMT in the cellular calcium response to extracellular stimuli in the brain.

PCMT1 knockdown in HEK293 and U-87 MG cells did not affect either Akt or Erk1/2 phosphorylation levels under our experimental conditions. *Pcmt1* knockout in HT22 mouse hippocampal cells did not produce detectable effects on Akt phosphorylation either, but we could find a transient increase in ERK1/2 phosphorylation levels in the knockout cells compared to control cells after exposure to EGF. Our main conclusions from this work are that the regulation of the insulin/IGF-1 signalling pathway by PCMT seems to rely on interactions that are too complex to reproduce in simple cell culture models and that can only be meaningfully addressed in the context of the living brain. This is less the case for the effect of PCMT on the MAPK signalling pathway, which can be observed in simple cell culture. However, type of stimulator used, stimulator concentration, exposure time to the stimulator, and extent of reduction of PCMT expression are all factors critically impacting this effect. We ended up finding conditions under which ERK1/2 hyperphosphorylation could be reproducibly observed in PCMT knockout cells; these conditions can now be used to investigate molecular mechanisms underlying the observed effect in a convenient experimental setting.

We have also established a new vertebrate whole organism model for investigation of the physiological role of PCMT. After demonstrating that zebrafish expresses two PCMT homologs (Pcmt and Pcmtl) with isoaspartyl methyltransferase activity, we characterized their expression during development and their tissular distribution. Maternal transcript for both genes are transmitted to the progeny, reflecting the importance of both genes during the very first stages of development. Both enzymes were ubiquitously expressed in all organs tested with the highest levels in the brain and testes or ovaries, consistent with what has been reported for other species. Both enzymes catalyse the transfer of a methyl group from the cofactor SAM to isoaspartyl residues with very similar kinetics. MO-meditated knockdown of both genes simultaneously led to developmental abnormalities, locomotor impairment, and a perturbed calcium response.

For future perspectives, it would be interesting to reveal the differences between Pcmt and Pcmtl that justify conservation of expression of both the proteins by zebrafish. The data that we gathered so far revealed no large differences between Pcmt and Pcmtl in terms of gene expression, tissue distribution

and catalytic function. However, we did not investigate the subcellular localization of the enzymes. Such studies may reveal different compartmentalization of both enzymes similar to what has been found in *A. thaliana*, where one of the PCMT paralogs is targeted to the nucleus. It could also be that after gene duplication, both Pcmt and Pcmtl retained the isoaspartyl methyltransferase function, but that one of them retained another ancestral function, which was lost in the other. Further enzymatic and functional analyses of the zebrafish proteins may shed more light on possible alternative functions of PCMT.

Concerning the effect of PCMT on the calcium response that we uncovered in the zebrafish model and subsequently confirmed in the HT22 cell model, the low intracellular IP_3 levels that we detected upon *Pcmt1* knockout in the HT22 cells suggest that phospholipase C may be an interesting enzyme to study with respect to its susceptibility to isoaspartyl damage and a protective function of PCMT. It is currently not known whether PCMT interacts with PLC and whether or not this interaction plays a role in the effect of PCMT deficiency on the cellular calcium response. Another possible mechanistic explanation for the effects of PCMT deficiency on calcium fluxes, which cannot be ignored given a body of pre-existing evidence, involves the calcium binding protein calmodulin. As the isoaspartyl methyltransferase activity seems to be required for the role of PCMT in calcium regulation, based on our observations in the zebrafish model, the most straightforward calmodulin-associated mechanism would be that PCMT deficiency decreases the calcium binding affinity of calmodulin (due to non-repaired isoaspartyl residues) or its calcium binding capacity (due to increased proteolytic degradation of calmodulin because of higher isoaspartyl content). Support for these hypotheses could be obtained for example by measuring calmodulin protein levels as well as isoaspartyl content in calmodulin (by mass spectrometry; (YANG *et al.* 2013)) in *pcmt/l* morphant larvae versus control larvae.

Moreover, a recent proteomic study supports a role of PCMT in glutamate metabolism that might lead to seizures as well (YANG *et al.* 2013). We also obtained, during the work of this thesis, some preliminary data in our *Pcmt1* knockout HT22 cell line supporting differential response to glutamate toxicity compared to control cells. While 3 mM glutamate was found to be toxic and affects HT22 cell viability, *Pcmt1* knockout were resistant to the same concentration of glutamate. One possible explanation could be a damage in glutamate receptor in cells deficient in Pcmt1 leading to lower sensitivity to glutamate. It would be interesting to pursue the investigation of glutamate toxicity in our cell model which might reveal new findings on the effect of PCMT on glutamate metabolism.

Generation of a *pcmt/l* double knockout zebrafish line using CRISPR/Cas9 technology would enable us to study the effect of isoaspartyl residue accumulation, which is positively correlated with age, on physiological functions at later stages of development. The high expression levels of PCMT in the brain

and its interaction with various proteins associated to neurodegenerative diseases, which typically develop at later age stages, suggest that PCMT may play a protective role in neurodegenerative diseases. In this context, the study of the effects of PCMT deficiency certainly makes more sense at later age stages. Towards this end, it would also be interesting to study PCMT deficiency in combination with a neurodegenerative disease model such as for example zebrafish lines expressing α-synuclein. A *pcmt/l* knockout line would maybe also enable the study of seizures associated with PCMT deficiency and which may only develop at later age. The lower efficiency of MOs at developmental stages later than 5 dpf limited us from this point of view in this thesis, where we did not detect a difference in electrical brain activity by EEG in the young animals tested. Finally, a *pcmt/l* knockout zebrafish model may be instrumental in investigating the role of PCMT in insulin/IGF-1 signalling in the brain, given a number of afore mentioned practical advantages over the mouse model and that it addresses the apparent requirement for these studies to be implemented in the context of a living brain, as suggested by the work in this thesis.

6 Appendix

6.1 Plasmid maps

6.1.1 Plasmids for lentivirus production and shRNA

6.1.1.1 pENTR™/U6

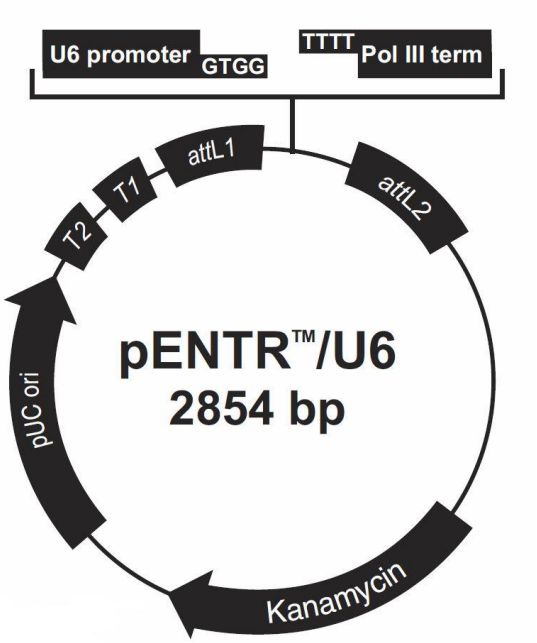

Feature	Bases	Benefit
***rrn*B T1 and T2 transcription terminators**	427-470 268-295 (C)	Reduces potential toxicity in *E. coli* by preventing basal expression of the double-stranded oligonucleotide of interest.
M13 forward (-20) priming site	537-552	Allow sequencing of the insert.
***att*L1 and *att*L2 sites**	569-668 (C) 979-1078	Bacteriophage λ-derived recombination sequences that allow recombinational cloning of a gene of interest in the entry construct with a Gateway® destination vector (Landy, 1989).
Human U6 promoter	705-968	Allows RNA polymerase III-dependent expression of the short hairpin RNA (shRNA) (Kunkel et al., 1986; Kubkel and Pederson, 1988).
U6 forward priming site		Allow sequencing of the insert.
5' overhangs	965-968 (C) 969-972	Allows ligase-mediated directional cloning of the double-stranded oligonucleotide of the insert.
Pol III terminator	969-974	Allows efficient termination of RNA Polymerase III-dependent transcription.
M13 reverse priming site	1119-1135	Allow sequencing of the insert.
Kanamycin resistance gene	1248-2057	Allows selection of the plasmid in *E. coli*.
pUC origin of replication (*ori*)	2178-2851	Permits high-copy replication and maintenance in *E. coli*.

6.1.1.2 pLenti6/BLOCK-iT™

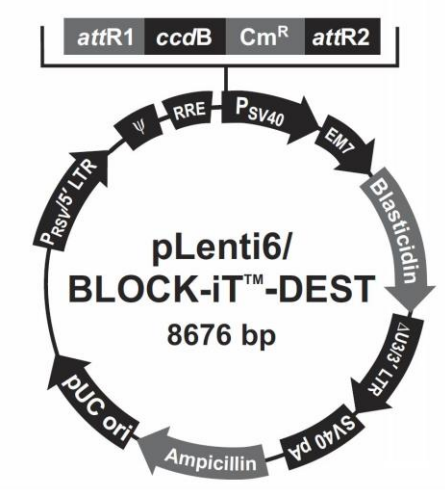

Feature	Bases	Benefit
Rous Sarcoma Virus (RSV) enhancer/promoter	1-229	Allows Tat-independent production of viral mRNA (Dull et al., 1998).
HIV-1 truncated 5' LTR	230-410	Permits viral packaging and reverse transcription of the viral mRNA (Luciw, 1996).
5' splice donor and 3' acceptors	520	Enhances the biosafety of the vector by facilitating removal of the Ψ packaging sequence and RRE such that expression of the gene of interest in the transduced host cell is no longer Rev-dependent (Dull et al., 1998).
HIV-1 psi (Ψ) packaging signal	521-565	Allows viral packaging (Luciw, 1996).
HIV-1 Rev response element (RRE)	1075-1308	Permits Rev-dependent nuclear export of unspliced viral mRNA (Kjems et al., 1991; Malim et al., 1989).
***att*R1 and *att*R2 sites**	1868-1992 4008-4132	Bacteriophage λ-derived recombination sequences that permit recombinational cloning of the gene of interest from Gateway.
***ccd*B gene**	2421-2726 (C)	Permits negative selection of the plasmid.
Chloramphenicol resistance gene (Cm^R)	3068-3727 (C)	Allows counterselection of the plasmid.
SV40 early promoter and origin	4281-4590	Allows high-level expression of the selection marker and episomal replication in cells expressing the SV40 large T antigen.
EM7 promoter	4645-4711	Synthetic prokaryotic promoter for expression of the selection marker in E. coli.
Blasticidin (bsd) resistance gene	4712-5110	Permits selection of stably transduced mammalian cell lines (Kimura et al., 1994).
ΔU3 HIV-1 truncated 3' LTR	5916-5430	Allows viral packaging but self-inactivates the 5' LTR for biosafety purposes (Dull et al., 1998). The element also contains a polyadenylation signal for transcription termination and polyadenylation of mRNA in transduced cells.
SV40 polyadenylation signal	5502-5636	Allows transcription termination and polyadenylation of mRNA.
***bla* promoter**	6492-6590	Allows expression of the ampicillin resistance gene.
Ampicillin resistance gene (β-lactamase)	6591-7451	Allows selection of the plasmid in *E. coli*.
pUC origin	7596-8269	Permits high-copy replication and maintenance in *E. coli*.

6.1.1.3 pLP1

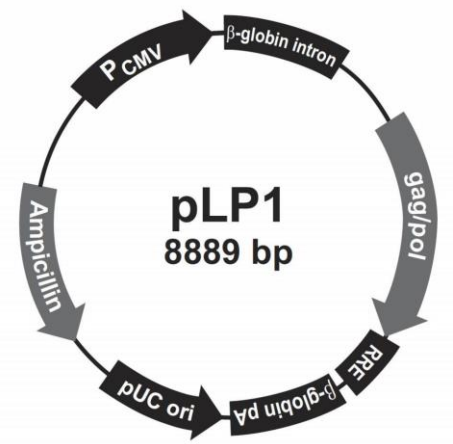

Feature	Bases	Benefit
Human cytomegalovirus (CMV) promoter	1-747	Permits high-level expression of the HIV-1 *gag* and *pol* genes in mammalian cells (Andersson et al., 1989; Boshart et al., 1985; Nelson et al., 1987).
Human β-globin intron	880-1320	Enhances expression of the *gag* and *pol* genes in mammalian cells.
HIV-1 *gag* coding sequence	1355-2857	Encodes the viral core proteins required for forming the structure of the lentivirus (Luciw, 1996).
HIV-1 *pol* coding sequence	2650-2857	Encodes the viral replication enzymes required for the replication and integration of the lentivirus (Luciw, 1996).
HIV-1 Rev response element (RRE)	5686-5919	Permits Rev-dependent expression of the *gag* and *pol* genes.
pUC origin of replication (*ori*)	6995-7668 (C)	Permits high-copy replication and maintenance in *E. coli*.
Ampicillin (*bla*) resistance gene	7813-8673 (C)	Allows selection of the plasmid in *E. coli*.

6.1.1.4 pLP2

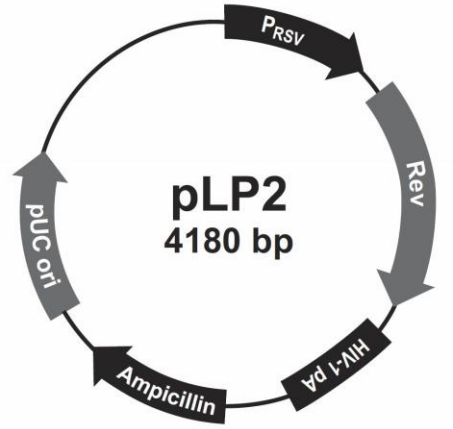

Feature	Bases	Benefit
RSV enhancer/promoter	1-271	Permits high-level expression of the *rev* gene (Gorman *et al.*, 1982).
HIV-1 Rev ORF	391-741	Encodes the Rev protein that interacts with the RRE on pLP1 and on the pLenti6/BLOCK-iT™-DEST expression vector to induce Gag and Pol expression, which promotes

		the nuclear export of the unspliced viral RNA for packaging into viral particles.
HIV-1 LTR polyadenylation signal	850-971	Allows efficient transcription termination and polyadenylation of mRNA.
Ampicillin (*bla*) resistance gene	2015-2875	Allows selection of the plasmid in *E. coli*.
pUC origin of replication (*ori*)	3020-3693	Permits high-copy replication and maintenance in *E. coli*.

6.1.1.5 pLP/VSVG

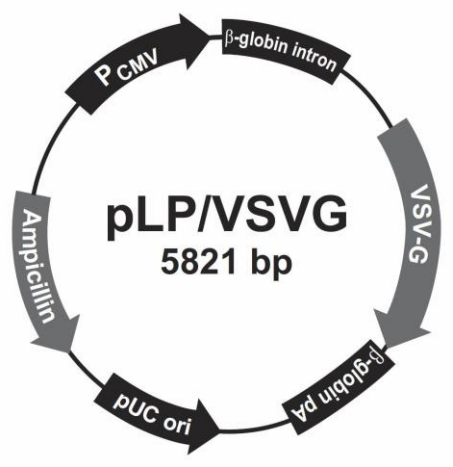

Feature	Bases	Benefit
Human CMV promoter	1-747	Permits high-level expression of the VSV-G gene in mammalian cells (Andersson et al., 1989; Boshart et al., 1985; Nelson et al., 1987).
Human β-globin intron	880-1320	Enhances expression of the VSV-G gene in mammalian cells.
VSV G glycoprotein (VSV-G)	1346-2881	Encodes the envelope G glycoprotein from Vesicular Stomatitis Virus to allow production of a pseudotyped retrovirus with a broad host range (Burns *et al*., 1993; Emi *et al*., 1991; Yee *et al*., 1994)
Human β-globin polyadenylation signal	3004-3769	Allows efficient transcription termination and polyadenylation of mRNA.
pUC origin of replication (*ori*)	3927-4600 (C)	Permits high-copy replication and maintenance in *E. coli*.
Ampicillin (*bla*) resistance gene	4745-5606 (C)	Allows selection of the plasmid in *E. coli*.

6.1.2 Plasmid for CRISPR/Cas9 pX459

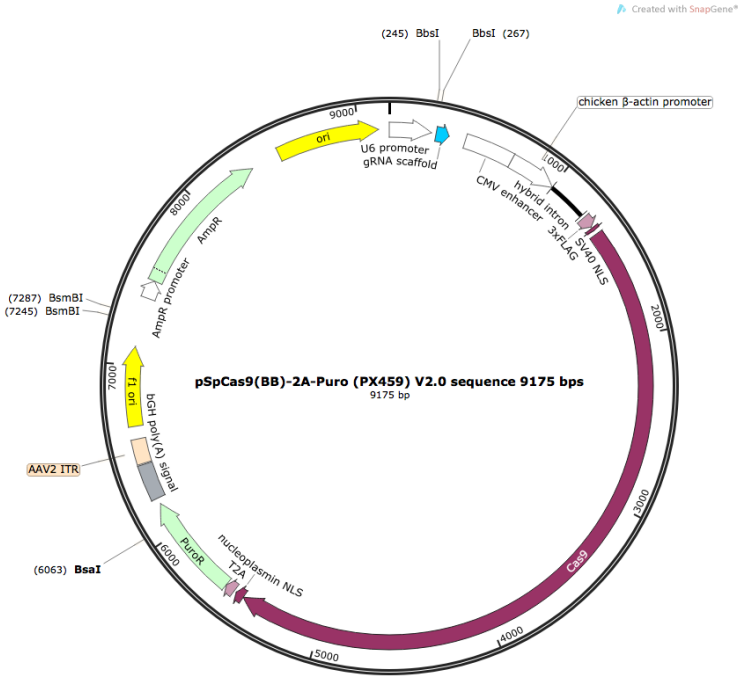

Feature	Benefit
U6 promoter	Allows RNA polymerase III-dependent expression of the gRNA
Human CMV promoter	Permits high-level expression of the Cas9 gene in mammalian cells.
Cas9	Encodes Cas9
PuroR	Permits selection of transfected mammalian cell lines
Human β-globin polyadenylation signal	Allows efficient transcription termination and polyadenylation of mRNA.
Ampicillin (*bla*) resistance gene	Allows selection of the plasmid in *E. coli*.
pUC origin of replication (*ori*)	Permits high-copy replication and maintenance in *E. coli*.

6.1.3 Plasmid for recombinant protein expression: pET100

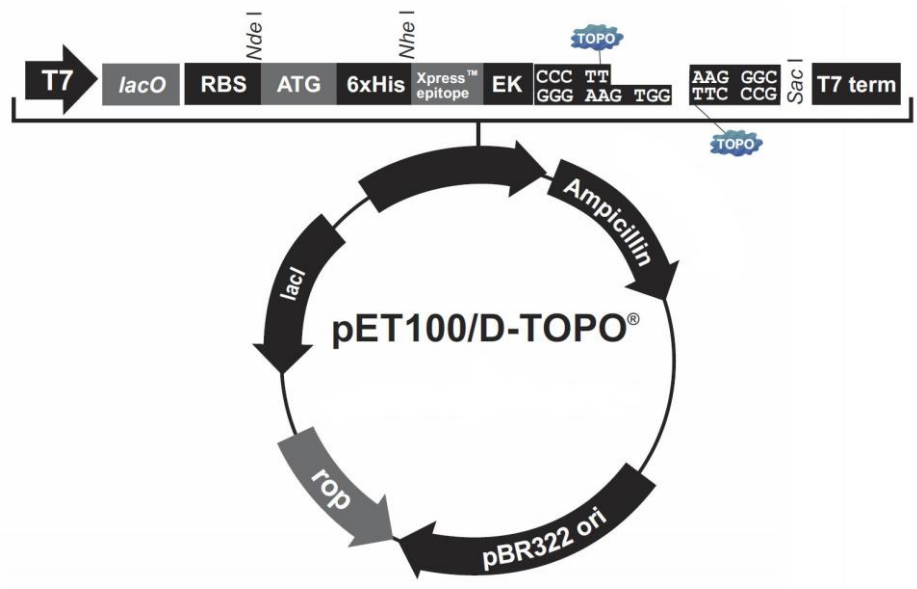

Feature	Bases	Benefit
T7 promoter	209-225	Permits high-level, IPTG-inducible expression of your recombinant protein in E. coli strains expressing the T7 RNA polymerase.
T7 forward priming site	209-228	Allow sequencing in the sense orientation
***lac* operator (lacO)**	228-252	Binding site for lac repressor that serves to reduce basal expression of your recombinant protein.
Ribosome binding site	282-288	Optimally spaced from the TOPO® Cloning site for efficient translation of PCR product.
N-terminal 6×His tag	309-326	Permits purification of recombinant fusion protein on metal-chelating resin (i.e. ProBond™ or Ni-NTA). In addition, allows detection of recombinant protein with the Anti-HisG Antibodies.
Xpress™ epitope (Asp-Leu-Tyr-Asp-Asp-Asp-Asp-Lys)	366-389	Allows detection of the fusion protein by Anti-Xpress™ Antibodies.
Enterokinase (EK) recognition site (Asp-Asp-Asp-Asp-Lys)	375-389	Allows removal of the N-terminal tag from your recombinant protein using an enterokinase such as EKMax™.
T7 Revers priming site	466-485	Allows sequencing of the insert.
T7 transcription termination region	427-555	Sequence from bacteriophage T7 which permits efficient transcription termination.
***bla* promoter**	856-954	Allows expression of the ampicillin resistance gene.
Ampicillin resistance gene (β-lactamase)	955-1815	Allows selection of the plasmid in *E. coli*.
***ROP* ORF**	3001-3192 (C)	Interacts with the pBR322 origin to facilitate low-copy replication in *E. coli*.
***lacI* ORF**	4507-5595 (C)	Encodes lac repressor which binds to the T7*lac* promoter to block basal transcription of the gene of interest and to the *lacUV5* promoter in the host chromosome to repress transcription of T7 RNA polymerase

6.1.4 Plasmids for zebrafish

6.1.4.1 pCS2+

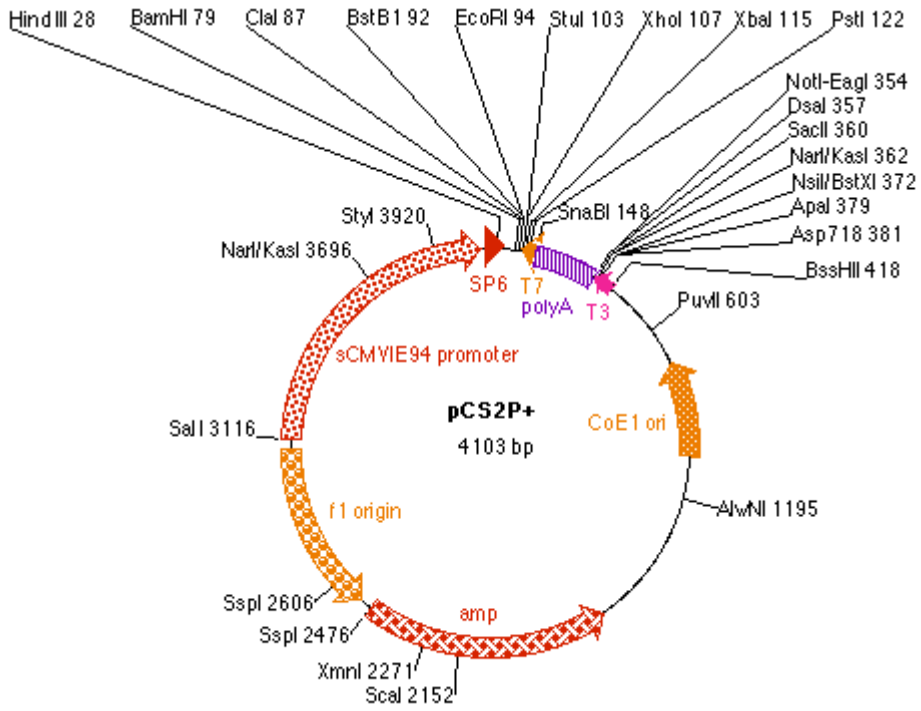

Feature	Bases	Benefit
Sp6 primer	35-52	Allows *in vitro* transcription of ORF
SV40_PA_terminator	145-273 (C)	Allows transcription termination and polyadenylation of mRNA.
Ampicillin resistance gene (β-lactamase)	1591-2451 (C)	Allows selection of the plasmid in *E. coli*.
f1 origin	2600-2905 (C)	Permits high-copy replication and maintenance in *E. coli*.

6.1.4.2 pZFF001

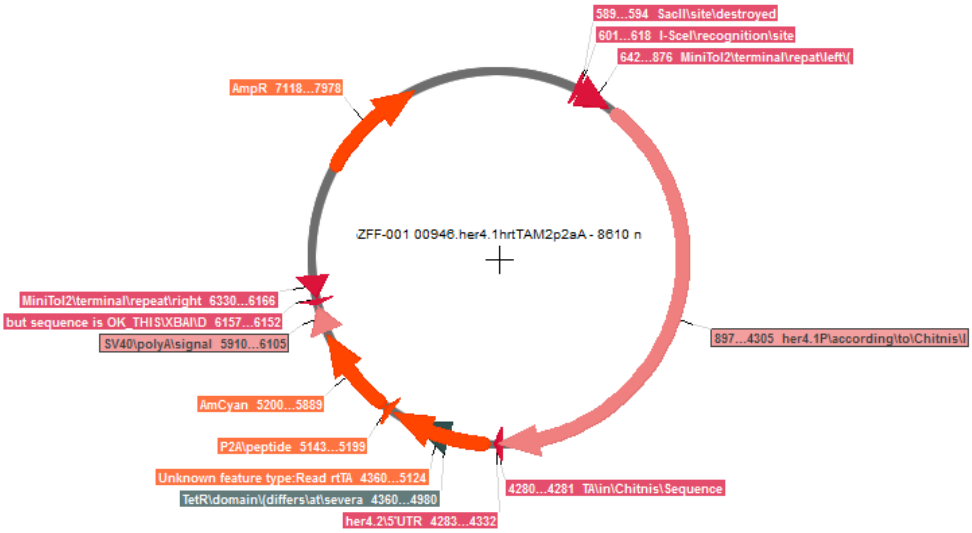

Feature	Benefit
MiniTol2	Permits transgenesis of exogenous gene into the zebrafish genome
Her4.1 promoter	Permits expression in neuronal cells
P2A peptide	Self-cleaving peptide that allow cleavage of expressed protein of interest from reporter fluorescent protein AmCyan
AmCyan	Fluorescence reporter protein
SV40 polyadenylation signal	Allows transcription termination and polyadenylation of mRNA.
Ampicillin resistance gene (β-lactamase)	Allows selection of the plasmid in *E. coli*.

6.1.4.3 pGEMT

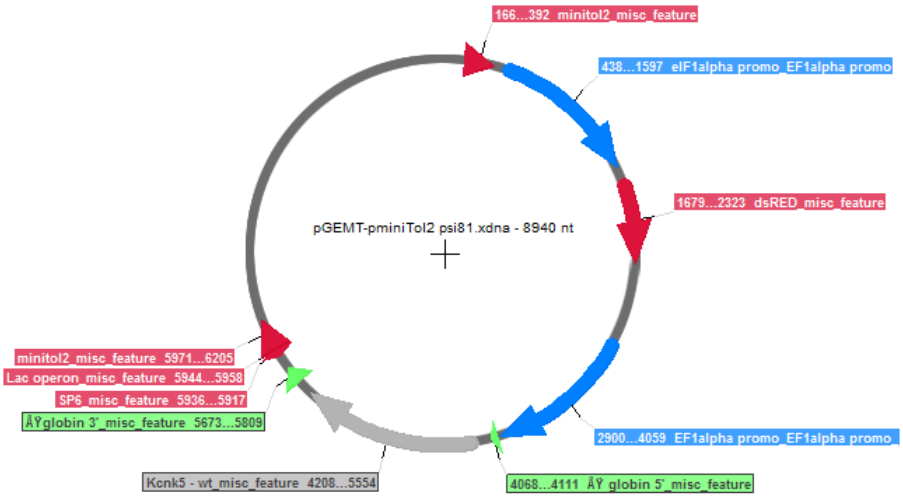

Feature	Benefit
MiniTol2	Permits transgenesis of exogenous gene into the zebrafish genome.
eEF1α promoter	Permits expression in eukaryotic cells
dsRED	Fluorescence reporter protein
Ampicillin resistance gene (β-lactamase)	Allows selection of the plasmid in *E. coli*.

6.2 LCMS

6.2.1 Ionisation

- Sheath gas flow rate 20 AU
- Auxiliary gas flow rate 5 AU
- Sweep gas flow rate 3 AU
- Spray voltage 2.5 kV
- Capillary temperature 250°C
- S-lens RF level 50 V
- Auxiliary gas heater temperature 100°C

6.2.2 Nucleotides method

- Targeted single ion monitoring (tSIM)
- Runtime 10 minutes
- polarity negative
- Mass resolution 35000
- AGC Target 200000 200000
- Maximum injection time 200 ms
- Isolation window 0.4 m/z

		Adduct neg mode	Mass adduct neg mode	detection window
AMP	C10H14N5O7P	-H	346.0552594	0 - 3
ADP	C10H15N5O10P2	-H	426.0215899	2 - 3.7
ATP	C10H16N5O13P3	-H	505.9879205	2.7 - 5
GMP	C10H14N5O8P	-H	362.050174	2.3 - 4.1
GDP	C10H15N5O11P2	-H	442.0165046	3.4 - 5.6
GTP	C10H16N5O14P3	-H	521.9828351	4.4 - 10

6.2.3 Inositol (3,4,5)-trisphosphate method

- Targeted single ion monitoring (tSIM)
- Runtime 20 minutes
- polarity positive
- Mass resuolution 70000
- AGC Target 200000 3000000
- Maximum injection time 200 ms
- Isolation window 0.4 m/z

		Adduct neg mode	Mass adduct neg mode	detection window
D-myo-inositol 1,4,5-triphosphate	C6H15O15P3	+H	420.9702047026	

7 References

AFRIKANOVA, T., A. S. SERRUYS, O. E. BUENAFE, R. CLINCKERS, I. SMOLDERS *et al.*, 2013 Validation of the zebrafish pentylenetetrazol seizure model: locomotor versus electrographic responses to antiepileptic drugs. PLoS One **8:** e54166.

ALTSCHUL, S. F., T. L. MADDEN, A. A. SCHAFFER, J. ZHANG, Z. ZHANG *et al.*, 1997 Gapped BLAST and PSI-BLAST: a new generation of protein database search programs. Nucleic Acids Res **25:** 3389-3402.

ALTSCHUL, S. F., J. C. WOOTTON, E. M. GERTZ, R. AGARWALA, A. MORGULIS *et al.*, 2005 Protein database searches using compositionally adjusted substitution matrices. FEBS J **272:** 5101-5109.

ASWAD, D. W., and E. A. DEIGHT, 1983 Endogenous substrates for protein carboxyl methyltransferase in cytosolic fractions of bovine brain. J Neurochem **41:** 1702-1709.

AXELROD, J., and J. DALY, 1965 Pituitary gland: enzymic formation of methanol from S-adenosylmethionine. Science **150:** 892-893.

BAKER, K. E., and R. PARKER, 2004 Nonsense-mediated mRNA decay: terminating erroneous gene expression. Curr Opin Cell Biol **16:** 293-299.

BANFIELD, K. L., T. A. GOMEZ, W. LEE, S. CLARKE and P. L. LARSEN, 2008 Protein-repair and hormone-signaling pathways specify dauer and adult longevity and dauer development in Caenorhabditis elegans. J Gerontol A Biol Sci Med Sci **63:** 798-808.

BARABAN, S. C., 2007 Emerging epilepsy models: insights from mice, flies, worms and fish. Curr Opin Neurol **20:** 164-168.

BARABAN, S. C., M. R. TAYLOR, P. A. CASTRO and H. BAIER, 2005 Pentylenetetrazole induced changes in zebrafish behavior, neural activity and c-fos expression. Neuroscience **131:** 759-768.

BARBARIC, I., G. MILLER and T. N. DEAR, 2007 Appearances can be deceiving: phenotypes of knockout mice. Brief Funct Genomic Proteomic **6:** 91-103.

BARBIERI, M., M. BONAFE, C. FRANCESCHI and G. PAOLISSO, 2003 Insulin/IGF-I-signaling pathway: an evolutionarily conserved mechanism of longevity from yeast to humans. Am J Physiol Endocrinol Metab **285:** E1064-1071.

BENNETT, E. J., J. BJERREGAARD, J. E. KNAPP, D. A. CHAVOUS, A. M. FRIEDMAN *et al.*, 2003 Catalytic implications from the Drosophila protein L-isoaspartyl methyltransferase structure and site-directed mutagenesis. Biochemistry **42:** 12844-12853.

BERRIDGE, M. J., M. D. BOOTMAN and H. L. RODERICK, 2003 Calcium signalling: dynamics, homeostasis and remodelling. Nature reviews Molecular cell biology **4:** 517-529.

BIDINOSTI, M., Y. MARTINEAU, F. FRANK and N. SONENBERG, 2010 Repair of isoaspartate formation modulates the interaction of deamidated 4E-BP2 with mTORC1 in brain. J Biol Chem **285:** 19402-19408.

BILLINGSLEY, M. L., and C. D. BALABAN, 1985 Protein-O-carboxylmethyltransferase in the rat brain: high regional levels in the substantia nigra, locus coeruleus and paraventricular nucleus. Brain Res **358:** 96-103.

BILLINGSLEY, M. L., S. KIM and D. M. KUHN, 1985a Immunohistochemical localization of protein-O-carboxylmethyltransferase in rat brain neurons. Neuroscience **15:** 159-171.

BILLINGSLEY, M. L., R. L. KINCAID and W. LOVENBERG, 1985b Stoichiometric methylation of calcineurin by protein carboxyl O-methyltransferase and its effects on calmodulin-stimulated phosphatase activity. Proc Natl Acad Sci U S A **82:** 5612-5616.

BILLINGSLEY, M. L., P. A. VELLETRI, W. LOVENBERG, D. KUHN, J. R. GOLDENRING *et al.*, 1985c Is Ca2+-calmodulin-dependent protein phosphorylation in rat brain modulated by carboxylmethylation? J Neurochem **44:** 1442-1450.

BOIVIN, D., D. BILODEAU and R. BELIVEAU, 1995 Immunochemical characterization of L-isoaspartyl-protein carboxyl methyltransferase from mammalian tissues. Biochem J **309 (Pt 3):** 993-998.

BOUCHARD, P., C. GAGNON, D. M. PHILLIPS and C. W. BARDIN, 1980 The localization of protein carboxyl-methylase in sperm tails. J Cell Biol **86:** 417-423.

BURNASHEV, N., and A. ROZOV, 2005 Presynaptic Ca2+ dynamics, Ca2+ buffers and synaptic efficacy. Cell Calcium **37:** 489-495.

CAMPISI, J., and J. VIJG, 2009 Does damage to DNA and other macromolecules play a role in aging? If so, how? J Gerontol A Biol Sci Med Sci **64:** 175-178.

CARSON, M. J., R. R. BEHRINGER, R. L. BRINSTER and F. A. MCMORRIS, 1993 Insulin-like growth factor I increases brain growth and central nervous system myelination in transgenic mice. Neuron **10:** 729-740.

CHAVOUS, D. A., L. E. HAKE, R. J. LYNCH and C. M. O'CONNOR, 2000 Translation of a unique transcript for protein isoaspartyl methyltransferase in haploid spermatids: implications for protein storage and repair. Mol Reprod Dev **56:** 139-144.

CHAVOUS, D. A., F. R. JACKSON and C. M. O'CONNOR, 2001 Extension of the Drosophila lifespan by overexpression of a protein repair methyltransferase. Proc Natl Acad Sci U S A **98:** 14814-14818.

CHEN, J., V. AVDONIN, M. A. CIORBA, S. H. HEINEMANN and T. HOSHI, 2000 Acceleration of P/C-type inactivation in voltage-gated K(+) channels by methionine oxidation. Biophys J **78:** 174-187.

CHEN, Y., X. SONG, S. YE, L. MIAO, Y. ZHU *et al.*, 2013 Structural insight into enhanced calcium indicator GCaMP3 and GCaMPJ to promote further improvement. Protein Cell **4:** 299-309.

CIMMINO, A., R. CAPASSO, F. MULLER, I. SAMBRI, L. MASELLA *et al.*, 2008 Protein isoaspartate methyltransferase prevents apoptosis induced by oxidative stress in endothelial cells: role of Bcl-Xl deamidation and methylation. PLoS One **3:** e3258.

CLARKE, S., 1987 Propensity for spontaneous succinimide formation from aspartyl and asparaginyl residues in cellular proteins. Int J Pept Protein Res **30:** 808-821.

CLARKE, S., 2003 Aging as war between chemical and biochemical processes: protein methylation and the recognition of age-damaged proteins for repair. Ageing Res Rev **2:** 263-285.

COHEN, P., 2000 The regulation of protein function by multisite phosphorylation--a 25 year update. Trends Biochem Sci **25:** 596-601.

COLLARD, F., 2004 Characterization of fructosamine 3-kinase related protein, pp. Université catholique de Louvain.

COLLARD, F., G. DELPIERRE, V. STROOBANT, G. MATTHIJS and E. VAN SCHAFTINGEN, 2003 A mammalian protein homologous to fructosamine-3-kinase is a ketosamine-3-kinase acting on psicosamines and ribulosamines but not on fructosamines. Diabetes **52:** 2888-2895.

COLLINS, T. J., P. LIPP, M. J. BERRIDGE and M. D. BOOTMAN, 2001 Mitochondrial Ca2+ uptake depends on the spatial and temporal profile of cytosolic Ca2+ signals. Journal of Biological Chemistry **276:** 26411-26420.

CONANT, G. C., and K. H. WOLFE, 2008 Turning a hobby into a job: how duplicated genes find new functions. Nat Rev Genet **9:** 938-950.

COPPEDE, F., and L. MIGLIORE, 2015 DNA damage in neurodegenerative diseases. Mutat Res **776:** 84-97.

CORTI, A., and F. CURNIS, 2011 Isoaspartate-dependent molecular switches for integrin-ligand recognition. J Cell Sci **124:** 515-522.

CUNLIFFE, V. T., 2016 Building a zebrafish toolkit for investigating the pathobiology of epilepsy and identifying new treatments for epileptic seizures. J Neurosci Methods **260:** 91-95.

CURNIS, F., R. LONGHI, L. CRIPPA, A. CATTANEO, E. DONDOSSOLA *et al.*, 2006 Spontaneous formation of L-isoaspartate and gain of function in fibronectin. J Biol Chem **281:** 36466-36476.

DAI, S., W. NI, A. N. PATANANAN, S. G. CLARKE, B. L. KARGER *et al.*, 2013 Integrated proteomic analysis of major isoaspartyl-containing proteins in the urine of wild type and protein L-isoaspartate O-methyltransferase-deficient mice. Anal Chem **85:** 2423-2430.

DAVID, C. L., C. L. SZUMLANSKI, C. G. DEVRY, J. O. PARK-HAH, S. CLARKE *et al.*, 1997 Human erythrocyte protein L-isoaspartyl methyltransferase: heritability of basal activity and genetic polymorphism for thermal stability. Arch Biochem Biophys **346:** 277-286.

DELPIERRE, G., and E. VAN SCHAFTINGEN, 2003 Fructosamine 3-kinase, an enzyme involved in protein deglycation. Biochem Soc Trans **31:** 1354-1357.

DESROSIERS, R. R., E. A. ROMANIK and C. M. O'CONNOR, 1990 Selective carboxyl methylation of structurally altered calmodulins in Xenopus oocytes. J Biol Chem **265:** 21368-21374.

DEVRY, C. G., and S. CLARKE, 1999 Polymorphic forms of the protein L-isoaspartate (D-aspartate) O-methyltransferase involved in the repair of age-damaged proteins. J Hum Genet **44:** 275-288.

DHO, S. H., B. E. DEVERMAN, C. LAPID, S. R. MANSON, L. GAN *et al.*, 2013 Control of cellular Bcl-xL levels by deamidation-regulated degradation. PLoS Biol **11:** e1001588.

DIAUGUSTINE, R. P., B. W. GIBSON, W. ABERTH, M. KELLY, C. M. FERRUA *et al.*, 1987 Evidence for isoaspartyl (deamidated) forms of mouse epidermal growth factor. Anal Biochem **165:** 420-429.

DILIBERTO, E. J., JR., and J. AXELROD, 1974 Characterization and substrate specificity of a protein carboxymethylase in the pituitary gland. Proc Natl Acad Sci U S A **71:** 1701-1704.

DILIBERTO, E. J., JR., and J. AXELROD, 1976 Regional and subcellular distribution of protein carboxymethylase in brain and other tissues. J Neurochem **26:** 1159-1165.

DIMITRIJEVIC, A., Z. QIN and D. W. ASWAD, 2014 Isoaspartyl formation in creatine kinase B Is associated with loss of enzymatic activity; implications for the linkage of isoaspartate accumulation and neurological dysfunction in the PIMT knockout mouse. PLoS One **9:** e100622.

DOYLE, H. A., R. J. GEE and M. J. MAMULA, 2003 A failure to repair self-proteins leads to T cell hyperproliferation and autoantibody production. J Immunol **171:** 2840-2847.

DRAPER, B. W., P. A. MORCOS and C. B. KIMMEL, 2001 Inhibition of zebrafish fgf8 pre-mRNA splicing with morpholino oligos: a quantifiable method for gene knockdown. Genesis **30:** 154-156.

DREW, B., and C. LEEUWENBURGH, 2002 Aging and the role of reactive nitrogen species. Ann N Y Acad Sci **959:** 66-81.

DRIEVER, W., L. SOLNICA-KREZEL, A. F. SCHIER, S. C. NEUHAUSS, J. MALICKI *et al.*, 1996 A genetic screen for mutations affecting embryogenesis in zebrafish. Development **123:** 37-46.

DUNG, T. T., Y. S. YI, J. HEO, W. S. YANG, J. H. KIM *et al.*, 2016 Critical role of protein L-isoaspartyl methyltransferase in basic fibroblast growth factor-mediated neuronal cell differentiation. BMB Rep.

EAKIN, C. M., A. J. BERMAN and A. D. MIRANKER, 2006 A native to amyloidogenic transition regulated by a backbone trigger. Nat Struct Mol Biol **13:** 202-208.

EDGAR, D. H., and D. B. HOPE, 1974 Neurophysin methylation in extracts of bovine posterior pituitary gland: hormone binding ability. FEBS Lett **49:** 145-148.

EKKER, S. C., 2000 Morphants: a new systematic vertebrate functional genomics approach. Yeast **17:** 302-306.

FANGHANEL, J., H. AKIYAMA, C. UCHIDA and T. UCHIDA, 2006 Comparative analysis of enzyme activities and mRNA levels of peptidyl prolyl cis/trans isomerases in various organs of wild type and Pin1-/- mice. FEBS Lett **580:** 3237-3245.

FARRAR, C., C. R. HOUSER and S. CLARKE, 2005a Activation of the PI3K/Akt signal transduction pathway and increased levels of insulin receptor in protein repair-deficient mice. Aging Cell **4:** 1-12.

FARRAR, C. E., C. S. HUANG, S. G. CLARKE and C. R. HOUSER, 2005b Increased cell proliferation and granule cell number in the dentate gyrus of protein repair-deficient mice. J Comp Neurol **493:** 524-537.

FENG, Y., C. CHEN, Y. HAN, Z. CHEN, X. LU *et al.*, 2016 Expanding CRISPR/Cas9 Genome Editing Capacity in Zebrafish Using SaCas9. G3 (Bethesda) **6:** 2517-2521.

FIRE, A., S. XU, M. K. MONTGOMERY, S. A. KOSTAS, S. E. DRIVER *et al.*, 1998 Potent and specific genetic interference by double-stranded RNA in Caenorhabditis elegans. Nature **391:** 806-811.

FRANCO, M. C., Y. YE, C. A. REFAKIS, J. L. FELDMAN, A. L. STOKES *et al.*, 2013 Nitration of Hsp90 induces cell death. Proc Natl Acad Sci U S A **110:** E1102-1111.

FRIEDBERG, F., 1988 Calcium binding protein families: The 'E–F Hand'Family. Biochemical Education **16:** 35-36.

FRIEDRICH, M. G., S. E. HANCOCK, M. J. RAFTERY and R. J. TRUSCOTT, 2016 Isoaspartic acid is present at specific sites in myelin basic protein from multiple sclerosis patients: could this represent a trigger for disease onset? Acta Neuropathol Commun **4:** 83.

FU, J. C., L. DING and S. CLARKE, 1991 Purification, gene cloning, and sequence analysis of an L-isoaspartyl protein carboxyl methyltransferase from Escherichia coli. J Biol Chem **266:** 14562-14572.

FUJITA, T., K. SUZUKI, T. TADA, Y. YOSHIHARA, R. HAMAOKA *et al.*, 1998 Human erythrocyte bisphosphoglycerate mutase: inactivation by glycation in vivo and in vitro. J Biochem **124:** 1237-1244.

GAGNON, C., J. AXELROD, N. MUSTO, M. DYM and C. W. BARDIN, 1979 Protein carboxyl-methylation in rat testes: a study of inherited and X-ray-induced seminiferous tubule failure. Endocrinology **105:** 1440-1445.

GAGNON, C., S. KELLY, V. MANGANIELLO, M. VAUGHAN, C. ODYA *et al.*, 1981 Modification of calmodulin function by enzymatic carboxylic methylation. Nature **291:** 515-516.

GAO, J., D. H. YIN, Y. YAO, H. SUN, Z. QIN *et al.*, 1998 Loss of conformational stability in calmodulin upon methionine oxidation. Biophys J **74:** 1115-1134.

GATCH, M. B., C. J. WALLIS and H. LAL, 2001 Effects of calcium channel blockers on pentylenetetrazol drug discrimination in rats. Alcohol **23:** 141-147.

GEE, K. R., K. A. BROWN, W. N. CHEN, J. BISHOP-STEWART, D. GRAY *et al.*, 2000 Chemical and physiological characterization of fluo-4 Ca(2+)-indicator dyes. Cell Calcium **27:** 97-106.

GEIGER, T., and S. CLARKE, 1987 Deamidation, isomerization, and racemization at asparaginyl and aspartyl residues in peptides. Succinimide-linked reactions that contribute to protein degradation. J Biol Chem **262:** 785-794.

GIACOMELLO, M., I. DRAGO, P. PIZZO and T. POZZAN, 2007 Mitochondrial Ca2+ as a key regulator of cell life and death. Cell Death Differ **14:** 1267-1274.

GO, C., and O. C. SNEAD, 3RD, 2008 Pharmacologically intractable epilepsy in children: diagnosis and preoperative evaluation. Neurosurg Focus **25:** E2.

GORG, B., N. QVARTSKHAVA, P. VOSS, T. GRUNE, D. HAUSSINGER *et al.*, 2007 Reversible inhibition of mammalian glutamine synthetase by tyrosine nitration. FEBS Lett **581:** 84-90.

GOW, A. J., D. DURAN, S. MALCOLM and H. ISCHIROPOULOS, 1996 Effects of peroxynitrite-induced protein modifications on tyrosine phosphorylation and degradation. FEBS Lett **385:** 63-66.

GRIENBERGER, C., and A. KONNERTH, 2012 Imaging Calcium in Neurons. Neuron **73:** 862-885.

HAFFTER, P., M. GRANATO, M. BRAND, M. C. MULLINS, M. HAMMERSCHMIDT *et al.*, 1996 The identification of genes with unique and essential functions in the development of the zebrafish, Danio rerio. Development **123:** 1-36.

HARRIS, R. J., B. KABAKOFF, F. D. MACCHI, F. J. SHEN, M. KWONG *et al.*, 2001 Identification of multiple sources of charge heterogeneity in a recombinant antibody. Journal of Chromatography B: Biomedical Sciences and Applications **752:** 233-245.

HASHEMITABAR, M., S. SABBAGH, M. ORAZIZADEH, A. GHADIRI and M. BAHMANZADEH, 2015 A proteomic analysis on human sperm tail: comparison between normozoospermia and asthenozoospermia. J Assist Reprod Genet.

HOFFMAN, J. L., 1986 Chromatographic analysis of the chiral and covalent instability of S-adenosyl-L-methionine. Biochemistry **25:** 4444-4449.

HOLTZINGER, A., and T. EVANS, 2005 Gata4 regulates the formation of multiple organs. Development **132:** 4005-4014.

HOLZENBERGER, M., J. DUPONT, B. DUCOS, P. LENEUVE, A. GELOEN *et al.*, 2003 IGF-1 receptor regulates lifespan and resistance to oxidative stress in mice. Nature **421:** 182-187.

HORVATH, P., and R. BARRANGOU, 2010 CRISPR/Cas, the immune system of bacteria and archaea. Science **327:** 167-170.

HOWE, K., M. D. CLARK, C. F. TORROJA, J. TORRANCE, C. BERTHELOT *et al.*, 2013 The zebrafish reference genome sequence and its relationship to the human genome. Nature **496:** 498-503.

HSU, Y. R., W. C. CHANG, E. A. MENDIAZ, S. HARA, D. T. CHOW *et al.*, 1998 Selective deamidation of recombinant human stem cell factor during in vitro aging: isolation and characterization of the aspartyl and isoaspartyl homodimers and heterodimers. Biochemistry **37:** 2251-2262.

HUANG, R.-Q., C. L. BELL-HORNER, M. I. DIBAS, D. F. COVEY, J. A. DREWE *et al.*, 2001 Pentylenetetrazole-Induced Inhibition of Recombinant γ-Aminobutyric Acid Type A (GABA_A) Receptors: Mechanism and Site of Action. Journal of Pharmacology and Experimental Therapeutics **298:** 986-995.

HUEBSCHER, K. J., J. LEE, G. ROVELLI, B. LUDIN, A. MATUS *et al.*, 1999 Protein isoaspartyl methyltransferase protects from Bax-induced apoptosis. Gene **240:** 333-341.

ICHIKAWA, J. K., and S. CLARKE, 1998 A highly active protein repair enzyme from an extreme thermophile: the L-isoaspartyl methyltransferase from Thermotoga maritima. Arch Biochem Biophys **358:** 222-231.

INGROSSO, D., S. D'ANGELO, E. DI CARLO, A. F. PERNA, V. ZAPPIA *et al.*, 2000 Increased methyl esterification of altered aspartyl residues in erythrocyte membrane proteins in response to oxidative stress. Eur J Biochem **267:** 4397-4405.

JEPPESEN, D. K., V. A. BOHR and T. STEVNSNER, 2011 DNA repair deficiency in neurodegeneration. Progress in Neurobiology **94:** 166-200.

JOHNSON, B. A., and D. W. ASWAD, 1990 Fragmentation of isoaspartyl peptides and proteins by carboxypeptidase Y: release of isoaspartyl dipeptides as a result of internal and external cleavage. Biochemistry **29:** 4373-4380.

JOHNSON, B. A., and D. W. ASWAD, 1993 Kinetic properties of bovine brain protein L-isoaspartyl methyltransferase determined using a synthetic isoaspartyl peptide substrate. Neurochem Res **18:** 87-94.

JOHNSON, B. A., N. E. FREITAG and D. W. ASWAD, 1985 Protein carboxyl methyltransferase selectively modifies an atypical form of calmodulin. Evidence for methylation at deamidated asparagine residues. J Biol Chem **260:** 10913-10916.

JOHNSON, B. A., E. L. LANGMACK and D. W. ASWAD, 1987a Partial repair of deamidation-damaged calmodulin by protein carboxyl methyltransferase. J Biol Chem **262:** 12283-12287.

JOHNSON, B. A., E. D. MURRAY, JR., S. CLARKE, D. B. GLASS and D. W. ASWAD, 1987b Protein carboxyl methyltransferase facilitates conversion of atypical L-isoaspartyl peptides to normal L-aspartyl peptides. J Biol Chem **262:** 5622-5629.

JOHNSON, B. A., S. Q. NGO and D. W. ASWAD, 1991a Widespread phylogenetic distribution of a protein methyltransferase that modifies L-isoaspartyl residues. Biochem Int **24:** 841-847.

JOHNSON, B. A., J. M. SHIROKAWA, J. W. GEDDES, B. H. CHOI, R. C. KIM *et al.*, 1991b Protein L-isoaspartyl methyltransferase in postmortem brains of aged humans. Neurobiol Aging **12:** 19-24.

JOHNSON, R. N., P. A. METCALF and J. R. BAKER, 1983 Fructosamine: a new approach to the estimation of serum glycosylprotein. An index of diabetic control. Clin Chim Acta **127:** 87-95.

JUNG, G., J. RYU, J. HEO, S. J. LEE, J. Y. CHO *et al.*, 2011 Protein L-isoaspartyl O-methyltransferase inhibits amyloid beta fibrillogenesis in vitro. Pharmazie **66:** 529-534.

KAGAN, R. M., and S. CLARKE, 1994 Widespread occurrence of three sequence motifs in diverse S-adenosylmethionine-dependent methyltransferases suggests a common structure for these enzymes. Arch Biochem Biophys **310:** 417-427.

KAGAN, R. M., and S. CLARKE, 1995 Protein L-isoaspartyl methyltransferase from the nematode Caenorhabditis elegans: genomic structure and substrate specificity. Biochemistry **34:** 10794-10806.

KAGAN, R. M., H. J. MCFADDEN, P. N. MCFADDEN, C. O'CONNOR and S. CLARKE, 1997 Molecular phylogenetics of a protein repair methyltransferase. Comp Biochem Physiol B Biochem Mol Biol **117:** 379-385.

KAMISAKI, Y., K. WADA, K. BIAN, B. BALABANLI, K. DAVIS *et al.*, 1998 An activity in rat tissues that modifies nitrotyrosine-containing proteins. Proc Natl Acad Sci U S A **95:** 11584-11589.

KAYAALP, E., E. TREACY, P. J. WATERS, S. BYCK, P. NOWACKI *et al.*, 1997 Human phenylalanine hydroxylase mutations and hyperphenylalaninemia phenotypes: a metanalysis of genotype-phenotype correlations. Am J Hum Genet **61:** 1309-1317.

KENYON, C., J. CHANG, E. GENSCH, A. RUDNER and R. TABTIANG, 1993 A C. elegans mutant that lives twice as long as wild type. Nature **366:** 461-464.

KENYON, C. J., 2010 The genetics of ageing. Nature **464:** 504-512.

KHARE, S., C. L. LINSTER and S. G. CLARKE, 2011 The interplay between protein L-isoaspartyl methyltransferase activity and insulin-like signaling to extend lifespan in Caenorhabditis elegans. PLoS One **6:** e20850.

KIM, D., K. S. JUN, S. B. LEE, N.-G. KANG, D. S. MIN *et al.*, 1997a Phospholipase C isozymes selectively couple to specific neurotransmitter receptors. Nature **389:** 290-293.

KIM, E., J. D. LOWENSON, S. CLARKE and S. G. YOUNG, 1999 Phenotypic analysis of seizure-prone mice lacking L-isoaspartate (D-aspartate) O-methyltransferase. J Biol Chem **274:** 20671-20678.

KIM, E., J. D. LOWENSON, D. C. MACLAREN, S. CLARKE and S. G. YOUNG, 1997b Deficiency of a protein-repair enzyme results in the accumulation of altered proteins, retardation of growth, and fatal seizures in mice. Proc Natl Acad Sci U S A **94:** 6132-6137.

KIMMEL, C. B., W. W. BALLARD, S. R. KIMMEL, B. ULLMANN and T. F. SCHILLING, 1995 Stages of embryonic development of the zebrafish. Dev Dyn **203:** 253-310.

KINDRACHUK, J., J. PARENT, G. F. DAVIES, M. DINSMORE, S. ATTAH-POKU *et al.*, 2003 Overexpression of L-isoaspartate O-methyltransferase in Escherichia coli increases heat shock survival by a mechanism independent of methyltransferase activity. J Biol Chem **278:** 50880-50886.

KOK, F. O., M. SHIN, C. W. NI, A. GUPTA, A. S. GROSSE *et al.*, 2015 Reverse Genetic Screening Reveals Poor Correlation between Morpholino-Induced and Mutant Phenotypes in Zebrafish. Dev Cell **32:** 97-108.

KOSUGI, S., T. FURUCHI, M. KATANE, M. SEKINE, T. SHIRASAWA *et al.*, 2008 Suppression of protein l-isoaspartyl (d-aspartyl) methyltransferase results in hyperactivation of EGF-stimulated MEK-ERK signaling in cultured mammalian cells. Biochem Biophys Res Commun **371:** 22-27.

KOVTUN, I. V., and C. T. MCMURRAY, 2001 Trinucleotide expansion in haploid germ cells by gap repair. Nat Genet **27:** 407-411.

KOWLURU, R. A., D. B. HEIDORN, S. P. EDMONDSON, M. W. BITENSKY, A. KOWLURU *et al.*, 1989 Glycation of calmodulin: chemistry and structural and functional consequences. Biochemistry **28:** 2220-2228.

KREMER, L. S., K. DANHAUSER, D. HEREBIAN, D. PETKOVIC RAMADZA, D. PIEKUTOWSKA-ABRAMCZUK *et al.*, 2016 NAXE Mutations Disrupt the Cellular NAD(P)HX Repair System and Cause a Lethal Neurometabolic Disorder of Early Childhood. Am J Hum Genet **99:** 894-902.

KUSCHEL, L., A. HANSEL, R. SCHONHERR, H. WEISSBACH, N. BROT *et al.*, 1999 Molecular cloning and functional expression of a human peptide methionine sulfoxide reductase (hMsrA). FEBS Lett **456:** 17-21.

LEE, J. C., S. U. KANG, Y. JEON, J. W. PARK, J. S. YOU *et al.*, 2012 Protein L-isoaspartyl methyltransferase regulates p53 activity. Nat Commun **3:** 927.

LEVINE, R. L., L. MOSONI, B. S. BERLETT and E. R. STADTMAN, 1996 Methionine residues as endogenous antioxidants in proteins. Proc Natl Acad Sci U S A **93:** 15036-15040.

LI, C., and S. CLARKE, 1992 Distribution of an L-isoaspartyl protein methyltransferase in eubacteria. J Bacteriol **174:** 355-361.

LIESCHKE, G. J., and P. D. CURRIE, 2007 Animal models of human disease: zebrafish swim into view. Nat Rev Genet **8:** 353-367.

LILLIS, K. P., C. DULLA, A. MAHESHWARI, D. COULTER, I. MODY *et al.*, 2015 WONOEP appraisal: molecular and cellular imaging in epilepsy. Epilepsia **56:** 505-513.

LINDAHL, T., P. MODRICH and A. SANCAR, 2016 The 2015 Nobel Prize in Chemistry The Discovery of Essential Mechanisms that Repair DNA Damage. J Assoc Genet Technol **42:** 37-41.

LINK, V., A. SHEVCHENKO and C. P. HEISENBERG, 2006 Proteomics of early zebrafish embryos. BMC Dev Biol **6:** 1.

LINSTER, C. L., E. VAN SCHAFTINGEN and A. D. HANSON, 2013 Metabolite damage and its repair or pre-emption. Nat Chem Biol **9:** 72-80.

LIOU, Y.-C., A. SUN, A. RYO, X. Z. ZHOU, Z.-X. YU *et al.*, 2003 Role of the prolyl isomerase Pin1 in protecting against age-dependent neurodegeneration. Nature **424:** 556-561.

LISTER, J. A., C. P. ROBERTSON, T. LEPAGE, S. L. JOHNSON and D. W. RAIBLE, 1999 nacre encodes a zebrafish microphthalmia-related protein that regulates neural-crest-derived pigment cell fate. Development **126:** 3757-3767.

LIU, J., L. LI and W. Z. SUO, 2009 HT22 hippocampal neuronal cell line possesses functional cholinergic properties. Life Sci **84:** 267-271.

LOWENSON, J. D., and S. CLARKE, 1991 Structural elements affecting the recognition of L-isoaspartyl residues by the L-isoaspartyl/D-aspartyl protein methyltransferase. Implications for the repair hypothesis. J Biol Chem **266:** 19396-19406.

LOWENSON, J. D., and S. CLARKE, 1992 Recognition of D-aspartyl residues in polypeptides by the erythrocyte L-isoaspartyl/D-aspartyl protein methyltransferase. Implications for the repair hypothesis. J Biol Chem **267:** 5985-5995.

LOWENSON, J. D., E. KIM, S. G. YOUNG and S. CLARKE, 2001 Limited accumulation of damaged proteins in l-isoaspartyl (D-aspartyl) O-methyltransferase-deficient mice. J Biol Chem **276:** 20695-20702.

LU, P. J., G. WULF, X. Z. ZHOU, P. DAVIES and K. P. LU, 1999 The prolyl isomerase Pin1 restores the function of Alzheimer-associated phosphorylated tau protein. Nature **399:** 784-788.

MACKAY, K. B., J. D. LOWENSON and S. G. CLARKE, 2012 Wortmannin reduces insulin signaling and death in seizure-prone Pcmt1-/- mice. PLoS One **7:** e46719.

MACLAREN, D. C., R. M. KAGAN and S. CLARKE, 1992 Alternative splicing of the human isoaspartyl protein carboxyl methyltransferase RNA leads to the generation of a C-terminal -RDEL sequence in isozyme II. Biochem Biophys Res Commun **185:** 277-283.

MARTIN-JIMENEZ, R., M. CAMPANELLA and C. RUSSELL, 2015 New zebrafish models of neurodegeneration. Curr Neurol Neurosci Rep **15:** 555.

MARTYNYUK, A. E., D. A. UCAR, D. D. YANG, W. M. NORMAN, P. R. CARNEY *et al.*, 2007 Epilepsy in phenylketonuria: a complex dependence on serum phenylalanine levels. Epilepsia **48:** 1143-1150.

MCCUBREY, J. A., L. STEELMAN, M. MAYO, P. ALGATE, R. DELLOW *et al.*, 1991 Growth-promoting effects of insulin-like growth factor-1 (IGF-1) on hematopoietic cells: overexpression of introduced IGF-

1 receptor abrogates interleukin-3 dependency of murine factor-dependent cells by a ligand-dependent mechanism. Blood **78:** 921-929.

MCFADDEN, P. N., and S. CLARKE, 1987 Conversion of isoaspartyl peptides to normal peptides: implications for the cellular repair of damaged proteins. Proc Natl Acad Sci U S A **84:** 2595-2599.

MEEKER, N. D., S. A. HUTCHINSON, L. HO and N. S. TREDE, 2007 Method for isolation of PCR-ready genomic DNA from zebrafish tissues. Biotechniques **43:** 610, 612, 614.

MIZOBUCHI, M., K. MURAO, R. TAKEDA and Y. KAKIMOTO, 1994 Tissue-specific expression of isoaspartyl protein carboxyl methyltransferase gene in rat brain and testis. J Neurochem **62:** 322-328.

MORRISON, G. J., R. GANESAN, Z. QIN and D. W. ASWAD, 2012 Considerations in the identification of endogenous substrates for protein L-isoaspartyl methyltransferase: the case of synuclein. PLoS One **7:** e43288.

MOSKOVITZ, J., E. FLESCHER, B. S. BERLETT, J. AZARE, J. M. POSTON *et al.*, 1998 Overexpression of peptide-methionine sulfoxide reductase in Saccharomyces cerevisiae and human T cells provides them with high resistance to oxidative stress. Proc Natl Acad Sci U S A **95:** 14071-14075.

MUDGETT, M. B., and S. CLARKE, 1993 Characterization of plant L-isoaspartyl methyltransferases that may be involved in seed survival: purification, cloning, and sequence analysis of the wheat germ enzyme. Biochemistry **32:** 11100-11111.

MUDGETT, M. B., and S. CLARKE, 1994 Hormonal and environmental responsiveness of a developmentally regulated protein repair L-isoaspartyl methyltransferase in wheat. J Biol Chem **269:** 25605-25612.

MULLINS, M. C., M. HAMMERSCHMIDT, P. HAFFTER and C. NUSSLEIN-VOLHARD, 1994 Large-scale mutagenesis in the zebrafish: in search of genes controlling development in a vertebrate. Curr Biol **4:** 189-202.

MURPHEY, R. D., and L. I. ZON, 2006 Small molecule screening in the zebrafish. Methods **39:** 255-261.

O'CONNOR, C. M., B. J. GERMAIN, K. M. GUTHRIE, D. W. ASWAD and C. F. MILLETTE, 1989 Protein carboxyl methyltransferase activity specific for age-modified aspartyl residues in mouse testes and ovaries: evidence for translation during spermiogenesis. Gamete Res **22:** 307-319.

O'CONNOR, M. B., and C. M. O'CONNOR, 1998 Complex interactions of the protein L-isoaspartyl methyltransferase and calmodulin revealed with the yeast two-hybrid system. J Biol Chem **273:** 12909-12913.

OGASAWARA, M., M. OTANI, M. TAKANO, M. SHUDOU, Y. INABA *et al.*, 2016 The protective role of protein L-isoaspartyl (D-aspartate) O-methyltransferase for maintenance of mitochondrial morphology in A549 cell. Exp Lung Res **42:** 245-262.

OGE, L., G. BOURDAIS, J. BOVE, B. COLLET, B. GODIN *et al.*, 2008 Protein repair L-isoaspartyl methyltransferase 1 is involved in both seed longevity and germination vigor in Arabidopsis. Plant Cell **20:** 3022-3037.

ONOZUKA, M., I. NAKAGAKI and S. SASAKI, 1989 Pentylenetetrazole-induced seizure activity produces an increased release of calcium from endoplasmic reticulum by mediating cyclic AMP-dependent protein phosphorylation in rat cerebral cortex. Gen Pharmacol **20:** 627-634.

OTA, I. M., and S. CLARKE, 1989a Calcium affects the spontaneous degradation of aspartyl/asparaginyl residues in calmodulin. Biochemistry **28:** 4020-4027.

OTA, I. M., and S. CLARKE, 1989b Enzymatic methylation of L-isoaspartyl residues derived from aspartyl residues in affinity-purified calmodulin. The role of conformational flexibility in spontaneous isoaspartyl formation. J Biol Chem **264:** 54-60.

OTA, I. M., and S. CLARKE, 1990 Multiple sites of methyl esterification of calmodulin in intact human erythrocytes. Arch Biochem Biophys **279:** 320-327.

OTA, I. M., J. M. GILBERT and S. CLARKE, 1988 Two major isozymes of the protein D-aspartyl/L-isoaspartyl methyltransferase from human erythrocytes. Biochem Biophys Res Commun **151:** 1136-1143.

OUAZIA, D., L. C. LEVROS, JR., E. RASSART and R. R. DESROSIERS, 2015 The protein l-isoaspartyl (d-aspartyl) methyltransferase protects against dopamine-induced apoptosis in neuroblastoma SH-SY5Y cells. Neuroscience **295:** 139-150.

PARANANDI, M. V., and D. W. ASWAD, 1995 Spontaneous alterations in the covalent structure of synapsin I during in vitro aging. Biochem Biophys Res Commun **212:** 442-448.

PASTORINO, L., A. SUN, P. J. LU, X. Z. ZHOU, M. BALASTIK *et al.*, 2006 The prolyl isomerase Pin1 regulates amyloid precursor protein processing and amyloid-beta production. Nature **440:** 528-534.

PATANANAN, A. N., J. CAPRI, J. P. WHITELEGGE and S. G. CLARKE, 2014 Non-repair pathways for minimizing protein isoaspartyl damage in the yeast Saccharomyces cerevisiae. J Biol Chem **289:** 16936-16953.

PELHAM, H. R., 2000 Using sorting signals to retain proteins in endoplasmic reticulum. Methods Enzymol **327:** 279-283.

PERATHONER, S., J. M. DAANE, U. HENRION, G. SEEBOHM, C. W. HIGDON *et al.*, 2014 Bioelectric signaling regulates size in zebrafish fins. PLoS Genet **10:** e1004080.

PFAFFL, M. W., 2001 A new mathematical model for relative quantification in real-time RT-PCR. Nucleic Acids Res **29:** e45.

POIRIER, M. C., 2004 Chemical-induced DNA damage and human cancer risk. Nat Rev Cancer **4:** 630-637.

POTTER, S. M., W. J. HENZEL and D. W. ASWAD, 1993 In vitro aging of calmodulin generates isoaspartate at multiple Asn-Gly and Asp-Gly sites in calcium-binding domains II, III, and IV. Protein Sci **2:** 1648-1663.

POTTER, S. M., B. A. JOHNSON, A. HENSCHEN, D. W. ASWAD and A. W. GUZZETTA, 1992 The type II isoform of bovine brain protein L-isoaspartyl methyltransferase has an endoplasmic reticulum retention signal (...RDEL) at its C-terminus. Biochemistry **31:** 6339-6347.

PUIG, O., M. T. MARR, M. L. RUHF and R. TJIAN, 2003 Control of cell number by Drosophila FOXO: downstream and feedback regulation of the insulin receptor pathway. Genes Dev **17:** 2006-2020.

RAN, F. A., P. D. HSU, J. WRIGHT, V. AGARWALA, D. A. SCOTT *et al.*, 2013 Genome engineering using the CRISPR-Cas9 system. Nat Protoc **8:** 2281-2308.

RAO, V. R., and S. FINKBEINER, 2007 NMDA and AMPA receptors: old channels, new tricks. Trends Neurosci **30:** 284-291.

REISSNER, K. J., and D. W. ASWAD, 2003 Deamidation and isoaspartate formation in proteins: unwanted alterations or surreptitious signals? Cell Mol Life Sci **60:** 1281-1295.

REISSNER, K. J., M. V. PARANANDI, T. M. LUC, H. A. DOYLE, M. J. MAMULA *et al.*, 2006 Synapsin I is a major endogenous substrate for protein L-isoaspartyl methyltransferase in mammalian brain. J Biol Chem **281:** 8389-8398.

RINDERKNECHT, E., and R. E. HUMBEL, 1978 The amino acid sequence of human insulin-like growth factor I and its structural homology with proinsulin. J Biol Chem **253:** 2769-2776.

ROBINSON, N. E., and A. B. ROBINSON, 2001a Deamidation of human proteins. Proc Natl Acad Sci U S A **98:** 12409-12413.

ROBINSON, N. E., and A. B. ROBINSON, 2001b Molecular clocks. Proc Natl Acad Sci U S A **98:** 944-949.

ROHER, A. E., J. D. LOWENSON, S. CLARKE, C. WOLKOW, R. WANG *et al.*, 1993 Structural alterations in the peptide backbone of beta-amyloid core protein may account for its deposition and stability in Alzheimer's disease. J Biol Chem **268:** 3072-3083.

ROSS, C. A., and M. A. POIRIER, 2005 Opinion: What is the role of protein aggregation in neurodegeneration? Nat Rev Mol Cell Biol **6:** 891-898.

ROSSI, A., Z. KONTARAKIS, C. GERRI, H. NOLTE, S. HOLPER *et al.*, 2015 Genetic compensation induced by deleterious mutations but not gene knockdowns. Nature **524:** 230-233.

RUAN, H., X. D. TANG, M. L. CHEN, M. L. JOINER, G. SUN *et al.*, 2002 High-quality life extension by the enzyme peptide methionine sulfoxide reductase. Proc Natl Acad Sci U S A **99:** 2748-2753.

RUTHERFORD, K., and V. DAGGETT, 2009 The V119I polymorphism in protein L-isoaspartate O-methyltransferase alters the substrate-binding interface. Protein Eng Des Sel **22:** 713-721.

RUTHERFORD, K., and V. DAGGETT, 2010 Polymorphisms and disease: hotspots of inactivation in methyltransferases. Trends Biochem Sci **35:** 531-538.

RYU, J., J. SONG, J. HEO, Y. JUNG, S. J. LEE *et al.*, 2011 Cross-regulation between protein L-isoaspartyl O-methyltransferase and ERK in epithelial mesenchymal transition of MDA-MB-231 cells. Acta Pharmacol Sin **32:** 1165-1172.

SAITO, H., M. YAMASHITA, M. OGASAWARA, N. YAMADA, M. NIISATO *et al.*, 2016 Chaperone protein l-isoaspartate (d-aspartyl) O-methyltransferase as a novel predictor of poor prognosis in lung adenocarcinoma. Hum Pathol **50:** 1-10.

SALMON, A. B., G. KIM, C. LIU, J. D. WREN, C. GEORGESCU *et al.*, 2016 Effects of transgenic methionine sulfoxide reductase A (MsrA) expression on lifespan and age-dependent changes in metabolic function in mice. Redox Biol **10:** 251-256.

SALTER, M. W., and J. L. HICKS, 1995 ATP causes release of intracellular Ca2+ via the phospholipase C beta/IP3 pathway in astrocytes from the dorsal spinal cord. J Neurosci **15:** 2961-2971.

SAMBRI, I., R. CAPASSO, P. PUCCI, A. F. PERNA and D. INGROSSO, 2011 The microRNA 15a/16-1 cluster down-regulates protein repair isoaspartyl methyltransferase in hepatoma cells: implications for apoptosis regulation. J Biol Chem **286:** 43690-43700.

SARGAEVA, N. P., C. LIN and P. B. O'CONNOR, 2009 Identification of aspartic and isoaspartic acid residues in amyloid beta peptides, including Abeta1-42, using electron-ion reactions. Anal Chem **81:** 9778-9786.

SCHIENE, C., and G. FISCHER, 2000 Enzymes that catalyse the restructuring of proteins. Current Opinion in Structural Biology **10:** 40-45.

SCHINDELIN, J., I. ARGANDA-CARRERAS, E. FRISE, V. KAYNIG, M. LONGAIR *et al.*, 2012 Fiji: an open-source platform for biological-image analysis. Nat Methods **9:** 676-682.

SCHWALLER, B., 2007 Emerging Functions of the “Ca2+ Buffers” Parvalbumin, Calbindin D-28k and Calretinin in the Brain, pp. 197-221 in *Handbook of Neurochemistry and Molecular Neurobiology: Neural Protein Metabolism and Function*, edited by A. LAJTHA and N. BANIK. Springer US, Boston, MA.

SHAW, G., S. MORSE, M. ARARAT and F. L. GRAHAM, 2002 Preferential transformation of human neuronal cells by human adenoviruses and the origin of HEK 293 cells. FASEB J **16:** 869-871.

SHIMIZU, T., H. FUKUDA, S. MURAYAMA, N. IZUMIYAMA and T. SHIRASAWA, 2002 Isoaspartate formation at position 23 of amyloid beta peptide enhanced fibril formation and deposited onto senile plaques and vascular amyloids in Alzheimer's disease. J Neurosci Res **70:** 451-461.

SHIMIZU, T., A. WATANABE, M. OGAWARA, H. MORI and T. SHIRASAWA, 2000 Isoaspartate formation and neurodegeneration in Alzheimer's disease. Arch Biochem Biophys **381:** 225-234.

SHIRASAWA, T., R. ENDOH, Y. X. ZENG, K. SAKAMOTO and H. MORI, 1995 Protein L-isoaspartyl methyltransferase: developmentally regulated gene expression and protein localization in the central nervous system of aged rat. Neurosci Lett **188:** 37-40.

SIEVERS, F., A. WILM, D. DINEEN, T. J. GIBSON, K. KARPLUS *et al.*, 2011 Fast, scalable generation of high-quality protein multiple sequence alignments using Clustal Omega. Mol Syst Biol **7:** 539.

SMITH, C. D., M. CARSON, A. M. FRIEDMAN, M. M. SKINNER, L. DELUCAS *et al.*, 2002 Crystal structure of human L-isoaspartyl-O-methyl-transferase with S-adenosyl homocysteine at 1.6-A resolution and modeling of an isoaspartyl-containing peptide at the active site. Protein Sci **11:** 625-635.

STEPHENSON, R. C., and S. CLARKE, 1989 Succinimide formation from aspartyl and asparaginyl peptides as a model for the spontaneous degradation of proteins. J Biol Chem **264:** 6164-6170.

SUGAYA, E., and M. ONOZUKA, 1978 Intracellular calcium: its movement during pentylenetetrazole-induced bursting activity. Science **200:** 797-799.

SUMMERTON, J., and D. WELLER, 1997 Morpholino antisense oligomers: design, preparation, and properties. Antisense Nucleic Acid Drug Dev **7:** 187-195.

SZYMANSKA, G., J. D. LESZYK and C. M. O'CONNOR, 1998 Carboxyl methylation of deamidated calmodulin increases its stability in Xenopus oocyte cytoplasm. Implications for protein repair. J Biol Chem **273:** 28516-28523.

TAKEDA, R., M. MIZOBUCHI, K. MURAO, M. SATO and J. TAKAHARA, 1995 Characterization of three cDNAs encoding two isozymes of an isoaspartyl protein carboxyl methyltransferase from human erythroid leukemia cells. J Biochem **117:** 683-685.

TANG, R., A. DODD, D. LAI, W. C. MCNABB and D. R. LOVE, 2007 Validation of zebrafish (Danio rerio) reference genes for quantitative real-time RT-PCR normalization. Acta Biochim Biophys Sin (Shanghai) **39:** 384-390.

TAYLOR, J. S., Y. VAN DE PEER, I. BRAASCH and A. MEYER, 2001 Comparative genomics provides evidence for an ancient genome duplication event in fish. Philos Trans R Soc Lond B Biol Sci **356:** 1661-1679.

THAPAR, N., and S. CLARKE, 2000 Expression, purification, and characterization of the protein repair l-isoaspartyl methyltransferase from Arabidopsis thaliana. Protein Expr Purif **20:** 237-251.

THISSE, B., and C. THISSE, 2004 Fast Release Clones: A High Throughput Expression Analysis, pp. in *ZFIN Direct Data Submission*.

THISSE, C., and B. THISSE, 2008 High-resolution in situ hybridization to whole-mount zebrafish embryos. Nat Protoc **3:** 59-69.

THURMAN, D. J., E. BEGHI, C. E. BEGLEY, A. T. BERG, J. R. BUCHHALTER *et al.*, 2011 Standards for epidemiologic studies and surveillance of epilepsy. Epilepsia **52 Suppl 7:** 2-26.

TON, C., D. STAMATIOU, V. J. DZAU and C. C. LIEW, 2002 Construction of a zebrafish cDNA microarray: gene expression profiling of the zebrafish during development. Biochem Biophys Res Commun **296:** 1134-1142.

UNAL, E., B. KINDE and A. AMON, 2011 Gametogenesis eliminates age-induced cellular damage and resets life span in yeast. Science **332:** 1554-1557.

VAN SCHAFTINGEN, E., R. RZEM, A. MARBAIX, F. COLLARD, M. VEIGA-DA-CUNHA *et al.*, 2013 Metabolite proofreading, a neglected aspect of intermediary metabolism. J Inherit Metab Dis **36:** 427-434.

VAN SCHAFTINGEN, E., R. RZEM and M. VEIGA-DA-CUNHA, 2009 L: -2-Hydroxyglutaric aciduria, a disorder of metabolite repair. J Inherit Metab Dis **32:** 135-142.

VICENTE MIRANDA, H., O. M. EL-AGNAF and T. F. OUTEIRO, 2016 Glycation in Parkinson's disease and Alzheimer's disease. Mov Disord **31:** 782-790.

VICENTE MIRANDA, H., and T. F. OUTEIRO, 2010 The sour side of neurodegenerative disorders: the effects of protein glycation. J Pathol **221:** 13-25.

VIGNESWARA, V., S. CASS, D. WAYNE, E. L. BOLT, D. E. RAY *et al.*, 2013 Molecular ageing of alpha- and Beta-synucleins: protein damage and repair mechanisms. PLoS One **8:** e61442.

VIGNESWARA, V., J. D. LOWENSON, C. D. POWELL, M. THAKUR, K. BAILEY *et al.*, 2006 Proteomic identification of novel substrates of a protein isoaspartyl methyltransferase repair enzyme. J Biol Chem **281:** 32619-32629.

VILLA, S. T., Q. XU, A. B. DOWNIE and S. G. CLARKE, 2006 Arabidopsis Protein Repair L-Isoaspartyl Methyltransferases: Predominant Activities at Lethal Temperatures. Physiol Plant **128:** 581-592.

VINCI, C. R., and S. G. CLARKE, 2007 Recognition of age-damaged (R,S)-adenosyl-L-methionine by two methyltransferases in the yeast Saccharomyces cerevisiae. J Biol Chem **282:** 8604-8612.

WAGER, K., A. A. ZDEBIK, S. FU, J. D. COOPER, R. J. HARVEY *et al.*, 2016 Neurodegeneration and Epilepsy in a Zebrafish Model of CLN3 Disease (Batten Disease). PLoS One **11:** e0157365.

WANG, R., and M. G. BRATTAIN, 2007 The maximal size of protein to diffuse through the nuclear pore is larger than 60kDa. FEBS Lett **581:** 3164-3170.

WATANABE, A., K. TAKIO and Y. IHARA, 1999 Deamidation and isoaspartate formation in smeared tau in paired helical filaments. Unusual properties of the microtubule-binding domain of tau. J Biol Chem **274:** 7368-7378.

WATKINS, N. G., S. R. THORPE and J. W. BAYNES, 1985 Glycation of amino groups in protein. Studies on the specificity of modification of RNase by glucose. Journal of Biological Chemistry **260:** 10629-10636.

WEISSBACH, H., F. ETIENNE, T. HOSHI, S. H. HEINEMANN, W. T. LOWTHER *et al.*, 2002 Peptide methionine sulfoxide reductase: structure, mechanism of action, and biological function. Arch Biochem Biophys **397:** 172-178.

WESTERFIELD, M., 2000 *The Zebrafish Book. A guide for the laboratory use of zebrafish (Danio rerio)*. University of Oregon Press.

WHITE, R., K. ROSE and L. ZON, 2013 Zebrafish cancer: the state of the art and the path forward. Nat Rev Cancer **13:** 624-636.

WIGGANS, A. J., G. K. CASS, A. BRYANT, T. A. LAWRIE and J. MORRISON, 2015 Poly(ADP-ribose) polymerase (PARP) inhibitors for the treatment of ovarian cancer. Cochrane Database Syst Rev**:** CD007929.

WOJDA, U., E. SALINSKA and J. KUZNICKI, 2008 Calcium ions in neuronal degeneration. IUBMB Life **60:** 575-590.

XIE, M., and R. L. SCHOWEN, 1999 Secondary structure and protein deamidation. J Pharm Sci **88:** 8-13.

XU, Q., M. P. BELCASTRO, S. T. VILLA, R. D. DINKINS, S. G. CLARKE *et al.*, 2004 A second protein L-isoaspartyl methyltransferase gene in Arabidopsis produces two transcripts whose products are sequestered in the nucleus. Plant Physiol **136:** 2652-2664.

YAMAMOTO, A., H. TAKAGI, D. KITAMURA, H. TATSUOKA, H. NAKANO *et al.*, 1998 Deficiency in protein L-isoaspartyl methyltransferase results in a fatal progressive epilepsy. J Neurosci **18:** 2063-2074.

YAN, G., Q. QIN, B. YI, K. CHUPRUN, H. SUN *et al.*, 2013 Protein-L-isoaspartate (D-aspartate) O-methyltransferase protects cardiomyocytes against hypoxia induced apoptosis through inhibiting proapoptotic kinase Mst1. Int J Cardiol **168:** 3291-3299.

YANG, H., J. D. LOWENSON, S. CLARKE and R. A. ZUBAREV, 2013 Brain proteomics supports the role of glutamate metabolism and suggests other metabolic alterations in protein l-isoaspartyl methyltransferase (PIMT)-knockout mice. J Proteome Res **12:** 4566-4576.

YANG, H., Y. LYUTVINSKIY, H. SOININEN and R. A. ZUBAREV, 2011 Alzheimer's disease and mild cognitive impairment are associated with elevated levels of isoaspartyl residues in blood plasma proteins. J Alzheimers Dis **27:** 113-118.

YANG, M. L., H. A. DOYLE, R. J. GEE, J. D. LOWENSON, S. CLARKE *et al.*, 2006 Intracellular protein modification associated with altered T cell functions in autoimmunity. J Immunol **177:** 4541-4549.

YE, Y., C. QUIJANO, K. M. ROBINSON, K. C. RICART, A. L. STRAYER *et al.*, 2007 Prevention of peroxynitrite-induced apoptosis of motor neurons and PC12 cells by tyrosine-containing peptides. J Biol Chem **282:** 6324-6337.

YOUNG, G. W., S. A. HOOFRING, M. J. MAMULA, H. A. DOYLE, G. J. BUNICK *et al.*, 2005 Protein L-isoaspartyl methyltransferase catalyzes in vivo racemization of Aspartate-25 in mammalian histone H2B. J Biol Chem **280:** 26094-26098.

ZHANG, Y., A. KECSKES, D. COPMANS, M. LANGLOIS, A. D. CRAWFORD *et al.*, 2015 Pharmacological characterization of an antisense knockdown zebrafish model of Dravet syndrome: inhibition of epileptic seizures by the serotonin agonist fenfluramine. PLoS One **10:** e0125898.

ZHONG, Z., K. DU, Q. YU, Y. E. ZHANG and S. HE, 2016 Divergent DNA Methylation Provides Insights into the Evolution of Duplicate Genes in Zebrafish. G3 (Bethesda).

ZHU, H., W. YANG, W. LU, J. ZHANG, G. M. SHAW *et al.*, 2006a A known functional polymorphism (Ile120Val) of the human PCMT1 gene and risk of spina bifida. Mol Genet Metab **87:** 66-70.

ZHU, J. X., H. A. DOYLE, M. J. MAMULA and D. W. ASWAD, 2006b Protein repair in the brain, proteomic analysis of endogenous substrates for protein L-isoaspartyl methyltransferase in mouse brain. J Biol Chem **281:** 33802-33813.

ZON, L. I., and R. T. PETERSON, 2005 In vivo drug discovery in the zebrafish. Nat Rev Drug Discov **4:** 35-44.